FACILITY FORM 602

N 66-80056
(ACCESSION NUMBER)

(THRU)

325
(PAGES)

None
(CODE)

CR-64956
(NASA CR OR TMX OR AD NUMBER)

(CATEGORY)

RE-ORDER NO. 65-333

VOL II

DOCUMENT NO. 65SD4286
1 MAY 1965

# SOLAR THERMIONIC FLIGHT EXPERIMENT STUDY FINAL REPORT

## Volume II - Mission Analysis ( Phase I )

PREPARED UNDER

CONTRACT NO. 950852

FOR

JET PROPULSION LABORATORY
CALIFORNIA INSTITUTE OF TECHNOLOGY
4800 OAK GROVE DRIVE
PASADENA, CALIFORNIA 91103

This work was performed for the Jet Propulsion Laboratory, California Institute of Technology, sponsored by the National Aeronautics and Space Administration under Contract NAS7-100.

GENERAL ELECTRIC
SPACECRAFT DEPARTMENT
*A Department of the Missile and Space Division*
Valley Forge Space Technology Center
P.O. Box 8555 • Philadelphia 1, Penna.

RE-ORDER No. 65-323
Vol II

VOLUME II

TABLE OF CONTENTS


| Section | | Page |
|---|---|---|
| 1. | INTRODUCTION TO MISSION ANALYSIS | 1-1 |
| 1.1 | Objective | 1-1 |
| 1.2 | Study Ground Rules | 1-2 |
| 2. | LAUNCH VEHICLE | 2-1 |
| 2.1 | Introduction | 2-1 |
| 2.2 | Launch Vehicles Considered | 2-1 |
| 2.3 | Promising Launch Vehicles | 2-3 |
| 2.4 | Performance | 2-5 |
| 2.4.1 | Description and Flight Record | 2-5 |
| 2.4.2 | Fairing Configurations | 2-20 |
| 2.4.3 | Payload-Orbit Capability | 2-28 |
| 2.4.4 | Launch Vibration and Acceleration Environment | 2-30 |
| 2.5 | Cost and Reliability | 2-73 |
| 2.6 | Summary and Conclusions | 2-76 |
| 2.7 | References | 2-81 |
| 3. | ORBIT ANALYSIS | 3-1 |
| 3.1 | Introduction | 3-1 |
| 3.2 | Definitions | 3-1 |
| 3.3 | Basic Characteristics and Shadow Comparison for Various Orbits | 3-4 |
| 3.3.1 | Circular Orbit With a Five to Three Light-to-Shadow Ratio | 3-4 |
| 3.3.2 | Circular Polar Orbit | 3-9 |
| 3.3.3 | Sun-Synchronous Daylight Orbit | 3-12 |
| 3.3.4 | Modified Sun-Synchronous Orbit (MSO) | 3-20 |
| 3.3.5 | Elliptical Orbit With a High Light-to-Shadow Ratio | 3-26 |
| 3.3.6 | Stationary Earth Synchronous Orbit | 3-29 |
| 3.3.7 | Solar Probe Orbit | 3-31 |
| 3.4 | Communications Considerations | 3-33 |
| 3.5 | Launch Vehicle Requirements | 3-39 |
| 3.6 | Summary and Conclusions | 3-39 |
| 3.7 | References | 3-44 |
| 4. | SOLAR THERMIONIC SYSTEM PERFORMANCE | 4-1 |
| 4.1 | Introduction | 4-1 |
| 4.2 | Thermionic Converter Performance | 4-1 |
| 4.2.1 | Selection of Emitter Material | 4-2 |
| 4.2.2 | Estimated Converter Performance | 4-7 |

RE-ORDER No. 65-323
Vol II

TABLE OF CONTENTS (CONT.)


| Section | | | Page |
|---|---|---|---|
| | 4.3 | Generator Performance | 4-16 |
| | 4.4 | Concentrator-Absorber Performance | 4-21 |
| | | 4.4.1 Assumed Concentrator Parameters | 4-22 |
| | | 4.4.2 Concentrator-Absorber Performance Calculations | 4-34 |
| | | 4.4.3 Rim Angle Selection | 4-42 |
| | 4.5 | Thermionic System Performance | 4-44 |
| | 4.6 | Selection of Converter Operating Point | 4-48 |
| | 4.7 | Summary and Conclusions | 4-50 |
| | 4.8 | References | 4-51 |
| 5. | SECONDARY EXPERIMENTS | | 5-1 |
| | 5.1 | Introduction | 5-1 |
| | 5.2 | Engineering Experiments | 5-3 |
| | | 5.2.1 Radiation Effects on Solar Cells | 5-3 |
| | | 5.2.2 Solar Thermoelectrics | 5-9 |
| | | 5.2.3 Thermal Coatings | 5-17 |
| | | 5.2.4 V-Ridge Concentrating Photovoltaics | 5-25 |
| | | 5.2.5 Thin-Film Solar Cells | 5-30 |
| | | 5.2.6 Solar Concentrator Reflective Surfaces | 5-37 |
| | | 5.2.7 Thermal Contact Resistance | 5-44 |
| | | 5.2.8 Infrared Detector | 5-51 |
| | | 5.2.9 Laser Experiment | 5-55 |
| | | 5.2.10 Low Thrust Electric Engine | 5-60 |
| | 5.3 | Scientific Experiments | 5-65 |
| | | 5.3.1 Interplanetary Dust (Micrometeoroids) | 5-66 |
| | | 5.3.2 Solar Wind (Interplanetary Plasma) | 5-71 |
| | | 5.3.3 Proton and Electron Spectra and Direction | 5-76 |
| | | 5.3.4 Interplanetary Magnetic Field | 5-80 |
| | | 5.3.5 Heavy Nuclei | 5-86 |
| | | 5.3.6 Solar X-Rays | 5-88 |
| | | 5.3.7 Solar $\gamma$-Rays | 5-91 |
| | | 5.3.8 Measurement of Planetary Albedo | 5-93 |
| | | 5.3.9 Measurements of Ultraviolet Radiation Flux | 5-97 |
| | | 5.3.10 Lyman-Alpha Experiment | 5-101 |
| | 5.4 | Selection of Secondary Experiments | 5-105 |
| | | 5.4.1 Orbit Compatibility | 5-105 |
| | | 5.4.2 Priority Grouping of Experiments | 5-113 |
| | 5.5 | Summary and Conclusions | 5-114 |
| | 5.6 | References | 5-117 |




3

RE-ORDER No. 65-323
VOL II

TABLE OF CONTENTS (CONT.)


| Section | | Page |
|---|---|---|
| 6. | MISSION SELECTION | 6-1 |
| 6.1 | Introduction | 6-1 |
| 6.2 | Orbit Comparisons | 6-1 |
| 6.3 | Launch Vehicle Selection | 6-5 |
| 6.4 | Solar Thermionic System Performance | 6-7 |
| 6.5 | Secondary Experiment Selection | 6-8 |
| 6.6 | Summary and Conclusions | 6-13 |




4

RE-ORDER No. 65-323
VOL II

## LIST OF ILLUSTRATIONS


| Figure | | Page |
|---|---|---|
| 2-1 | Fairings for ATLAS-AGENAD, TAT-AGENA D, and THOR-AGENA D Launch Vehicles | 2-22 |
| 2-2 | Special AGENA Fairings Developed for Advent Program | 2-23 |
| 2-3 | Fairings for THOR-ABLESTAR Launch Vechicle | 2-25 |
| 2-4 | Low Drag Fairings for DELTA and TAD Launch Vehicles | 2-26 |
| 2-5 | Bulbous Fairings for DELTA and TAD Launch Vehicles | 2-27 |
| 2-6 | Fairings for IMPROVED DELTA Launch Vehicle | 2-29 |
| 2-7 | DELTA Model DSV-3B Circular Orbit Capabilities (Low Drag Spacecraft Fairing) | 2-31 |
| 2-8 | DELTA Model DSV-3B Elliptical Orbit Capabilities (Low Drag Spacecraft Fairing - ETR Launch Site) | 2-32 |
| 2-9 | DELTA Model DSV-3B Elliptical Orbit Capabilities (Log Drag Spacecraft Fairing - WTR Launch Site) | 2-33 |
| 2-10 | DELTA Model DSV-3B Circular Orbit Capabilities (Bulbous Spacecraft Fairing) | 2-34 |
| 2-11 | DELTA Model DSV-3C Circular Orbit Capabilities (Low Drag Spacecraft Fairing) | 2-35 |
| 2-12 | DELTA Model DSV-3C Elliptical Orbit Capabilities (Low Drag Spacecraft Fairing - ETR Launch Site) | 2-36 |
| 2-13 | DELTA Model DSV-3C Elliptical Orbit Capabilities (Low Drag Spacecraft Fairing - WTR Launch Site) | 2-37 |
| 2-14 | DELTA Model DSV-3C Circular Orbit Capabilities (Bulbous Spacecraft Fairing) | 2-38 |
| 2-15 | Polar Circular Orbit Capabilities - Trust Augmented DELTA | 2-39 |
| 2-16 | Elliptical Orbit Capability - Trust Augmented DELTA (ETR Launch Site) | 2-40 |
| 2-17 | Elliptical Orbit Capability - Thrust Augmented DELTA, Subrange Africa (ETR Launch Site) | 2-41 |
| 2-18 | Elliptical Orbit Capability - Thrust Augmented DELTA, Overflys Africa (ETR Launch Site) | 2-42 |
| 2-19 | Highly Elliptical Orbit Capability - Thrust Augmented DELTA (ETR Launch Site) | 2-43 |
| 2-20 | IMPROVED DELTA (DSV-3G) Two Stage Circular Orbit Capability (ETR Launch Site) | 2-45 |
| 2-21 | IMPROVED DELTA Three Stage Circular Orbit Capability (ETR Launch Site) | 2-46 |
| 2-22 | IMPROVED DELTA (DSV-3E) Polar Circular Orbit Capability (ETR Launch Site) | 2-47 |




5

RE-ORDER No. 65-323
VOL II

LIST OF ILLUSTRATIONS (CONT.)


| Figure | | Page |
|---|---|---|
| 2-23 | IMPROVED DELTA (DSV-3E) Elliptical Orbit Capability (ETR Launch Site) | 2-48 |
| 2-24 | IMPROVED DELTA (DSV-3E) Elliptical Orbit Capability (ETR Launch Site) | 2-49 |
| 2-25 | IMPROVED DELTA (DSV-3E) Elliptical Orbit Capability (ETR Launch Site) | 2-50 |
| 2-26 | IMPROVED DELTA (DSV-3E) Elliptical Orbit Capability (ETR Launch Site) | 2-51 |
| 2-27 | IMPROVED DELTA (DSV-3E) Elliptical Orbit Capability (ETR Launch Site) | 2-52 |
| 2-28 | IMPROVED DELTA, Three Stage Elliptical Orbit Capability (ETR Launch Site) | 2-53 |
| 2-29 | IMPROVED DELTA, Three Stage Elliptical Orbit Capability for Various Configurations (ETR Launch Site) | 2-54 |
| 2-30 | IMPROVED DELTA, Three Stage Elliptical Orbit Capability for Various Configurations (ETR Launch Site) | 2-55 |
| 2-31 | IMPROVED DELTA Escape Capability | 2-56 |
| 2-32 | IMPROVED DELTA (DSV-3G), Circular Orbit Capability (WTR Launch Site) | 2-57 |
| 2-33 | IMPROVED DELTA (DSV-3E) Polar Elliptical Orbit Capability (WTR Launch Site) | 2-58 |
| 2-34 | IMPROVED DELTA, Three Stage Elliptical Polar Orbit Capability (WTR Launch Site) | 2-59 |
| 2-35 | IMPROVED DELTA, Three Stage Elliptical Polar Orbit Capability (WTR Launch Site) | 2-60 |
| 2-36 | IMPROVED DELTA, Three Stage Elliptical Polar Orbit Capability (WTR Launch Site) | 2-61 |
| 2-37 | IMPROVED DELTA, Three Stage Elliptical Polar Orbit Capability (WTR Launch Site) | 2-62 |
| 2-38 | IMPROVED DELTA* Three Stage Elliptical Polar Orbit Capability (WTR Launch Site) | 2-63 |
| 2-39 | DELTA, Three Stage Circular Orbit Capability (ETR Launch Site) | 2-65 |
| 2-40 | DELTA, Three Stage Elliptical Orbit Capability (ETR Launch Site) | 2-66 |
| 2-41 | DELTA, Three Stage Elliptical Orbit Capability (ETR Launch Site) | 2-67 |




6

RE-ORDER No. 65-323
VOL II

LIST OF ILLUSTRATIONS (CONT.)


| Figure | | Page |
|---|---|---|
| 2-42 | DELTA, Three Stage Polar Circular Orbit Capability (ETR Launch Site) | 2-68 |
| 2-43 | Payload Capability THOR (Block II) ABLESTAR-I, Circular Orbit | 2-69 |
| 2-44 | DELTA Typical Axial Acceleration Time History | 2-71 |
| 3-1 | Maximum Shadow Time for Circular Orbits | 3-5 |
| 3-2 | Orbital Period for Various Circular and Eliptic Orbits | 3-6 |
| 3-3 | Percentage of Darkness as a Function of Inclination of Orbit with Respect to Sun Vector for Various Circular Orbit Altitudes | 3-7 |
| 3-4 | Shadow History for 325-Nautical Mile Circular Orbit | 3-8 |
| 3-5 | Shadow History for Polar Orbits | 3-10 |
| 3-6 | Effects of Combined Launch Delay and Inclination Error on Polar Orbit Shadow History | 3-11 |
| 3-7 | Inclination Angle Required to Achieve Sun-Synchronous Orbit for Various Circular Orbital Altitudes | 3-13 |
| 3-8 | Retrograde Inclination for Eccentric Sun-Synchronous Orbits | 3-14 |
| 3-9 | Shadow History for Sun-Synchronous Noon or Midnight Orbit | 3-16 |
| 3-10 | Seasonal Geometry for Sun-Synchronous Daylight Orbit | 3-17 |
| 3-11 | Region of Continuous Daylight for Sun-Synchronous Daylight Circular Orbits | 3-18 |
| 3-12 | Shadow History for Sun Synchronous Daylight Orbits | 3-19 |
| 3-13 | Yearly Drift of Sun-Synchronous Circular Orbits Due to Inclination Error | 3-21 |
| 3-14 | Effects of Inclination Error on Shadow History for Sun-Synchronous Orbits | 3-22 |
| 3-15 | Effects of Launch Delay on Shadow Histories for Sun-Synchronous Orbits | 3-23 |
| 3-16 | Effect of Combined Launch Delay and Inclination Errors on a Typical Sun-Synchronous Orbit. | 3-24 |
| 3-17 | Modified Sun-Synchronous Orbit Preliminary Launch Window | 3-25 |
| 3-18 | Shadow Histories for Nominal and Deviant Modified Sun-Synchronous Orbits | 3-27 |
| 3-19 | Shadow History for Elliptical Orbit | 3-28 |
| 3-20 | Stationary Orbit Shadow History | 3-30 |




7

LIST OF ILLUSTRATIONS (CONT.)


| Figure | | Page |
|---|---|---|
| 3-21 | Perihelion Performance vs. Spacecraft Weight for Solar Probe Orbit | 3-32 |
| 3-22 | Ecliptic Trajectory in Rotating Sun-Central Coordinate System Using ATLAS-AGENA D-X-259 | 3-34 |
| 3-23 | Communications Gap as a Function of Altitude for Circular Orbits | 3-36 |
| 3-24 | Semi-Synchronous Circular Orbit Conditions | 3-38 |
| 3-25 | Solar Intensity vs. Distance From Sun | 3-43 |
| 4-1 | Output Power Density of Solar Energy Thermionic Converters With Rhenium and Tantalum Emitters at 2000°K | 4-3 |
| 4-2 | Cesium Conduction Loss | 4-9 |
| 4-3 | Measured Bombardment Power Input vs. Average Current for VIII-P-1 Converter | 4-10 |
| 4-4 | Work Function and Saturation Current of Rhenium at 2000°K vs. Reservoir Temperature | 4-11 |
| 4-5 | Electron Cooling Loss vs. Saturation Current at 2000°K | 4-14 |
| 4-6 | Output Power Density of Rhenium Converters | 4-15 |
| 4-7 | Converter Performance at Peak Power $V_o$ = 0.70 Volts | 4-18 |
| 4-8 | Converter Performance at Peak Efficiency $V_o$ = 0.85 Volts | 4-20 |
| 4-9 | Reflectivity Samples | 4-24 |
| 4-10 | Measured Spectral Reflectance for Liberty Mirror Coating 747 (Sample 5) | 4-25 |
| 4-11 | Solar Spectrum in Space | 4-27 |
| 4-12 | Definition of Geometric Error Nomenclature | 4-28 |
| 4-13 | Y-Cumulative Distribution Function for the TAPCO S/N-2 Concentrator | 4-29 |
| 4-14 | Converter - Absorber Efficiency vs. Concentrator Geometric Error for Zero - Orientation Error | 4-31 |
| 4-15 | Concentrator - Absorber Efficiency vs. Rim Angle for Various Values of Orientation Error | 4-35 |
| 4-16 | Concentrator - Absorber Efficiency Vs. Rim Angle for Various Values of Geometric Error | 4-35 |
| 4-17 | Energy Entering Aperture vs. Aperture Diameter (Concentrator Diameter = 2 Feet) | 4-36 |
| 4-18 | Energy Entering Aperture vs. Aperture Diameter (Concentrator Diameter = 3.5 Feet. ) | 4-37 |
| 4-19 | Energy Entering Aperture vs. Aperture Diameter (Concentrator Diameter = 5 Feet) | 4-38 |




8

65-72
VOL II

LIST OF ILLUSTRATIONS (CONT.)


| Figure | | Page |
|---|---|---|
| 4-20 | Blackbody Radiation Loss vs. Aperture Diameter | 4-39 |
| 4-21 | Net Energy Available vs. Concentrator Diameter at Optimum Aperture | 4-40 |
| 4-22 | Optimum Aperture Diameter vs. Concentrator Diameter | 4-41 |
| 4-23 | Energy Entrance Conditions, 45 and 60 Degree Rim Angles | 4-43 |
| 4-24 | Generator Net Energy Required and Power Output vs. Converter Emitter Area | 4-46 |
| 4-25 | Thermionic Generator Power Output vs. Concentrator Diameter | 4-47 |
| 4-26 | Thermionic System Effeciency vs. Concentrator Diameter | 4-49 |
| 5-1 | Schematic of Solar Cell Radiation Effects Experiment | 5-7 |
| 5-2 | Construction Details of Solar Thermoelectric Panel | 5-10 |
| 5-3 | Schematic Diagram, Solar Thermoelectric Test Panel | 5-15 |
| 5-4 | Temperature of Sensor for 19 June 1961 | 5-18 |
| 5-5 | Comparison of Experimental Temperature of Explorer XI Sensor for 6/19/61 and 10/8/61 (Approximately Same Thermodynamic Orbit) | 5-19 |
| 5-6 | Thermal Surface Environment Effects Sensor | 5-22 |
| 5-7 | Construction Details of Radiation Sensor | 5-23 |
| 5-8 | Mounting of Radiation Sensor | 5-23 |
| 5-9 | S-16 Orbiting Solar Observatory Radiation Sensor Plate | 5-24 |
| 5-10 | Photovoltaic V-Ridge Concentration Panel | 5-26 |
| 5-11 | V-Ridge Concentrator Experiment Schematic | 5-29 |
| 5-12 | Reflective Surfaces Experiment Configuration | 5-41 |
| 5-13 | Thermal Contact Resistance Experiment Module | 5-49 |
| 5-14 | Assembly Technique for Several Modules | 5-49 |
| 5-15 | Sensor Head Configuration - Schematic | 5-54 |
| 5-16 | Infrared Detector Electronics, Block Diagram | 5-54 |
| 5-17 | Piezo-Electric Modulatable Retroreflector | 5-58 |
| 5-18 | S-66 Satellite Retro-reflector Panel | 5-58 |
| 5-19 | Family of Experimental Electric Engines | 5-62 |
| 5-20 | Electric Engine on Thrust Stand (In Instrumented Vacuum Chambers) | 5-63 |




9

65-325
Vol II

LIST OF TABLES


| Number | | Page |
|---|---|---|
| 2-1 | ATLAS-AGENA A (B) (D) Flight Record (Through July 28, 1964) | 2-7 |
| 2-2 | THOR-ABLESTAR Flight Record (Through July 28, 1964) | 2-10 |
| 2-3 | THOR-AGENA and TAT-AGENA Flight Record (Through July 28, 1964) | 2-13 |
| 2-4 | DELTA Flight Record (Through July 28, 1964) | 2-18 |
| 2-5 | Launch Vehicle Steady State and Vibration Loading Expected During Powered Flight (350-Pound Spacecraft) | 2-72 |
| 2-6 | NASA Recommended Qualification and Flight Acceptance Vibration on DSV-3B, 3C, 3D or 3E Vehicles | 2-74 |
| 2-7 | Launch Vehicle Cost and Reliability | 2-75 |
| 2-8 | Comparison of Launch Vehicles. | 2-78 |
| 2-9 | Attractive Launch Vehicles | 2-79 |
| 4-1 | Reproducibility of Solar Energy Thermionic Converter Performance (Emitter Area = $2CM^2$) | 4-5 |
| 4-2 | Comparison of Rhenium and Tantalum as Emitter Material | 4-6 |
| 4-3 | Electron Cooling Loss at 2000°K | 4-13 |
| 4-4 | Emitter Sleeve Heat Loss and Voltage Drop (Sleeve Thickness = 0.0025 inches) | 4-13 |
| 4-5 | Lead Voltage Drop and Power Density for Various Voltages and Emitter Areas | 4-17 |
| 4-6 | Converter Performance at Peak Power ($V_0$ = 0.700 Volts) | 4-17 |
| 4-7 | Converter Performance at Peak Efficiency | 4-19 |
| 5-1 | Calculated Performance of Solar Panel Illuminated with 130 Watts/Square Foot Solar Intensity at Normal Incidence | 5-16 |
| 5-2 | Experiment Sample Selection and Separation of Effects | 5-43 |
| 5-3 | Summary of Secondary Experiment Characteristics and Requirements | 5-107 |
| 5-4 | Orbit Compatibility of Secondary Experiments | 5-111 |
| 5-5 | Priority Grouping of Secondary Experiments | 5-115 |
| 6-1 | Advantages and Disadvantages of Various Orbits | 6-2 |
| 6-2 | Recommended Orbits | 6-3 |
| 6-3 | Recommended Launch Vehicle | 6-5 |
| 6-4 | Thermionic System Performance Parameters | 6-9 |
| 6-5 | Recommended Secondary Experiments | 6-10 |
| 6-6 | Summary of Selected Missions | 6-14 |




10

REPORT NO. 65-375
VOL II

# SECTION 1

# INTRODUCTION TO MISSION ANALYSIS

# SECTION 1

# INTRODUCTION TO MISSION ANALYSIS

## 1.1 OBJECTIVE

The objective of this first phase of the study is to select the most attractive missions* for conducting a solar thermionic flight experiment.

To determine the most desirable missions requires consideration of numerous factors, some of the more significant of which are:

- Compatibility with the solar thermionic experiment
- Maximum size solar thermionic system permitted
- Effect on spacecraft weight (battery requirements, radiation shielding required, etc.)
- Weight of spacecraft that can be orbited
- Availability, cost and reliability of launch vehicle required
- Accuracy of orbit injection required
- Compatibility with secondary experiments
- Value of secondary experiments
- Attitude control requirements
- Effect on life of the experiment
- Simplifying the spacecraft design
- MAXIMIZING THE CHANCES OF A SUCCESSFUL MISSION

This phase of the study evaluates various missions on the basis of these factors and selects the most promising.

*In this context, mission refers to a specific combination of orbit, launch vehicle, thermionic experiment size, secondary experiments, etc., that go to make up the flight experiment.

65-323
Vol II

## 1.2 STUDY GROUND RULES

The constraints placed on the study are summarized here since they influence mission selection. Five basic types of orbits were specified for consideration:

a. Circular orbit with a five to three light to dark ratio
b. Sun-synchronous daylight orbit
c. Elliptical orbit with a high light to shadow ratio
d. Stationary earth synchronous orbit
e. Solar probe orbit.

In addition to the specified orbits, three ground rules were established at the outset of the study:

a. The thermionic system must generate a minimum of 100 watts

b. The number of ground stations needed and the demands on these stations are to be minimized in order to avoid priority problems and reduce the cost of data acquisition and handling.

c. The study is based on a spacecraft design life of one year. As the study develops, it will be apparent that an experiment life on the order of one year is needed for complete evaluation of such factors as the effects of the space environment on the concentrator reflective surface.

For the Mission Analysis portion of the study, the spacecraft weight was assumed to be 350 pounds. This estimate was developed from the results of an earlier General Electric sponsored study, entitled "A Preliminary Look at the Feasibility of a Solar Thermionic Piggy-Back Experiment."* This 350 pound estimate is broken down as follows:

*"A Preliminary Look at the Feasibility of a Solar Thermionic Piggy-Back Experiment," by E.W. Williams. An internal General Electric Spacecraft Department Report, ASP-TM-003, January 18, 1963.



13

| | |
|---|---|
| Primary Experiment | 30 |
| Secondary Experiments | 95 |
| Telemetry, Tracking and Command Subsystem | 50 |
| Attitude Control Subsystem | 75 |
| Power Subsystem | 50 |
| Spacecraft Structure and Thermal Control | 50 |
| | 350 Pounds Total |

Obviously, the spacecraft weight will vary with the particular mission, so the 350-pound figure can only be considered typical. When the spacecraft designs are completed, their weight will be estimated and the effects of any deviations from 350 pounds determined.

After, having selected the most attractive missions, Phase II of the study will develop the conceptual spacecraft designs for carrying them out.

RE-ORDER No. 65-323
VOL II

# SECTION 2

# LAUNCH VEHICLE

PRINCIPLE CONTRIBUTOR:

E.W. Williams

# SECTION 2
# LAUNCH VEHICLES

## 2.1 INTRODUCTION

This section considers those launch vehicles that might be suitable for use in a solar thermionic flight experiment program. The relative merits of the various vehicles are compared and recommendations made regarding the most suitable launch vehicles for achieving the various orbits of interest.

## 2.2 LAUNCH VEHICLES CONSIDERED

A list of the launch vehicles considered in this study is given below:

| | |
|---|---|
| ATLAS D | THOR AGENA D |
| ATLAS AGENA B | TAT-AGENA D (TAT-THRUST AUGMENTED THOR) |
| ATLAS AGENA D | DELTA |
| SCOUT | TAD (THRUST AUGMENTED DELTA) |
| THOR ABLESTAR | IMPROVED DELTA |
| THOR AGENA B | |

This list is made up of all major launch vehicles that are currently being used in the space program plus the IMPROVED DELTA, which at present, is under development.

The IMPROVED DELTA is an advanced version of the standard DELTA launch vehicle. Its distinguishing characteristics are greater payload launch capability and larger payload fairings. This vehicle is scheduled to become operational in the third quarter of 1965 (Reference 2-1). Excluding the IMPROVED DELTA, each of the vehicles listed has been used to orbit satellites within the past year.

Vol II

Launch vehicles being used exclusively with IRBM or ICBM programs were not considered.

Launch vehicles which are still in the development stage were not considered (IMPROVED DELTA is an exception) for the following reasons:

a. The expected difficulty in obtaining any launch vehicle which is not presently operational, for a program of this type. Advanced launch vehicles which become operational in the next few years will be in demand for higher priority programs.

b. The uncertainty associated with when these boosters will be available.

c. The lack of available performance data.

The IMPROVED DELTA was included because it is not an entirely new vehicle and the above disadvantages do not apply. Sufficient performance data is now available and all indications are that the vehicle will be available in the third quarter of 1965, as scheduled. There will undoubtedly be other space programs interested in this vehicle, but the priority problem is not one of the same magnitude as it would be if the vehicle were a TITAN III.

Actually, failure to include those launch vehicles other than IMPROVED DELTA that are scheduled to become operational in the next few years should have no effect on the results of this study. At present, it appears that the earliest possible launch date for a solar thermionic flight experiment would be the latter part of 1967*. Only four additional launch vehicles are scheduled (Reference 2-3) to become operational before 1969: SATURN C-1, SATURN C-1B, TITAN III and CENTAUR. Each of these boosters has far greater payload-orbit capability than is needed for this application, and therefore, would not be suitable.

*This is based on estimates of how long it will take to develop an experimental solar thermionic flight vehicle (Reference 2-2) and discussions held with JPL personnel involved in their solar thermionic effort.

## 2.3 PROMISING LAUNCH VEHICLES

All of the launch vehicles listed in the preceding section are not suitable for orbiting a primary solar thermionic experiment. Three criteria were applied to reduce the list to those launch vehicles warranting detailed considerations.

a. The chances of the launch vehicle being available over the next four years should be good.

b. The payload fairing must be able to accommodate a minimum solar concentrator diameter of 42 inches.

c. As a minimum payload-orbit capability the launch vehicle must be able to place 350 pounds in a 325-natutical mile circular earth orbit.

The basis for selecting these constraints and their effect on the list of launch vehicles to be considered is discussed below.

If a logical progression is followed in the development of solar thermionics, a flight experiment should be orbited within the next four years. Therefore, to be considered, a launch vehicle should be operational over this four year period. Except for ATLAS-AGENA B and THOR-AGENA B, there are no indications at present that those launch vehicles listed in Section 2.2 will not be operational over the next four year period. However, there are indications that AGENA B is phasing out. The last seventeen AGENA flights (through July 28, 1964) have employed the "D" series of the AGENA. The AGENA D is an advanced version of AGENA B. The AGENA D has greater length, thrust, and propellant capacity. The AGENA D is the production model of the AGENA series in which the electronics have been standardized and packaged.. Desired alterations are accomplished through the use of "kits." In the AGENA B case, the electronics are not standard and vary from vehicle to vehicle. The payload fairings are essentially the same for AGENA B and D. Since it appears likely that the AGENA B will soon be extinct, the ATLAS AGENA B and THOR AGENA B will not be considered further.

A ground rule of this study requires that the solar thermionic system produce a minimum of 100 watts. In order to generate 100 watts, a concentrator diameter of 42 inches (see Section 4.5) is required. Except for the SCOUT, each of the launch vehicles listed in Section 2.2 has a standard payload fairing capable of housing a 42 inch solar concentrator. The SCOUT vehicle is available with three standard fairings, the largest of which accommodates a maximum diameter of 30 inches. Since this is less than the required 42 inches, the SCOUT will be dropped from further consideration.

Using the work performed in Reference 2-4 as a basis, a spacecraft designed to conduct a solar thermionic flight experiment is expected to weigh approximately 350 pounds. Of the five types of orbits considered in this study, the 325-nautical mile circular orbit represents the minimum energy requirements placed on the launch vehicle. Therefore, if the launch vehicle is unable to place 350 pounds in a 325-nautical mile circular orbit, it could not achieve any of the orbits under consideration and should not be considered further. Only ATLAS D and SCOUT, of the launch vehicles listed in Section 2.2, fail to meet this requirement.

In light of the preceding, the launch vehicle systems with the required capability are:

| | |
|---|---|
| ATLAS-AGENA D | DELTA |
| THOR-ABLESTAR | TAD |
| THOR-AGENA D | IMPROVED DELTA |
| TAT-AGENA D | |

It remains now to consider each of these launch vehicles in more detail and determine which ones could best do the job of orbiting a primary solar thermionic experimental spacecraft.

## 2.4 PERFORMANCE

The significant performance parameters are outlined in this section. A brief description of each launch vehicle system is included in addition to information on its payload-orbit capability, available fairings, launch vibration environment, cost, and reliability.

### 2.4.1 DESCRIPTION AND FLIGHT RECORD

A brief description of each launch vehicle system follows. Only a limited amount of information is included on the ATLAS and AGENA vehicles because of their classified status.

#### 2.4.1.1 ATLAS-AGENA D

The ATLAS-AGENA D is a two stage Air Force launch vehicle. The ATLAS-AGENA series has been in operation as a space booster for over five years. This vehicle system has also been used by NASA in the Ranger and Mariner programs.

The first stage ATLAS is a liquid propellant booster developed by General Dynamics. The rocket engines for the ATLAS are built by Rocketdyne Division of North American Aviation.

Lockheed is the prime contractor on the second stage AGENA D. This stage employs a liquid propellant rocket engine developed by Bell Aerosystems. It burns hypergolic (IRFNA-UDMH) propellants and has restart capability.

The ATLAS-AGENA flight record (Reference 2-5) is summarized in Table 2-1. This launch vehicle system has successfully orbited its payload on 31 out of 39 missions (through July 28, 1964).

65-323
Vol II

Table 2-1. ATLAS-AGENA A (B) (D) Flight Record (Through July 28, 1964)

| Flight Number | Mission | Launch Date | Remarks |
|---|---|---|---|
| 1 (A)* | MIDAS 1 | 2/26/60 | Failed to orbit - second stage failed to separate |
| 2 (A) | MIDAS 2 | 5/24/60 | Successful launch |
| 3 (A) | SAMOS 1 | 10/11/60 | Failed to orbit - second stage ignited but did not go into orbit |
| 4 (A) | SAMOS 2 | 1/31/61 | Successful launch |
| 5 (B) | MIDAS 3 | 7/12/61 | Successful launch |
| 6 (B) | RANGER 1 | 8/23/61 | Failed to achieve deep space orbit |
| 7 (B) | SAMOS 3 | 9/9/61 | Failed to orbit - exploded on launch pad |
| 8 (B) | MIDAS 4 | 10/21/61 | Successful launch |
| 9 (B) | RANGER 2 | 11/18/61 | Failed to achieve deep space orbit |
| 10 (B) | USAF CLASSIFIED | 11/22/61 | Failed to orbit |
| 11 (B) | USAF CLASSIFIED | 12/22/61 | Successful launch |
| 12 (B) | RANGER 3 USAF | 1/26/62 | Successful launch |
| 13 (B) | USAF CLASSIFIED | 3/7/62 | Successful launch |
| 14 (B) | USAF CLASSIFIED | 4/9/62 | Successful launch |
| 15 (B) | RANGER 4 | 4/23/62 | Successful launch |
| 16 (B) | USAF CLASSIFIED | 4/26/62 | Successful launch |
| 17 (B) | USAF CLASSIFIED | 6/17/62 | Successful launch |
| 18 (B) | USAF CLASSIFIED | 7/18/62 | Successful launch |
| 19 (B) | MARINER 1 | 7/22/62 | Destroyed by range safety officer |
| 20 (B) | USAF CLASSIFIED | 8/5/62 | Successful launch |
| 21 (B) | MARINER 2 | 8/26/62 | Successful launch |
| 22 (B) | RANGER 5 | 10/18/62 | Successful launch |
| 23 (B) | USAF CLASSIFIED | 11/11/62 | Successful launch |
| 24 (B) | USAF CLASSIFIED | 12/17/62 | Failed to orbit |
| 25 (B) | USAF CLASSIFIED | 5/9/63 | Successful launch |
| 26 (D) | USAF CLASSIFIED | 7/12/63 | Successful launch |
| 27 (B) | USAF CLASSIFIED | 7/19/63 | Successful launch |
| 28 (D) | USAF CLASSIFIED | 9/6/63 | Successful launch |
| 29 (D) | USAF CLASSIFIED | 10/16/63 | Successful launch |
| 30 (D) | USAF CLASSIFIED | 10/25/63 | Successful launch |
| 31 (D) | USAF CLASSIFIED | 12/18/63 | Successful launch |
| 32 (B) | RANGER 6 | 1/30/64 | Successful launch |
| 33 (D) | USAF CLASSIFIED | 2/25/64 | Successful launch |
| 34 (D) | USAF CLASSIFIED | 3/11/64 | Successful launch |
| 35 (D) | USAF CLASSIFIED | 4/23/64 | Successful launch |
| 36 (D) | USAF CLASSIFIED | 5/19/64 | Successful launch |
| 37 (D) | USAF CLASSIFIED | 7/6/64 | Successful launch |
| 38 (D) | NDS 3<br>NDS 4<br>TRS 6 | 7/17/64 | Successful launch |
| 39 (D) | RANGER 7 | 7/28/64 | Successful launch |

Notes
*AGENA Series indicated by letter in parentheses



21

Launch capability for the ATLAS-AGENA D exist at both the Eastern Test Range (ETR) and the Western Test Range (WTR)*.

2.4.1.2 THOR-ABLESTAR

THOR-ABLESTAR is a standard two-stage launch vehicle used by both the Navy and the Air Force for launching earth satellites. This vehicle system has been in use for five years.

The THOR first state, built by Douglas, is powered by an MB-3 Block II main engine and two vernier engines. All first stage engines are single-start, bi-propellant rocket engines of calibrated thrust, manufactured by Rocketdyne division of North American Aviation. The first stage propellants are RJ-1 and Liquid Oxygen.

The ABLESTAR upper stage is manufactured by the Space-General Corporation. This stage consists of a single engine which burns hypergolic (IRFNA-UDMH) propellants and has restart capability. Attitude control is maintained during powered flight by gimballing the engine and with roll control provided by cold gas nozzles; during coast flight by a cold gas pitch, yaw, and roll control nozzle system.

The THOR-ABLESTAR flight record (Reference 2-5) is summarized in Table 2-2. This launch vehicle system has successfully orbited its payload in nine out of fourteen attempts (through July 28, 1964). Design changes have been made in both stages in an attempt to prevent a recurrence of the failures experienced to date. The THOR-ABLESTAR vehicle has been totally successful in three out of its last four launches. The predicted over-all reliability of the second stage ABLESTAR is 97 percent (Reference 2-6) based on continuous data collection from component, subsystem and system testing.

*The Atlantic Missile Range (AMR) and Pacific Missile Range (PMR) nomenclature has recently been superseded by Eastern Test Range (ETR) and Western Test Range (WTR) respectively.

RE-ORDER No. 65-323
Vol II

Table 2-2. THOR-ABLESTAR Flight Record (Through July 28, 1964)

| Flight Number | Mission | Launch Date | Remarks |
|---|---|---|---|
| 1 | TRANSIT 1B | 4/13/60 | Met all mission objectives except circularity of orbit due to guidance non-nominal performance |
| 2 | TRANSIT 2A and GREB 1 | 6/22/60 | Met all mission objectives except circularity of orbit. Control system problem |
| 3 | COURIER 1A | 8/18/60 | THOR failure |
| 4 | COURIER 1B | 10/4/60 | Met all objectives |
| 5 | TRANSIT 3A and GREB 2 | 11/30/60 | THOR failure |
| 6 | TRANSIT 3B and LOFTI 1 | 2/21/61 | Met all objectives except circularity or orbit. Failure to restart due to ABLESTAR programmer |
| 7 | TRANSIT 4A, INJUN and GREB 2 | 6/28/61 | Met all objectives except INJUN and GREB 3 did not separate from each other |
| 8 | TRANSIT 4B and TRAAC | 11/16/61 | Met all objectives |
| 9 | COMPOSITE 1 | 1/24/62 | Failed to orbit - insufficient second stage thrust |
| 10 | ANNA 1 | 5/10/62 | Failed to orbit - second stage ignition malfunction |
| 11 | ANNA 1B | 10/31/62 | Met all objectives |
| 12 | USAF/USN CLASSIFIED | 9/28/63 | Met all objectives |
| 13 | USAF/USN CLASSIFIED | 12/5/63 | Met all objectives |
| 14 | USAF/USN CLASSIFIED | 4/21/64 | Failed to orbit |

Launch capability for the THOR-ABLESTAR is currently maintained at the Eastern and Western Test Ranges.

2.4.1.3 THOR-AGENA D and TAT-AGENA D

THOR-AGENA D is a two stage launch vehicle system used by both NASA and the Air Force. The THOR-AGENA series has been operational for over six years and represents the most widely used launch vehicle in the space program.

The first stage THOR and second stage AGENA D were described earlier in Sections 2.4.1.2 and 2.4.1.1 respectively.

TAT stands for Thrust Augmented THOR and TAT-AGENA D is simply a standard THOR-AGENA D in which the THOR has been augmented. The THOR is augmented by adding three Thiokol solid propellant rockets. This increases the THOR thrust from 172,000 to 333,550 pounds. TAT is used by the Air Force to orbit payloads too heavy for the THOR-AGENA but which would not utilize all the capacity of ATLAS-AGENA.

The THOR-AGENA and TAT-AGENA flight records (Reference 2-5) are summarized in Table 2-3. The THOR-AGENA series has successfully launched 64 out of 79 payloads. The THOR-AGENA D has been successful 20 out of 22 times. The Space Log (Reference 2-5) shows only eight TAT-AGENA D launches with the payload being successfully orbited five times.

Launch facilities for the THOR-AGENA D and TAT-AGENA D are maintained at the Western Test Range.

2.4.1.4 DELTA and TAD

The DELTA launch vehicle is a three-stage space research vehicle developed by Douglas Aircraft Company for the National Aeronautics and Space Administration. It is used to

Table 2-3. THOR-AGENA and TAT-AGENA Flight Record (Through July 28, 1964) (Sheet 1 of 2)

| Flight Number | Mission | Launch Date | Remarks |
|---|---|---|---|
| 1 (A)* | DISCOVERER 1 | 2/28/59 | Successful launch |
| 2 (A) | DISCOVERER 2 | 4/13/59 | Successful launch |
| 3 (A) | DISCOVERER 3 | 6/3/59 | Failed to orbit |
| 4 (A) | DISCOVERER 4 | 6/25/59 | Failed to orbit |
| 5 (A) | DISCOVERER 5 | 8/13/59 | Successful launch |
| 6 (A) | DISCOVERER 6 | 8/19/59 | Successful launch |
| 7 (A) | DISCOVERER 7 | 11/7/59 | Successful launch |
| 8 (A) | DISCOVERER 8 | 11/20/59 | Successful launch |
| 9 (A) | DISCOVERER 9 | 1/4/60 | Failed to orbit |
| 10 (A) | DISCOVERER 10 | 1/19/60 | Failed to orbit |
| 11 (A) | DISCOVERER 11 | 4/15/60 | Successful launch |
| 12 (A) | DISCOVERER 12 | 6/29/60 | Failed to orbit |
| 13 (A) | DISCOVERER 13 | 8/10/60 | Successful launch |
| 14 (A) | DISCOVERER 14 | 8/18/60 | Successful launch |
| 15 (A) | DISCOVERER 15 | 9/13/60 | Successful launch |
| 16 (B) | DISCOVERER 16 | 10/26/60 | Failed to orbit |
| 17 (B) | DISCOVERER 17 | 11/12/60 | Failed to orbit |
| 18 (B) | DISCOVERER 18 | 12/4/60 | Successful launch |
| 19 (B) | DISCOVERER 19 | 12/20/60 | Successful launch |
| 20 (B) | DISCOVERER 20 | 2/17/61 | Successful launch |
| 21 (B) | DISCOVERER 21 | 2/18/61 | Successful launch |
| 22 (B) | DISCOVERER 22 | 3/30/61 | Failed to orbit |
| 23 (B) | DISCOVERER 23 | 4/8/61 | Successful launch |
| 24 (B) | DISCOVERER 24 | 6/8/61 | Failed to orbit |
| 25 (B) | DISCOVERER 25 | 6/16/61 | Successful launch |
| 26 (B) | DISCOVERER 26 | 7/7/61 | Successful launch |
| 27 (B) | DISCOVERER 27 | 7/21/61 | Failed to orbit |
| 28 (B) | DISCOVERER 28 | 8/3/61 | Failed to orbit |
| 29 (B) | DISCOVERER 29 | 8/30/61 | Successful launch |
| 30 (B) | DISCOVERER 30 | 9/12/61 | Successful launch |
| 31 (B) | DISCOVERER 31 | 9/17/61 | Successful launch |
| 32 (B) | DISCOVERER 32 | 10/13/61 | Successful launch |
| 33 (B) | DISCOVERER 33 | 10/23/61 | Failed to orbit |
| 34 (B) | DISCOVERER 34 | 11/5/61 | Successful launch |
| 35 (B) | DISCOVERER 35 | 11/15/61 | Successful launch |
| 36 (B) | DISCOVERER 36 OSCAR 1 | 12/12/61 | Successful launch |
| 37 (B) | DISCOVERER 37 | 1/13/62 | Failed to orbit |
| 38 (B) | USAF CLASSIFIED | 2/21/62 | Successful launch |
| 39 (B) | DISCOVERER 38 | 2/27/62 | Successful launch |
| 40 (B) | USAF CLASSIFIED | 4/17/62 | Successful launch |
| 41 (B) | USAF CLASSIFIED | 4/28/62 | Successful launch |
| 42 (B) | USAF CLASSIFIED | 5/15/62 | Successful launch |
| 43 (B) | USAF CLASSIFIED | 5/29/62 | Successful launch |
| 44 (B) | USAF CLASSIFIED | 6/2/62 | Successful launch |
| 45 (B) | USAF CLASSIFIED | 6/18/62 | Successful launch |
| 46 (B) | USAF CLASSIFIED | 6/22/62 | Successful launch |
| 47 (D) | USAF CLASSIFIED | 6/27/62 | Successful launch |
| 48 (B) | USAF CLASSIFIED | 7/20/62 | Successful launch |

Notes

* AGENA Series indicated by letter in parentheses

RE-ORDER No. 65-223 Vol II

Table 2-3. THOR-AGENA and TAT-AGENA Flight Record (Through July 28, 1964) (Sheet 2 of 2)

| Flight Number | Mission | Launch Date | Remarks |
|---|---|---|---|
| 49 (B) | USAF CLASSIFIED | 7/2[illegible]/62 | Successful launch |
| 50 (D) | USAF CLASSIFIED | 8/1/62 | Successful launch |
| 51 (D) | USAF CLASSIFIED | 8/20/62 | Successful launch |
| 52 (B) | USAF CLASSIFIED | 9/1/62 | Successful launch |
| 53 (B) | USAF CLASSIFIED | 9/17/62 | Successful launch |
| 54 (B) | ALOUETTE | 9/28/62 | Successful launch |
| 55 (D) | USAF CLASSIFIED | 9/29/62 | Successful launch |
| 56 (B) | USAF CLASSIFIED | 10/9/62 | Successful launch |
| 57 (D) | USAF CLASSIFIED | 10/26/62 | Successful launch |
| 58 (B) | USAF CLASSIFIED | 11/5/62 | Successful launch |
| 59 (B) | USAF CLASSIFIED | 11/24/62 | Successful launch |
| 60 (D) | USAF CLASSIFIED | 12/4/62 | Successful launch |
| 61 (D) | USAF/USN CLASSIFIED | 12/12/62 | Successful launch |
| 62 (D) | USAF CLASSIFIED | 12/14/62 | Successful launch |
| 63 (D) | USAF CLASSIFIED | 1/7/63 | Successful launch |
| 64 (D) | USAF CLASSIFIED | 1/16/63 | Successful launch |
| 65 (D)** | USAF CLASSIFIED | 2/28/63 | Failed to orbit - first use of TAT |
| 66 (D)** | USAF CLASSIFIED | 3/18/63 | Failed to orbit - used TAT |
| 67 (D) | USAF CLASSIFIED | 4/1/63 | Successful launch |
| 68 (D) | USAF CLASSIFIED | 4/26/63 | Failed to orbit |
| 69 (D) | USAF CLASSIFIED | 5/18/63 | Successful launch |
| 70 (D) | USAF CLASSIFIED | 6/12/63 | Successful launch |
| 71 (D) | LOFTI 2A<br>GREB 1<br>RADOSE<br>CLASSIFIED<br>SURCAL | 6/15/63 | Successful launch |
| 72 (D) | CLASSIFIED<br>HITCH-HIKER 1 | 6/26/63 | Successful launch |
| 73 (B) | USAF CLASSIFIED | 6/29/63 | Successful launch |
| 74 (D) | USAF CLASSIFIED | 7/18/63 | Successful launch |
| 75 (D) | USAF CLASSIFIED | 7/30/63 | Successful launch |
| 76 (D)** | USAF CLASSIFIED | 8/24/63 | Successful launch - used TAT |
| 77 (D) | USAF CLASSIFIED | 8/29/63 | Successful launch |
| 78 (D)** | USAF CLASSIFIED | 9/23/63 | Successful launch - used TAT |
| 79 (D)** | USAF CLASSIFIED | 10/29/63 | Successful launch - used TAT |
| 80 (D) | USAF CLASSIFIED | 11/9/63 | Failed to orbit |
| 81 (D) | USAF CLASSIFIED | 11/27/63 | Successful launch |
| 82 (D)** | USAF CLASSIFIED | 12/20/63 | Failed to orbit - used TAT |
| 83 (D) | USAF CLASSIFIED | 12/21/63 | Successful launch |
| 84 (D)** | USAF/USN<br>CLASSIFIED<br>GGSE<br>EGRS<br>GREB 5 | 1/11/64 | Successful launch used TAT |
| 85 (D) | USAF CLASSIFIED | 1/19/64 | Successful launch |
| 86 (B) | ECHO 2 | 1/25/64 | Successful launch |
| 87 (D)** | USAF CLASSIFIED | 2/15/64 | Successful launch - used TAT |

Notes

** Launches employing TAT

launch various spacecraft into either earth orbit, solar orbit, or deep space probes. There are two standard DELTA configurations: the DSV-3B which uses the X-248 third stage motor and the DSV-3C which uses a higher performance X-258 third stage motor.

The DELTA first stage is a basic THOR booster previously described in Section 2.4.1.2.

The propellants of the second-stage propulsion system are inhibited red fuming nitric acid (oxidizer) and unsymmetrical dimethylhydrazine (fuel). In addition to its principal function, the second-stage propulsion system allows pitch and yaw control by gimbaling the thrust chamber. The second stage rocket engine is manufactured by Aerojet General.

The DELTA third-stage motor is a solid propellant rocket manufactured by Allegheny Ballistics Laboratory.

DELTA vehicles have proven their reliability with 22 successful launches out of 24 attempts (through July 28, 1964). The DELTA flight record is summarized in Table 2-4 (Reference 2-5).

The Eastern Test Range has been used exclusively for all launches, but plans for the necessary DELTA facilities at the Western Test Range have been prepared and these facilities are scheduled to be available in the first quarter of 1966 (Reference 2-1). The DELTA program now uses Complex 17 at Cape Kennedy. The complex includes launch pads 17A and 17B and provides the DELTA program with simultaneous checkout capability for two vehicles.

The TAD (Thrust Augmented DELTA) was used successfully to launch SYNCOM 2 in July 1963. This represents the only application of TAD to date (through October 30, 1964). The TAD vehicle consists of a standard DSV-3B DELTA modified with three 53,850 pound thrust rocket motors attached to the first stage; they increase liftoff thrust from its nominal 172,000 to 333,550 pounds. These solid propellant boosters are manufactured by Thiokol. This approach for augmenting the first stage THOR booster is identical to the system used on the TAT-AGENA D launch vehicle. Launch pad 17A at ETR is used for TAD launches.

RE-ORDER No. 65-323
VOL II

Table 2-4. DELTA Flight Record (Through July 28, 1964)

| Flight Number | Mission | Launch Date | Remarks |
|---|---|---|---|
| 1 | ECHO A-10 | 5/13/60 | Failed to orbit - second stage attitude control malfunction |
| 2 | ECHO 1 | 8/12/60 | Successful launch |
| 3 | TIROS 2 | 11/23/60 | Successful launch |
| 4 | EXPLORER 10 | 3/25/61 | Successful launch |
| 5 | TIROS 3 | 7/12/61 | Successful launch |
| 6 | EXPLORER 12 | 8/15/61 | Successful launch |
| 7 | TIROS 4 | 2/8/62 | Successful launch |
| 8 | OSO 1 | 3/7/62 | Successful launch |
| 9 | AEIEL | 4/26/62 | Successful launch |
| 10 | TIROS 5 | 6/19/62 | Successful launch |
| 11 | TELSTAR 1 | 7/10/62 | Successful launch |
| 12 | TIROS 6 | 9/18/62 | Successful launch |
| 13 | EXPLORER | 10/2/62 | Successful launch |
| 14 | EXPLORER 15 | 10/27/62 | Successful launch |
| 15 | RELAY 1 | 12/13/62 | Successful launch |
| 16 | SYNCOM 1 | 2/14/63 | Successful launch |
| 17 | EXPLORER 17 | 4/2/63 | Successful launch |
| 18 | TELSTAR 2 | 5/7/63 | Successful launch |
| 19 | TIROS 7 | 6/19/63 | Successful launch |
| 20 | SYNCOM 2* | 7/26/63 | Successful launch |
| 21 | EXPLORER 18 | 11/27/63 | Successful launch |
| 22 | TIROS 8 | 12/21/63 | Successful launch |
| 23 | RELAY 2 | 1/21/64 | Successful launch |
| 24 | BEACON EXPLORER | 3/19/64 | Failed to orbit - insufficient third stage thrust. |

Note

*Launch employed the thrust augmented DELTA.



28

2.4.1.5 IMPROVED DELTA (DSV-3E)

An IMPROVED DELTA, designated the DSV-3E, is presently under development. This vehicle is scheduled to be available in the third quarter of 1965. This is basically an augmented DELTA (DSV-3C) with a larger improved second stage and larger payload fairings. The first stage is a modified thrust augmented DELTA (TAD) booster. The second stage vehicle consists of two major components; the AJ10-118E liquid propellant propulsion system and the guidance compartment structure. The third stage/spacecraft fairing attaches to the forward face of the guidance compartment structure and protects the third stage motor and spacecraft from aerodynamic heating during the boost flight.

The first stage liquid propellant booster is powered by a gimballed main engine and initially augmented by three externally mounted solid propellant motors equally spaced around the periphery of the stage. The three solid propellant motors are jettisoned simultaneously after solid propellant burnout. The AJ10-118E second stage pressure fed propulsion system utilizes IRFNA and UDMH as propellants. The thrust chamber assembly is mounted on a gimbal system for attitude control (pitch and yaw) during powered flight. Roll control during powered and coast flight and pitch and yaw control during coast flight is achieved by the second stage cold gas system. The second stage guidance compartment structure houses the flight control system, the radio guidance system, the velocity cutoff system, instrumentation, range safety system, tracking and power systems.

The primary difference between the IMPROVED DELTA second stage propulsion system (AJ10-118E) and the present DELTA second stage propulsion system (AJ10-118D) is in the tankage and aft skirt assemblies. The tankage diameter has been increased from 32 inches to 54.7 inches, thus more than doubling the propellant capacity. The aft skirt has been revised to attach to the larger diameter tankage. The second-to-third stage interstage structure includes the spin table and is mounted at the forward end of the guidance compartment structure and will support the third stage vehicle. The third stage propulsion system is the ABL X258-E2 solid propellant rocket motor which is also used on the standard DELTA (DSV-3C). A spacecraft attachment fitting is mounted to the forward shoulder of the third

stage motor to support various spacecrafts. The spacecraft attachment fittings includes provisions for separating the spacecraft, at the spacecraft-support structure interface, from the expended third stage motor.

The larger diameter of the IMPROVED DELTA second stage allows larger diameter payload fairings than were possible with the standard DELTA (DSV-3C). The IMPROVED DELTA uses the standard AGENA D fairings which greatly increases its payload volume capability over the DSV-3C.

The IMPROVED DELTA represents a very versatile launch vehicle. It can be used in the configuration described above which constitutes a three stage vehicle with first stage augmentation. If the first stage augmentation is not needed the DSV-3E can be employed as a non augmented three stage vehicle. Finally, for applications where an even smaller payload-orbit capability is required the third stage solid motor can be omitted and only the first two stages used. These various combinations have the following designations:

a. DSV-3E - Three stage vehicle with first stage augmentation
b. DSV-3F - Three stage vehicle without first stage augmentation
c. DSV-3G - Two stage vehicle (omit X-258 solid) with first stage agumentation
d. DSV-3H - Two stage vehicle without augmentation.

The IMPROVED DELTA then can be used as a two or three stage launch vehicle and with or without augmentation depending on the particular requirements.

### 2.4.2 FAIRING CONFIGURATIONS

The standard available fairings for each launch vehicle system are outlined in this section. This information is important since the available payload volume is a major factor in defining the maximum size thermionic system a given launch vehicle can accommodate. Since several of the launch vehicles employ the same last stage, they have essentially the same payload fairings.

### 2.4.2.1 Fairings for ATLAS-AGENA D, TAT-AGENA D and THOR-AGENA D

Because the AGENA has received wide application in the space program, there have been numerous fairing designs developed to be used with launch vehicle systems employing it as the final stage. Some of these fairings are associated with classified programs and information on these configurations is unavailable. Information was obtained on four fairings made for the AGENA D. Two of these, the AGENA short fairing and the AGENA long fairing, are shown in Figure 2-1. These fairings are basically the same except for length. They each accommodate a payload up to 57 inches in diameter, but the long fairing will handle a payload 195 inches long while the short fairing can only take an axial length of 88 inches. The long fairing is used on the Nimbus Program and is also referred to as the S-27. The S-27 is the largest of the AGENA D fairings. The two additional fairings, UNITAK and 823, are very similar in configuration to the long fairing shown in Figure 2-1. They are approximately the same length and 62 inches in diameter instead of 64 inches.

Either of these four fairings will meet the requirements of a solar thermionic experiment. However, since the required axial length is expected to be on the same order as the diameter the short fairing would be the most suitable.

As part of the Advent Program, Lockheed developed and flight qualified three special fairings of the configuration shown in Figure 2-2. These fairings were made for use with the AGENA B but could be used with the AGENA D if a special adapter were developed. Since Advent's cancellation, Lockheed has been looking for an application for these fairings. Their size is such that solar concentrator diameters up to approximately 7.5 feet could be accommodated. This fairing design does not appear particularly attractive, at least for the first experimental flight, because a system requiring a solar concentrator diameter greater than 44 to 55 inches does not appear desirable.

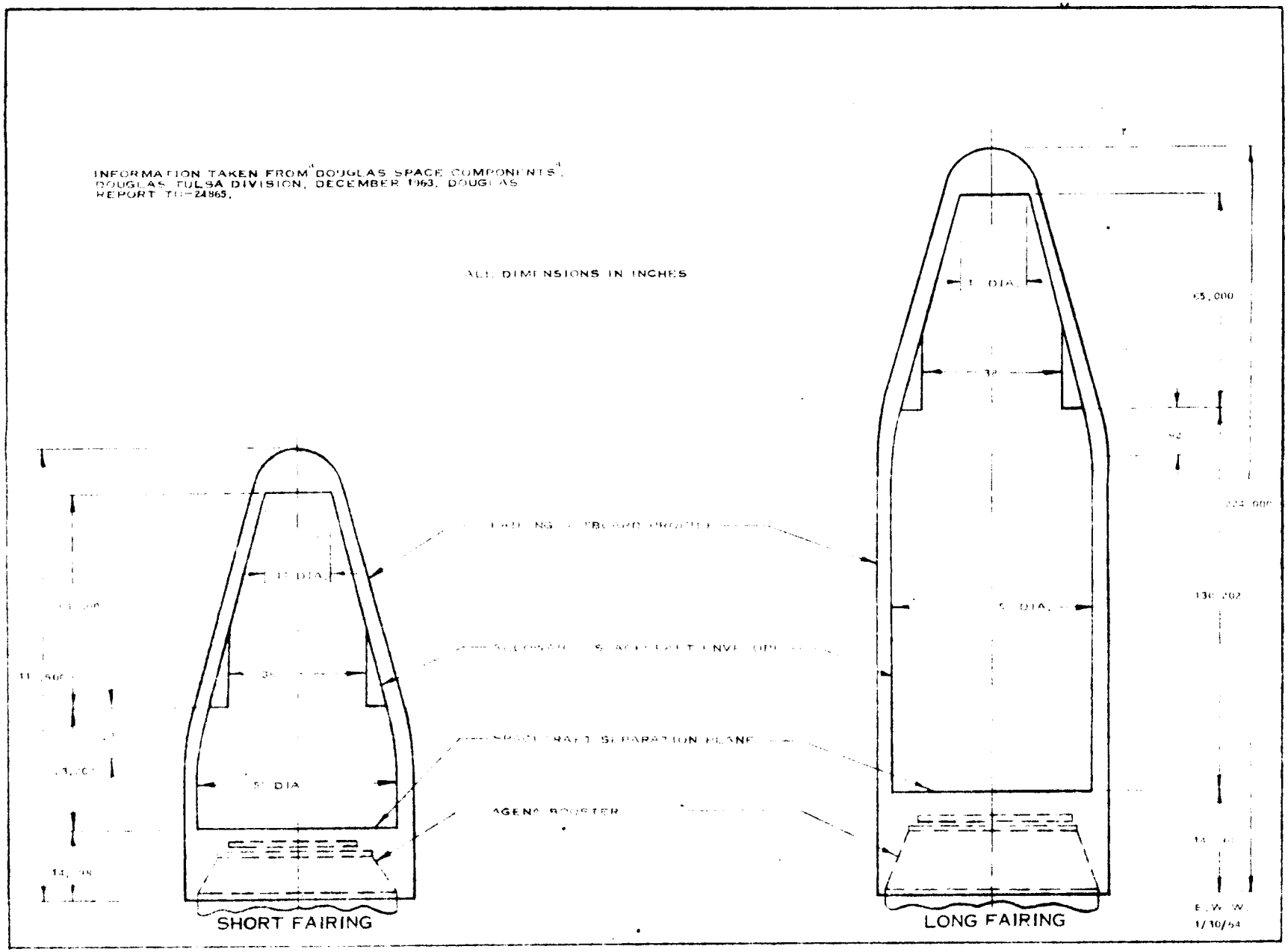


Figure 2-1. Fairings for ATLAS-AGENA D, TAT-AGENA D, and THOR-AGENA D Launch Vehicles

RECORDER No. 63-323

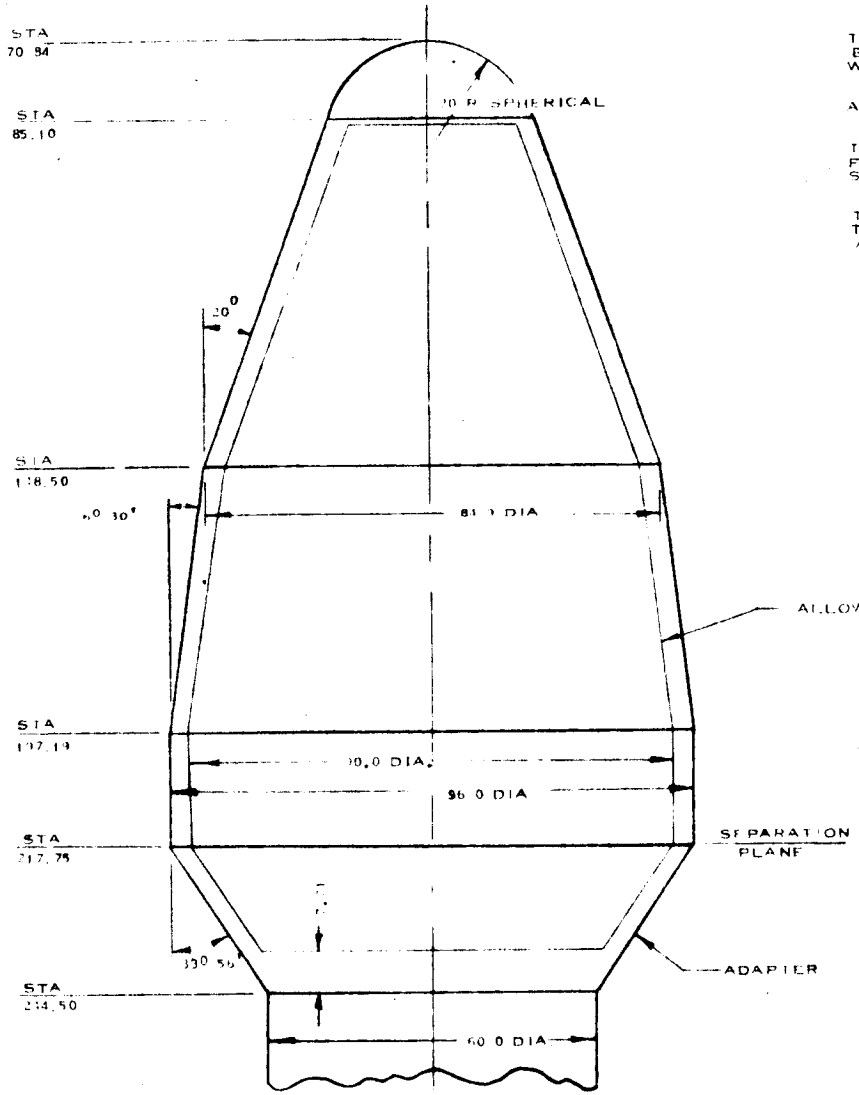


THIS FAIRING DESIGNED FOR USE WITH AGENA B. BY MODIFYING THE ADAPTER IT COULD BE USED WITH AGENA D.

ALL DIMENSIONS IN INCHES.

THREE OF THESE FAIRINGS HAVE BEEN DEVELOPED, FLIGHT QUALIFIED AND ARE AVAILABLE FOR SPACE MISSIONS.

THIS IS NOT A "CLAM SHELL" TYPE FAIRING AND THEREFORE IT MUST PASS OVER THE SPACECRAFT AT SEPARATION.

E.W.W.
5/2/64

Figure 2-2. Special AGENA Fairing Developed for Advent Program



33

2.4.2.2 Fairings for THOR-ABLESTAR

There are two standard fairings for the THOR-ABLESTAR vehicle. Details of these fairings are given in Figure 2-3. The smaller fairing is used when the payload will permit since it is 85 pounds lighter than the large one and improves the launch vehicle payload weight capability. Either of these fairings meets the experimental solar thermionic vehicle requirements. The short fairing appears ideal for a spacecraft design similar to the one resulting from the study conducted in Reference 2-4.

2.4.2.3 Fairings for DELTA and TAD

Two basic types of fairings are currently being used on the DELTA vehicle, a low drag fairing and a bulbous fairing. The low drag fairing is used whenever the spacecraft size permits because it has less aerodynamic drag than the bulbous fairing and allows the vehicle to perform with maximum efficiency. Details of the standard fairings are given in Figures 2-4 and 2-5.

The low drag fairing is available in two lengths, but since the maximum diameter payload they will accommodate is 29 inches they are not suitable for this application.

At present, the bulbous fairing is available in only one size. However, an extended bulbous fairing has been proposed by NASA and Douglas. Douglas estimates the extended bulbous fairing can be available for launch within six months after notification to proceed. The bulbous fairings will just satisfy the 42-inch diameter concentrator required to obtain 100 watts from the thermionic system. However, based on the results of the study performed in Reference 2-4 it will be difficult to package the vehicle into the standard bulbous fairing because of the short axial length available. From this standpoint, the extended bulbous fairing appears most attractive for this application.

INFORMATION TAKEN FROM "ABLESTAR SUMMARY DATA FOR FUTURE APPLICATIONS," SPACE GENERAL CORPORATION, JUNE 1963.

ALL DIMENSIONS IN INCHES

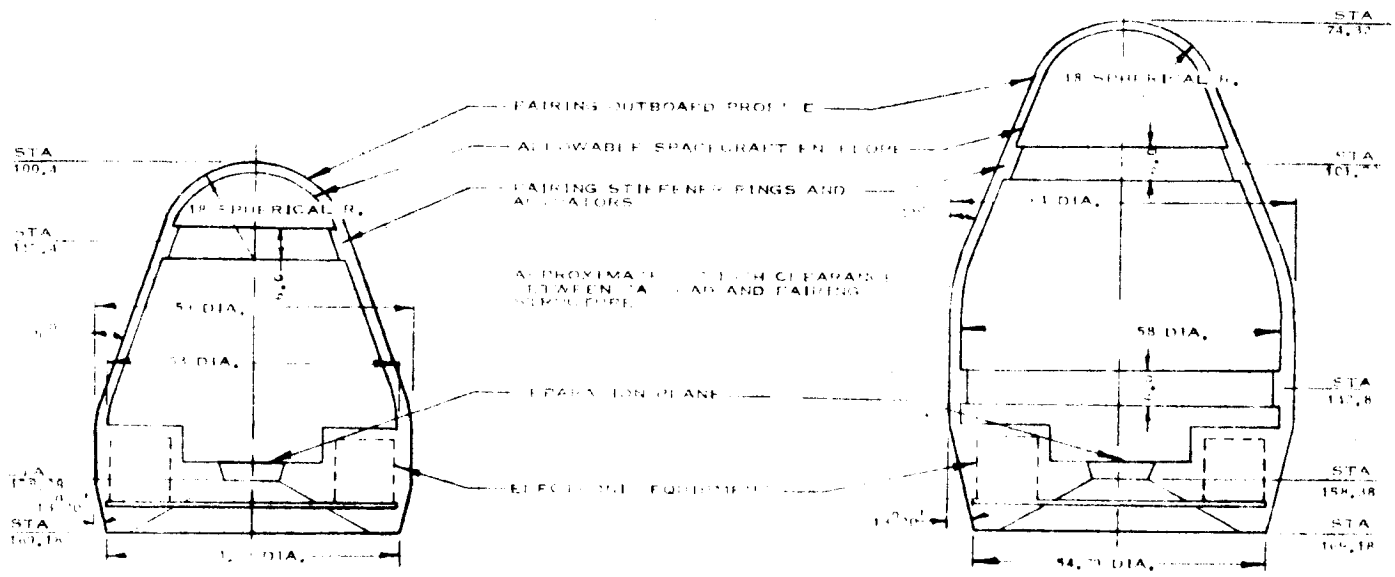


Figure 2-3. Fairings for THOR-ABLESTAR Launch Vehicle





VOL II

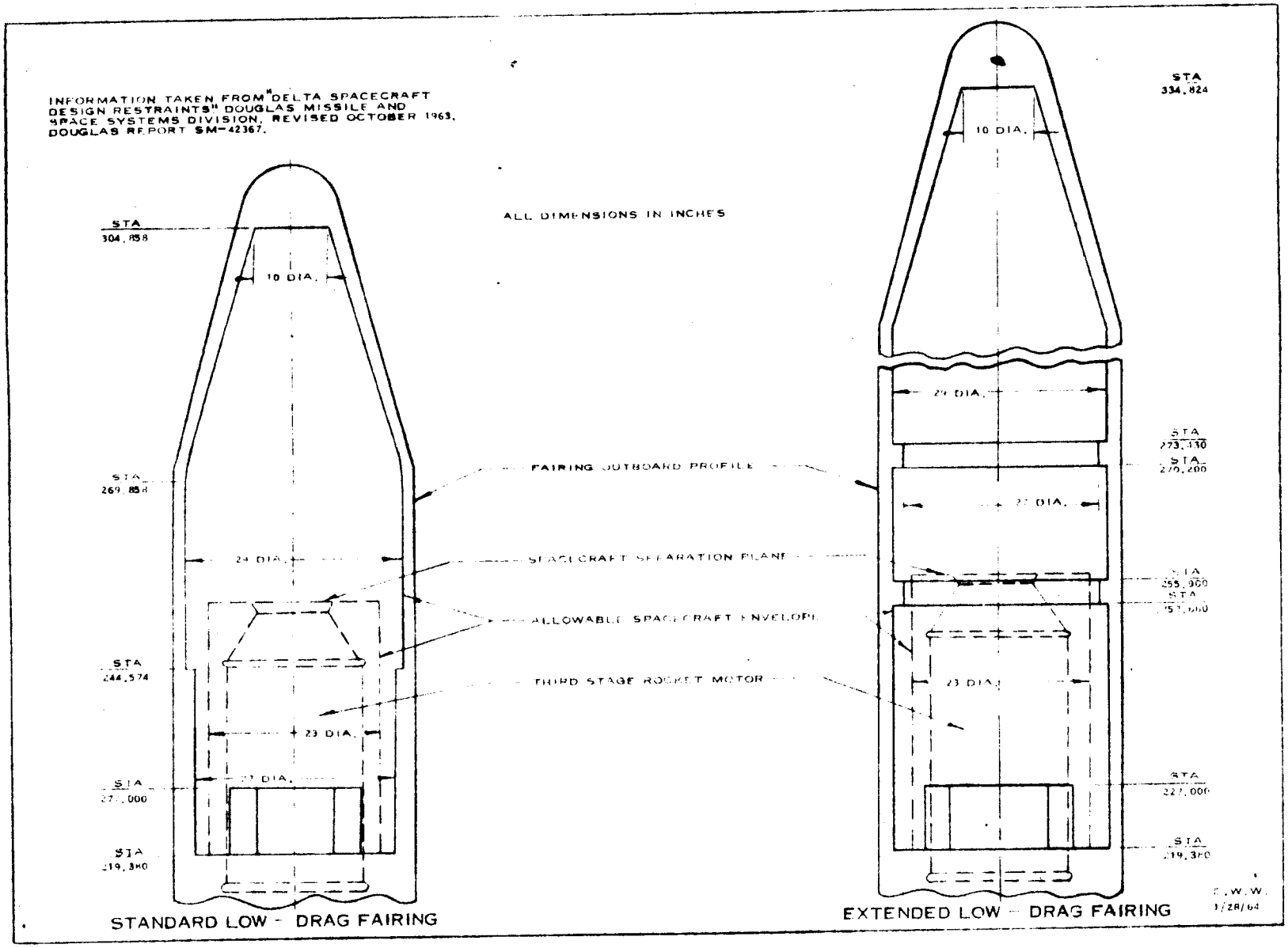


Figure 2-4. Low Drag Fairings for DELTA and TAD Launch Vehicles

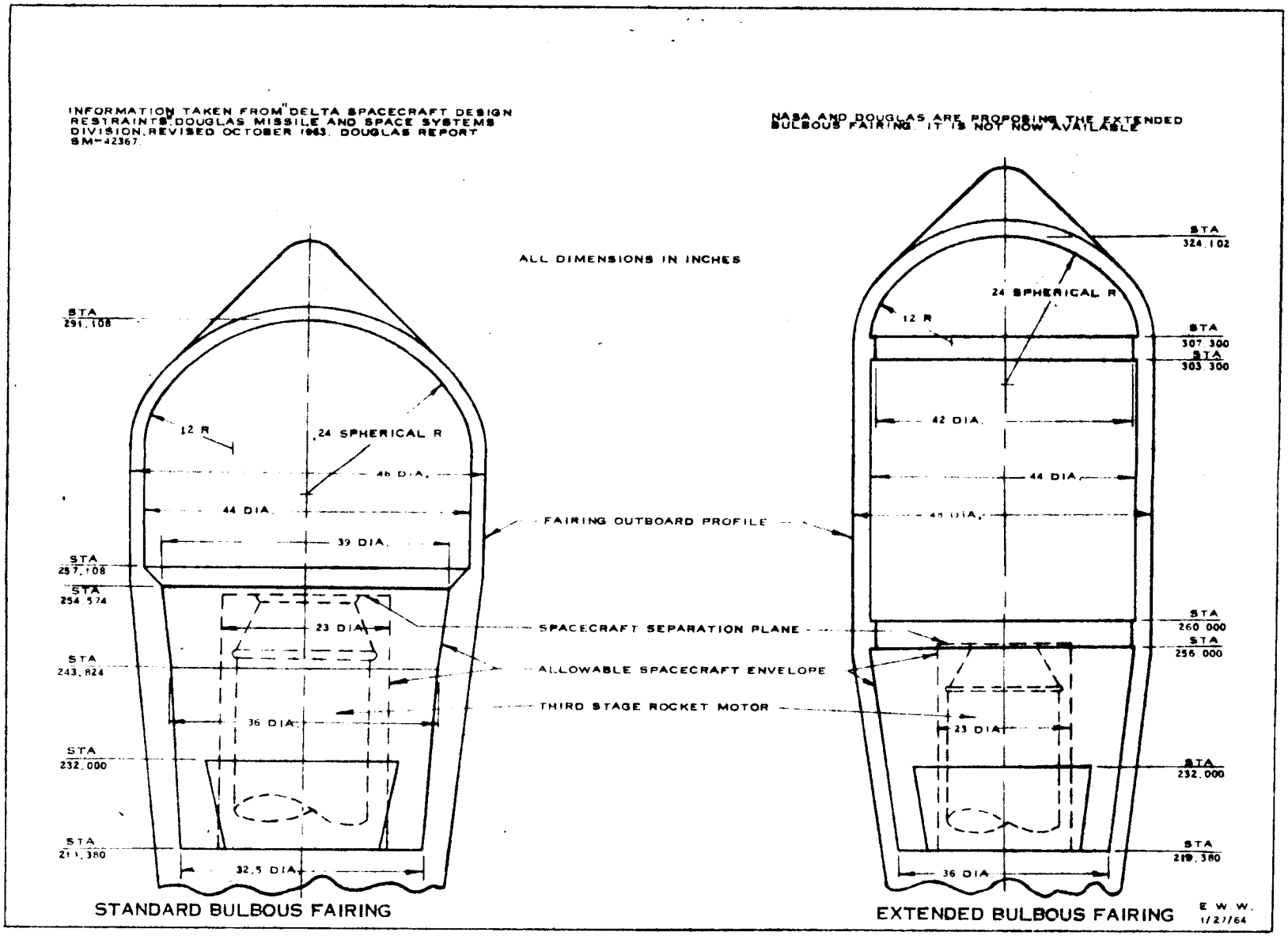


Figure 2-5. Bulbous Fairings for DELTA and TAD Launch Vehicles



37

2.4.2.4 Fairings for IMPROVED DELTA

The IMPROVED DELTA having a larger diameter second stage, can accommodate fairings and spacecraft of larger diameter. The two standard fairings for the IMPROVED DELTA are shown in Figure 2-6. Actually these are the basic AGENA D fairings (see Figure 2-1) which have been adapted to the IMPROVED DELTA configuration. The basic IMPROVED DELTA fairing is shown on the right of Figure 2-6. For cases where the X-258 third stage motor is not needed the payload volume can be increased significantly by direct mounting to the second stage as illustrated by the center configuration in Figure 2-6. Also shown is the short, A-12 fairing, which is available for second stage mounting in applications where the X-258 is not required.

These fairings will accommodate a maximum payload diameter of 57 inches compared with 44 inches for the DELTA (DSV-3C) bulbous fairing. This increased payload diameter capability is one of the major advantages of the IMPROVED DELTA.

2.4.3 PAYLOAD-ORBIT CAPABILITY

Payload-orbit capability plots are presented for the DELTA, TAD, IMPROVED DELTA, and THOR-ABLESTAR launch vehicle systems. This performance data was obtained from References 2-7, 2-8, and 2-6 respectively. Similar data for ATLAS-AGENA D, THOR-AGENA D and TAT-AGENA D is presented in Reference 2-9, but is not included here because of its classified nature.*

Figures 2-7 through 2-14 describe the DELTA payload-orbit capability. The TAD capability is given in Figures 2-15 through 2-19 and the IMPROVED DELTA in Figures 2-20 through 2-38. In addition, Reference 2-8 gives several payload-orbit plots comparing the standard

*As the report progresses, it will be shown that the ATLAS-AGENA D, THOR-AGENA D, and TAT-AGENA D launch vehicles are not attractive for the selected mission.

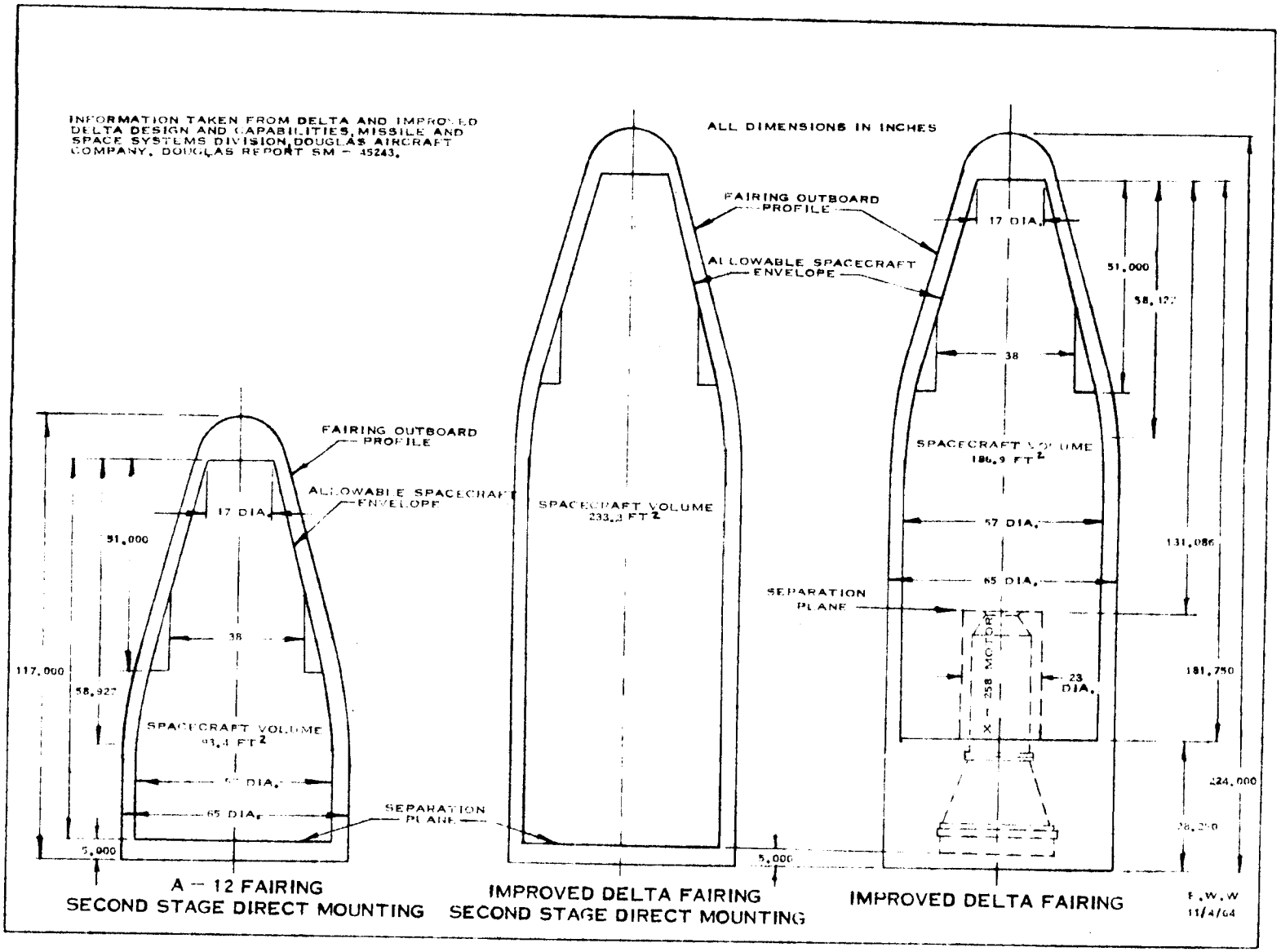


Figure 2-6. Fairings for IMPROVED DELTA Launch Vehicle



31

DELTA (DSV-3C), TAD (DSV-3D), and the IMPROVED DELTA (DSV-3E). These results are given in Figures 2-39 through 2-42. The THOR-ABLESTAR payload-orbit capability is summarized in Figure 2-43.

These figures give a fairly complete picture of the payload-orbit capability of the various launch vehicles. However, some caution should be exercised in using these curves. For example, Figure 2-7 indicates that DELTA can place a payload directly into polar orbit from ETR. This is true only if the range safety constraints are ignored which in a practical case never occurs. As a result polar orbits are generally obtained from WTR. Polar orbits can be obtained from ETR but this requires a "dog leg" (plane change) launch which is more complicated and makes less efficient use of the launch vehicles boost capability.

### 2.4.4 LAUNCH VIBRATION AND ACCELERATION ENVIRONMENT

Table 2-5 summarizes the maximum steady state and vibratory accelerations that are expected during powered flight for the various launch vehicles. The same loading conditions are indicated for the DELTA, TAD and IMPROVED DELTA vehicles. Obviously, there are differences between these vehicles but the variations are small. This is substantiated by Figure 2-44 which gives acceleration versus time for these three vehicles. The acceleration conditions for the DSV-3C and DSV-3D are essentially equal while the DSV-3E is always equal to or lower. The maximum values are used in Table 2-5.*

*The values given in Table 2-5 do not agree with those given in Figure 2-44 because the the spacecraft weights are different (Table 2-5 assumes a 350 pound spacecraft and Figure 2-44 is a 150 pound vehicle).



40

RE-ORDER No. 65-323
VOL II

# DELTA PAYLOAD - ORBIT CAPABILITY
## PERFORMANCE SUMMARY

| Figure | Launch Vehicle Configuration | Type of Orbit | Launch Site | Launch Azimuth Degrees | Orbit Inclination Degrees | Altitudes Apogee/Perigee Nautical Miles |
|---|---|---|---|---|---|---|
| 2-7 | DSV-3B | Circular | ETR | 108 | 33 | ≤ 2000 |
| | | | | 43 | 53 | |
| | | | | 146 | 90 | |
| | | | WTR | 182 | 90 | |
| 2-8 | DSV-3B | Elliptical | ETR | 108 | 33 | ≤ 400/200 |
| | | | | | | 300 |
| | | | | | | 400 |
| | | | | | | 500 |
| | | | | | | 600 |
| | | | | | | 700 |
| | | | | | | 800 |
| | | | | | | 900 |
| | | | | | | 1000 |
| 2-9 | DSV-3B | Elliptical | WTR | 182 | 90 | ≤ 200/200 |
| | | | | | | 300 |
| | | | | | | 400 |
| | | | | | | 500 |
| | | | | | | 600 |
| | | | | | | 700 |
| | | | | | | 800 |
| | | | | | | 900 |
| | | | | | | 1000 |
| 2-10 | DSV-3B | Circular | ETR | 108 | 33 | ≤ 2000 |
| | | | | 43 | 53 | |
| | | | | 146 | 90 | |
| | | | WTR | 182 | 90 | |
| 2-11 | DSV-3C | Circular | ETR | 108 | 33 | ≤ 2000 |
| | | | WTR | 182 | 90 | |
| 2-12 | DSV-3C | Elliptical | ETR | 108 | 33 | ≤ 40,000/200 |
| | | | | | | 400 |
| | | | | | | 600 |
| | | | | | | 800 |
| | | | | | | 1000 |
| 2-13 | DSV-3C | Elliptical | WTR | 182 | 90 | ≤ 40,000/200 |
| | | | | | | 400 |
| | | | | | | 600 |
| | | | | | | 800 |
| | | | | | | 1000 |
| 2-14 | DSV-3C | Circular | ETR | 108 | 33 | ≤ 2000 |
| | | | WTR | 182 | 90 | |

REPORT No. 65-323
VOL II

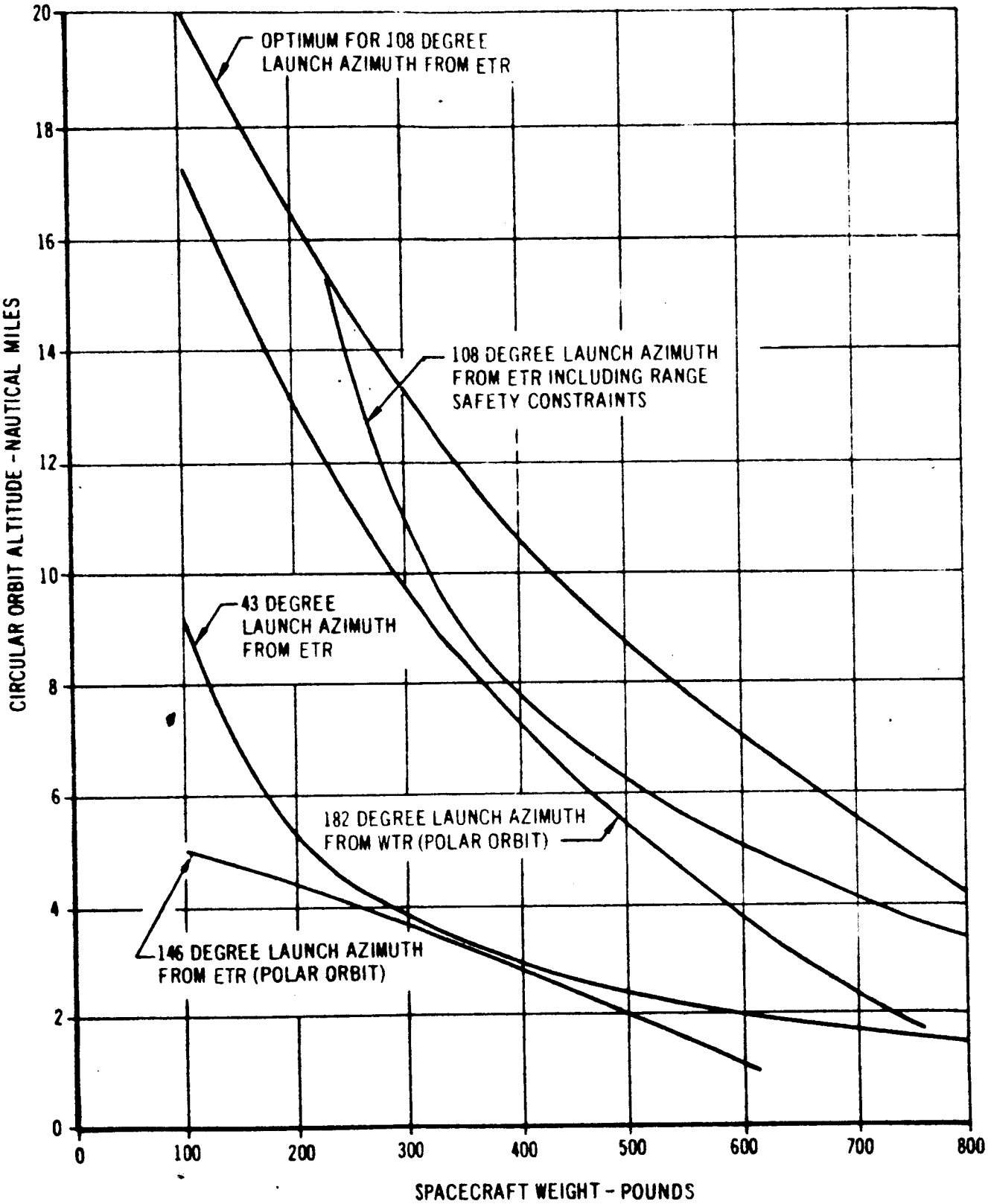


Figure 2-7. DELTA Model DSV-3B Circular Orbit Capabilities
(Low Drag Spacecraft Fairing)

RE-ORDER No. 65-323
Vol. II

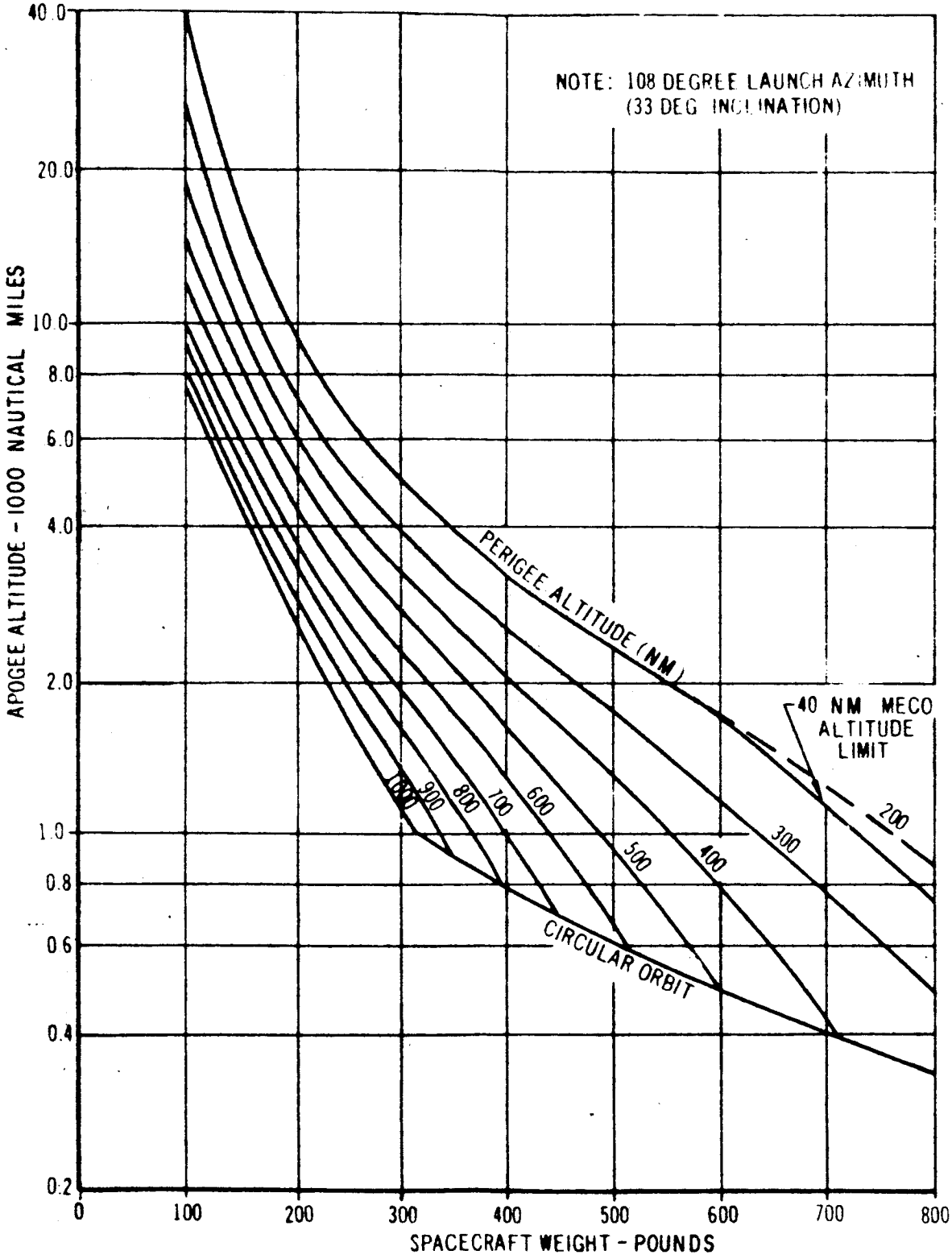


Figure 2-8. DELTA Model DSV-3B Elliptical Orbit Capabilities
(Low Drag Spacecraft Fairing - ETR Launch Site)

RE-ORDER No. 65-323
VOL II

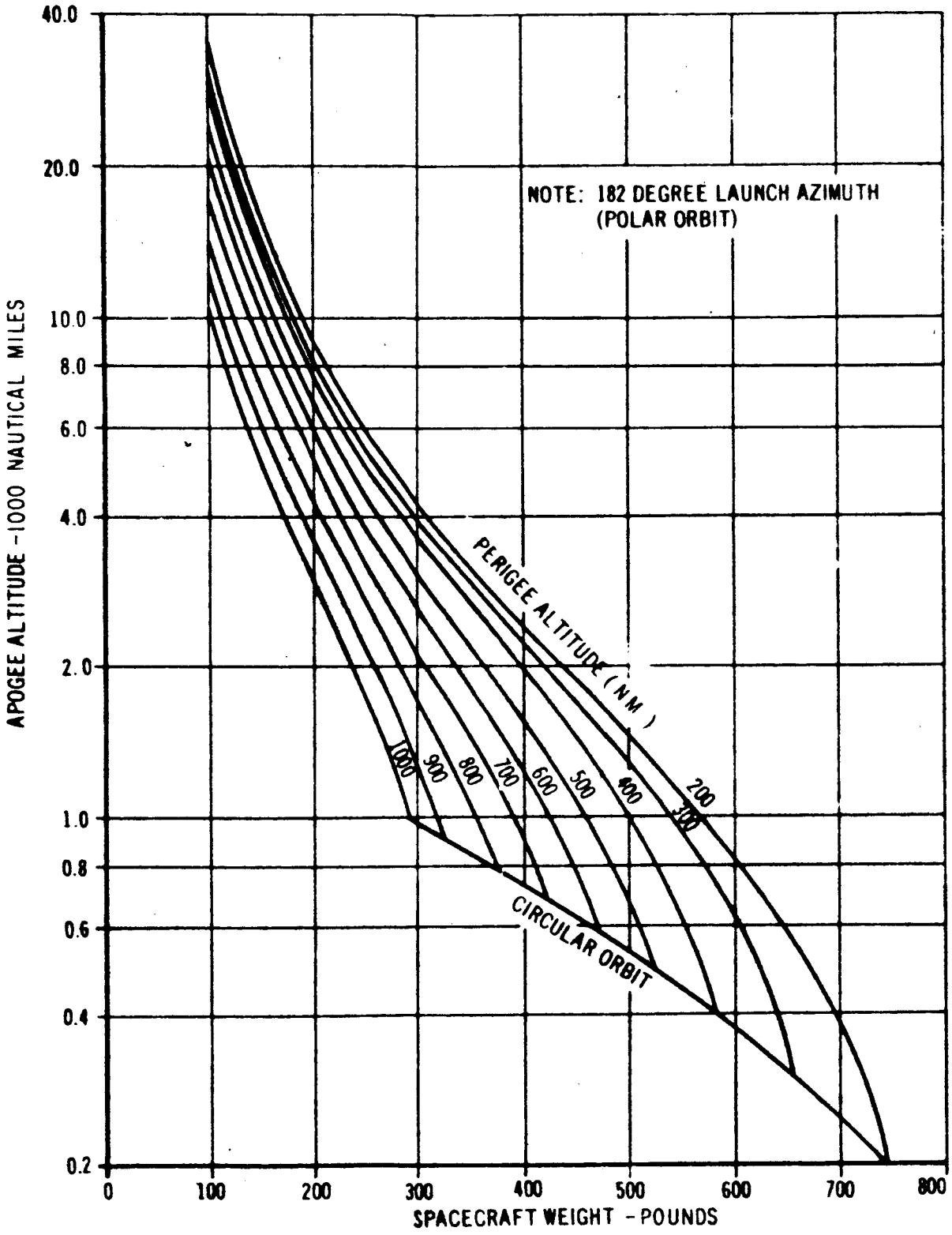


Figure 2-9. DELTA Model DSV-3B Elliptical Orbit Capabilities
(Low Drag Spacecraft Fairing - WTR Launch Site)



44

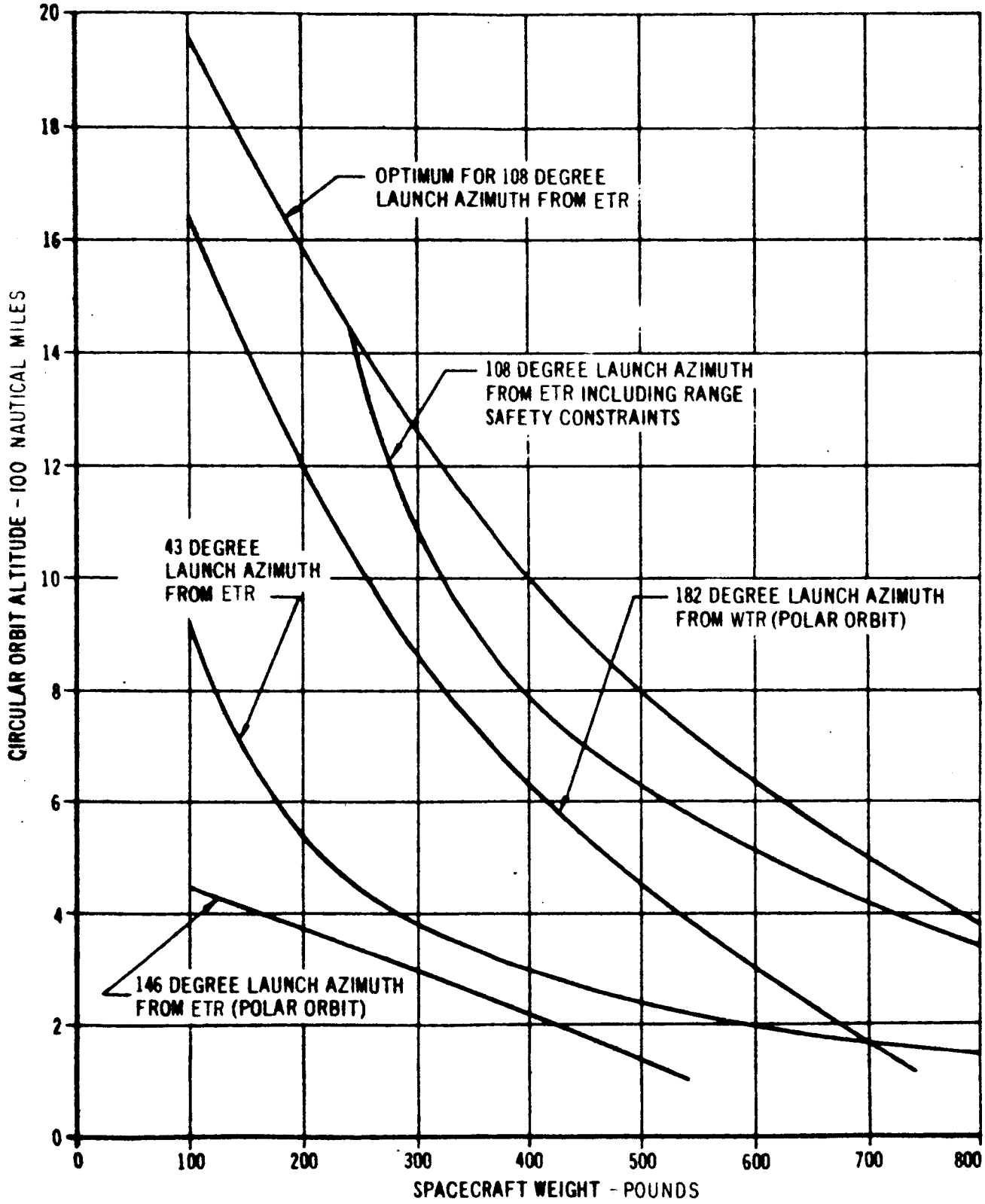


Figure 2-10. DELTA Model DSV-3B Circular Orbit Capabilities (Bulbous Spacecraft Fairing)

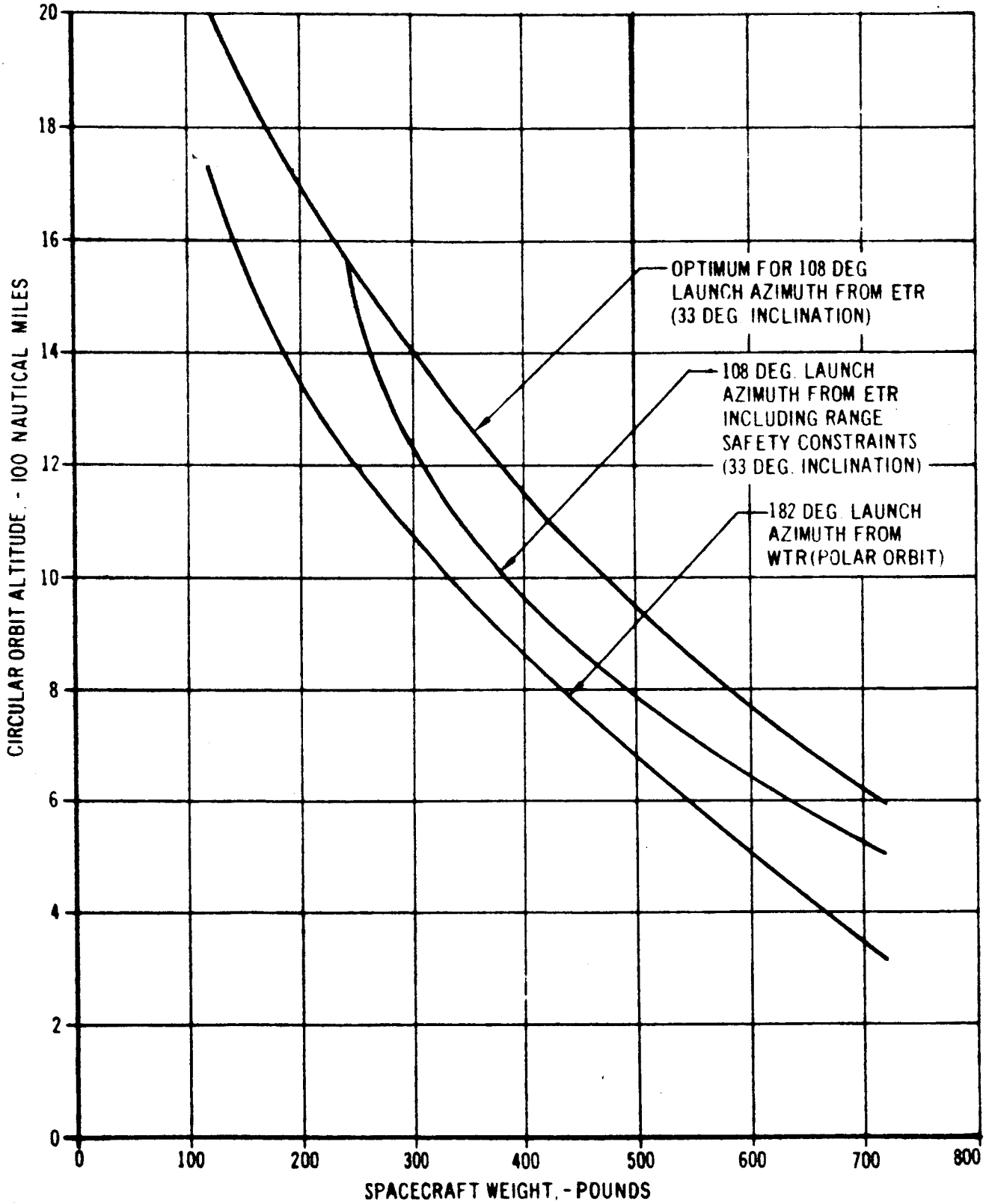


**Figure 2-11. DELTA Model DSV-3C Circular Orbit Capabilities (Low Drag Spacecraft Fairing)**

RE-ORDER No. 65-323
VOL II

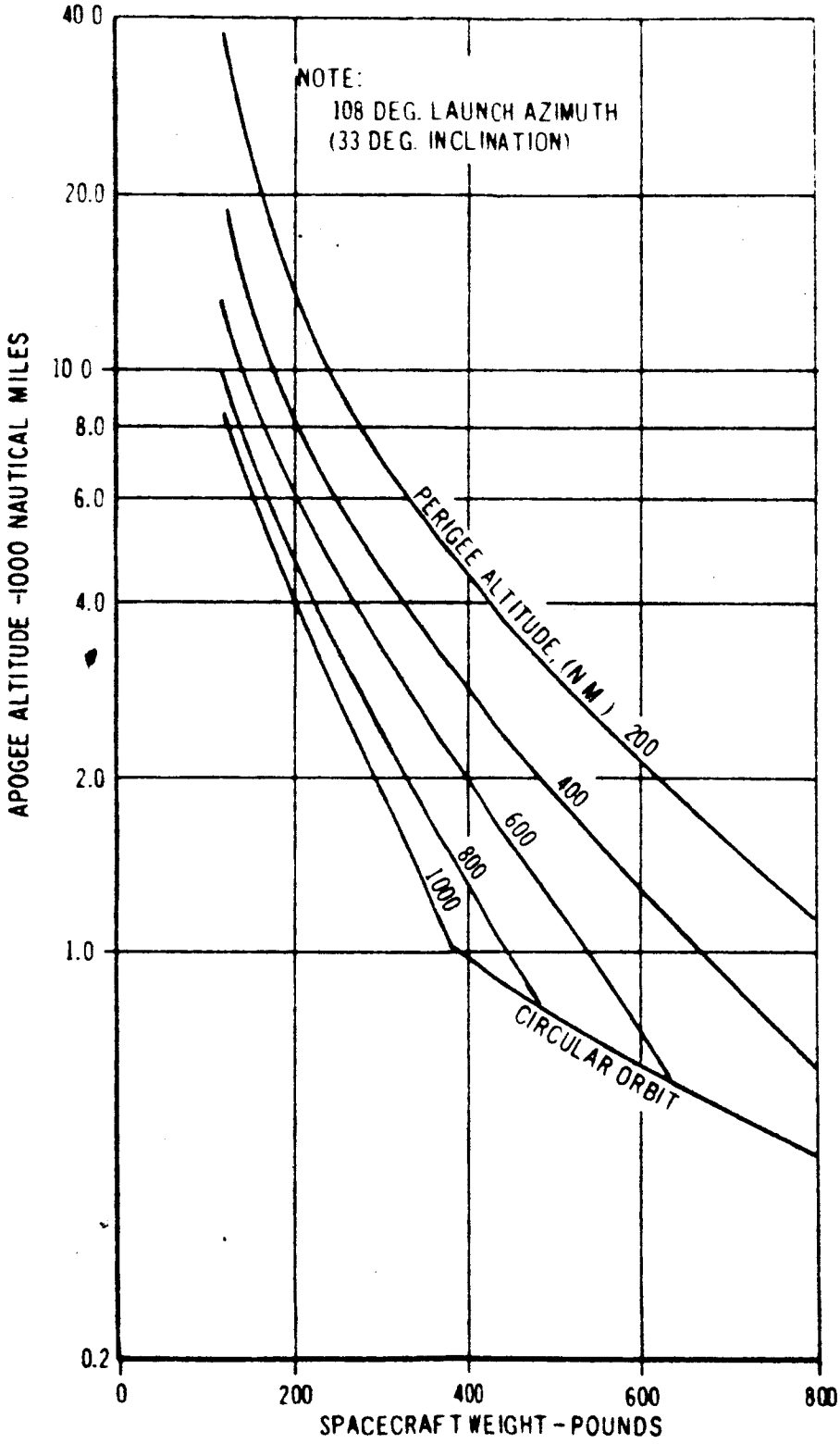


Figure 2-12. DELTA Model DSV-3C Elliptical Orbit Capabilities (Low Drag Spacecraft Fairing - ETR Launch Site)

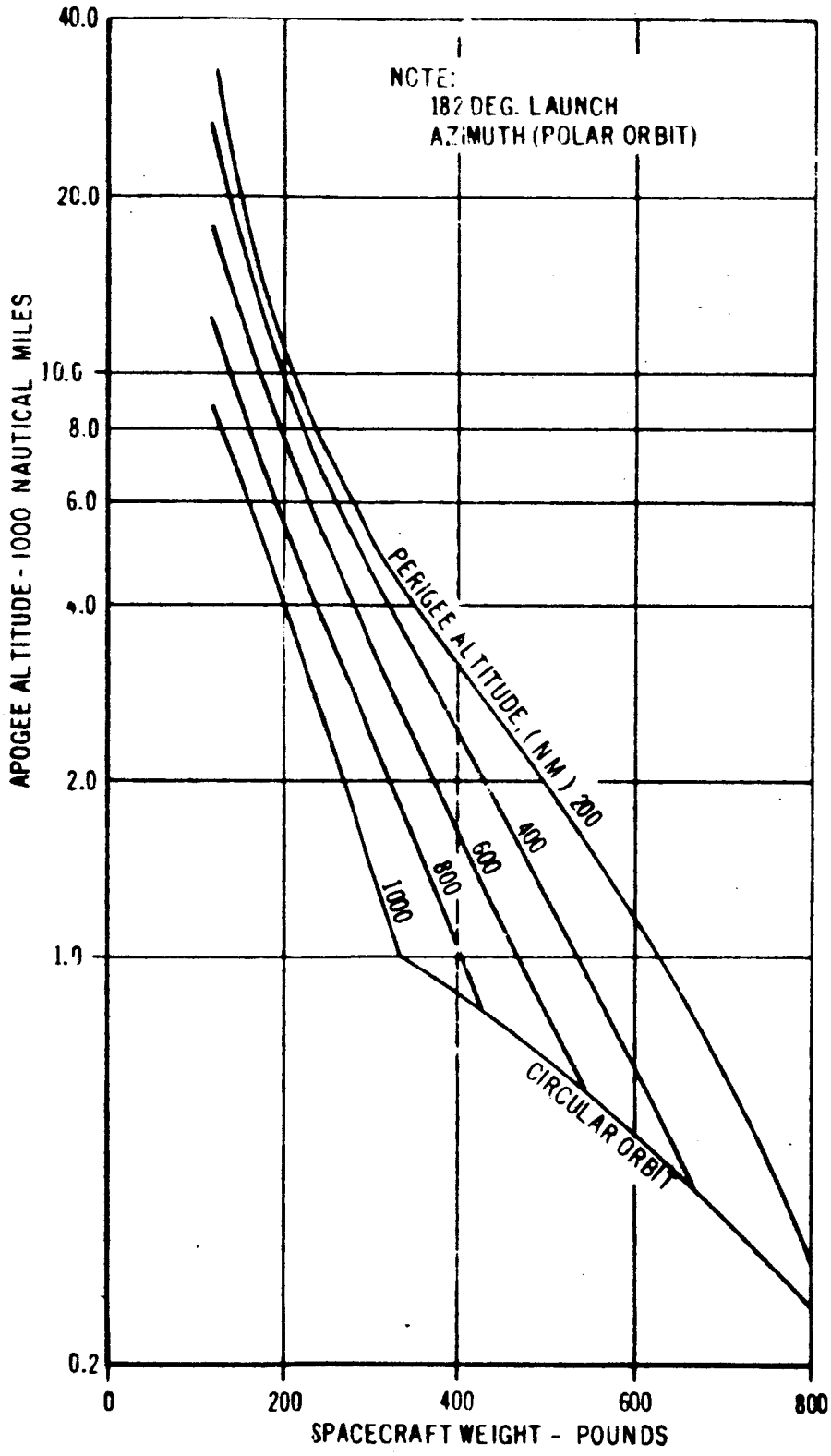


Figure 2-13. DELTA Model DSV-3C Elliptical Orbit Capabilities (Low Drag Spacecraft Fairing - WTR Launch Site)



48

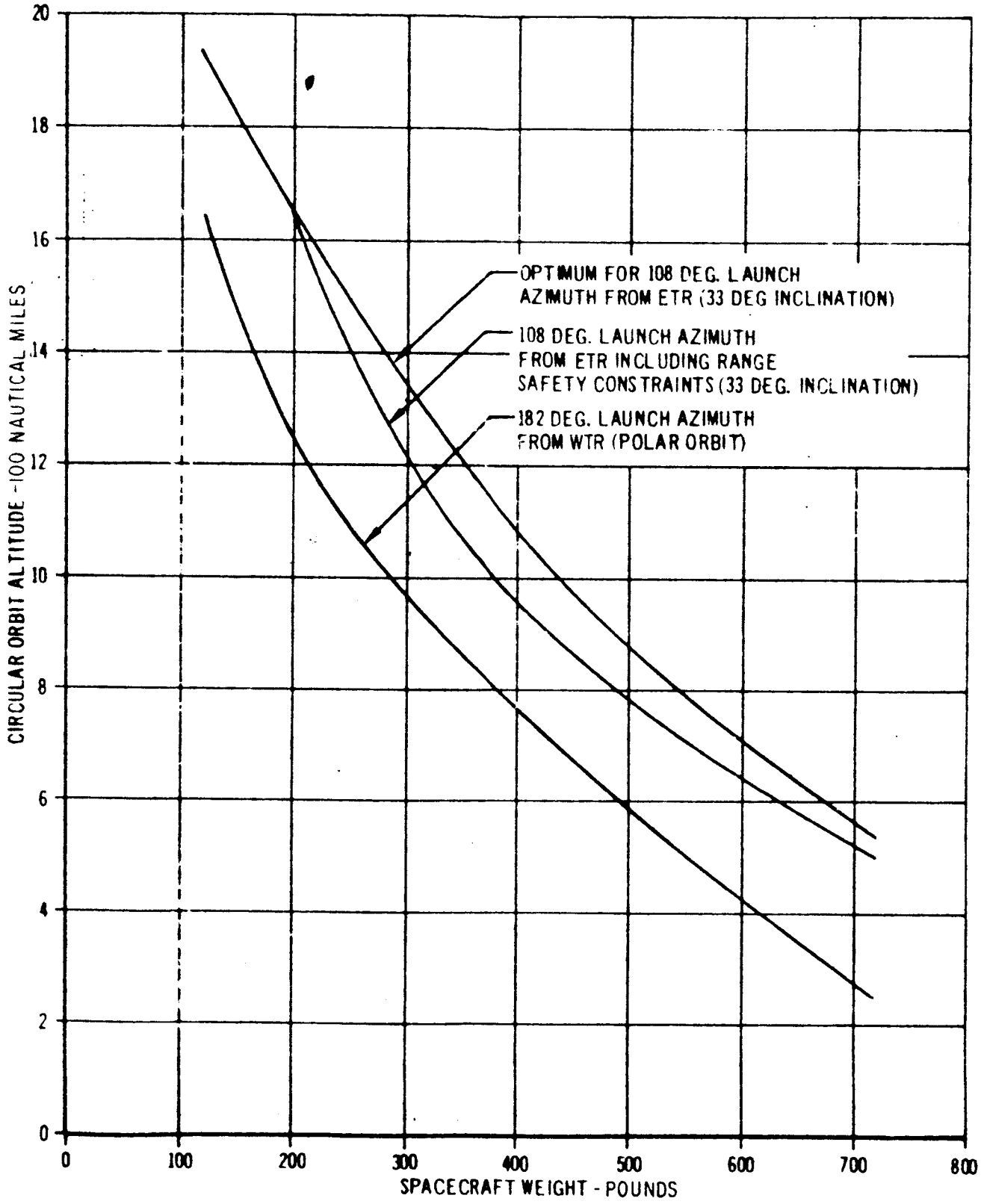


Figure 2-14. DELTA Model DSV-3C Circular Orbit Capabilities (Bulbous Spacecraft Fairing)



49

# TAD PAYLOAD-ORBIT CAPABILITY

## PERFORMANCE SUMMARY

| Figure | Launch Vehicle Configuration | Type of Orbit | Launch Site | Launch Azimuth Degrees | Orbit Inclination Degrees | Altitudes Apogee/Perigee Nautical Miles |
|---|---|---|---|---|---|---|
| 2-15 | DSV-3B<br>DSV-3D | Circular | WTR | 182 | 90 | ≤1400 |
| 2-16 (Range Safety not Considered) | DSV-3D | Elliptical | ETR | 108 | 33 | ≤20,000/200<br>400<br>600<br>800<br>1000 |
| 2-17 (Subranges Africa) | DSV-3D | Elliptical | ETR | 108 | 33 | ≤20,000/400<br>600<br>800<br>1000 |
| 2-18 (Overflys Africa) | DSV-3D | Elliptical | ETR | 108 | 33 | ≤20,000/200<br>400<br>600<br>800<br>1000 |
| 2-19 | DSV-3B<br>DSV-3D | Highly Elliptical | ETR | 108 | 33 | ≥100,000/105<br>110<br>115 |

RE-ORDER No. 65-323
VOL II

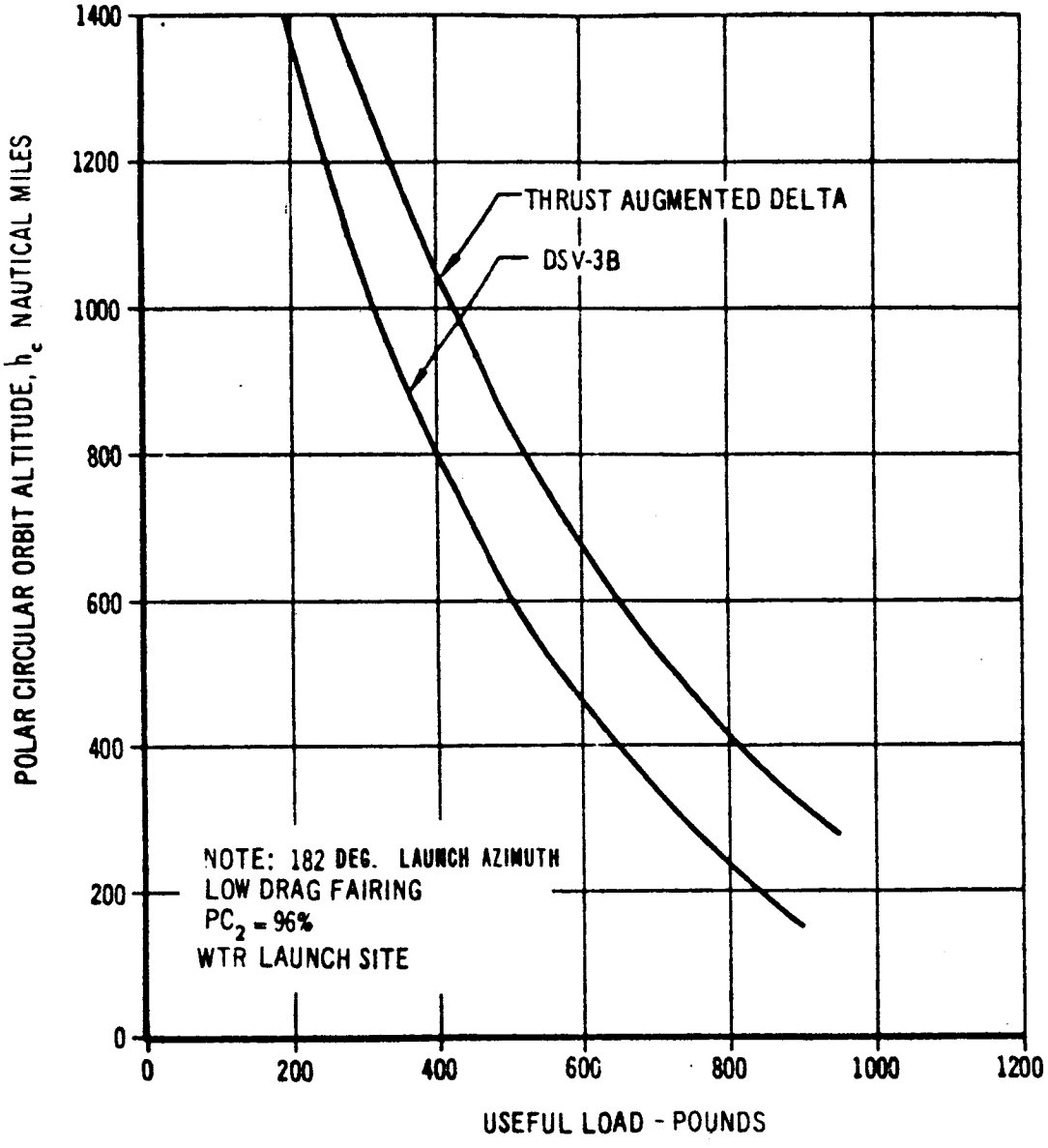


Figure 2-15. Polar Circular Orbit Capability - Trust Augmented DELTA

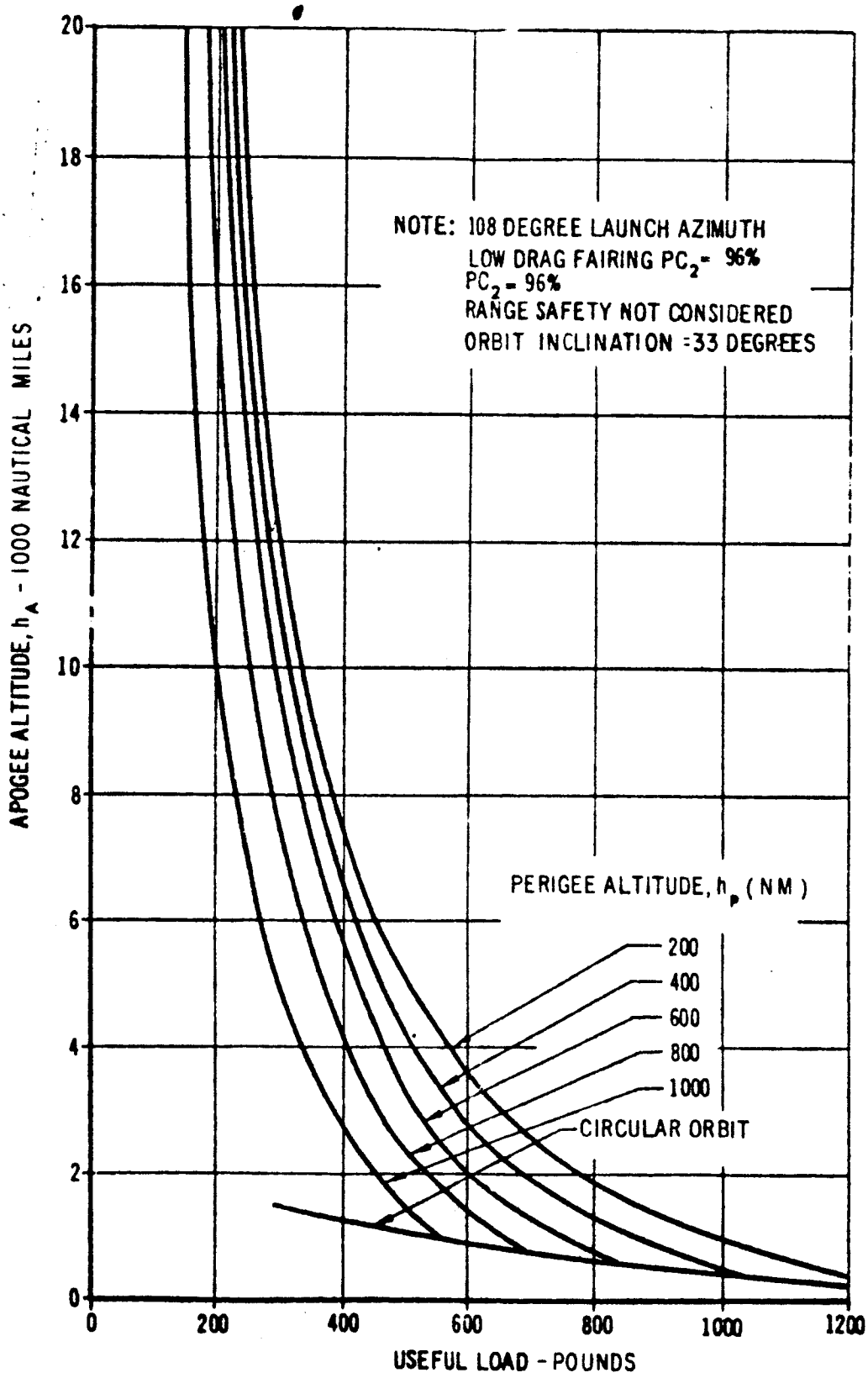


Figure 2-16. Elliptical Orbit Capability - Trust Augmented DELTA (ETR Launch Site)



52

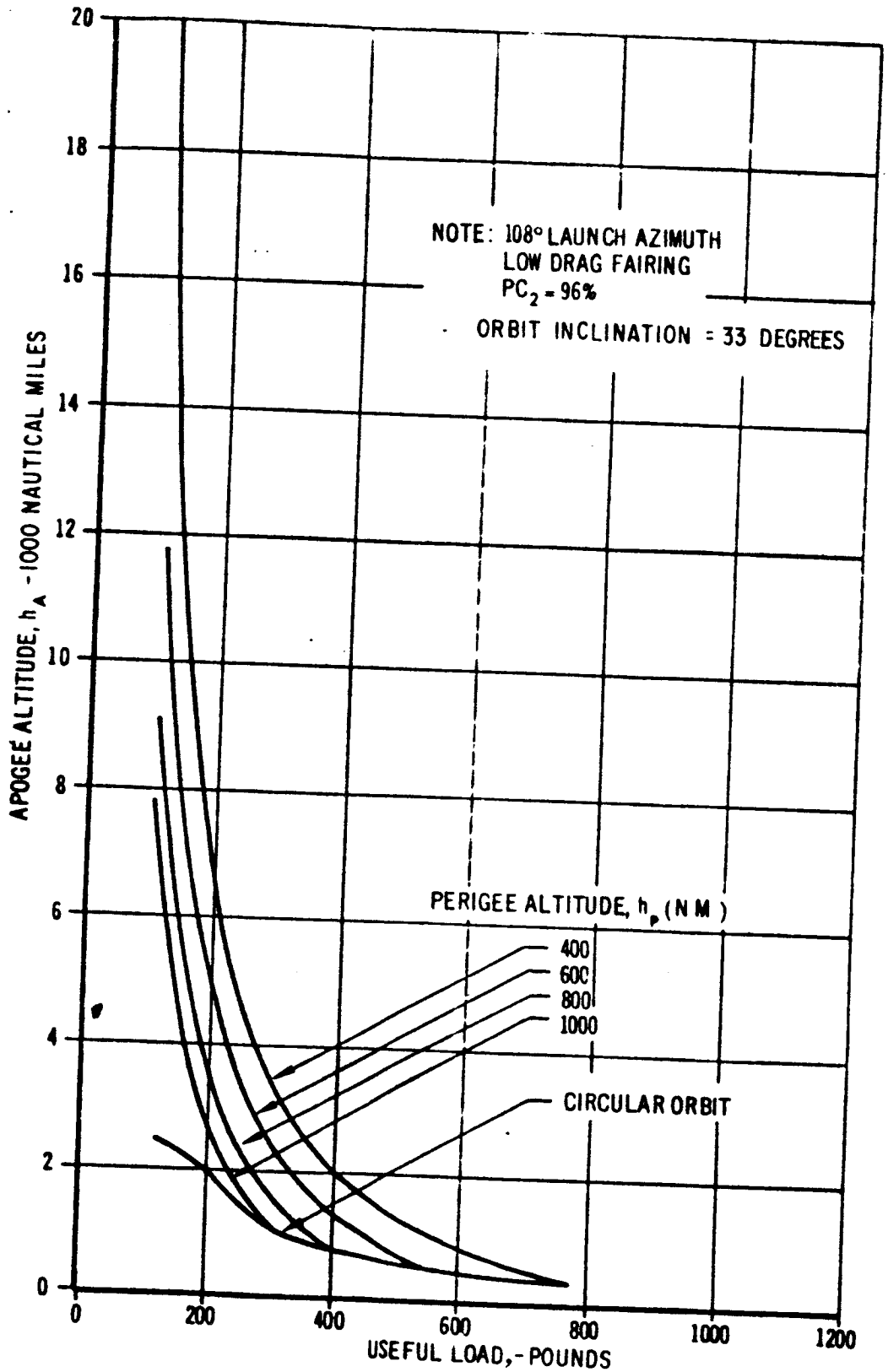


Figure 2-17. Elliptical Orbit Capability-Thrust Augmented DELTA, Subrange Africa (ETR Launch Site)

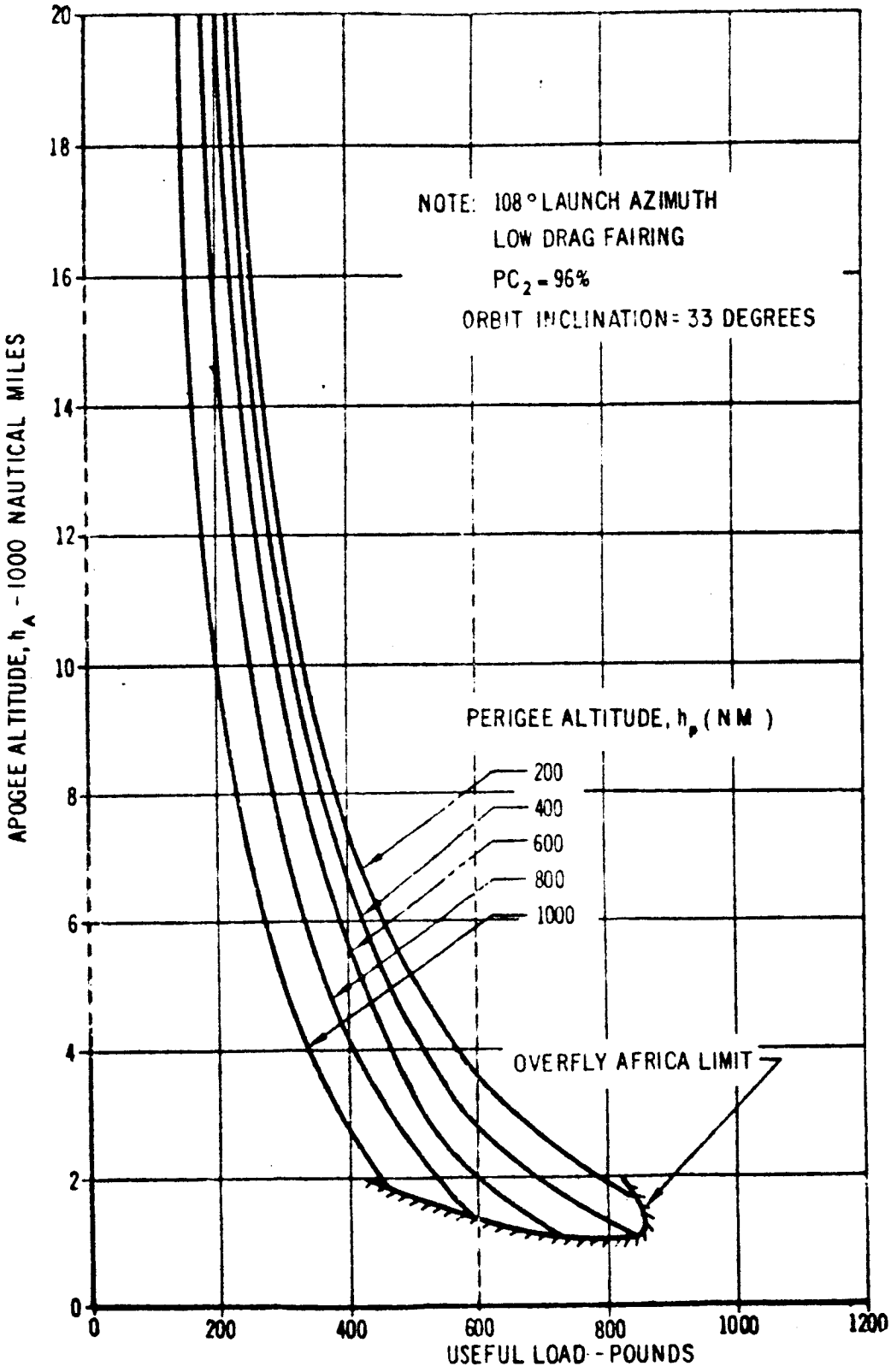


Figure 2-18. Elliptical Orbit Capability-Trust Augmented DELTA, Overflys Africa (ETR Launch Site)

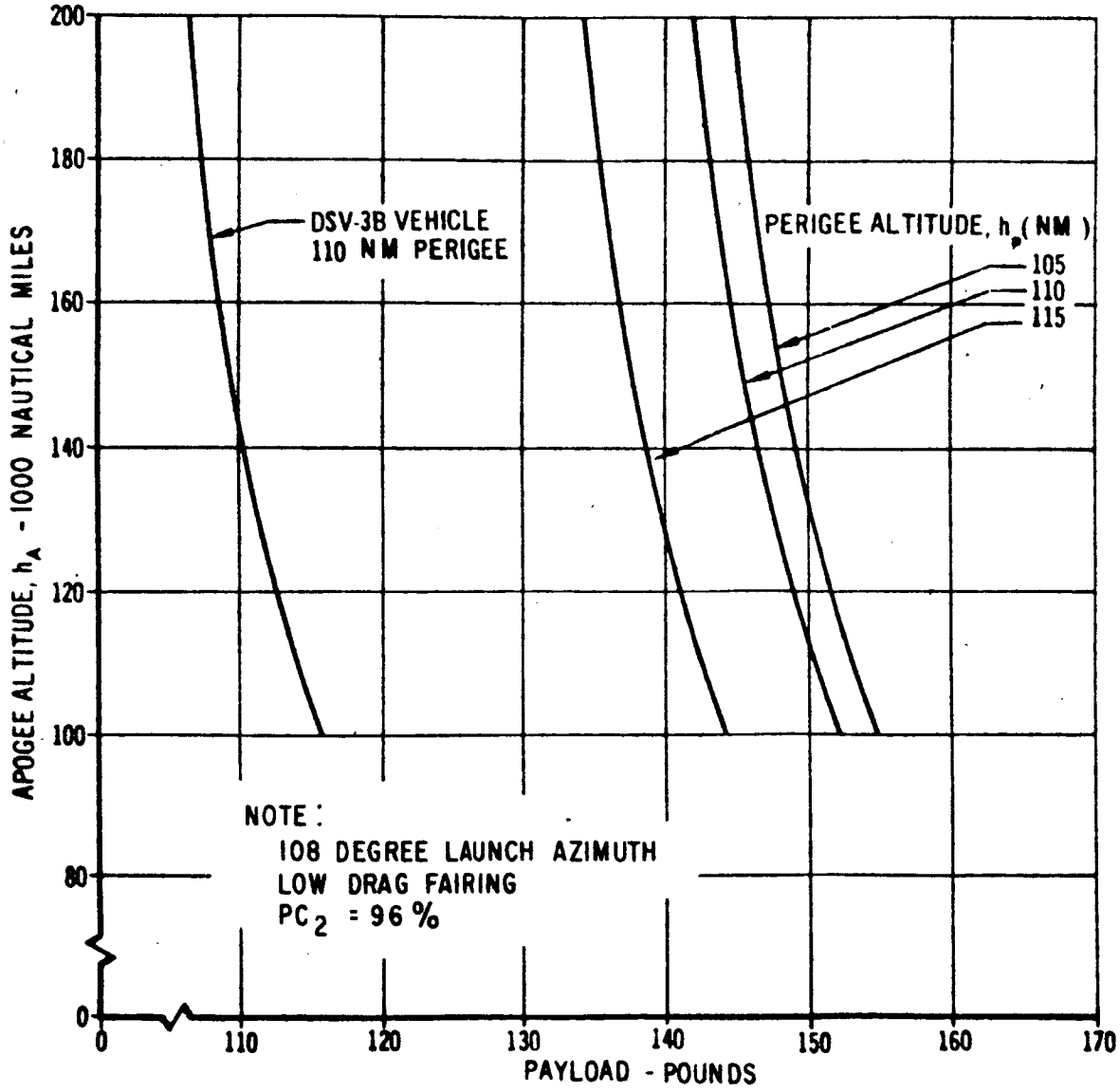


Figure 2-19. Highly Elliptical Orbit Capability-Trust Augmented DELTA (ETR Launch Site)

65-323

# IMPROVED DELTA PAYLOAD-ORBIT CAPABILITY

## PERFORMANCE SUMMARY

| Figure | Launch Vehicle Configuration | Type of Orbit | Launch Site | Launch Azimuth Degrees | Orbit Inclination Degrees | Altitudes Apogee/Perigee Nautical Miles |
|---|---|---|---|---|---|---|
| 2-20 | DSV-3G | Circular | ETR | 108 | 33 | ≤ 600 |
| 2-21 | DSV-3E<br>DSV-3F | Circular | ETR | 108 | 33 | ≤ 2500 |
| 2-22 | DSV-3E | Circular | ETR | 146 | 90 | ≤ 2000 |
| 2-23 | DSV-3E | Elliptical | ETR | 108 | 33 | ≥ 4000/100 |
| 2-24 | DSV-3E | Elliptical | ETR | 146 | 80<br>Prograde | ≥ 2000/400<br>600<br>800 |
| 2-25 | DSV-3E | Elliptical | ETR | 146 | 80<br>Retrograde | ≥ 400/400<br>600<br>800 |
| 2-26 | DSV-3E | Elliptical | ETR | 108 | 59 | ≥ 400/400<br>600<br>800 |
| 2-27 | DSV-3E | Elliptical | ETR | 146 | 59 | ≥ 400/400<br>600<br>800 |
| 2-28 | DSV-3E<br>DSV-3E<br>with 2L 1st. Stage | Elliptical | ETR | 108 | 33 | ≥ 10,000/100 |
| 2-29 | DSV-3E with 2L 1st Stage. Same as above with 30% Flox 1st Stage | Elliptical | ETR | 108 | 33 | ≥ 4000/100 |
| 2-30 | DSV-3E<br>DSV-3E<br>30% Flox<br>DSV-3E<br>$N_2O_4$/A-50<br>2nd. Stage<br>Fuel | Elliptical | ETR | 108 | 33 | ≥ 4000/100 |
| 2-31 | Escape Capability Chart for Various Configurations | | | | | |
| 2-32 | DSV-3G | Circular | WTR | 182 | 90 | ≤ 800 |
| 2-33 | DSV-3E | Elliptical | WTR | 182 | 90 | ≥ 4000/100 |
| 2-34 | DSV-3E<br>with Surveyor 3rd. Stage | Elliptical | WTR | 182 | 90 | ≥ 4000/100 |
| 2-35 | DSV-3E<br>DSV-3E<br>with 2L<br>1st. Stage | Elliptical | WTR | 182 | 90 | ≥ 4000/100 |
| 2-36 | DSV-3E<br>with 2L<br>1st. Stage | Elliptical | WTR | 182 | 90 | ≥ 4000/100 |
| 2-37 | DSV-3E<br>$N_2O_4$/A-50<br>2nd. Stage<br>Fuel | Elliptical | WTR | 182 | 90 | ≥ 4000/100 |
| 2-38 | DSV-3E<br>with 2L<br>1st. Stage<br>and Surveyor 3rd. Stage | Elliptical | WTR | 182 | 90 | ≥ 4000/100 |

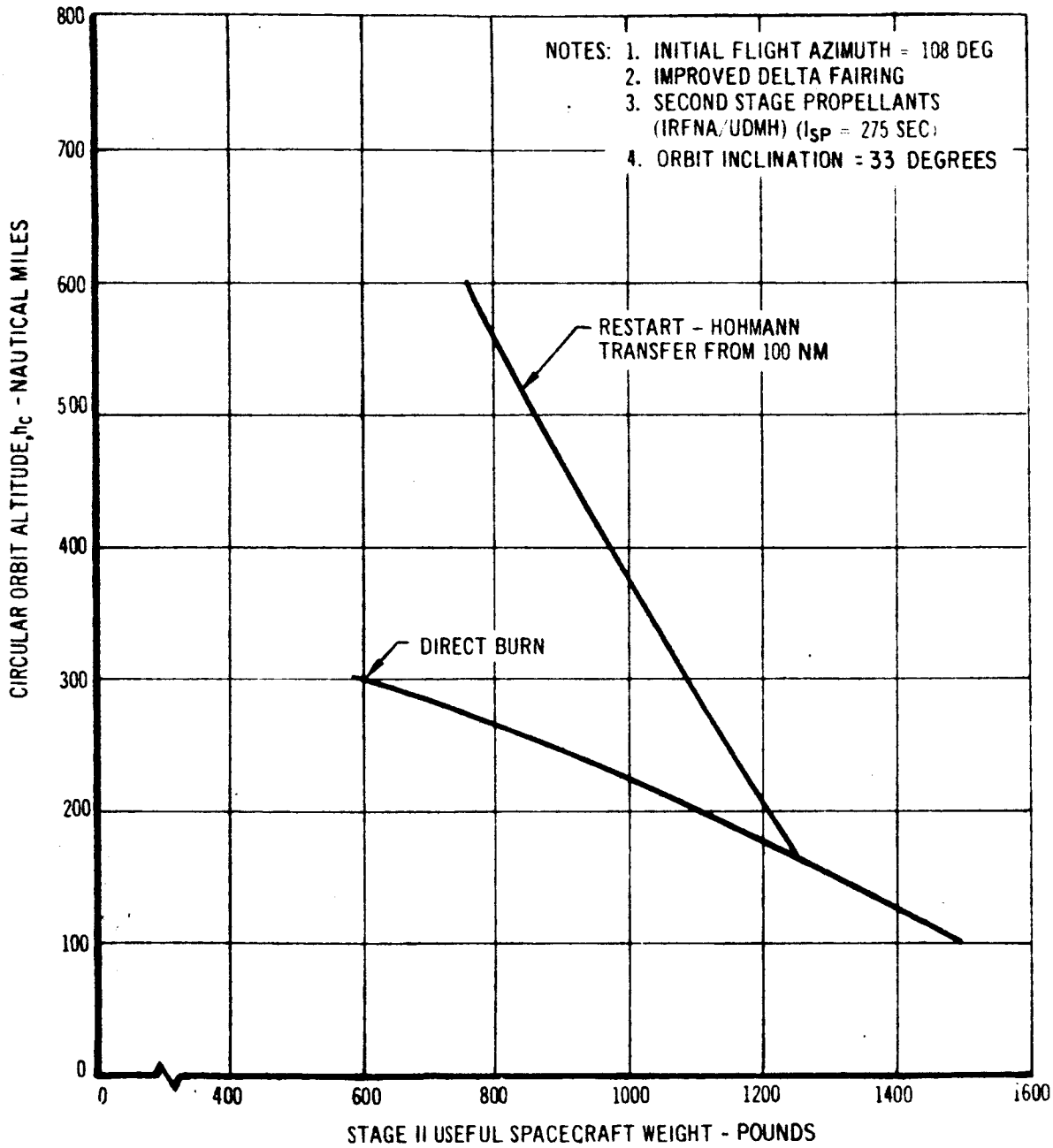


**Figure 2-20. IMPROVED DELTA (DSV-3G) Two Stage Circular Orbit Capability (ETR Launch Site)**

Vol II 65-323

NOTES

1. SECOND STAGE PROPELLANTS (IRFNA/UDMH) $I_{SP}$ 275 SECONDS
2. FIRST STAGE YAW MANEUVER FROM 90 TO 110 SEC
3. EXPENDED BOOSTER AND FAIRNG IMPACTS IN CARIBBEAN SEA
4. SECOND STAGE IMPACTS IN SOUTH PACIFIC
5. ORBIT INCLINATION 90 DEGREES
6. INITIAL FLIGHT AZIMUTH 146 DEGREES
7. THIRD STAGE X258 SOLID MOTOR

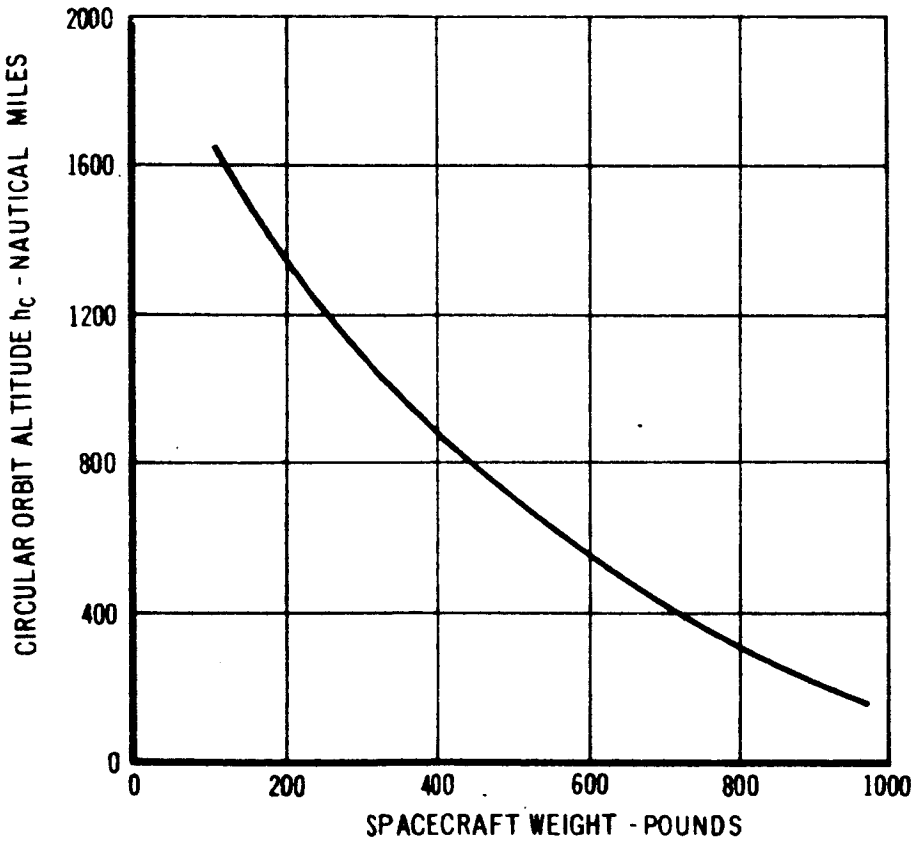


**Figure 2-22. IMPROVED DELTA (DSV-3E) Polar Circular Orbit Capability (ETR Launch Site)**

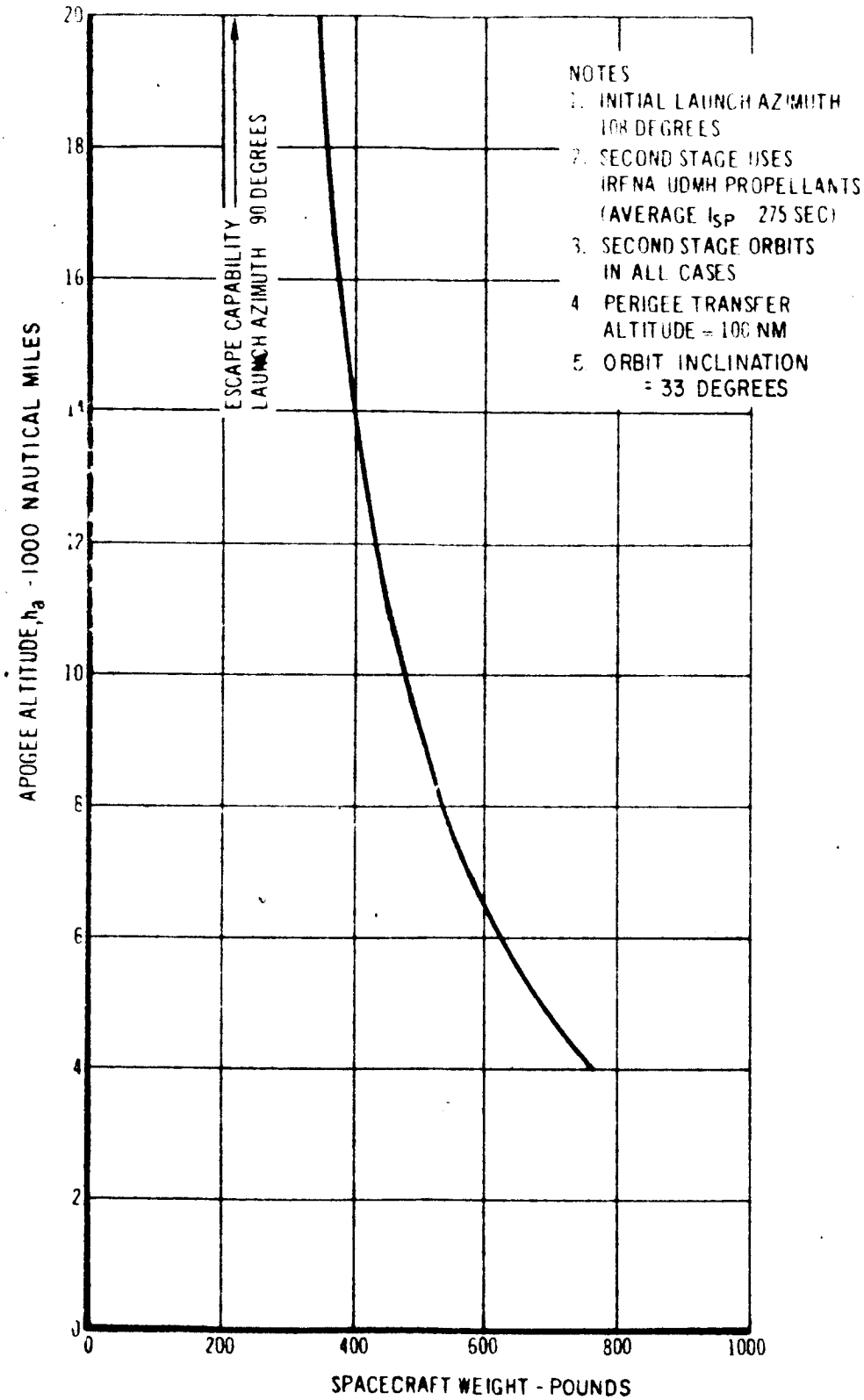


Figure 2-23. IMPROVED DELTA (DSV-3E) Elliptical Orbit Capability (ETR Launch Site)

65-323
Vol II

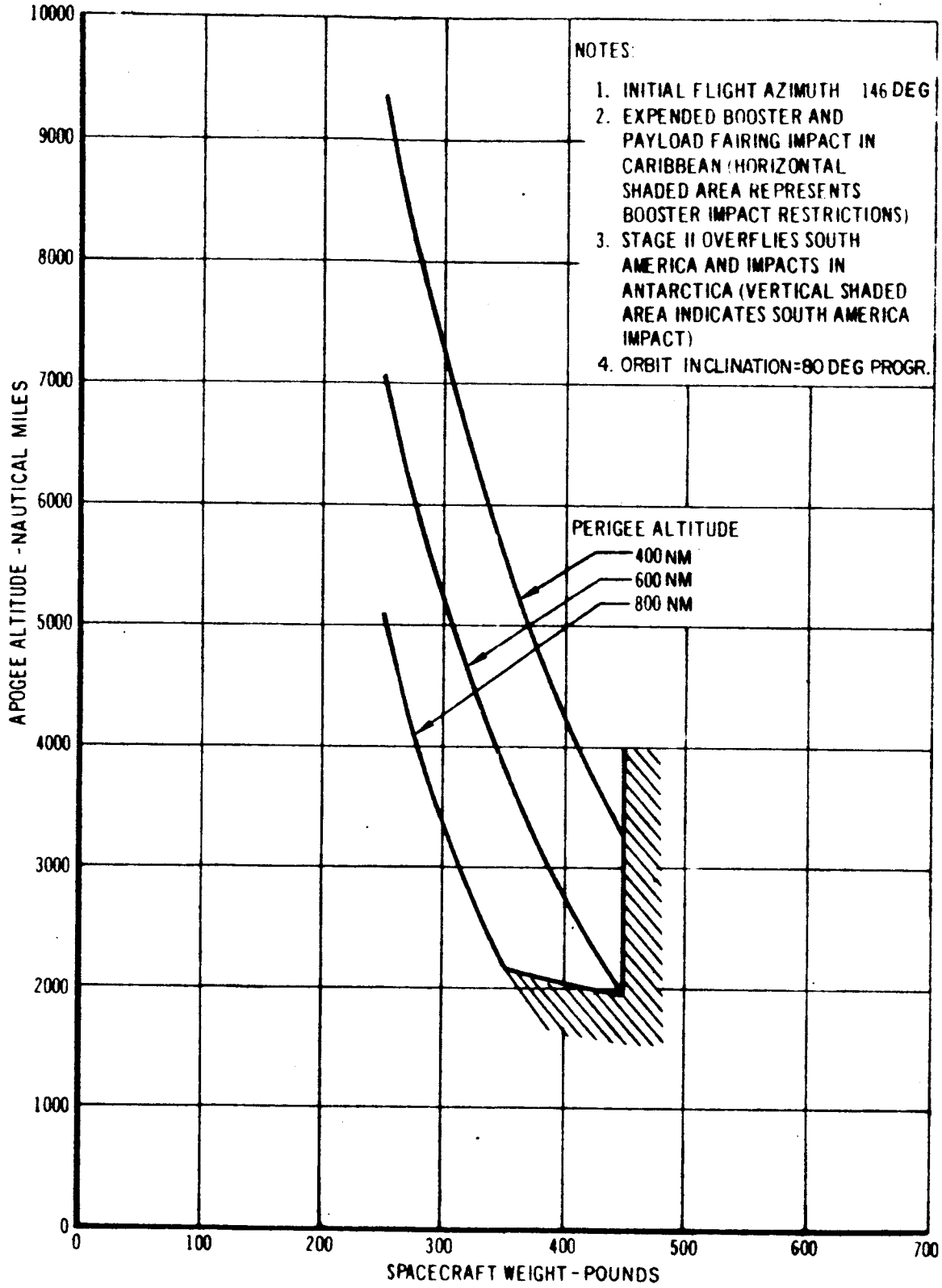


Figure 2-24. IMPROVED DELTA (DSV-3E) Elliptical Orbit Capability (ETR Launch Site)

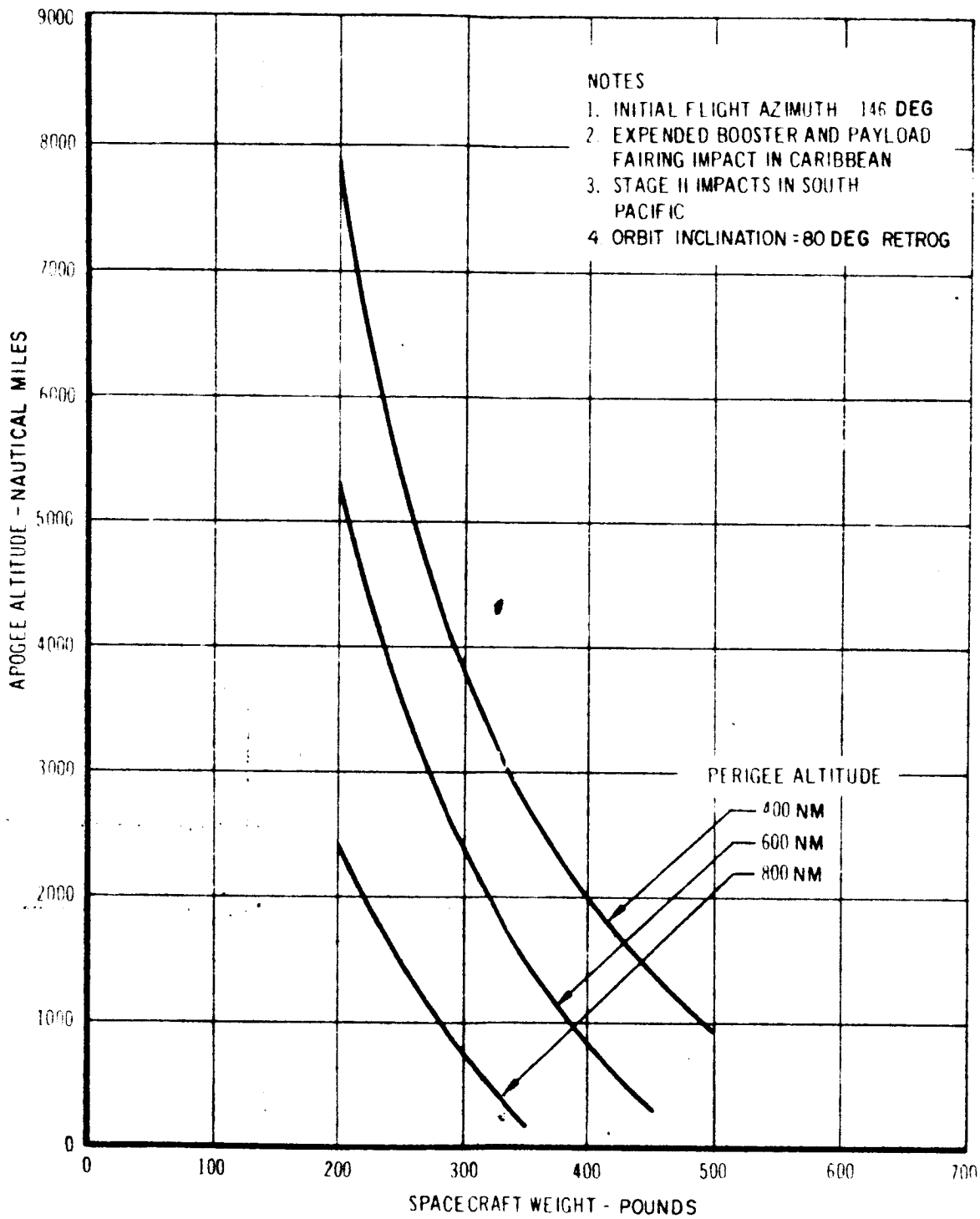


Figure 2-25. IMPROVED DELTA (DSV-3E) Elliptical Orbit Capability (ETR Launch Site)

RE-ORDER No. 65-323
VOL II

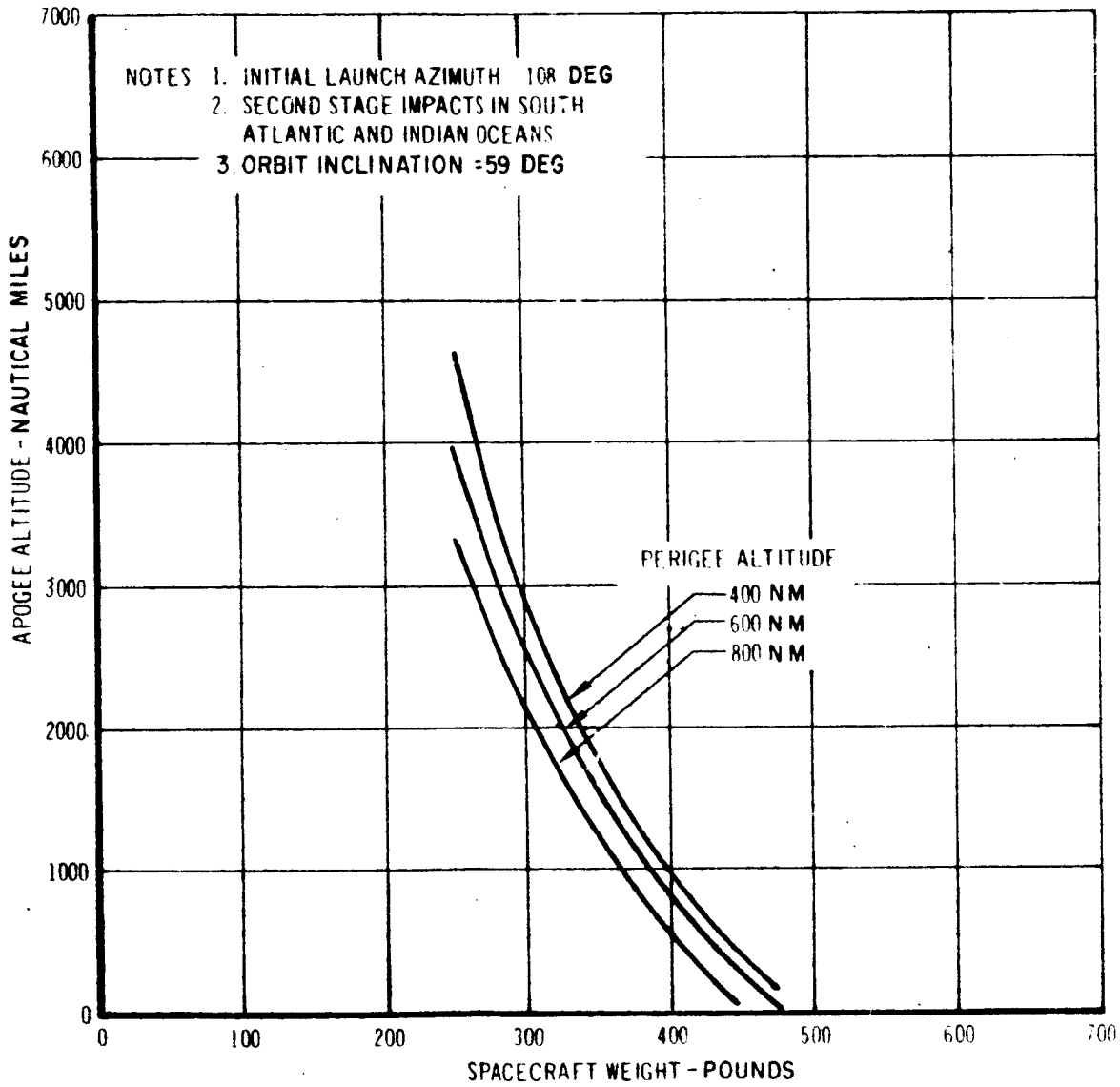


**Figure 2-26. IMPROVED DELTA (DSV-3E) Elliptical Orbit Capability (ETR Launch Site)**



63

RE-ORDER No. 65-323
Vol. II

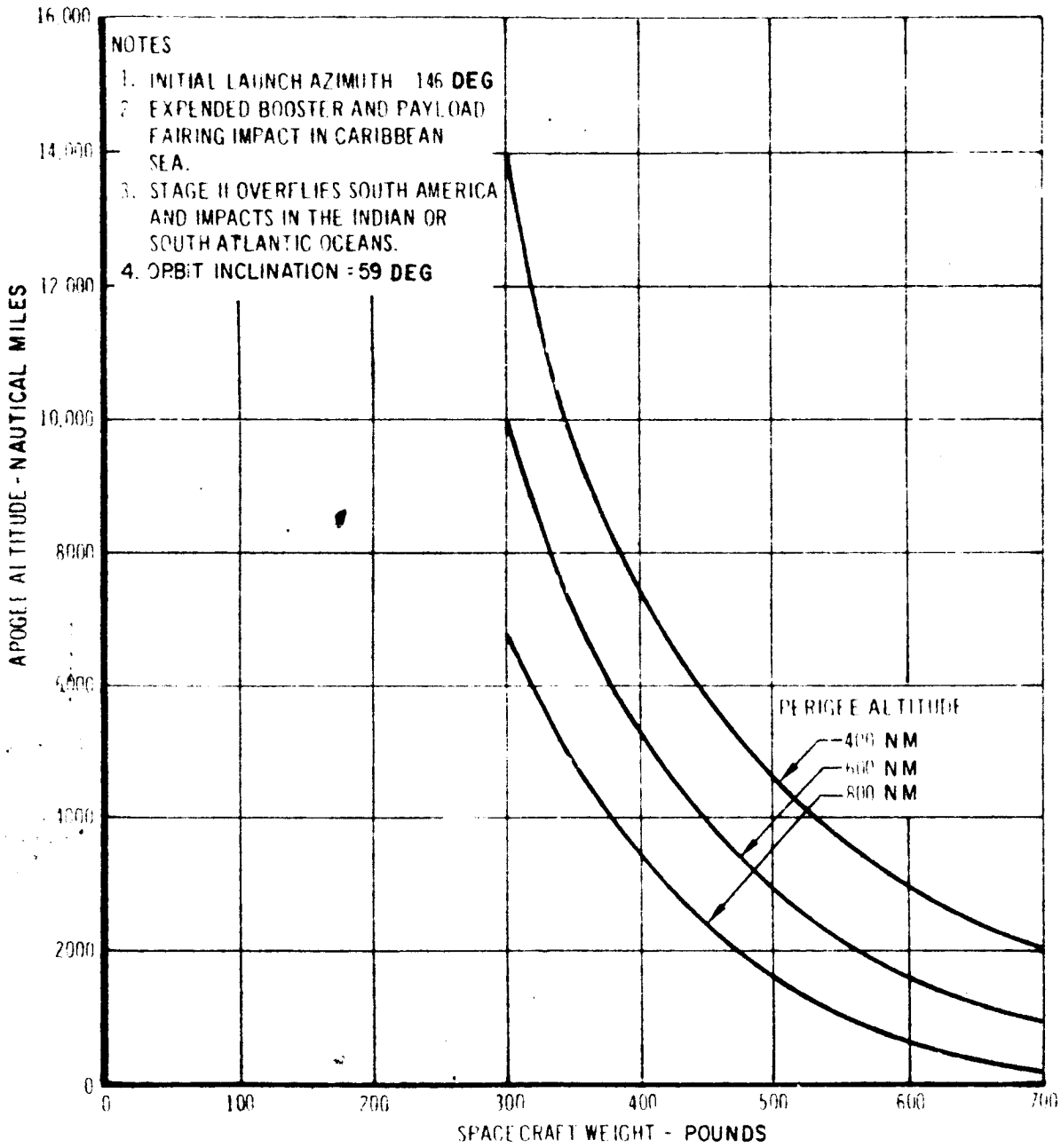


**Figure 2-27. IMPROVED DELTA (DSV-3E) Elliptical Orbit Capability (ETR Launch Site)**



64

RE-ORDER No. 65-323
Vol II

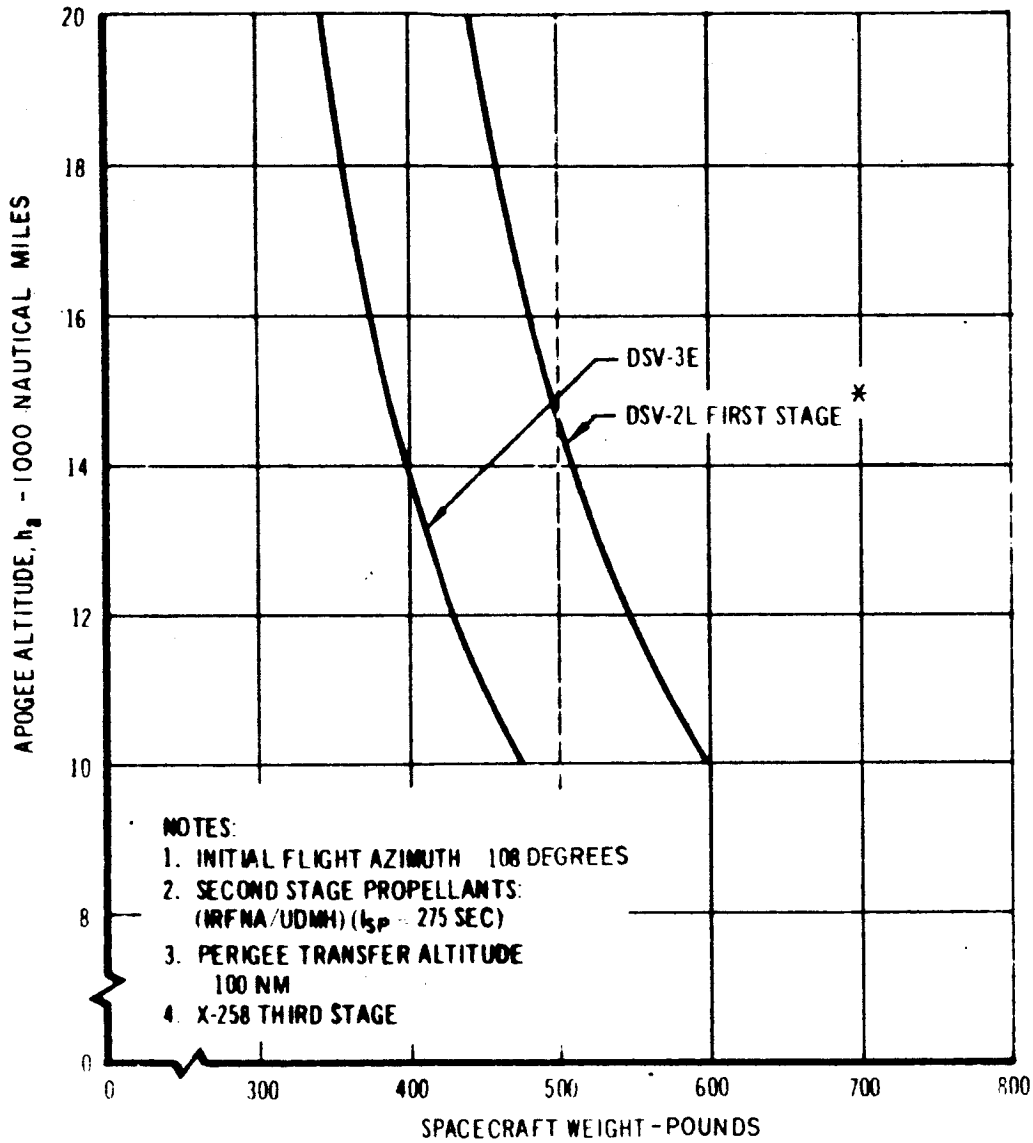


* THE DSV-2L IS A MODIFICATION OF THE BASIC THOR BOOSTER DESCRIBED IN SECTION 2.4.1.2. THE PRIMARY DIFFERENCE IS THAT THE DSV-2L HAS A GREATER PROPELLANT CAPABILITY.

Figure 2-28. IMPROVED DELTA Three Stage Elliptical Orbit Capability (ETR Launch Site)



65

RE-ORDER No. 65-323
VOL II

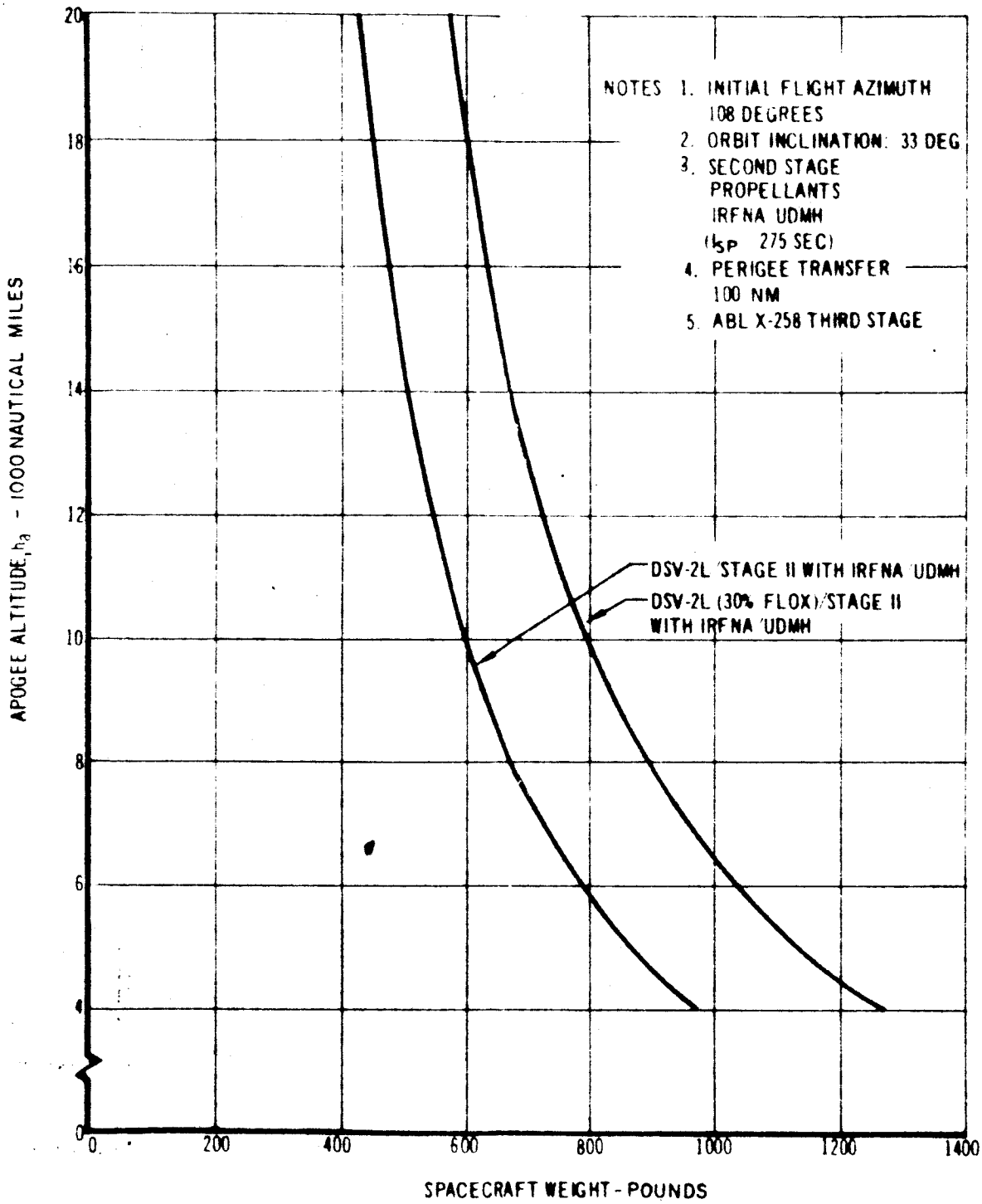


Figure 2-29. IMPROVED DELTA, Three Stage Elliptical Orbit Capability for Various Configurations (ETR Launch Site)

RE-ORDER No. 65-323
Vol II

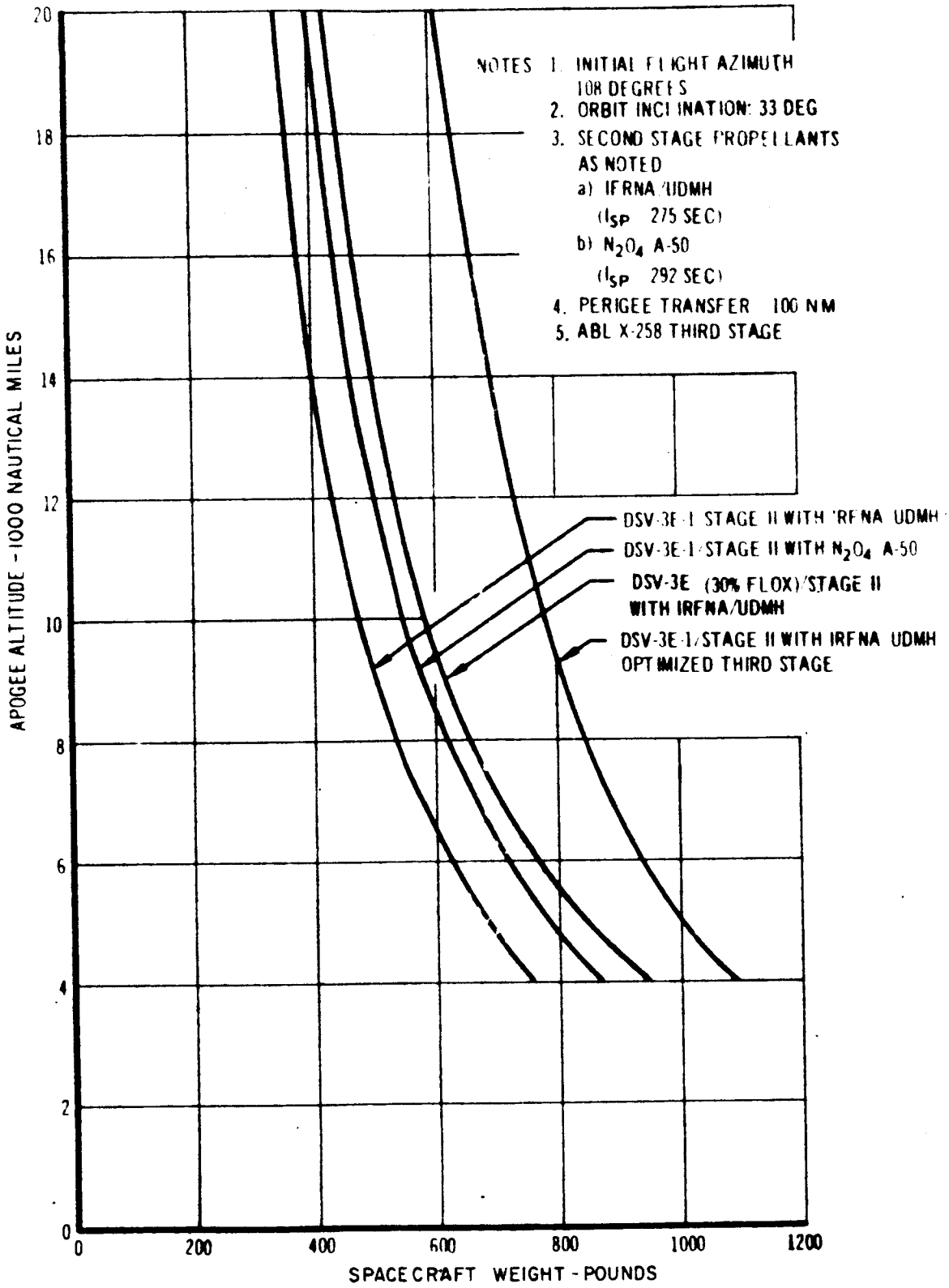


Figure 2-30. IMPROVED DELTA, Three Stage Elliptical Orbit Capability for Various Configurations (ETR Launch Site)

RE-ORDER No. 65-
VOL II

| NO. VEHICLE CONFIGURATION | ESCAPE PAYLOAD WEIGHT (POUNDS) |
|---|---|
| 1. IMPROVED DELTA (DSV-3E) | 220 |
| 2. DSV-3E WITH $N_2O_4$/A-50 AS SECOND STAGE PROPELLANTS | 255 |
| 3. DSV 3E WITH 30% FLOX IN FIRST STAGE | 260 |
| 4. STRAIGHT TANK THOR (DSV 2L) WITH DSV-3E SECOND & THIRD STAGES | 265 |
| 5. FLOXED DSV-2L WITH DSV-3E SECOND AND THIRD STAGES | 350 |
| 6. DSV-3E WITH OPTIMUM THIRD STAGE | 380 |
| 7. FLOXED DSV-2L WITH DSV-3E SECOND AND THIRD STAGES AND $N_2O_4$ A-50 SECOND STAGE PROPELLANTS | 390 |
| 8. SAME AS NO 7 EXCEPT FOR OPTIMUM THIRD STAGE | 630 |

NOTES:
1. ETR LAUNCH
2. 90 DEG LAUNCH AZIMUTH

Figure 2-31. IMPROVED DELTA Escape Capability

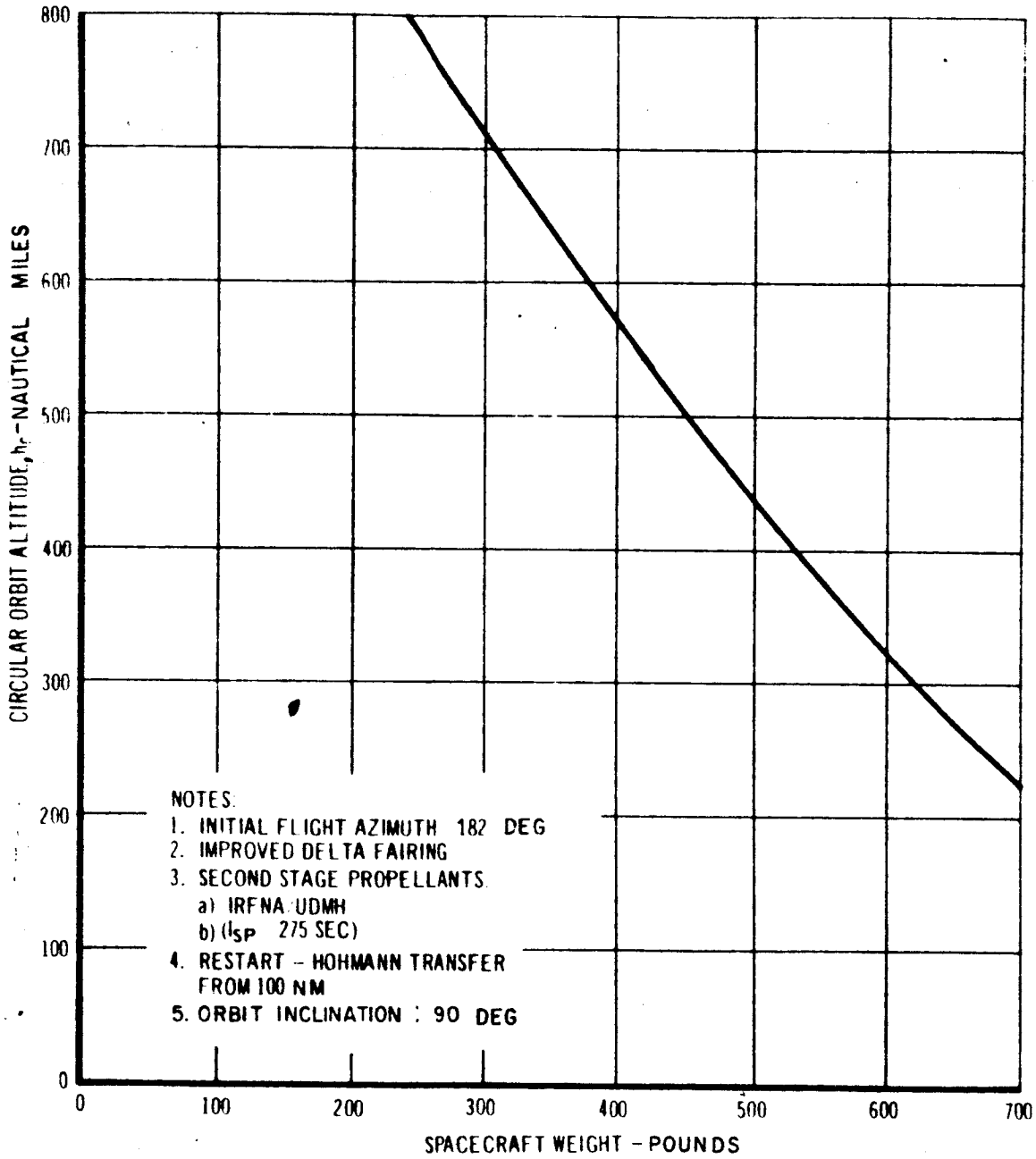


Figure 2-32. IMPROVED DELTA (DSV-3G), Circular Orbit Capability (WTR Launch Site)

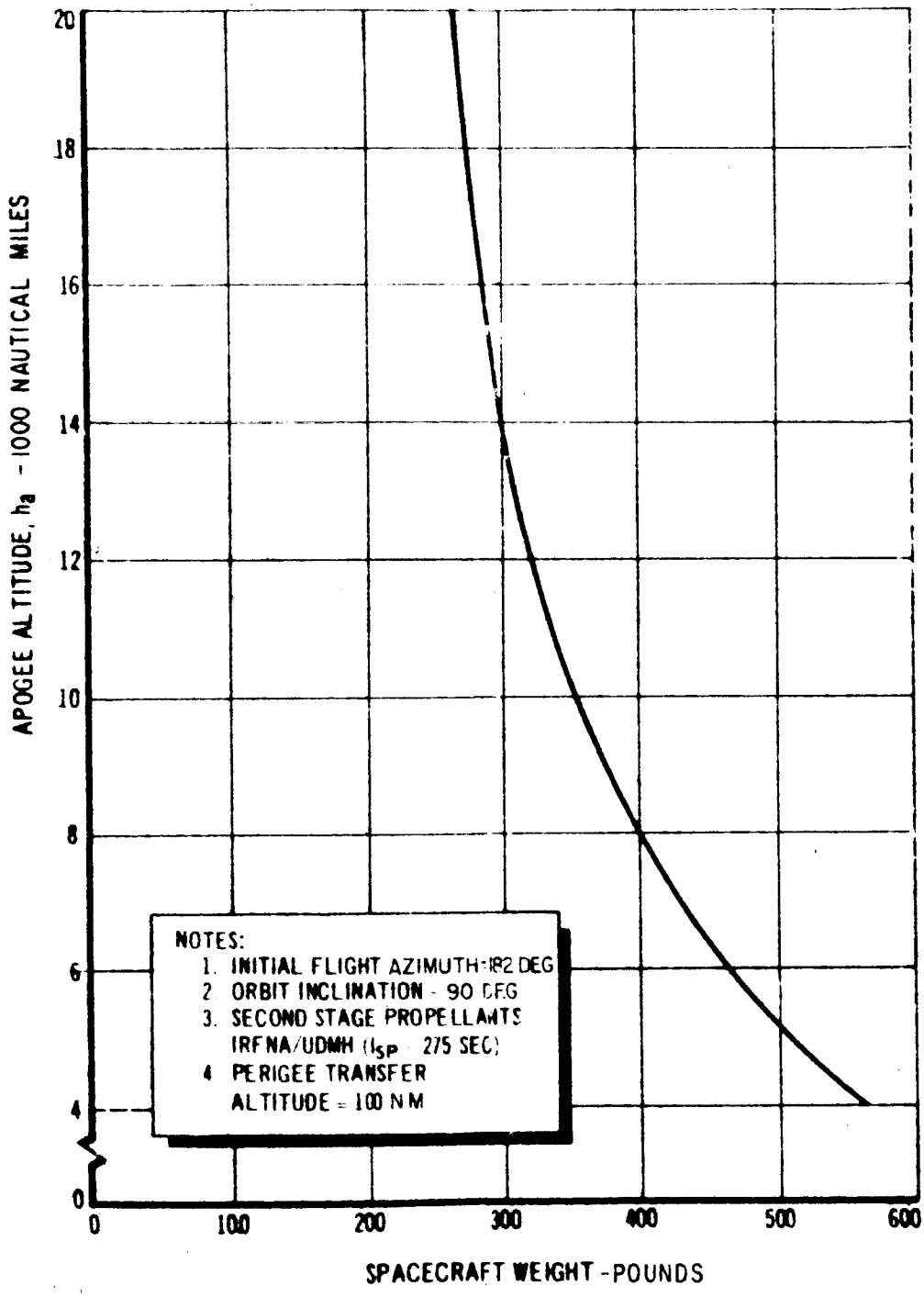


Figure 2-33. IMPROVED DELTA (DSV-3E) Polar Elliptical Orbit Capability (WTR Launch Site)

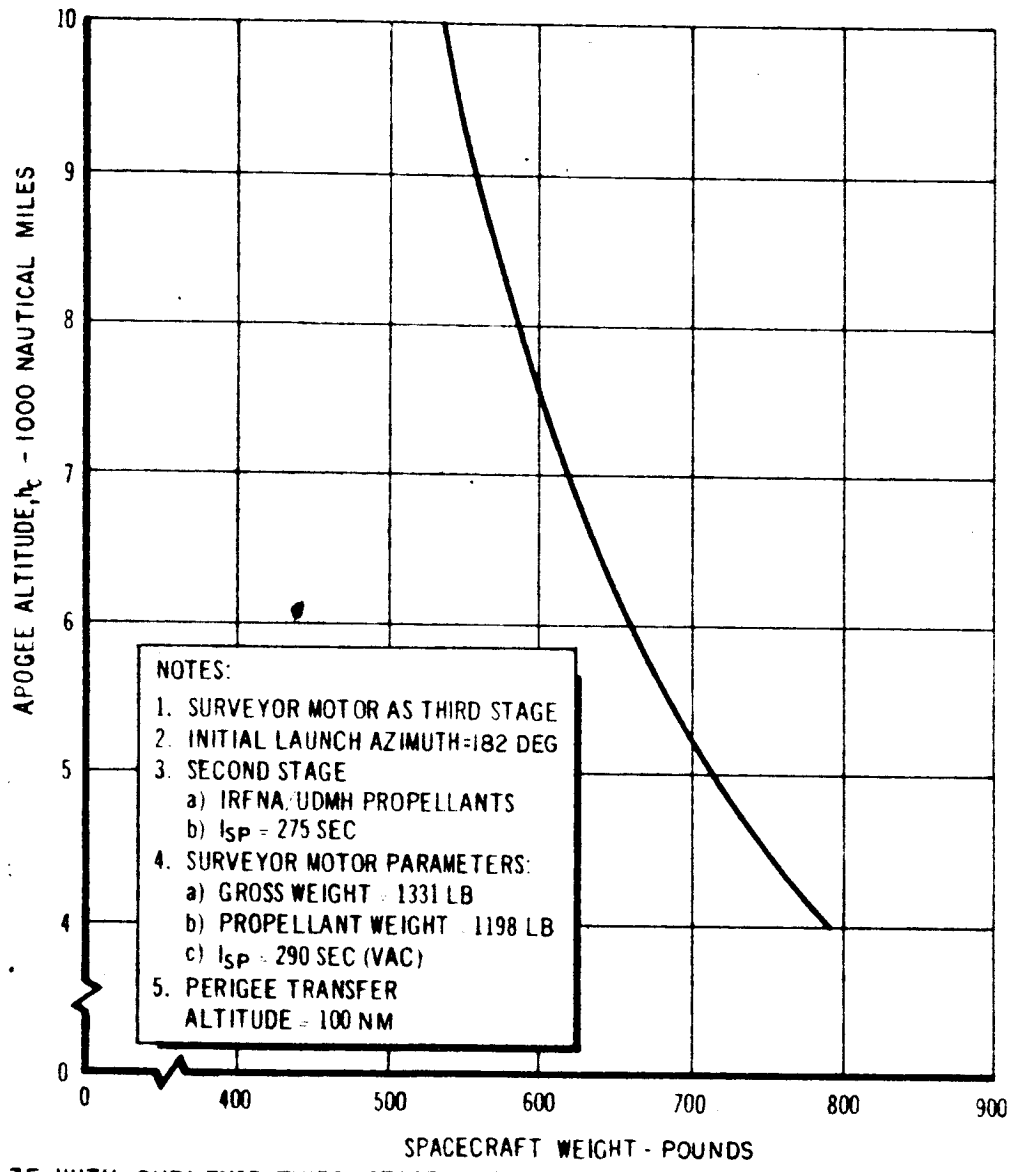


*DSV-3E WITH SURVEYOR THIRD STAGE MOTOR

Figure 3-34. IMPROVED DELTA*, Three Stage Elliptical Polar Orbit Capability (WTR Launch Site)

RE-ORDER No 65-323
VOL II

NOTES: 1. INITIAL FLIGHT AZIMUTH = 182 DEG
2. SECOND STAGE PROPELLANTS: (IRFNA/UDMH) ($I_{SP}$ = 275 SEC)
3. PERIGEE TRANSFER ALTITUDE = 100 NM
4. X-258 THIRD STAGE

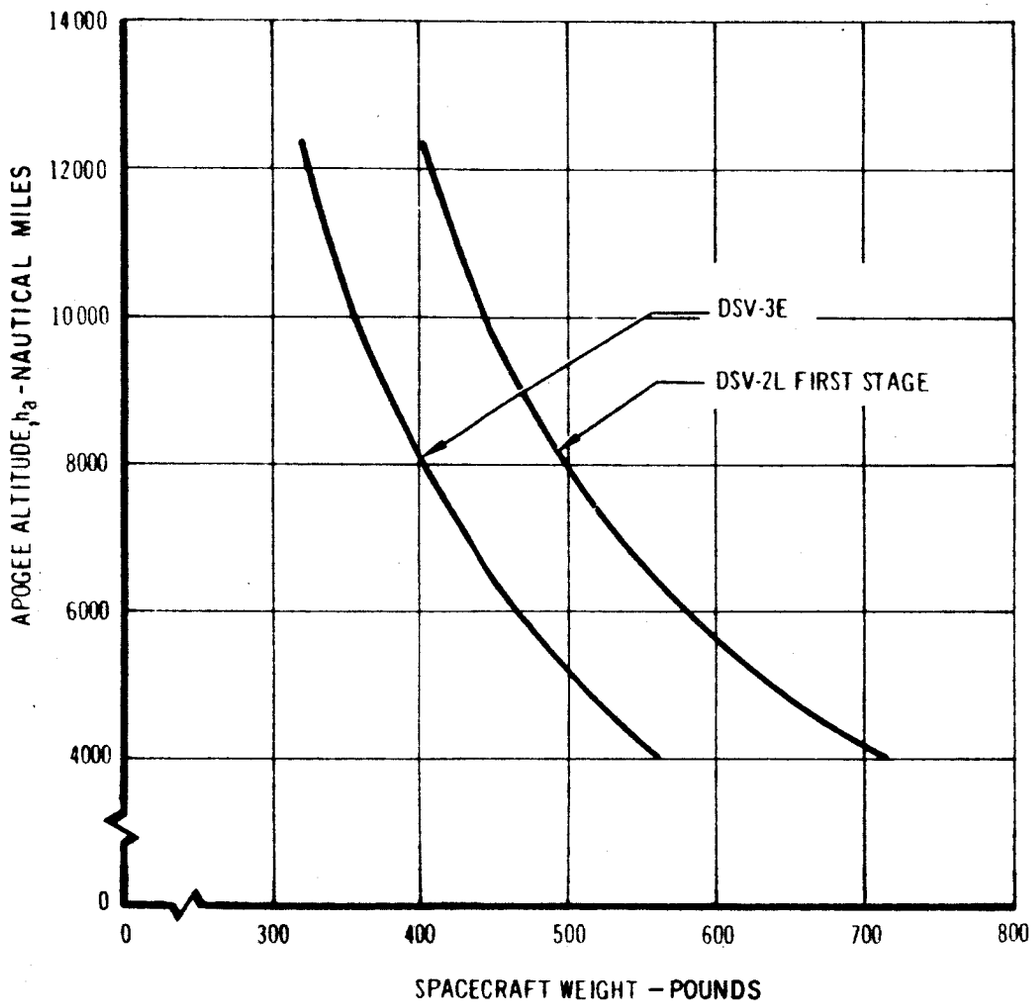


**Figure 2-35. IMPROVED DELTA, Three Stage Elliptical Polar Orbit Capability (WTR Launch Site)**



12

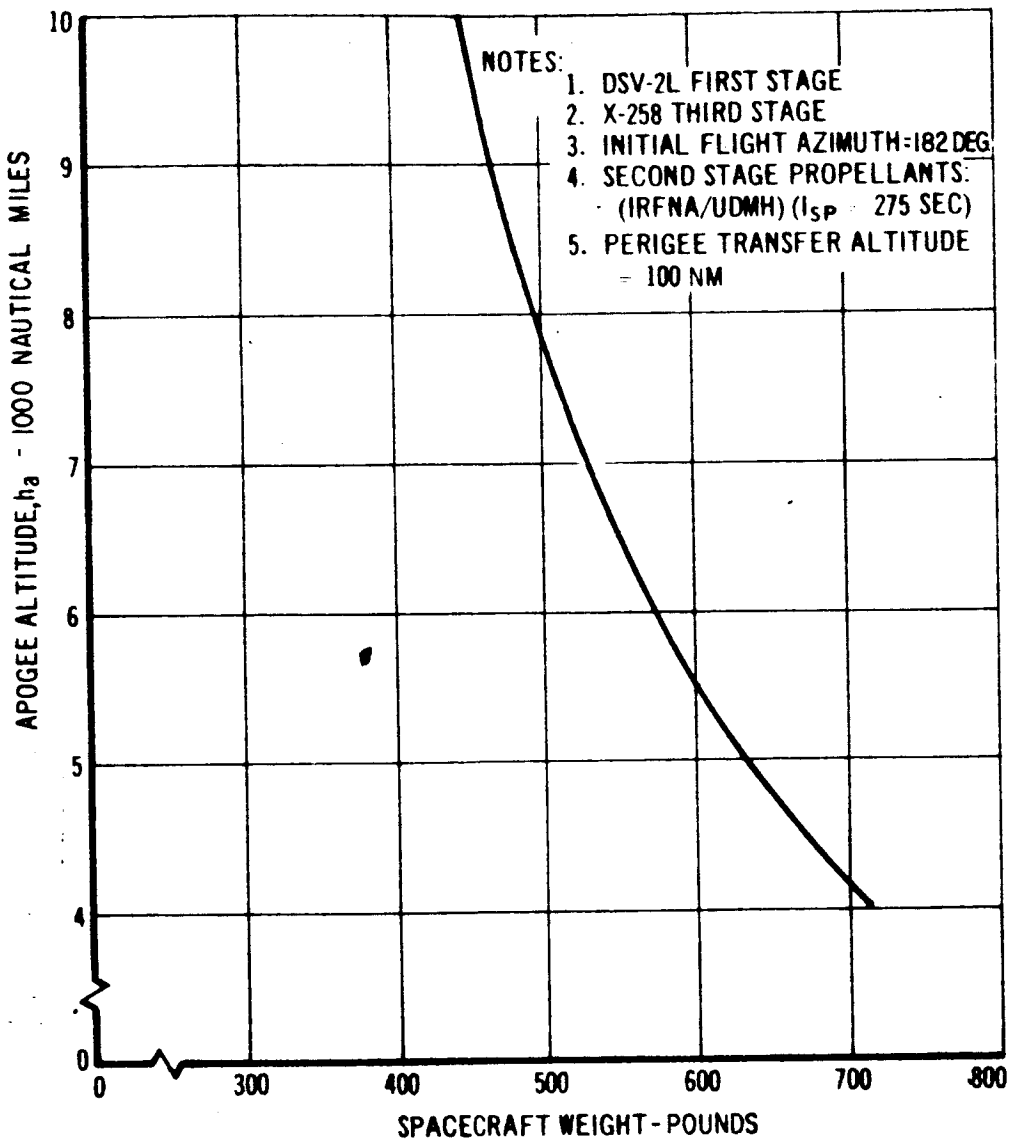


* DSV-3E WITH DSV-2L FIRST STAGE

Figure 2-36. IMPROVED DELTA*, Three Stage Elliptical Polar Orbit Capability (WTR Launch Site)



73

RE-ORDER No. 65-
VOL II

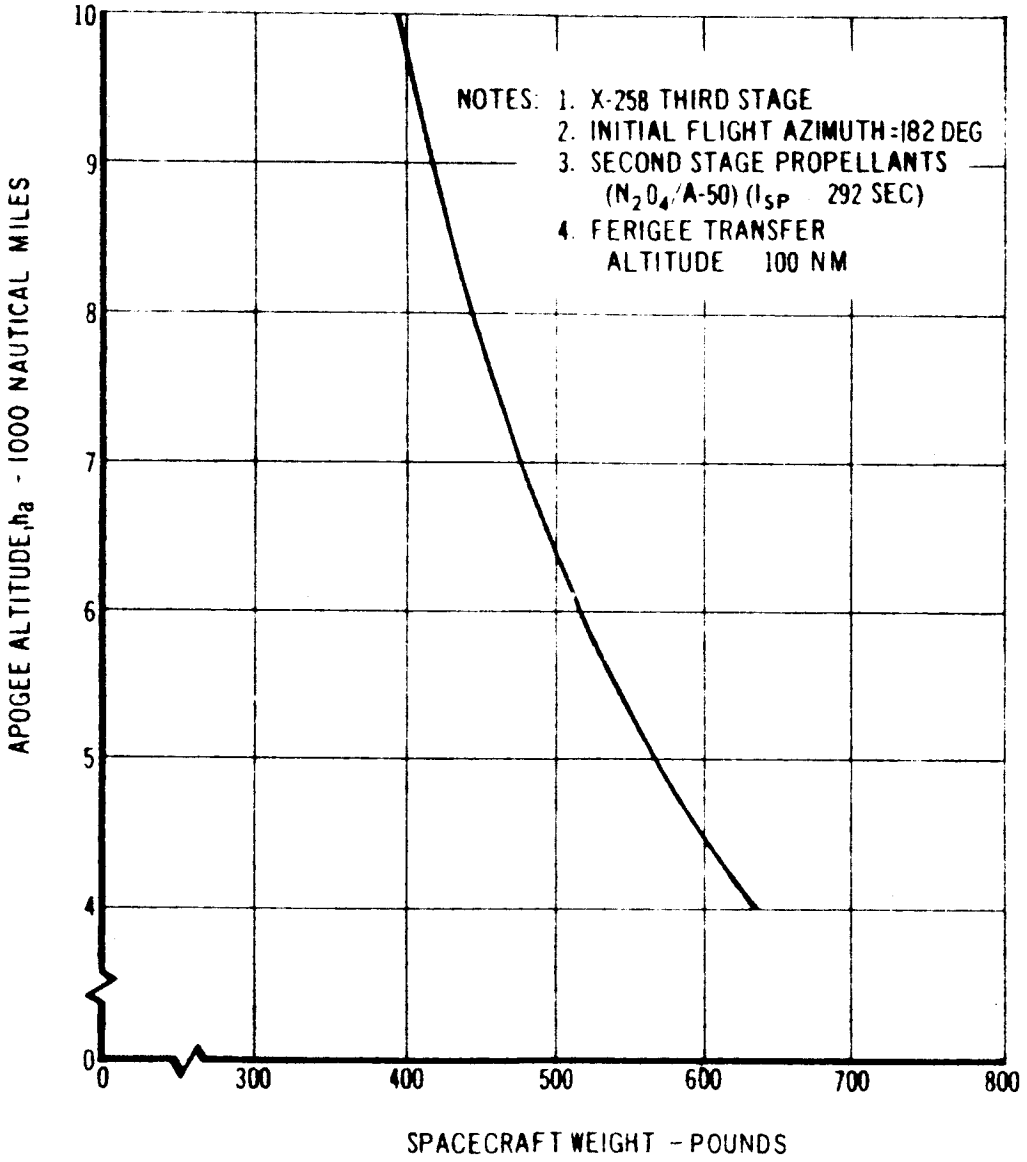


Figure 2-37. IMPROVED DELTA, Three Stage Elliptical Polar Orbit Capability (WTR Launch Site)

RE-ORDER NO. 65-323
VOL II

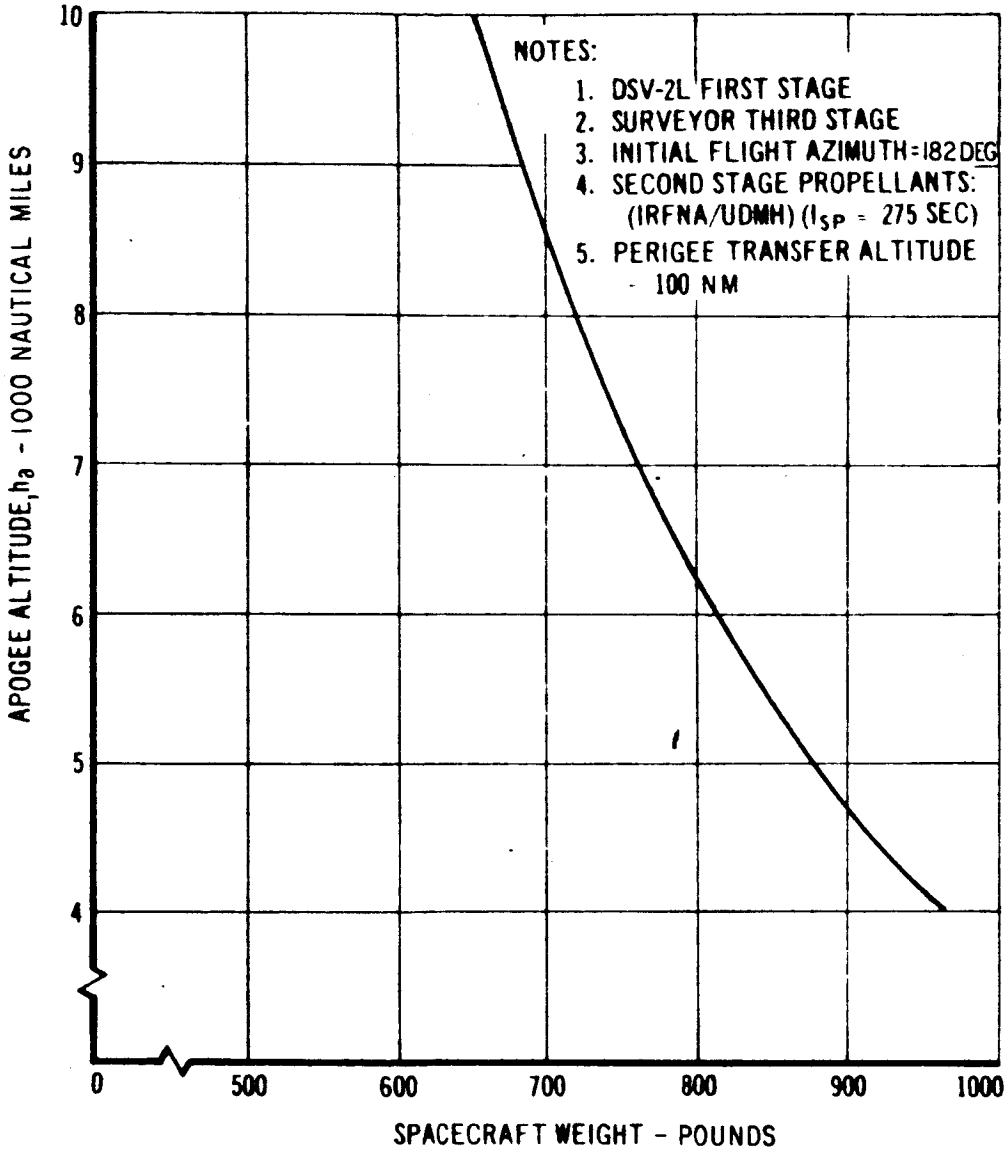


*DSV-3E WITH DSV-2L FIRST STAGE & SURVEYOR THIRD STAGE

Figure 2-38. IMPROVED DELTA* Three Stage Elliptical Polar Orbit Capability (WTR Launch Site)

# COMPARISON OF PAYLOAD-ORBIT CAPABILITY FOR VARIOUS DELTA VEHICLES

## PERFORMANCE SUMMARY

| Figure | Launch Vehicle Configuration | Type of Orbit | Launch Site | Launch Azimuth Degrees | Orbit Inclination Degrees | Altitudes Apogee/Perigee Nautical Miles |
|---|---|---|---|---|---|---|
| 2-39 | DSV-3C<br>DSV-3D<br>DSV-3E | Circular | ETR | 108 | 33 | ≈ 200 |
| 2-40 | DSV-3D<br>DSV-3E | Elliptical | ETR | 108 | 33 | ≈ 500/100 |
| 2-41 | DSV-3D<br>DSV-3E | Elliptical | WTR | 182 | 90 | ≈ 3000/100 |
| 2-42 | DSV-3C<br>DSV-3D | Circular | WTR | 182 | 90 | ≈ 300 |

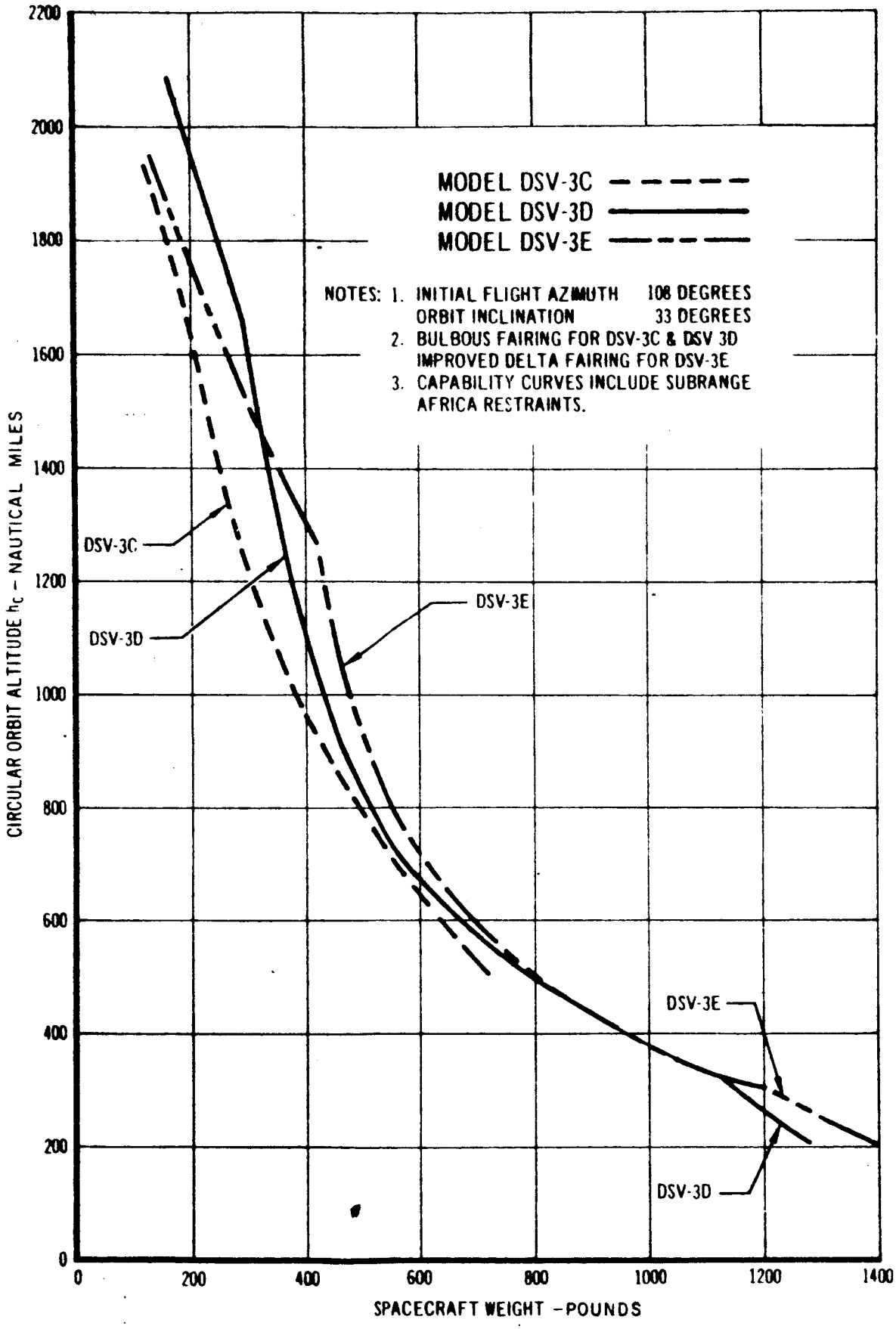


Figure 2-39. DELTA, Three Stage Circular Orbit Capability (ETR Launch Site)

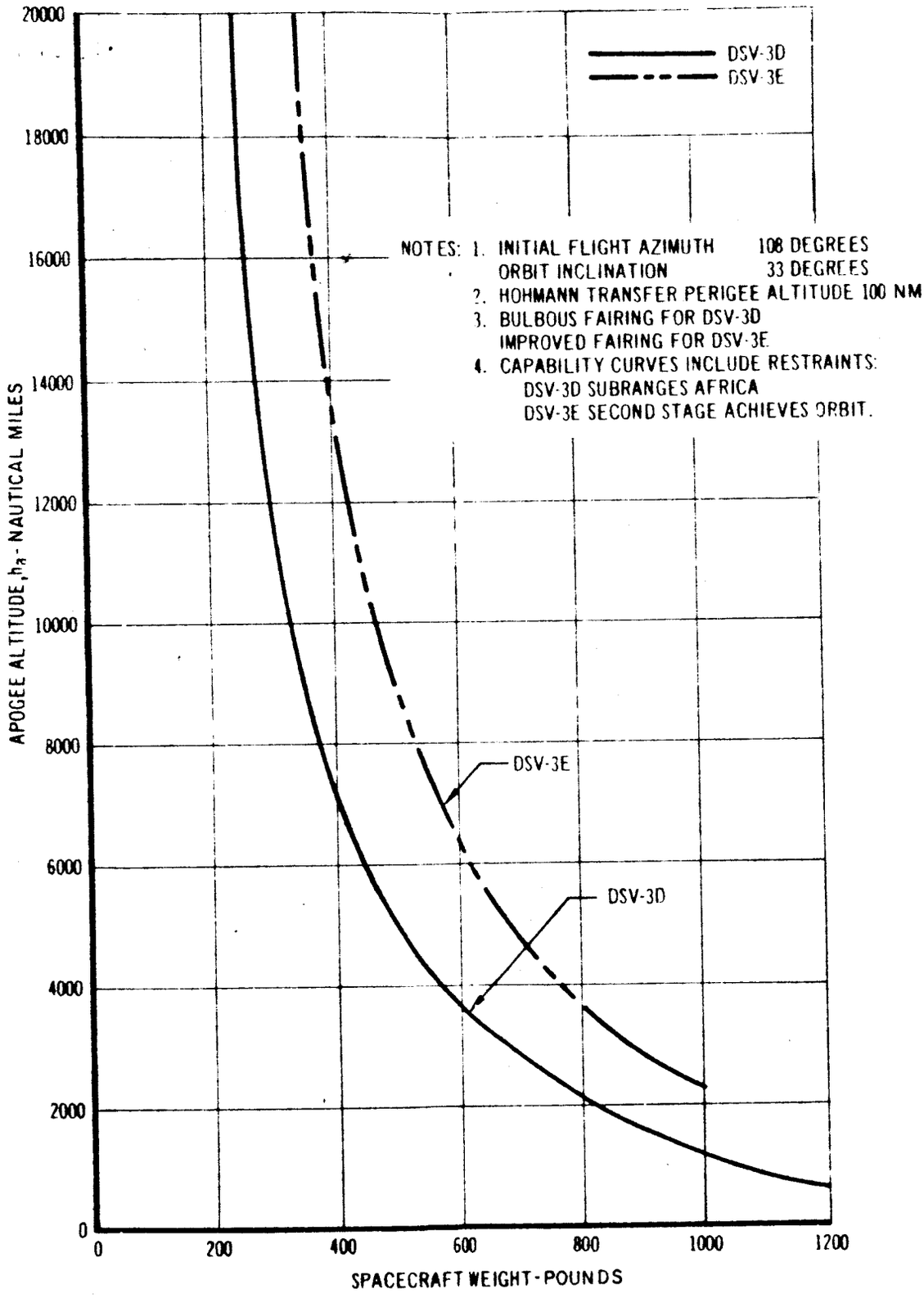


Figure 2-40. DELTA, Three Stage Elliptical Orbit Capability (ETR Launch Site)

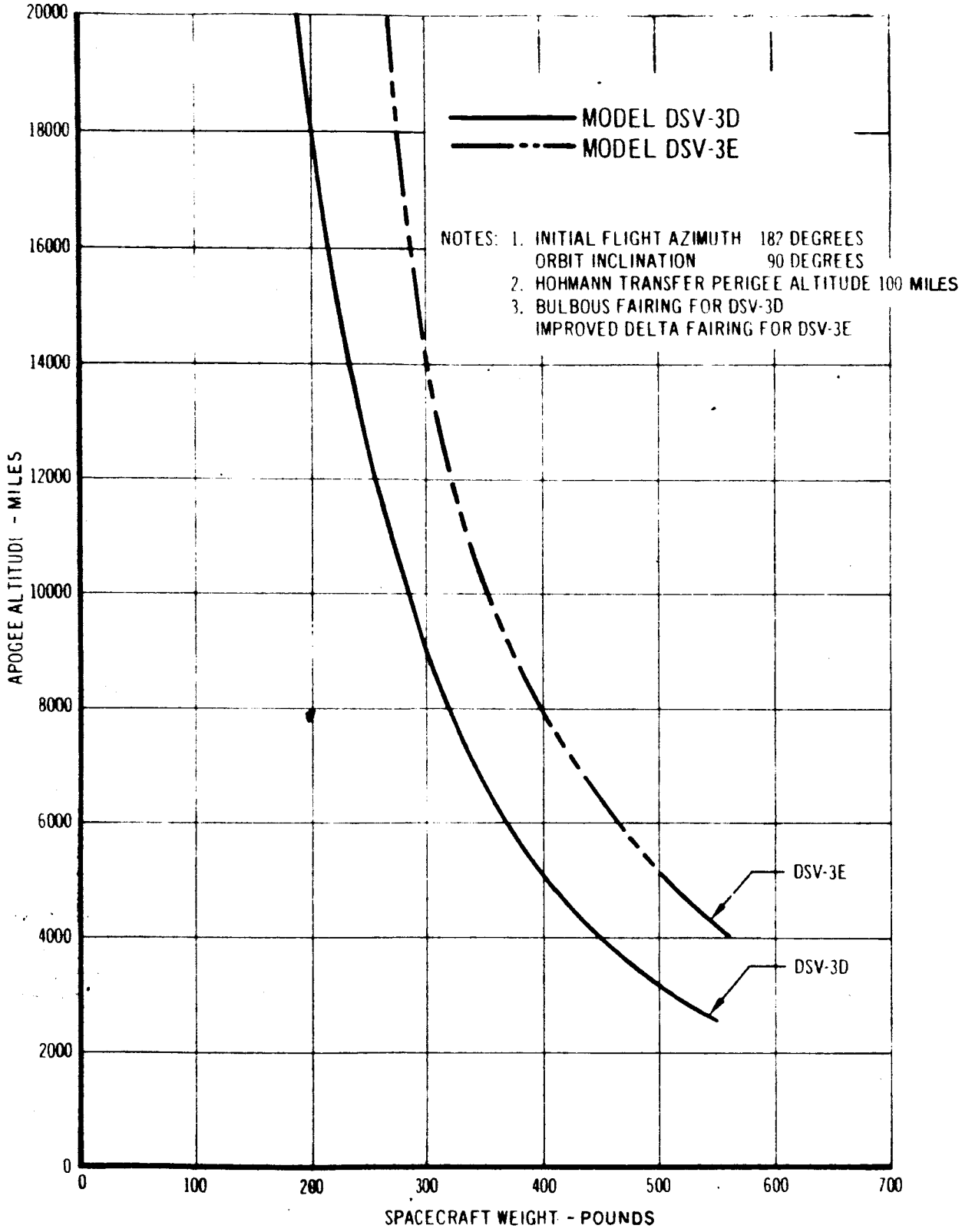


**Figure 2-41. DELTA, Three Stage Elliptical Orbit Capability (ETR Launch Site)**

RE-ORDER No. 65-323
Vol II

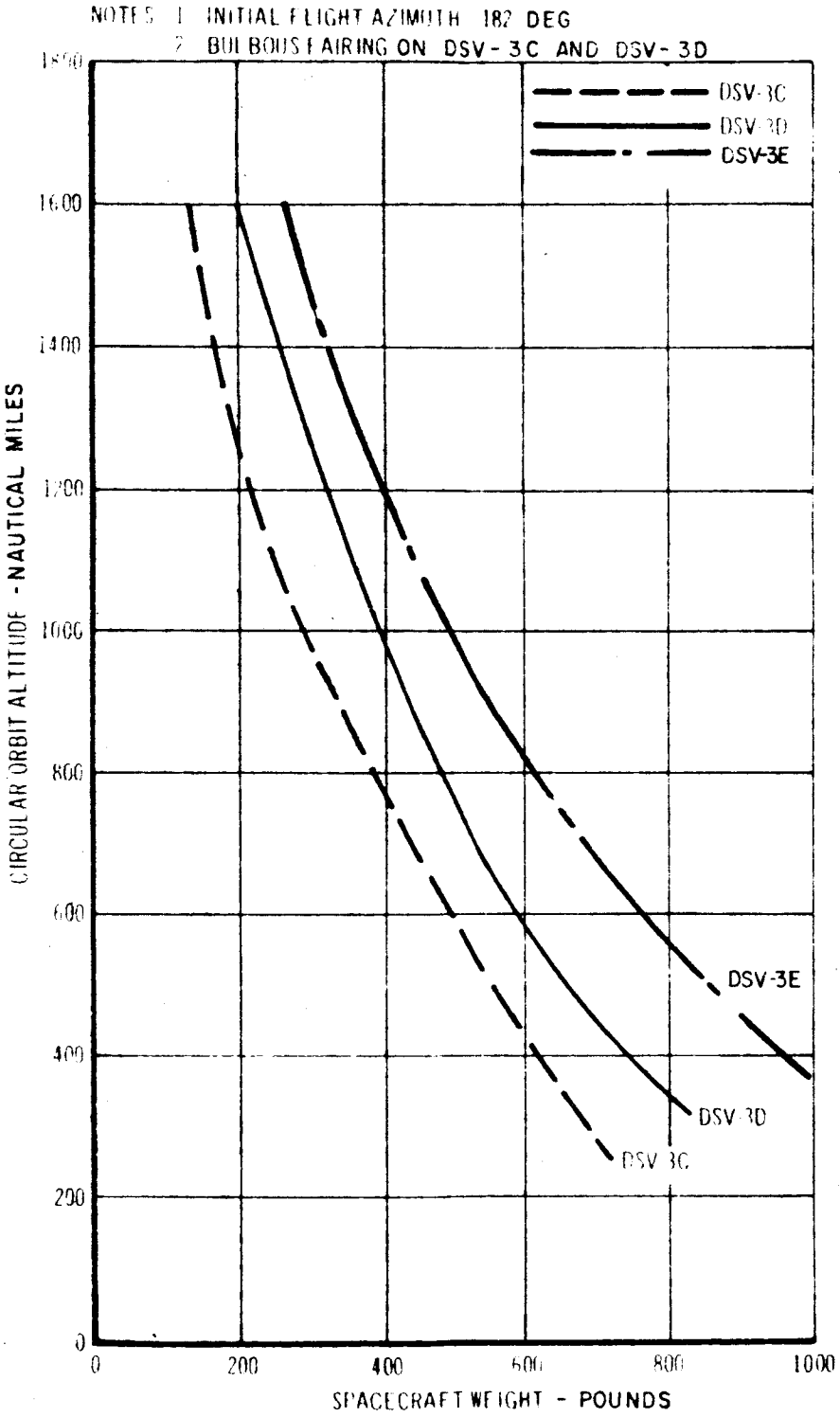


Figure 2-42. DELTA, Three Stage Polar Circular Orbit Capability (ETR Launch Site)



80

RE-ORDER No. 65-323
Vol II

# THOR-ABLESTAR PAYLOAD-ORBIT CAPABILITY

## PERFORMANCE SUMMARY

RE-ORDER No.

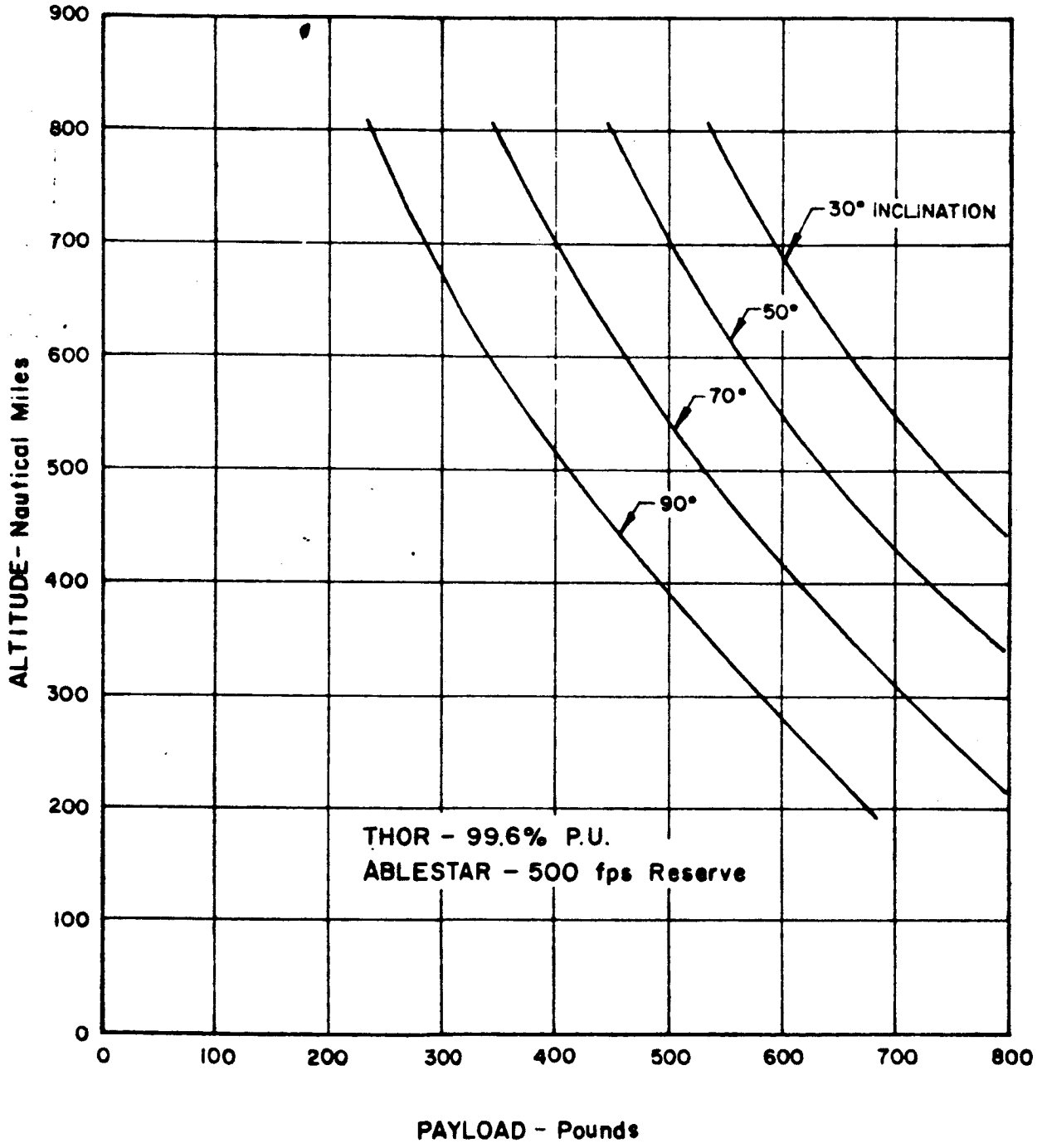


Figure 2-43. Payload Capability THOR (BlockII) ABLESTAR-I, Circular Orbit

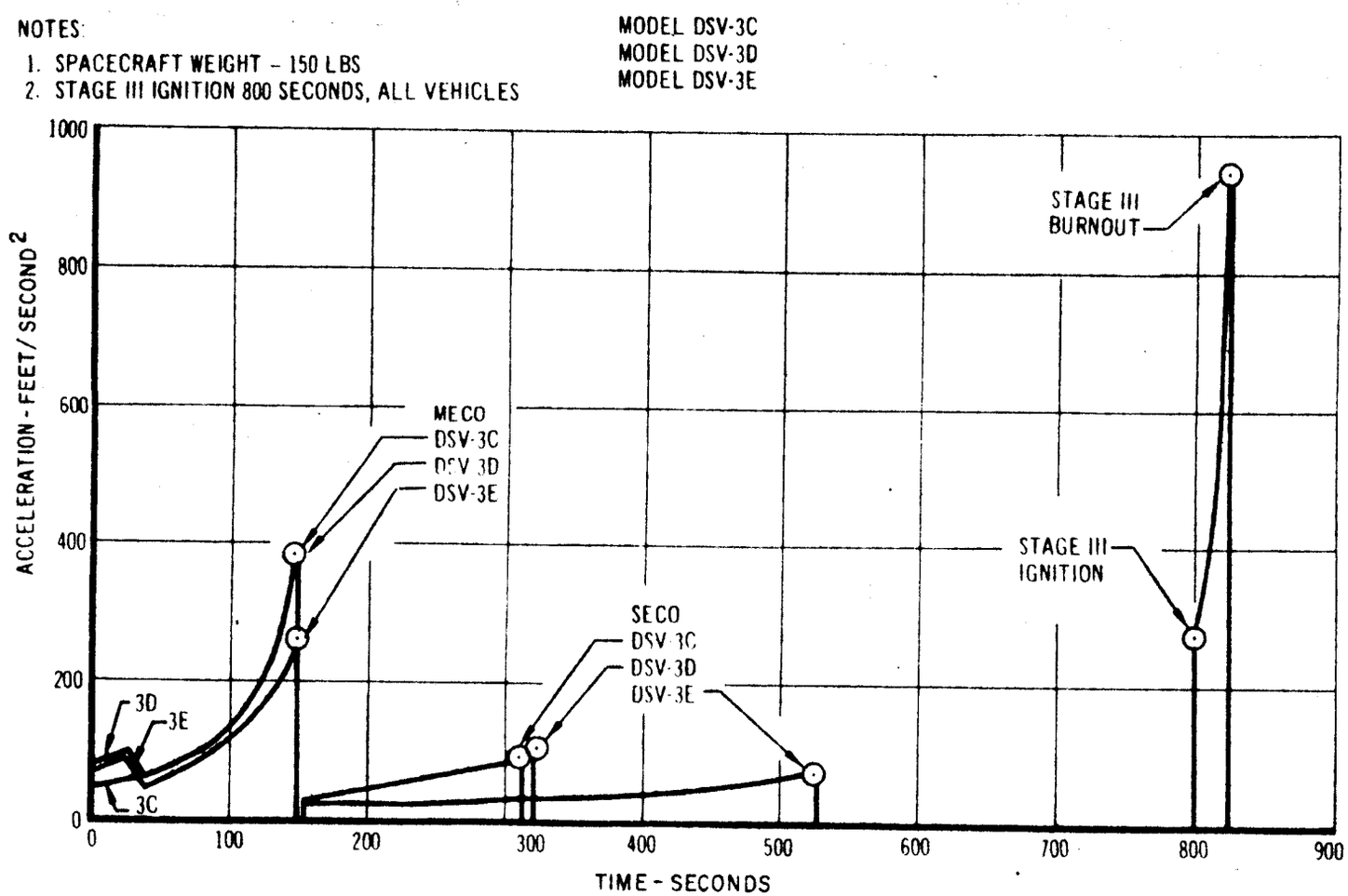


Figure 2-44. DELTA Typical Axial Acceleration Time History



RECEIVED NOV 6 5 - 3 3 3 3

# TABLE 2-5. LAUNCH VEHICLE STEADY STATE AND VIBRATION LOADING EXPECTED DURING POWERED FLIGHT (350-POUND SPACECRAFT)

| | | LAUNCH VEHICLE / LOAD DIRECTION | ATLAS-AGENA D | THOR-AGENA D | TAT-AGENA D | THOR-ABLESTAR | DELTA, TAD, AND IMPROVED DELTA |
|---|---|---|---|---|---|---|---|
| STEADY-STATE ACCELERATIONS | | Thrust Axis | Max q[1]: 2.3 g; Stage I Cutoff: 7.0 g | Max q: 2.1 g; MECO[2]: 6.1 g | | Available thrust, shear and bending diagrams indicate that maximum load levels occur during max q and THOR burnout. Values given for THOR-AGENA D are representative. | t = 120 sec: 6.2 g; Stage III Burnout: 15.3 g |
| | | Lateral Axis | 2.0 g; 1.0 g | 0.6 g; 0.06 g | | | 1.05 g; 0 g |
| FLIGHT VIBRATION | SINUSOIDAL | Thrust Axis | Frequency-cps / g rms<br>5-50: 0.7<br>50-100: 1.0<br>100-2000: 2.0 | Frequency-cps / g rms<br>5-16: 0.5<br>16-22: 2.1<br>22-150: 0.7<br>150-400: 1.4<br>400-2000: 3.5 | Frequency-cps / g rms<br>5-12: ±0.25 in. DA[3]<br>12-400: 2.8<br>400-2000: 5.3 | Frequency-cps / g rms<br>5-50: 2.0<br>50-2000: 3.5 | Frequency-cps / g rms<br>10-25: 1.4<br>25-50: 2.0<br>50-500: 5.0<br>500-2000: 10.0<br>Above are experienced along the three principle axes.<br>550-650: 20.0<br>Occurs during Stage III burnout |
| | | Lateral Axis | 5-50: 0.7 | 5-150: 0.35 | 5-9: ±0.25 in. DA<br>9-250: 1.4<br>250-400: 2.8<br>400-2000: 5.3 | | |
| | RANDOM | Thrust Axis | Frequency-cps / g rms<br>5-300: 0.02 $g^2$/cps<br>300-2000: 1.0$g^2$/cps | Frequency-cps / g rms<br>20-80: 0.02$g^2$/cps<br>80-1200: 0.02 to 0.03$g^2$/cps<br>1200-2000: 0.03 $g^2$/cps | | Frequency-cps / g rms<br>5-2000: 0.03$g^2$/cps | Frequency-cps / g rms<br>10-2000: 0.03 $g^2$/cps<br>During 1st and 2nd Stage burnout<br>Above applicable for all three axes |
| | | Lateral Axis | No significant lateral loading | Above applicable for all three axes | | | |
| REMARKS | | | | | Sinusoidal vibration conditions represent worst loading case. Therefore, steady-state acceleration and random vibration levels are omitted. | Above vibration levels are for equipment mounted in the forward compartment of the ABLESTAR Stage. Slightly lower input levels for the payload as a whole can be anticipated. | Angular accelerations (transient and steady state) as determined by spin rate and spacecraft roll moment of inertia are experienced during spin stabilization prior to third-stage ignition. |

1. Maximum q = Maximum Aerodynamic Loading
2. MECO = Main Engine Cut Off
3. DA = Double Amplitude

The values given in Table 2-5 are indicative of the actual flight levels experienced on the vehicle. However, in practice the spacecraft components are designed to qualification levels which are more severe than the actual flight levels. The prototype hardware is subjected to these qualification levels and the final flight hardware is subjected to flight acceptance levels which are less severe. As an example, the NASA recommended qualification and flight acceptance vibration levels for the DELTA DSV-3B, 3C, 3D or 3E vehicles are given in Table 2-6. As expected the qualification levels are significantly higher than the flight levels given in Table 2-5 and the flight acceptance levels slightly lower than the qualification levels.

Without conducting detailed structural analyses, it is difficult to draw significant conclusions regarding the effects of the launch environments given in Table 2-5 on spacecraft design. However, one point is apparent, those launch vehicles employing solid propellant stages (TAT-AGENA D, DELTA, TAD and IMPROVED DELTA) have significantly higher acceleration and vibration loads. It is beyond the scope of this study to determine if these higher loading conditions represent significant spacecraft structural design problems, but based on past experience it is believed that the conditions imposed by any of these launch vehicles could be handled without great difficult, or incurring undue weight penalties.

## 2.5 COST AND RELIABILITY

Cost and reliability estimates for each of the promising launch vehicle systems are given in Table 2-7. The cost estimates include all normal launch vehicle cost for injecting the payload into orbit (basic vehicle, pad preparation, etc.). If special alterations to the launch vehicle system are required these would represent additional cost. The references for the estimates are indicated.

Unfortunately, extensive flight experience does not exist for some of these vehicles. This reduces the validity of the reliability estimates and can be misleading. For example, Table 2-7 indicates a reliability of 100 percent for TAD. This results because TAD has only been used once and this was a successful launch.

Table 2-6. NASA Recommended Qualification and Flight Acceptance Vibration Levels for Spacecraft on DSV-3B, 3C, 3D, or 3E Vehicles

| SINUSOIDAL VIBRATION | Frequency, cps | Duration, Min | g's, O-Peak |
|---|---|---|---|
| I. QUALIFICATION LEVELS | | | |
| Thrust Axis | 10-50 | 1.17 | 3.8 |
| | 50-500 | 1.66 | 7.5 |
| | 500-2000 | 1.00 | 21.0 |
| Lateral Axis | 8-500 | 2.83 | 2.3 |
| | 500-2000 | 1.00 | 3.8 |
| Sweep Rate | 2 Octaves/Minute | | |
| II. FLIGHT ACCEPTANCE LEVELS | | | |
| Thrust Axis | 10-50 | .59 | 2.5 |
| | 50-500 | .83 | 5.0 |
| | 500-2000 | .50 | 14.0 |
| Lateral Axis | 8-500 | 1.42 | 1.5 |
| | 500-2000 | .50 | 2.5 |
| Sweep Rate | 4 Octaves/Minute | | |
| **RANDOM VIBRATION** | **Frequency, cps** | **Duration, Min** | **$g^2$/cps** |
| III. QUALIFICATION LEVELS | | | |
| All Axes | 20-2000 | 4.0 Each Axis | 0.07 $g^2$ |
| IV. FLIGHT ACCEPTANCE LEVELS | | | |
| All Axes | 20-2000 | 2.0 Each Axis | 0.03 $g^2$ |

Vol II

Table 2-7. Launch Vehicle Cost and Reliability

| LAUNCH VEHICLE | RELIABILITY[a] | COST-MILLIONS |
|---|---|---|
| ATLAS-AGENA D | 0.79 | 7.5[b] |
| THOR-AGENA D | 0.81 | 5.8[b] |
| TAT-AGENA D | 0.63 | 6.2[b] |
| THOR-ABLESTAR | 0.64 | 3.1[b] |
| DELTA (DSV-3C) | 0.91 | 2.9[c] |
| TAD (DSV-3D) | 1.0 | 3.2[c] |
| IMPROVED DELTA | | |
| DSV-3E | 0.91 (Est.) | 3.4[c] |
| DSV-3F | 0.91 (Est.) | 3.1[c] |
| DSV-3G | 0.91 (Est.) | 3.1[b] |
| DSV-3H | 0.91 (Est.) | 2.8[b] |

NOTES

a. Reliability estimates were obtained by dividing the successful launchings by the number of launch attempts (through July 28, 1964), except for the IMPROVED DELTA figures which are estimates since this vehicle has not been used to date. The entire launch vehicle series was considered in establishing the flight record. For example the reliability estimate for ATLAS-AGENA D is based on the flight record of the ATLAS-AGENA A, B and D.

b. Obtained from V. L. Johnson, Director of Launch Vehicle and Propulsion Programs, NASA Headquarters. Information obtained by phone on November 6, 1964.

c. Obtained from R. Goss, NASA Goddard Spacecraft Coordinator for the DELTA Launch Vehicle. Information obtained by phone on November 3, 1964. These figures were confirmed by V. L. Johnson in the phone conversation referenced above.

In some cases the actual vehicle reliability may be higher than the estimates given in Table 2-7. Since efforts are always being made to improve the reliability of each of these launch vehicles the basic reliability should be increasing, therefore, an estimate based on the total flight record should be lower than the current launch vehicle reliability. For example, Space General estimates the current reliability of the THOR-ABLESTAR to be 90 percent based on the most recent component tests.

Since launch vehicles are not mass produced items, and only a limited number of flights have actually been made the question of reliability is somewhat nebulous. One approach sometimes used is to consider the most recent portion of the flight record. The reasoning being that this should be more representative of the current vehicle performance and reflect the past efforts to improve the reliability. Estimating the reliability on the number of successful launches out of the past five attempts yields:

| | | |
|---|---|---|
| ATLAS-AGENA D | - | 1.00 |
| THOR-AGENA D | - | 0.80 |
| TAT-AGENA D | - | 0.80 |
| THOR-ABLESTAR | - | 0.60 |
| DELTA (DSV-3C) | - | 0.80 |

As expected these results are generally equal to or higher than those presented in Table 2-7.

Douglas estimates the IMPROVED DELTA reliability will be essentially equal to that of the standard DELTA since this class (DELTA, TAD and the IMPROVED DELTA configurations) of launch vehicles all employ the same basic engines, electronics, stabilization systems, etc.

## 2.6 SUMMARY AND CONCLUSIONS

The major launch vehicle performance parameters are summarized in Table 2-8. The polar orbit altitude that can be obtained for a 350 pound payload is presented to indicate the relative launch capability of the various vehicles. The final column in the table gives the "relative launch vibration rating." Increasing numbers are meant to imply a more severe

environment. For example, a (2) indicates that the launch environment is significantly worse than that for a vehicle with a (1) rating, but it does not mean that it is necessarily twice as severe.

An additional launch vehicle, the ATLAS-AGENA D-X-259, is included in Table 2-8. This vehicle combination has not been used to date, but has been under consideration (see Reference 2-10) by NASA-Ames for a solar probe mission. The ATLAS-AGENA D-X-259 has an important advantage over the basic ATLAS-AGENA D since it can place a 350 pound payload in a solar probe orbit with a perihelion of 0.34 AU. The ATLAS-AGENA D can obtain a perihelion of approximately 0.55 AU for the same spacecraft weight. To be of maximum scientific value, it is essential that the spacecraft pass as close to the sun as possible. This makes the ATLAS-AGENA D-X-259 an attractive vehicle for a solar probe mission and for this reason it was included here.

The ATLAS-AGENA D-X-259 would use the same payload fairings as the ATLAS-AGENA D. The X-259, which is the third stage engine on the SCOUT, would be mounted in the same manner as the third stage engine on the IMPROVED DELTA (see Figure 2-6) and as a result would occupy part of the normal payload volume.

In general, a launch vehicle selection for each of the orbits under consideration cannot be made on the basis of the information contained in this section alone. Consideration must be given to orbit mechanics, communications, thermionic system performance as a function of concentrator diameter, etc., before a final selection can be made. This is done in the following sections. However, the launch vehicles that look most promising for the orbits of interest can be identified and some general conclusions drawn. Table 2-9 lists, what appears at this point, to be the most attractive launch vehicles for achieving the orbits under consideration.

Table 2-9. Attractive Launch Vehicles

| Orbit | Attractive Launch Vehicles |
|---|---|
| A. 325 nm Circular Orbit | DELTA DSV-3C<br>IMPROVED DELTA DSV-3H<br>THOR-ABLESTAR |
| B. Sun-Synchronous Daylight Orbit* | TAD DSV-3D<br>IMPROVED DELTA DSV-3E |
| C. Elliptical Orbit with High Light to Shadow Ratio | TAD DSV-3D<br>IMPROVED DELTA DSV-3E |
| D. Stationary Earth Synchronous Orbit | ATLAS-AGENA D |
| E. Solar Probe | ATLAS-AGENA D<br>ATLAS-AGENA D-X-259 |

Of the launch vehicles considered** only the ATLAS-AGENA D has sufficient payload-orbit capability to place a 350 pound payload in a stationary earth synchronous orbit (19,300 nautical miles and zero inclination). Therefore, no further trade-offs are necessary to identify the launch vehicle associated with this type of orbit.

A similar situation exists in the case of the solar probe orbit. Only two vehicles, ATLAS-AGENA D and ATLAS-AGENA D-X-259 are capable of placing a 350 pound payload in an escape orbit. The ATLAS-AGENA D-X-259 permits a significantly closer approach to the sun (0.34 AU) than the ATLAS-AGENA D (0.55 AU). For this reason, the ATLAS-AGENA D is the preferred launch vehicle.

*The results of the work presented in Section 3 indicate that this type of orbit requires a near polar inclination at an altitude between 800 and 1800 nautical miles.

**This statement does not apply to the ATLAS-AGENA D-X-259 which is only included for consideration with solar probe orbits.

For the 325-nautical mile circular, sun-synchronous daylight, and elliptical orbits the choice of a launch vehicle is not as clear as in the two preceding cases. However, the DELTA class of vehicles (DELTA, TAD and IMPROVED DELTA) appear very attractive for the following reasons:

a. Based on over-all flight records, the DELTA and TAD vehicles have demonstrated a significantly higher reliability than any of the other vehicles considered. Since, in general, the IMPROVED DELTA will employ the same basic components, it is expected to have the same high reliability.

b. For equivalent payload-orbit capability, the DELTA series of launch vehicles has the lowest cost of the vehicles considered.

c. The development of the IMPROVED DELTA makes the DELTA series of vehicles extremely versatile. As a result, one of the DELTA configurations will generally closely approximate the required payload-orbit capability. This minimizes the chances of paying for booster capability that is not needed.

d. The payload fairings associated with the IMPROVED DELTA allow solar concentrator diameters essentially as large as those obtainable with any of the vehicles considered. These allowable concentrator diameters are sufficiently large to obtain the minimum acceptable thermionic generator output of 100 watts with a sizeable margin of safety (based on the results from Section 4 a concentrator diameter of 42 inches is required to obtain 100 watts). Having this safety margin can simplify the spacecraft design and offer some space for expansion should the component performance not come up to present estimates, thus necessitating a larger concentrator diameter.

e. The DELTA series are the only launch vehicles considered that are not engaged in orbiting classified military payloads. In addition, the DELTA series are NASA

vehicles. These two conditions should minimize priority problems in obtaining a vehicle and scheduling launches.

There are two possible disadvantages of the DELTA class of vehicles. First, there is no WTR launch capability for DELTA at present which makes obtaining polar, or near polar, orbits more difficult and less efficient. However, WTR launch capability is scheduled to be available in the first quarter of 1966 and, therefore, should present no problems for this program. Secondly, the DELTA series of vehicles have, in general, a more severe launch acceleration and vibration environment because of the solid stages employed. A detailed design analysis will have to be performed before the effects of this launch environment can be established, but based on past spacecraft design experience, no extremely difficult problems are anticipated. These two potential disadvantages are not considered serious at this point.

The ATLAS-AGENA D, THOR-AGENA D and TAT-AGENA D do not appear attractive for the 325-nautical mile circular, sun-synchronous daylight, and elliptical orbits because of their relatively high cost and low reliability. The high cost comes about partly because these vehicles generally have much higher payload-orbit capability than is required for these types of orbits. Another disadvantage of these three vehicles is that they are heavily involved in launching military payloads which could result in priority problems.

Work performed in the subsequent sections will have to be considered before any further conclusions can be drawn regarding final launch vehicle selections.

## 2.7 REFERENCES

2-1 Personal communications with the DELTA System Development Office for the Missile and Space Systems Division of the Douglas Aircraft Company (October 30, 1964)

2-2 E. Williams, "Availability of Solar Thermionics for the Early Voyager Missions," an internal General Electric, Missile and Space Division Document, PIR 9741-049, March 27, 1963.

Vol II 65-323


2-3 Dr. J. Hickey, "Space Launch Vehicles," General Electric, Missile and Space Division, January 1, 1963.

2-4 E. Williams, "A preliminary look at the Feasibility of a Solar Thermionic Piggy-Back Experiment," General Electric Company, Missile and Space Division, ASP-TM-003, January 18, 1963.

2-5 "Space Log," Volume 4, No. 1 and No. 2, Spring and Summer 1964 respectively, published by TRW Space Technology Laboratories.

2-6 "ABLESTAR Summary Data for Future Applications," Space General Report, June 1963.

2-7 "DELTA Spacecraft Design Restraints," Missile and Space Systems Division, Douglas Aircraft Company, Douglas Report SM-42367, Revised October 1963.

2-8 "DELTA and IMPROVED DELTA Design and Capabilities," Missile and Space Systems Division, Douglas Aircraft Company, Douglas Report SM-45243, August 25, 1964.

2-9 "Biosatellite Project," Volume 3, Classified Data, General Electric Missile and Space Division, RSD Proposal No. N-30232, Proposal submitted to NASA-Ames Research Center in response to RFP A-6824, June 13, 1963.

2-10 "Solar Probe Study Final Report," Volume 1, Study Summary, General Electric Spacecraft Department, Document No. 63SD779, September 3, 1963.

VOL II 65-323

SECTION 3

ORBIT ANALYSIS

PRINCIPAL CONTRIBUTOR:

B. GALMAN

# SECTION 3
# ORBIT ANALYSIS

## 3.1 INTRODUCTION

Five basic types of orbits were considered for the solar thermionic flight experiment.

a. Circular orbit with a five to three light-to-shadow ratio
b. Sun synchronous daylight orbit
c. Elliptical orbit with a high light to shadow ratio
d. Stationary earth synchronous orbit
e. Solar probe orbit.

This section investigates these orbits from the standpoint of shadow to light ratio, communications considerations, launch vehicle requirements, and the effect of launch delays and inclination errors; and draws conclusions regarding their suitability for a solar thermionic flight experiment.

## 3.2 DEFINITIONS

Since some of the terminology employed in this section may be unfamiliar to non-specialist, a number of terms are defined below for clarity.

a. Orbit - The path followed by a body moving in a gravitational field. Often employed synonomously with the term trajectory, although the latter implies, more correctly, an intersection with the planetary surface as in "ICBM Trajectory."

b. Circular Orbit - An orbit having constant distance with respect to the center of the principal attracting body. Orbits with variable distance are termed elliptical or eccentric.

c. Synchronous Orbit - An orbit which has a period equal to the daily planetary rotation (24 hours for earth). An inclined synchronous circular orbit daily retraces a figure "8" path on the earth. SYNCOM II is nominally in such an orbit. A synchronous circular orbit at zero inclination (in the plane of the equator) is termed "stationary" since its orbit trace a point on the planetary surface. This characteristic makes the circular stationary earth synchronous orbit of great interest for communications satellites. SYNCOM III is nominally in such an orbit.

d. Semi-Synchronous Orbits - A class of orbits having periods (the time to complete one orbit) which divide evenly into the number of hours in one day. Ground traces repeat daily for this type of orbit.

e. Sun-Synchronous Orbit - A class of orbits having nodal progression rate due to planetary oblateness equivalent to the mean apparent solar rate (0.9856 degrees/day for earth) such that the nodal axis (orbit plane, equatorial plane intersection) remains in constant phase with the sun. When the line of nodes of the orbit is normal to the planet sun vector, the orbit is termed daylight, twilight, or six o'clock. A more complete definition must include the injection time of day (the local sun time at the first North-South equatorial crossing).

f. Polar Orbit - An orbit whose plane is inclined 90 degrees to the equatorial plane. A characteristic of polar orbits is zero nodal rate, such that the orbital plane remains fixed in inertial space.

g. Retrograde Orbit - An orbit which is injected in a westerly direction such that the nodal axis "progresses" in the same direction as the earth's axial rotation. A prograde or posigrade orbit is injected in an easterly direction such that the nodal axis "regresses." A retrograde orbit may be alternately described as having an inclination of "97 degrees" (for instance) or "83 degrees retrograde."

h. Injection Time - In general, this refers to the burn-out point of the last propulsion stage; but, since this is dependant on the actual launch vehicle employed, a more convenient definition will be employed here. Injection time will be defined as the apparent solar time (or local sun time) at the first nodal North-to-South crossing.

i. Equinoxes - The nodal axis of the elliptic (plane of earth's orbit) and equatorial plane. The vernal equinox occurs in the spring around March 21 as the sun at 12 noon passes into the northern hemisphere. The autumnal equinox (about September 23) occurs six months later.

j. Solstices - The points at which the sun reaches its highest elevation above the equatorial plane. The summer solstice occurs about June 22; the winter solstice about December 22.

k. Shadow Cylinder - While the actual shadow formed by the earth is represented by two cone sections termed the umbra (shadow) and penumbra (semi-shadow), for present purposes it is deemed adequate to assume that the shadow volume is bounded by a cylinder having an earth radius.

l. Shadow Period - The time during a given orbital revolution when the spacecraft is in the earth's shadow.

m. Shadow Duration - Length of time when shadow is continually encountered.

n. Inclination - The angle from the equatorial plane to the orbit plane measured at the ascending node. An inclination greater than 90 degrees indicates a retrograde orbit; however, it is also common to quote the smaller angle (180-i) and term this retrograde inclination.

## 3.3 BASIC CHARACTERISTICS AND SHADOW COMPARISONS FOR VARIOUS ORBITS

Since the solar thermionic experiment requires a solar energy input to function, the light to shadow ratio and shadow history of the various orbits is of great importance. These particular characteristics influence the following areas:

a. The time in sunlight available for operating the solar thermionic experiment

b. The frequency with which the solar thermionic experiment will be subjected to severe thermal cycling

c. The percentage of the orbit period during which the spacecraft power requirements must be supplied by batteries.

The general characteristics and shadow histories of these basic types of orbits are considered below.

### 3.3.1 CIRCULAR ORBIT WITH A FIVE TO THREE LIGHT-TO-SHADOW RATIO

Figure 3-1 indicates the maximum shadow period for circular orbits as a function of orbit altitude. The maximum shadow occurs at those times of year when the sun falls in the plane of the spacecraft orbit. A light-to-shadow ratio of five to three (1.67) occurs at an altitude of 325 nautical miles and the percentage of time spent in shadow is 37.3 percent of the orbital period. From Figure 3-2, which gives orbital period as a function of altitude, the orbital period is 96.7 minutes for a 325-nautical mile circular orbit; the maximum shadow period is approximately 37 minutes. For cases when the sun vector is inclined to the orbital plane, Figure 3-3 indicates the decrease in shadow encountered with increasing inclinations.

Figure 3-4 shows a typical shadow history for a 325-nautical mile circular orbit with a 30-degree inclination. An inclination of 30 degrees was selected since this permits maximum

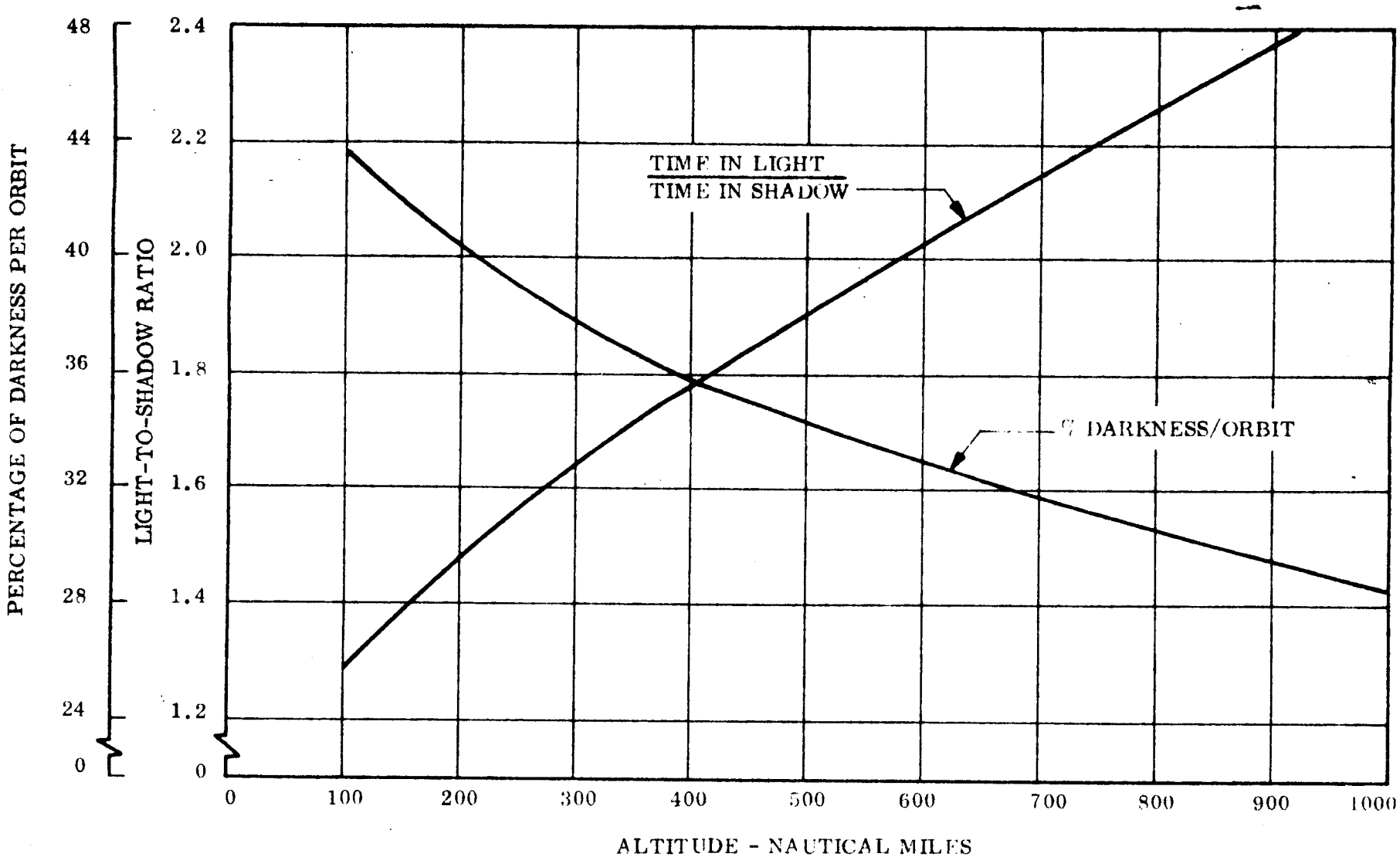


Figure 3-1. Maximum Shadow Time for Circular Orbits

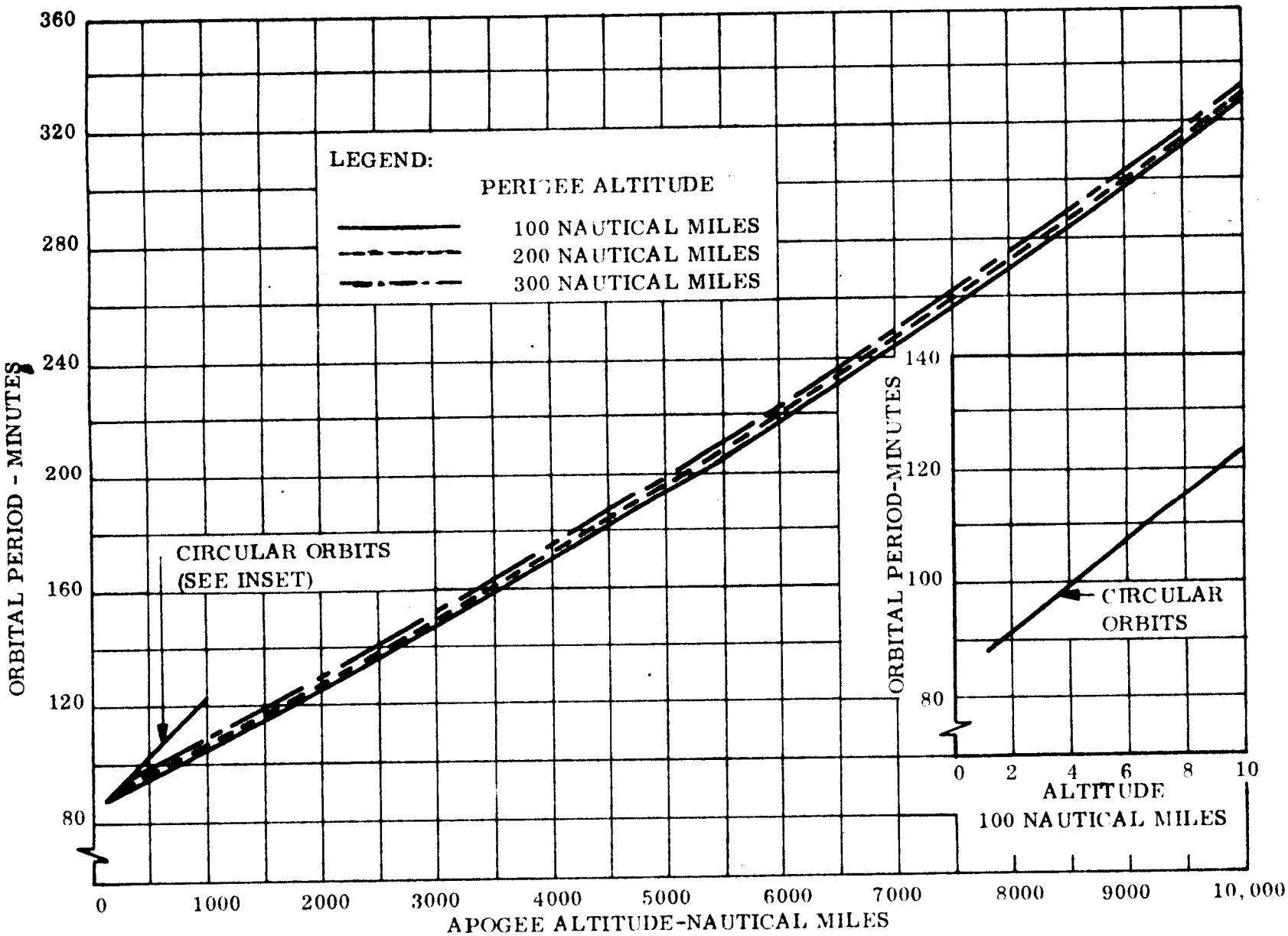


Figure 3-2. Orbital Period for Various Circular and Elliptic Orbits



65-323
Vol II

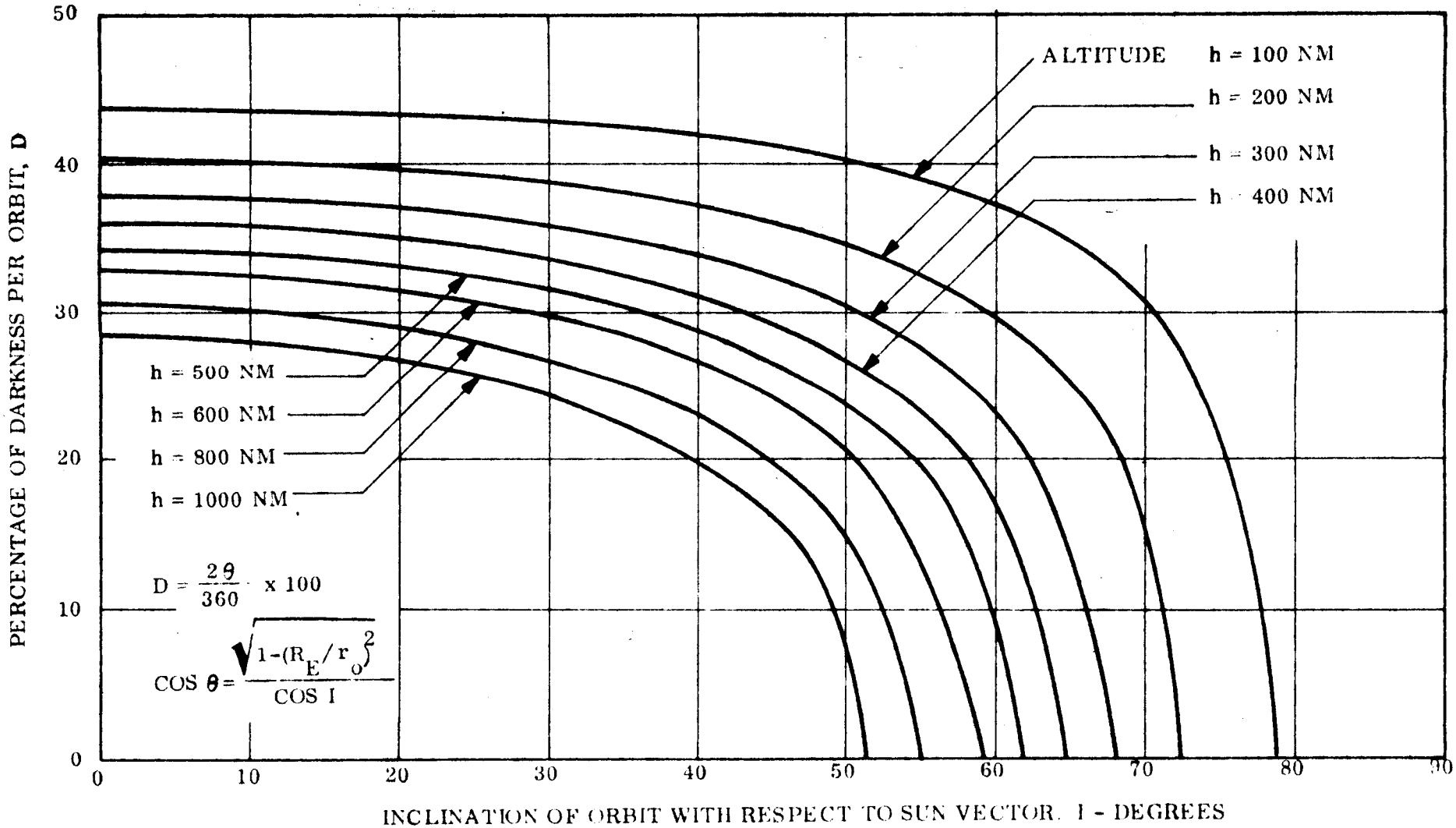


Figure 3-3. Percentage of Darkness as a Function of Inclination of Orbit With Respect to Sun Vector for Various Circular Orbit Altitudes

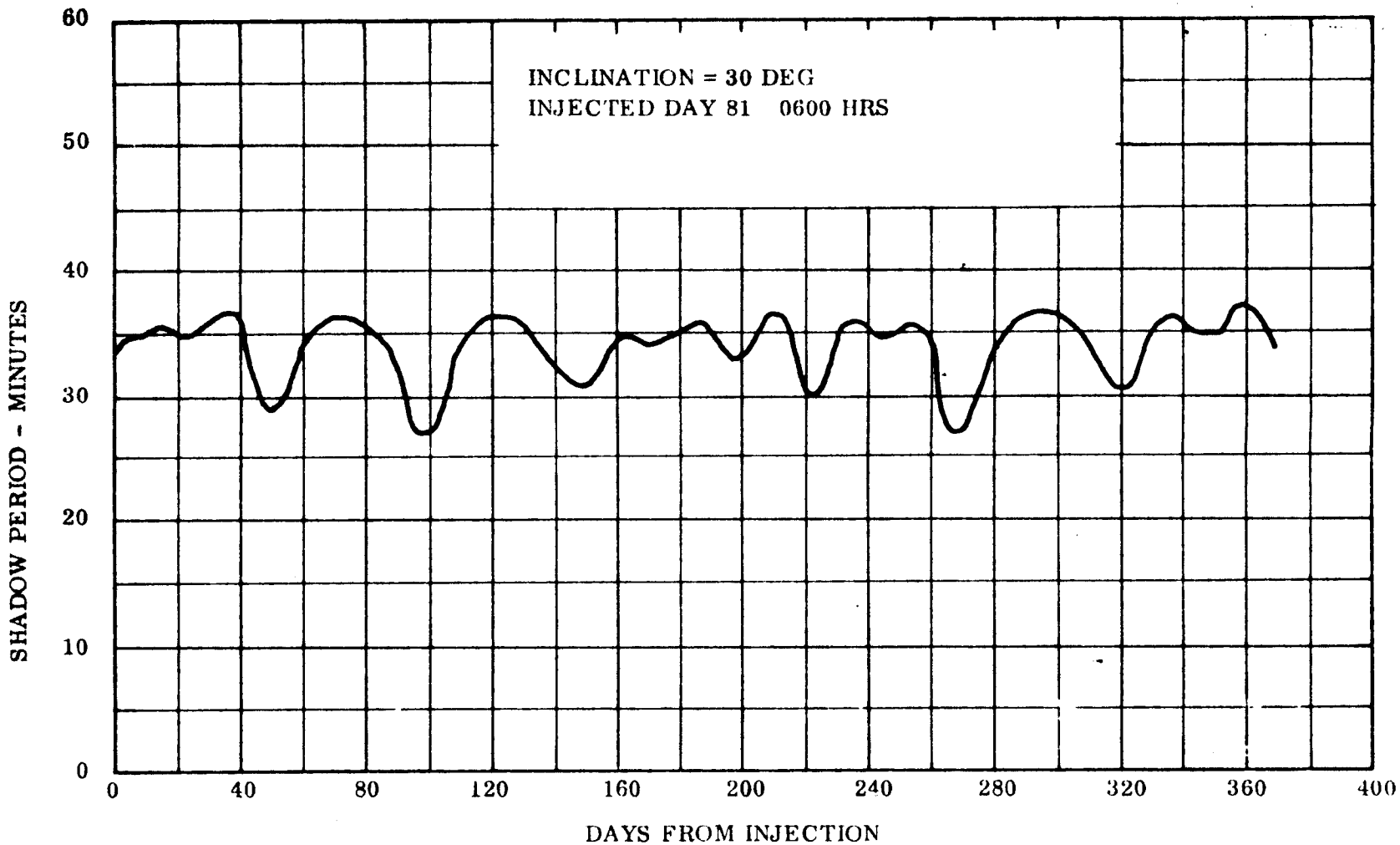


Figure 3-4. Shadow History for 325-Nautical Mile Circular Orbit

payload weight to be orbited from ETR*. In addition, a 30-degree inclination yields favorable ground station coverage (see Section 10-Volume III). The shadow history was computed using an IBM 7094 computer program previously developed for this purpose (Reference 3-1). Note that the shadow period remains fairly constant over the one-year duration. No particular significance is attached to the time of injection.

### 3.3.2 CIRCULAR POLAR ORBIT

A circular orbit with a 90-degree inclination (polar orbit) yields a very desirable orbit from the communications standpoint. Since the spacecraft passes over the poles on every orbit, it is in range of those ground stations located near the north pole on practically every pass. This suggests that the communications functions can probably be confined to one or two ground stations thus greatly simplifying the data collection and handling. This is discussed further in Section 10.4 (Volume III).

The polar orbit is generally obtained with a WTR launch. It can be obtained from ETR but this requires a dog leg launch to satisfy range safety constraints. Dog leg launches are more complicated and make less efficient use of the launch vehicle.

Figure 3-5 shows the characteristic of two identical shadow peaks per year for this class of orbits. The maximum shadow time occurs when the sun lies in the orbit plane; this happens twice a year. The maximum shadow period is not strongly dependent on altitude for the range shown, nor is it dependent on injection time of day or time of year. However, the duration and time of initiation is dependent on all three of these factors. Figure 3-6 shows the combined effects of launch delay (0.3 hour) and inclination error (1.0 degree) on time of shadow initiation and duration. It is apparent that initial shadow-free periods of more than a month or two are not obtainable with polar orbits.

*Without incurring range safety problems, the maximum inclination obtainable from AMR is approximately 33 degrees. Greater inclinations can be obtained but they require dog leg launches.

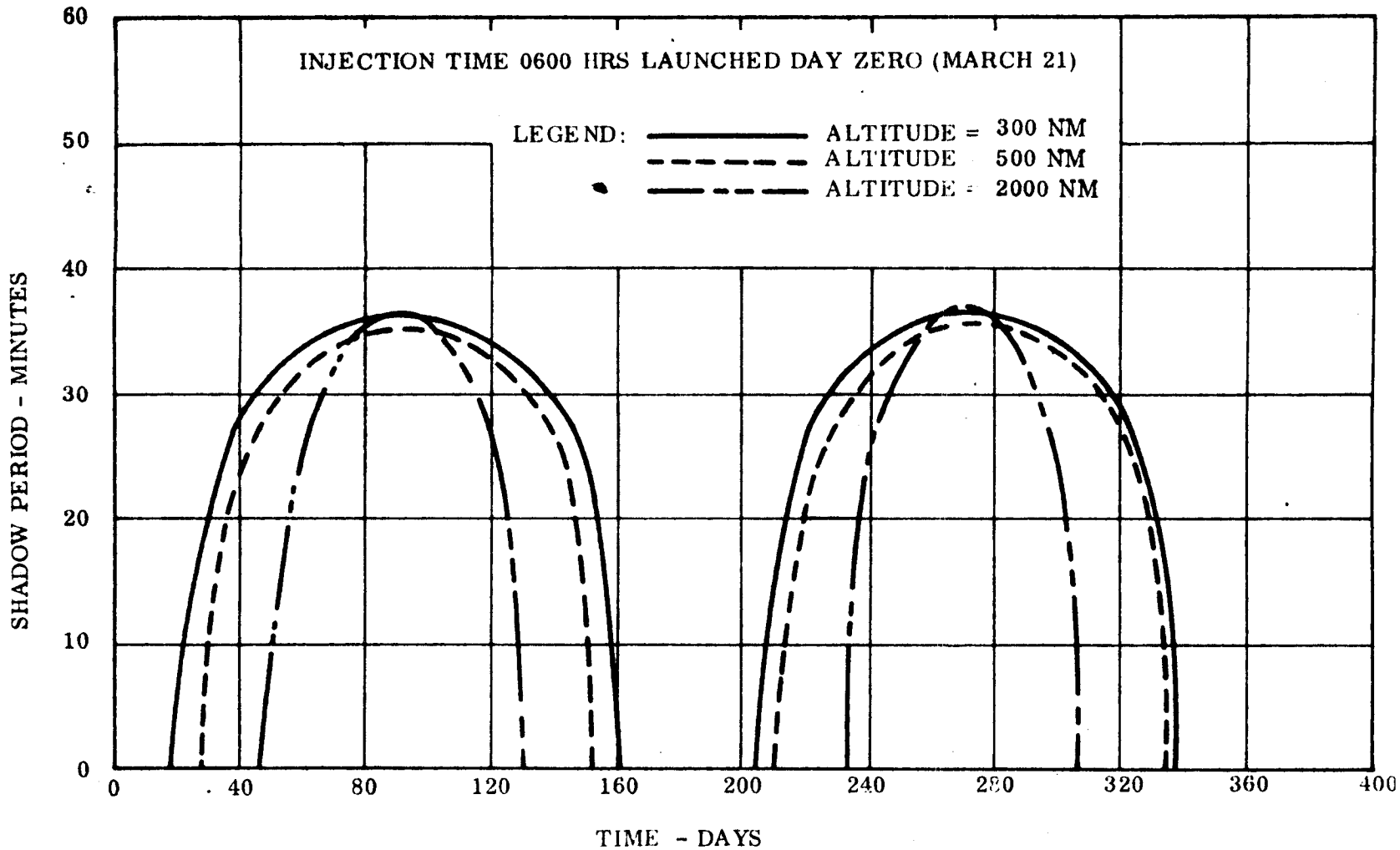


Figure 3-5. Shadow History for Polar Orbits

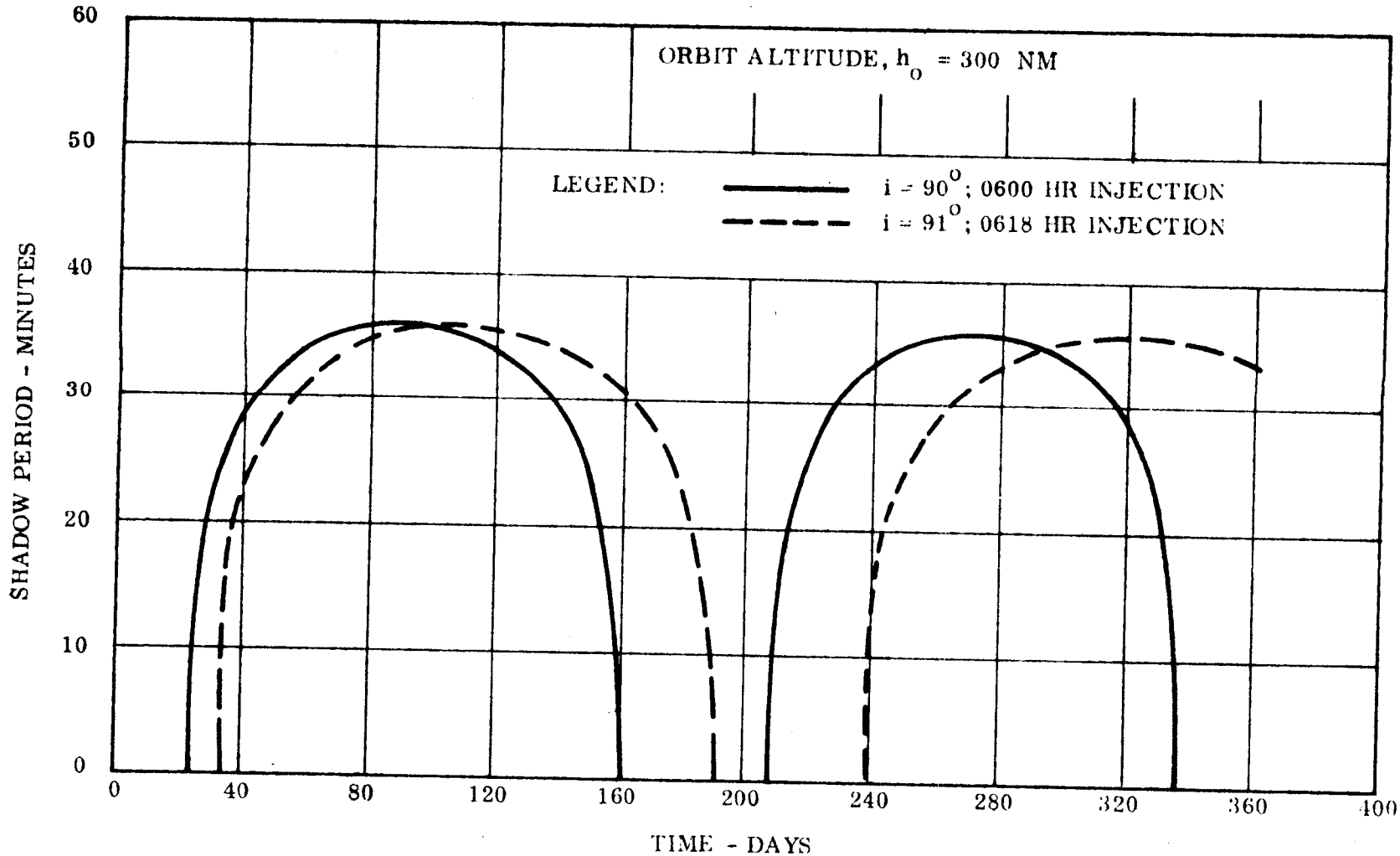


Figure 3-6. Effects of Combined Launch Delay and Inclination Error on Polar Orbit Shadow History

65-32
Vol II

### 3.3.3 SUN-SYNCHRONOUS DAYLIGHT ORBIT

The earth is not spherical but can better be described as an oblate spheroid. If it were a sphere, an orbiting satellite would (in the absence of other perturbing forces such as drag) continue to repeat its trace in inertial space. However, the earth's oblateness causes the orbit to change, and two principal motions can be identified. First, the line of apsides (line through the foci of the ellipse joining apogee and perigee) rotates in the orbit plane. Secondly, and more significant in the present context, is the motion of the line of nodes (axis formed by intersection of equatorial and orbit planes). For an easterly launch (inclination less than 90 degrees) the line of nodes rotates opposite to the earth's axial rotation (nodal regression), while for a westerly launch (inclination greater than 90 degrees) the line of nodes progresses in the same direction as the earth's rotation.

The inclination of a sun-synchronous orbit is given by:

$$i_s = \text{arc cos}\,(-0.4110849 \times 10^{-13}\, p^2\, a^{1.5})$$

Where:

$p = r_p\,(1 + e)$ = Semi-latus rectum

$a$ = Semi-major axis, nautical miles

$r_p$ = Perigee radius, nautical miles

$e$ = Orbit eccentricity

Figure 3-7 shows this function for circular orbits, and Figure 3-8 indicates the effect of orbit eccentricity. From Figure 3-7, it is apparent that increasingly westerly launches are required as orbital altitude increases. This places greater restrictions on a given



107

65-323
VOL II

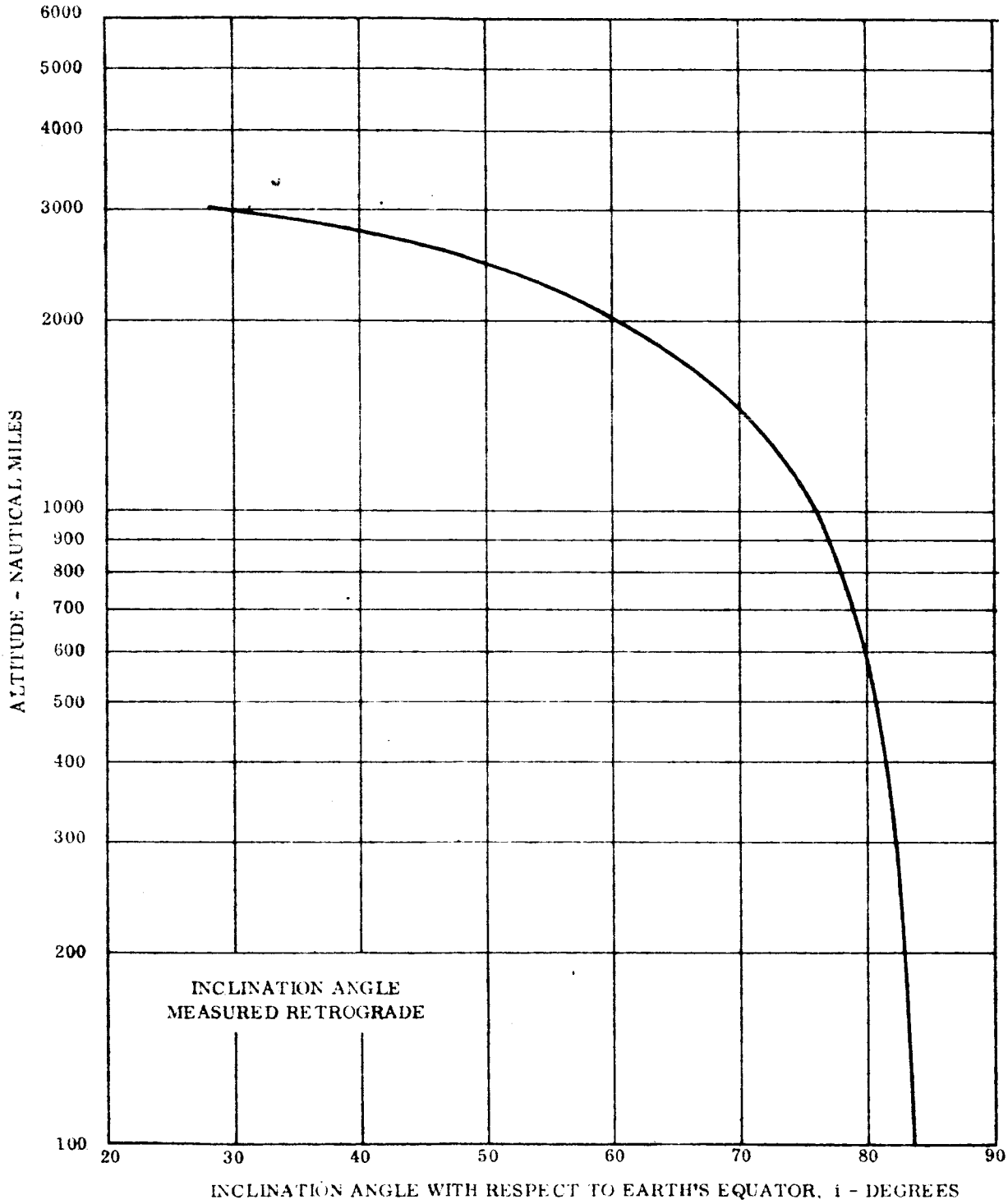


Figure 3-7. Inclination Angle Required to Achieve Sun-Synchronous Orbit for Various Circular Orbital Altitudes



108

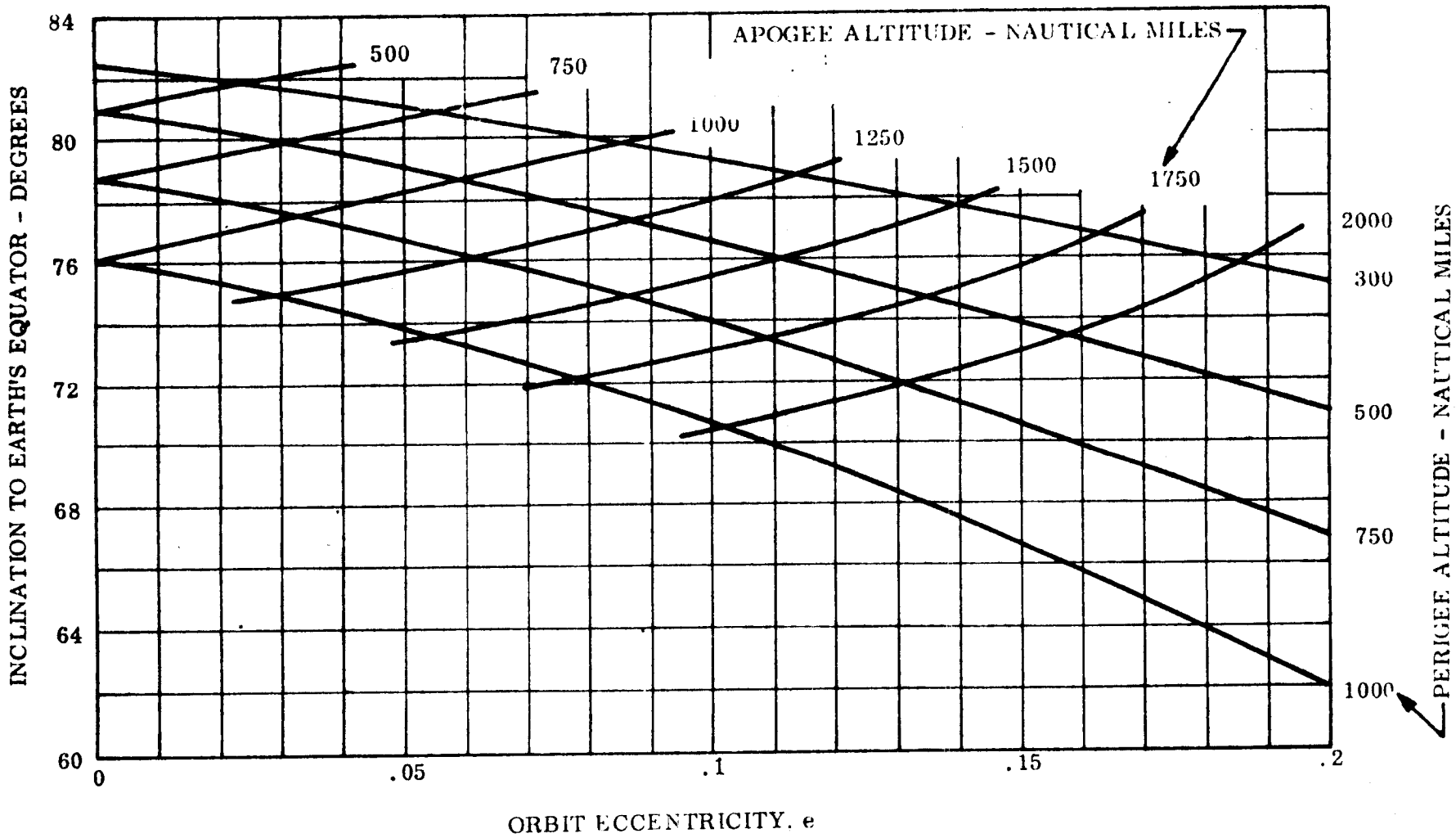


**Figure 3-8.** Retrograde Inclination for Eccentric Sun-Synchronous Orbits

launch vehicle's capabilities, since larger components of the earth's rotational velocity must be overcome.

When the nodal axis of the sun-synchronous orbit is positioned in the plane of the earth-sun vector (this plane being normal to the elliptic), a "noon" or "midnight" orbit results. Since the sun always lies in the orbit plane, then, a constant, maximum shadow history results, as illustrated by Figure 3-9. The Nimbus weather satellite employs such an orbit.

The sun-synchronous "daylight" orbit has its nodal axis positioned in the plane of the earth-sun vector at 6 am and 6 pm local solar time, and the seasonal geometry for this is illustrated by Figure 3-10. The sun, in effect, traverses an angle of 23.5 degrees above and below the equatorial plane during the course of a year. Note the effect of injection time of day on the orbit's inclination to the sun vector; this determines at which solstice the shadow period occurs. From the figure, it appears that increasing the orbital altitude eventually results in a condition where the orbit does not pass through the shadow cylinder at all. There is a "continuous daylight" region, but it is found to have an upper bound since orbit inclination begins to increase rapidly as altitude is increased; this is illustrated by Figure 3-11. The shadow region is determined, as for Figure 3-3, where the orbit inclination with respect to the sun vector $I_s$, at critical solstice, is equal to the retrograde orbit inclination $i_s$ minus the obliquity of the ecliptic ($I_o$ = 23.5 degrees). A region of continuous daylight orbits is found to exist from 825 to 1830 nautical miles. Since an error in inclination (I) of only two degrees results in shadow being encountered, the attainability (in practice) of continuous daylight for periods longer than a year is difficult, requiring very precise injection time and orbit inclination, or on-board propulsion for orbit adjustment.

For altitudes other than the continuous daylight band, a single shadow spike is encountered during the course of a year, as illustrated by Figure 3-12.

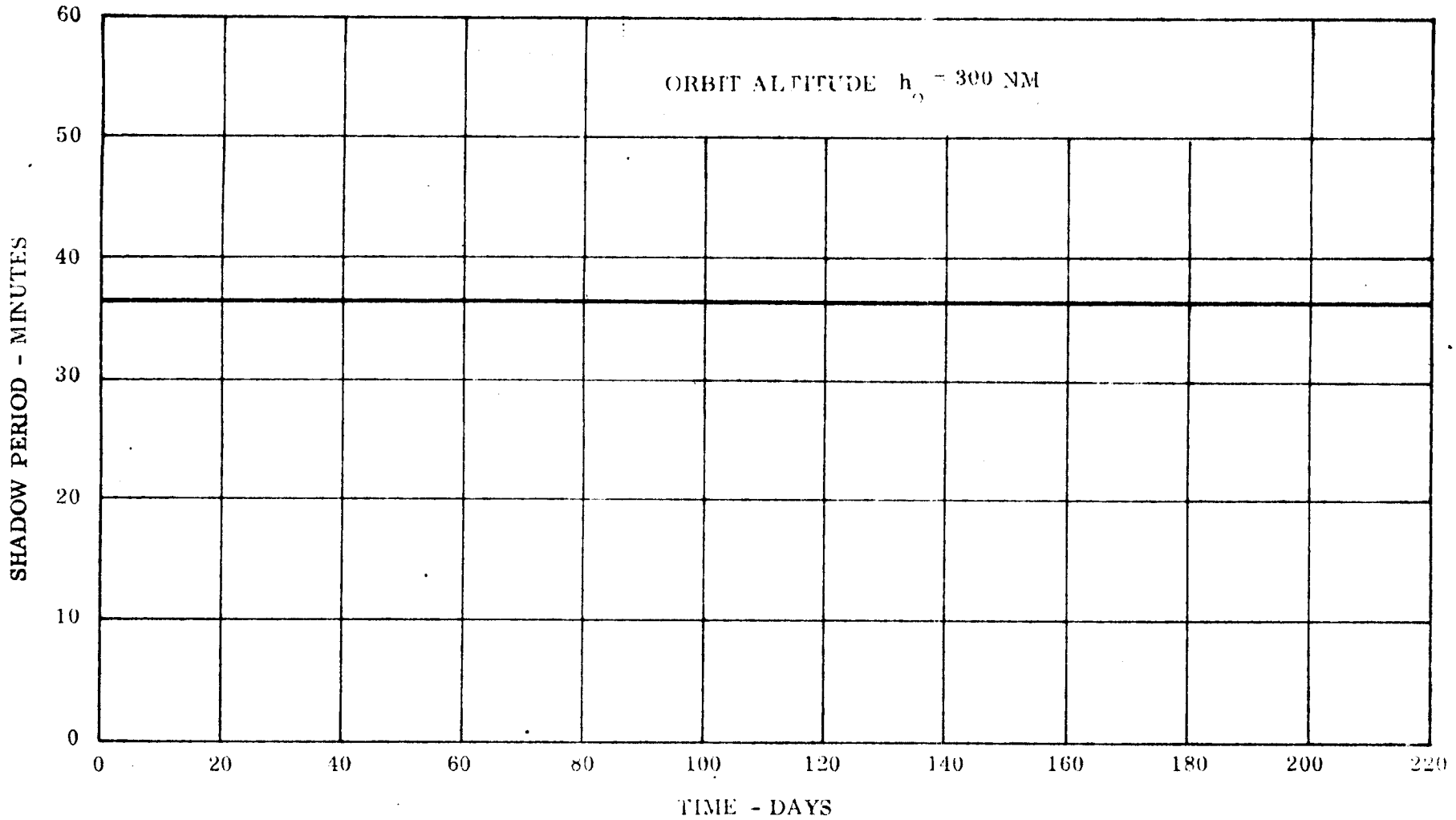


Figure 3-9. Shadow History for Sun-Synchronous Noon or Midnight Orbit

Vol. II

65-323
VOL. II

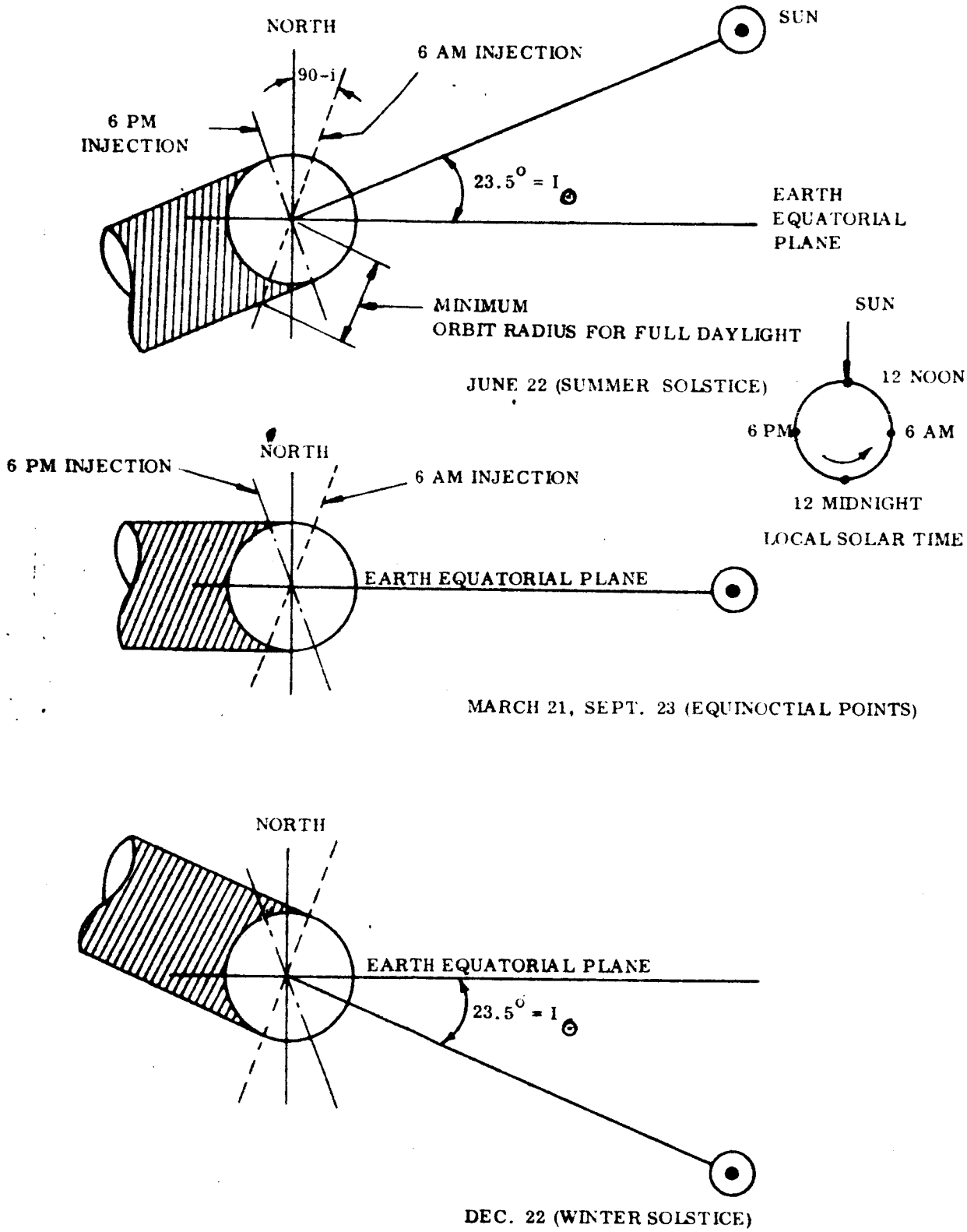


Figure 3-10. Seasonal Geometry for Sun-Synchronous Daylight Orbit

VOL II 65-323

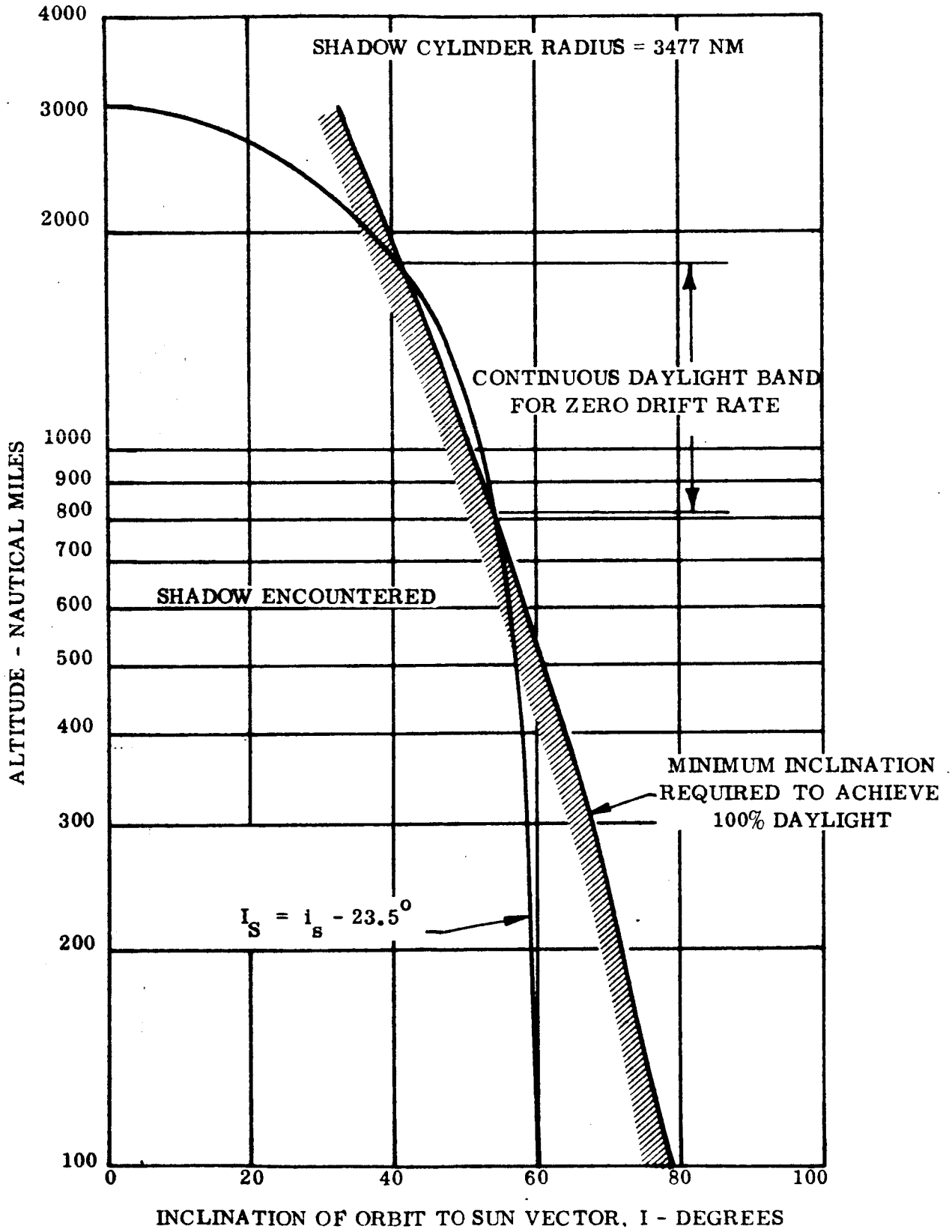


**Figure 3-11. Region of Continuous Daylight for Sun-Synchronous Daylight Circular Orbits**

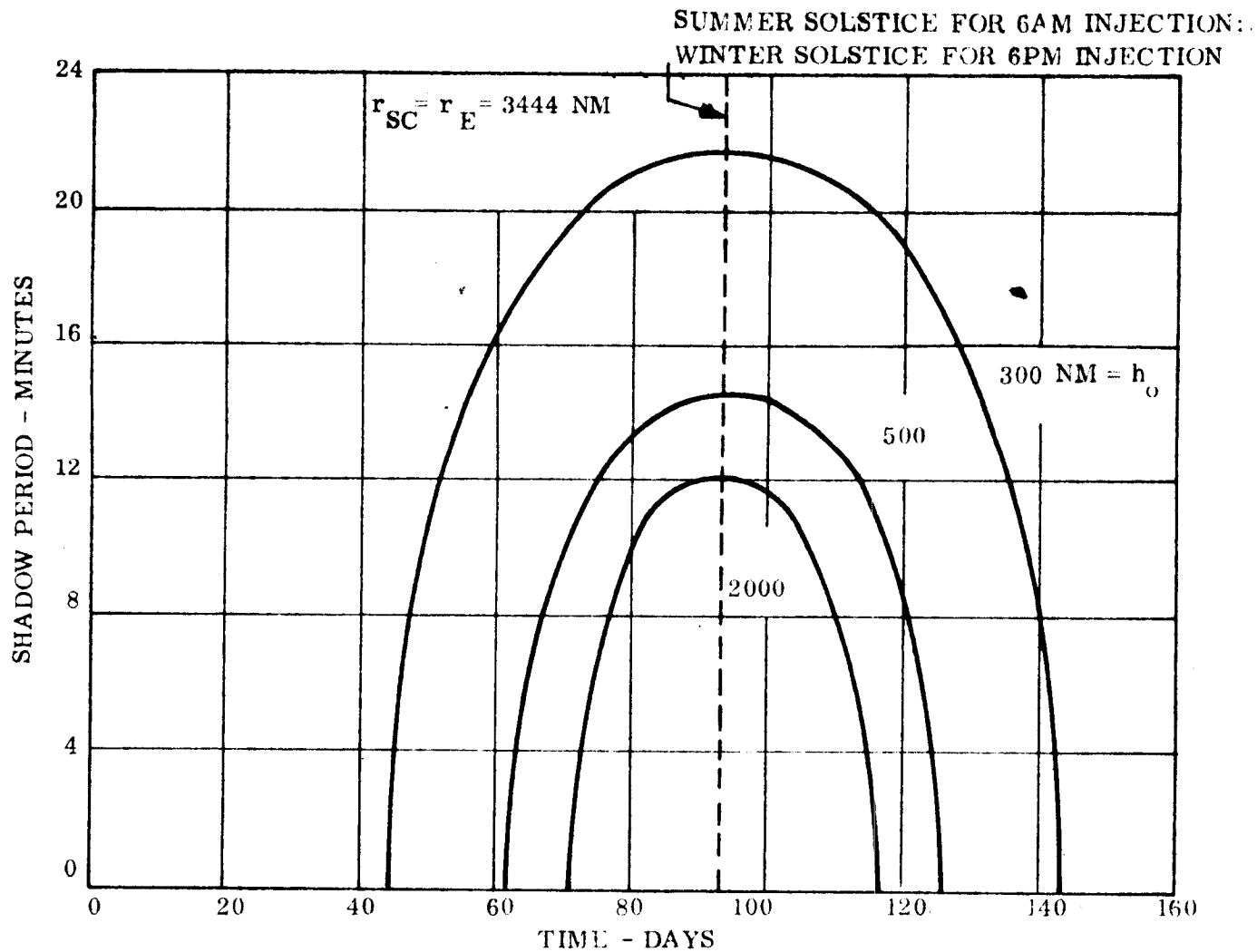


Figure 3-12. Shadow History for Sun-Synchronous Daylight Orbits

The chief sources of error in establishing sun-synchronous orbits are launch delays on the pad and injection inclination errors. The nodal axis will be initially misaligned by 15 degrees per hour of launch delay and will drift out of phase by up to 50 degrees per year per degree error in inclination as shown in Figure 3-13. Figure 3-14 indicates that inclination error can greatly increase shadow duration. Also, it will be shown in Section 3.3.4 that the time of shadow initiation can be affected significantly in some cases. Launch delays affect the magnitude, duration and time of shadow initiation (as illustrated by Figure 3-15). The combined effects of an 18-minute launch delay and one degree inclination error are shown in Figure 3-16. An earlier launch date would tend to magnify the effects of inclination error. An initial full daylight period of six months can readily be obtained before a shadow period is encountered.

### 3.3.4 MODIFIED SUN-SYNCHRONOUS ORBIT (MSO)

From the preceding discussion, a 1000-nautical mile altitude appears attractive for a sun-synchronous daylight orbit. This altitude is well within the capability of the more attractive launch vehicles as was shown in Section 2. This is a reasonable altitude from the communications standpoint. However, there is a potential problem with this orbit altitude. It is possible at this altitude, if the proper inclination is achieved, to have the spacecraft remain in continuous daylight for a very long period of time. Of course, this requires a very precise orbit injection and the period over which this continuous daylight can be maintained decreases as the errors in orbit injection increase. Although initially continuous daylight is desirable, it would also be advantageous to introduce a shadow period at some point during the mission life (one year) of the spacecraft. The time at which a shadow period is introduced can be easily controlled by a slight increase or decrease in inclination such that the nodal rate is perturbed sufficiently to induce shadow at the desired time. Figure 3-17 illustrates the effect of orbital inclination on the time shadow begins. The curve is almost symmetrical about the sun-synchronous inclination, so that in effect, two daily launch window regions are exhibited. The region of lower inclination is preferable, being less westerly and hence slightly easier for the launch vehicle to attain.

65-323
Vol II

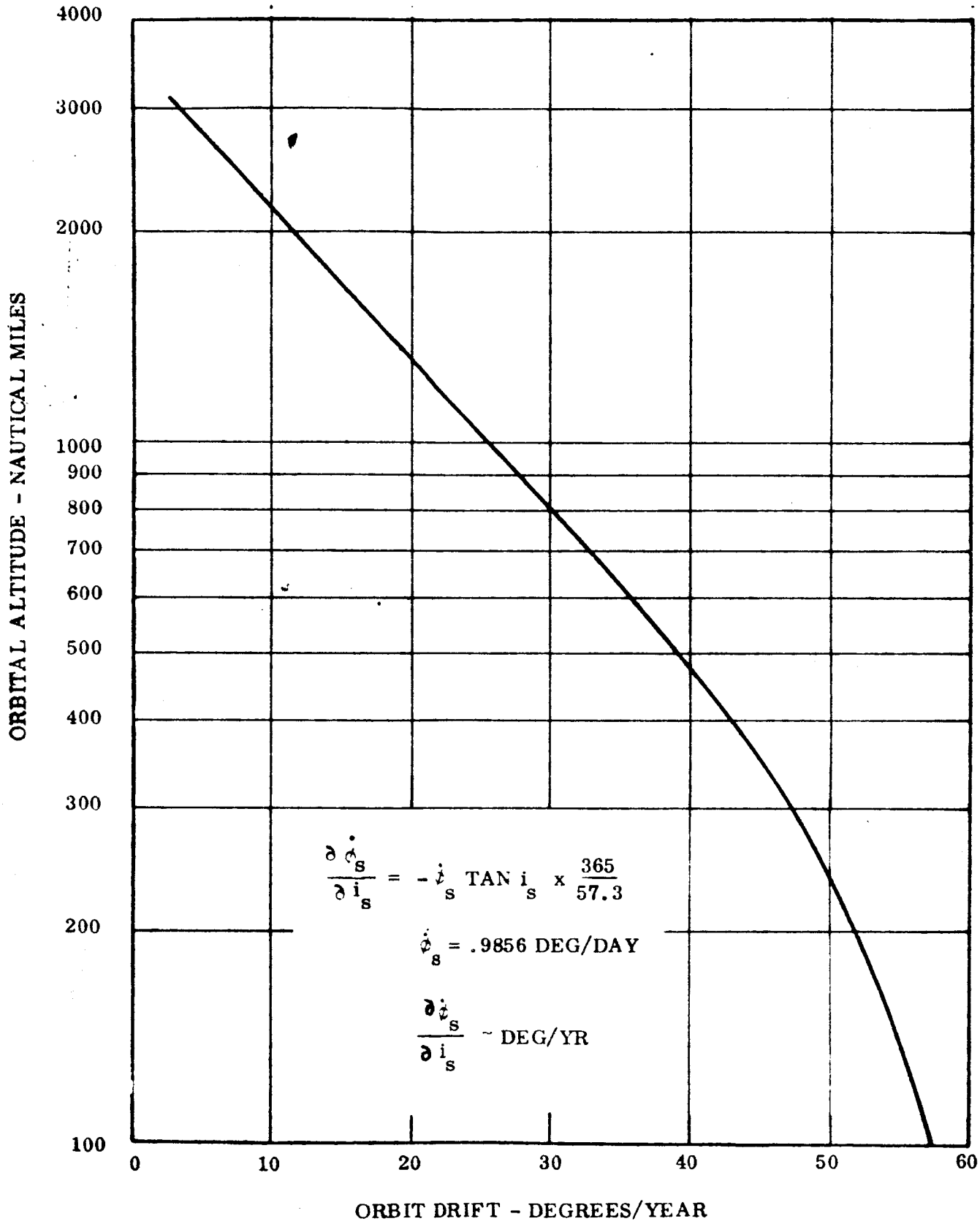


**Figure 3-13. Yearly Drift of Sun-Synchronous Circular Orbits Due to Inclination Error**



116

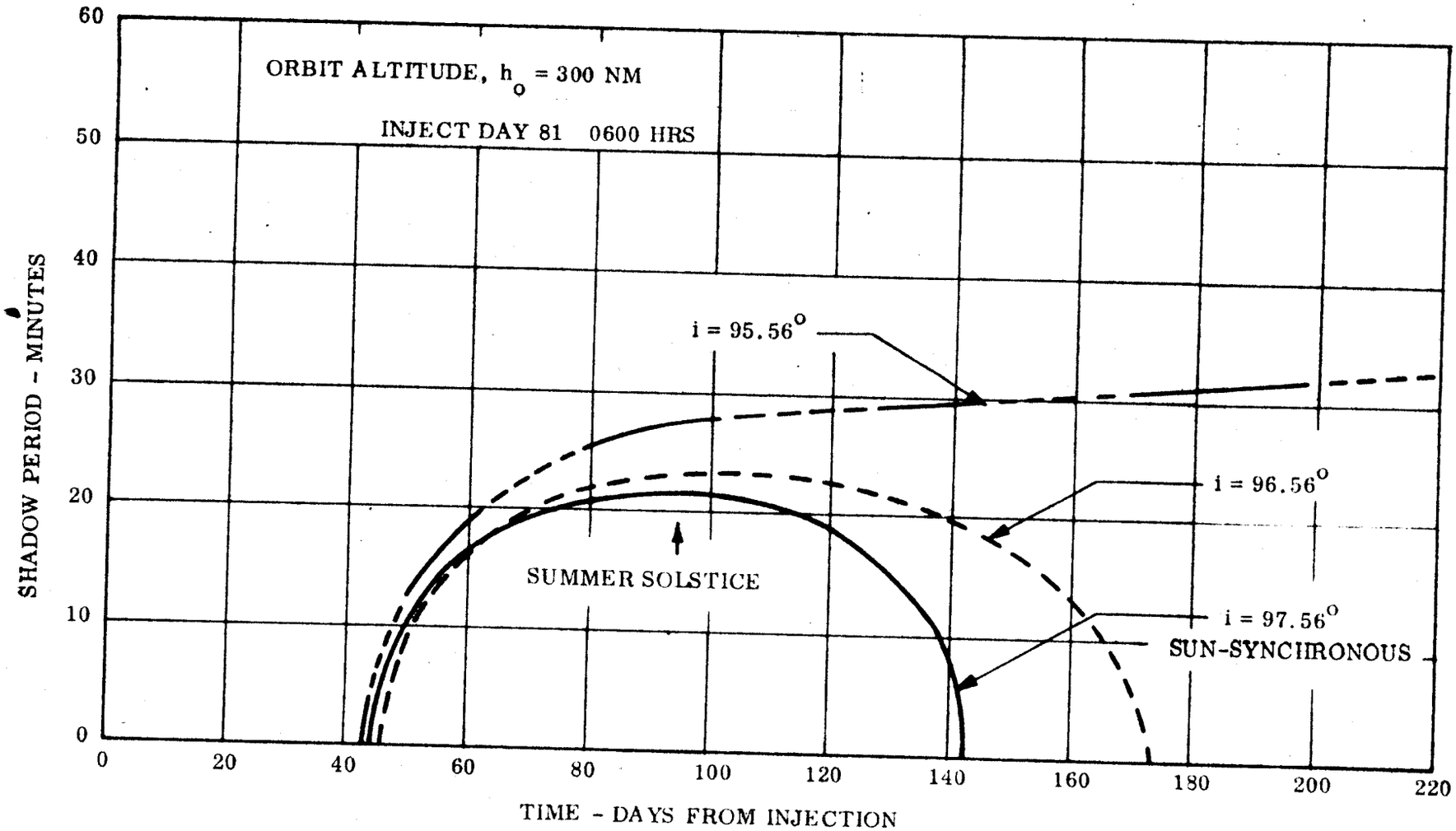


Figure 3-14. Effects of Inclination Error on Shadow History for Sun-Synchronous Orbits

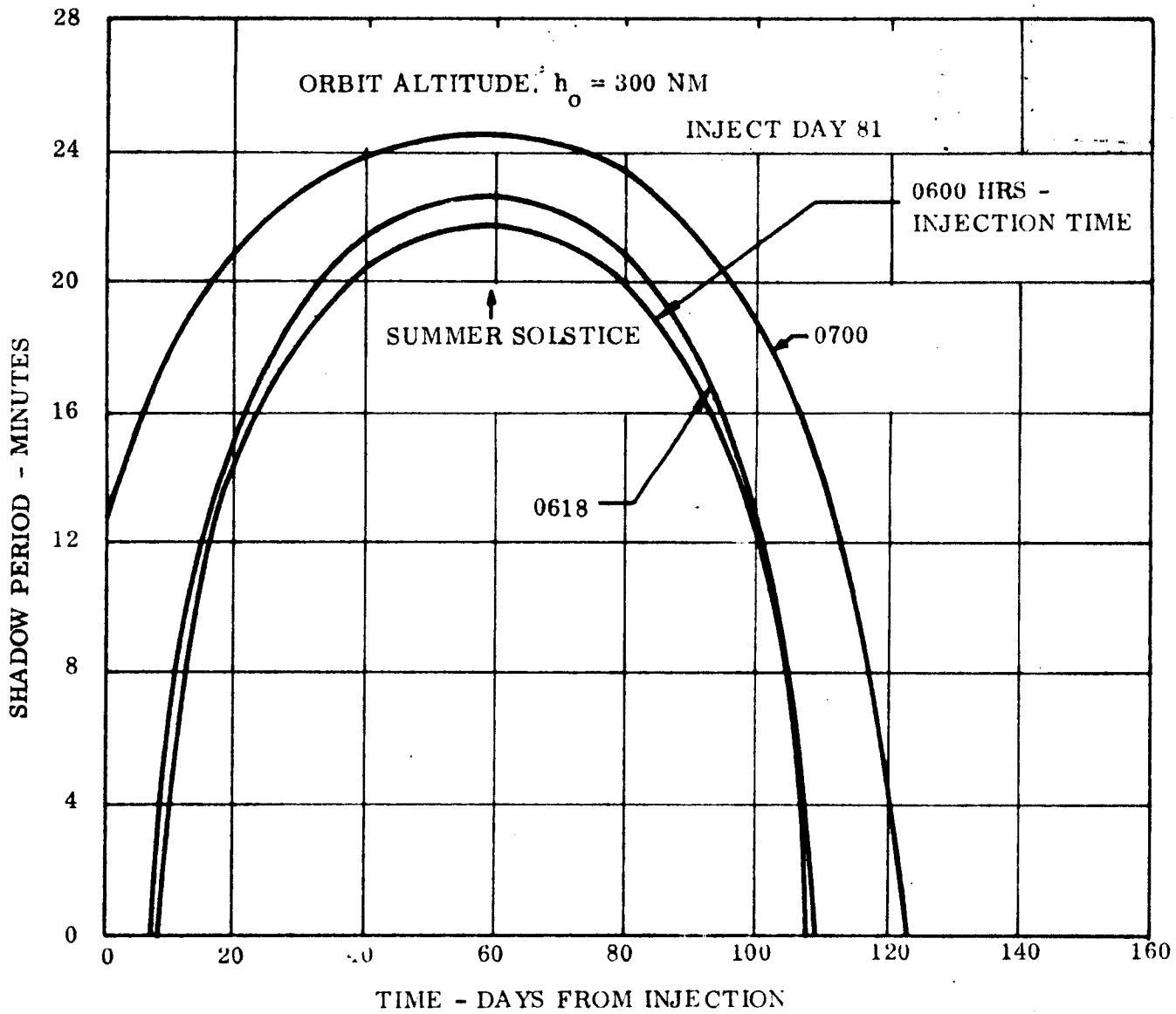


Figure 3-15. Effects of Launch Delay on Shadow Histories for Sun-Synchronous Orbits

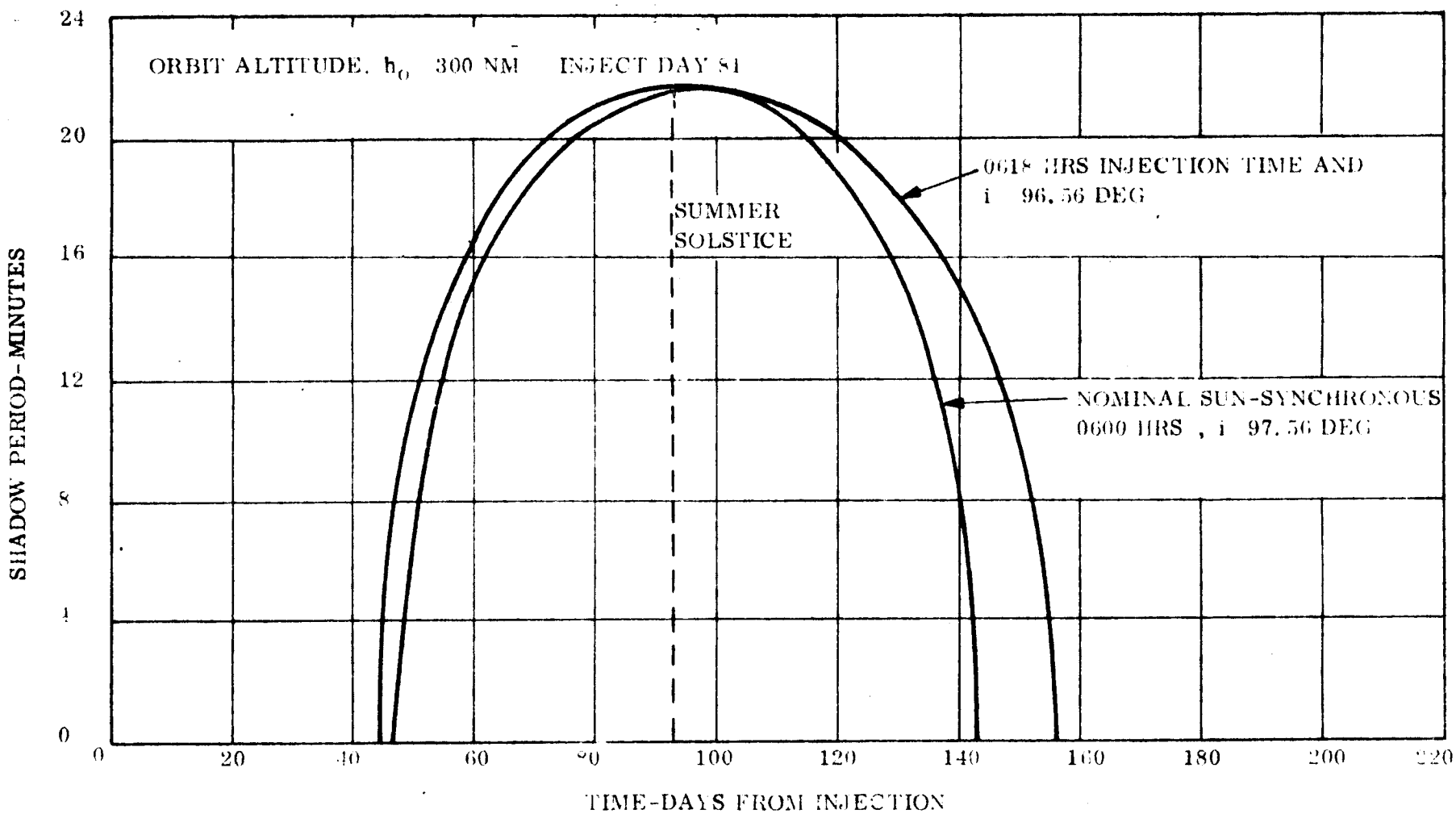


Figure 3-16. Effect of Combined Launch Delay and Inclination Errors on a Typical Sun-Synchronous Orbit

65-323
VOL II

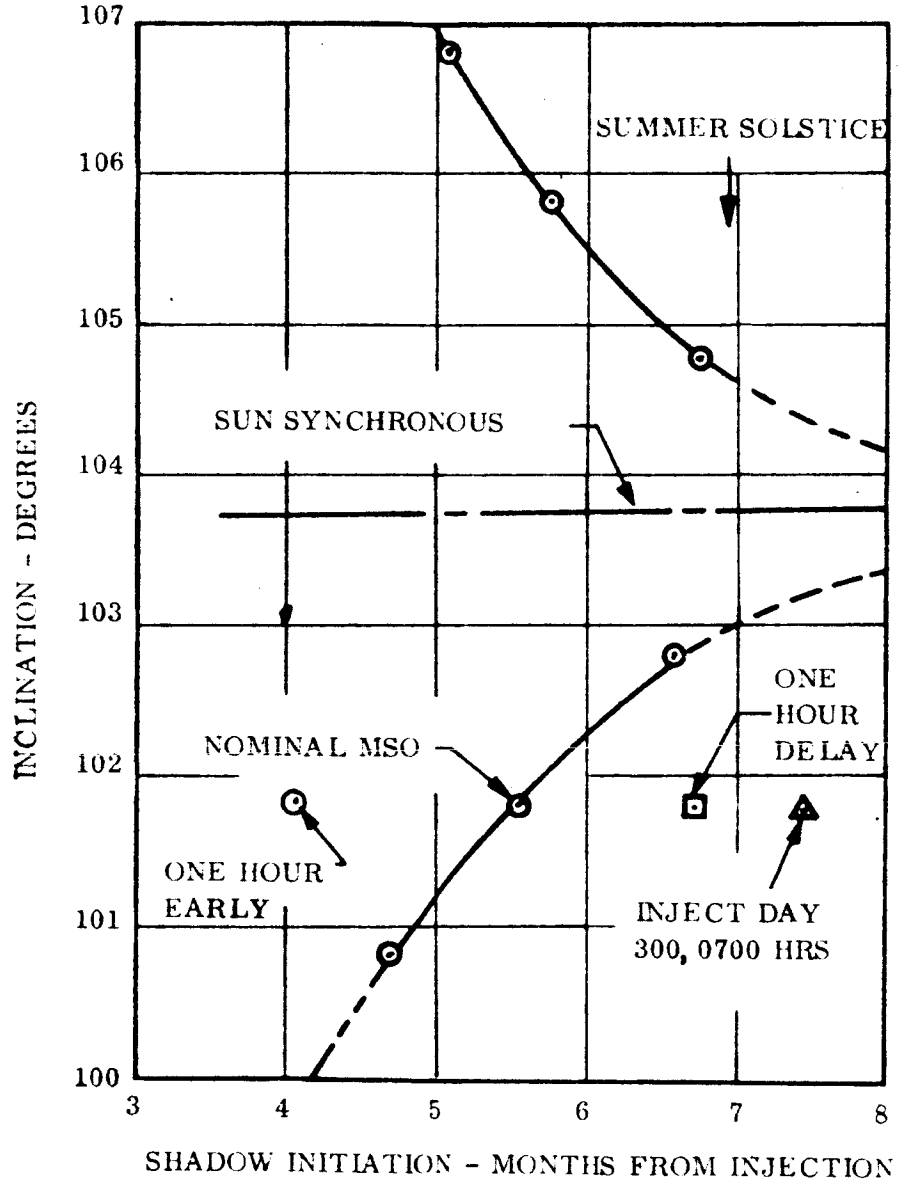


Figure 3-17. Modified Sun-Synchronous Orbit Preliminary Launch Window



120

65-323
Vol II

For the present, assume that approximately a six-month, continuous daylight period is desired. From Figure 3-17 an inclination of 101.84 degrees will provide 5.6 months of initial shadow-free operation. This could be adjusted in future iterations; however, a more comprehensive picture of the launch window should be sought first. This is likely to prove quite costly in computer time, and is beyond the scope of the present study.

Reasonable three sigma injection errors will not unduly affect shadow initiation time. For a ± 1.0 degree inclination error shadow can initiate from 4.7 to 6.6 months from injection. For a ±1.0 hour variation in injection time shadow can initiate from 4.1 to 6.8 months after injection, and a ±1.0 degree inclination error does not increase this period. The four error points shown on Figure 3-17 represent, in effect, an injection error ellipse.

Injection day 330 (November 26) was chosen because it occurs approximately seven months before summer solstice. If injection had occurred 30 days earlier, shadow would have initiated about three quarters of a month later as shown by Figure 3-17 (the point shown is for 0700 hours which corresponds to the one-hour delay point for day 330). This occurs because the solstice is correspondingly later, although the drift has accumulated for a month longer. Again, further studies are required to better define this aspect.

Shadow histories for the nominal and deviant orbits are given in Figure 3-18. As expected, as the sun-synchronous condition is approached, the shadow period and duration are shorter.

### 3.3.5 ELLIPTICAL ORBIT WITH A HIGH LIGHT-TO-SHADOW RATIO

The principal advantages of a highly elliptical orbit are the high percentage of orbit period spent in daylight and the opportunities the wide extremes in orbit altitude afford for making scientific measurements. For example, an elliptical orbit with an apogee of 25,000 nautical miles and a perigee of 200 nautical miles can easily be obtained with the majority of the launch vehicles discussed in Section 2. A typical shadow history for such an orbit is given in Figure 3-19. An orbit inclination of 45 degrees was selected because it yields an orbit from which valuable scientific measurements can be made of such phenomenon as the Van



121

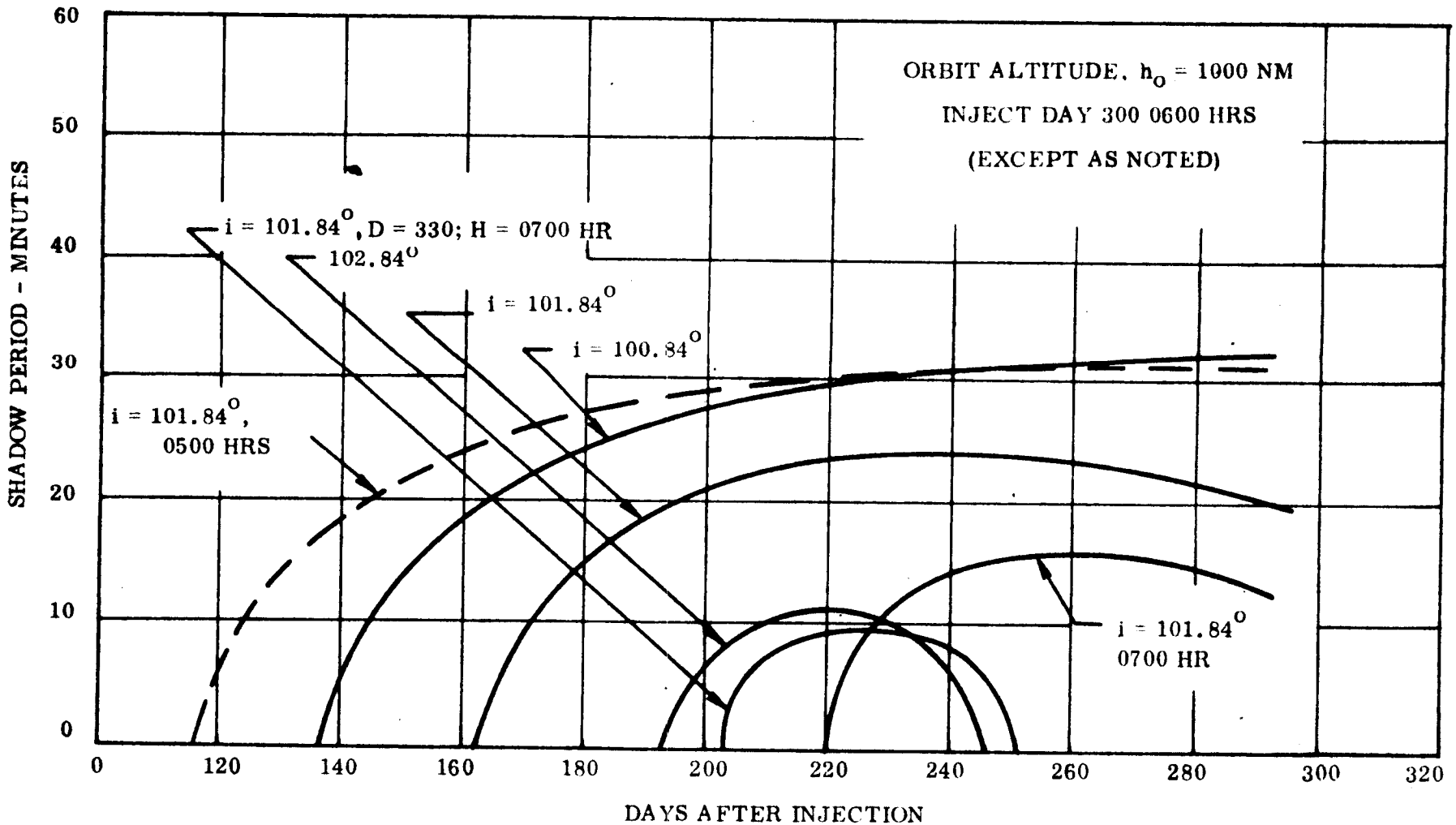


Figure 3-18. Shadow Histories for Nominal and Deviant Modified Sun-Synchronous Orbits



VOL II 65-323

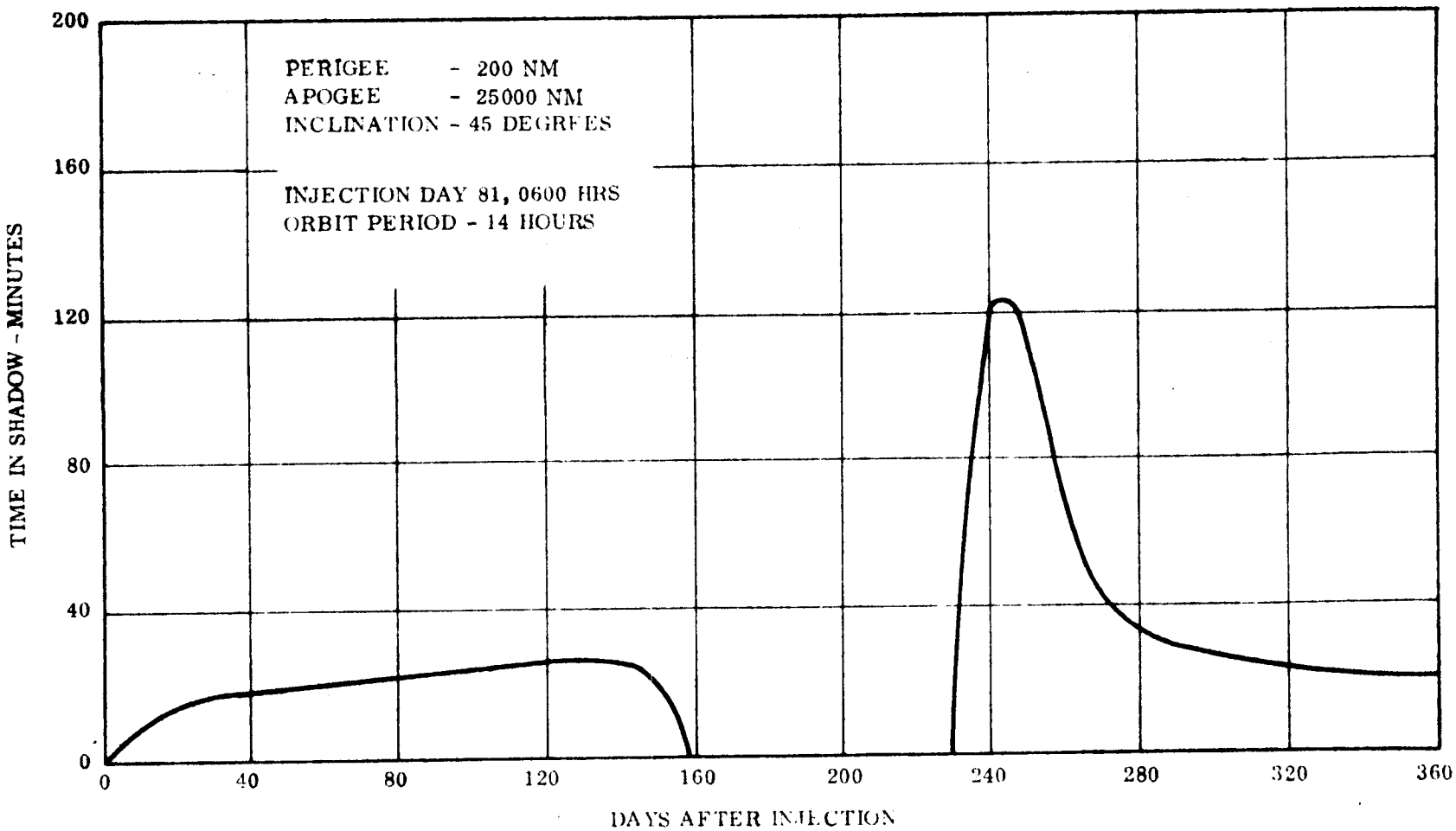


Figure 3-19. Shadow History for Elliptical Orbit

65-323
Vol II

Allen radiation belt and the earth's magnetic field. This orbit has a period of 14 hours. For at least 12 of the 14 hours, the spacecraft is always in daylight. However, shadow periods can be as long as two hours which is not desirable. The range of orbit altitude variation will allow measurements to be made across the entire Van Allen radiation belt.

Figure 3-19 indicates that it may be possible to obtain a shadow free period of approximately two months duration. However, expected injection errors would probably wash this out.

Shadow histories for elliptical orbits tend to be somewhat erratic in form (Reference 3-2) due to the nodal and apsidal rates. Therefore, the shadow history given in Figure 3-19 should not be considered representative for other elliptical orbits.

### 3.3.6 STATIONARY EARTH SYNCHRONOUS ORBIT

The synchronous circular orbit in the equatorial plane with its 24-hour period appears to a ground observer to remain stationary. It is thus an ideal communications relay, since fixed ground station antennas are possible. Relay III is an example of this application.

Figure 3-20 shows the characteristic shadow history for stationary earth synchronous satellites. These results are independent of the time of day at which orbit injection occurs. Twin peaks of 70 minutes maximum period occur in the spring and fall with about 20 days duration. For inclined, synchronous circular orbits a similar situation exists except that the peaks occur at the solstices. A period of almost five months in full daylight can be obtained prior to initiation of a shadow period. This is considered advantageous but the long (1.17 hours) shadow periods are a definite disadvantage for a solar thermionic flight experiment application.

The attainment of stationary earth synchronous orbits, in practice, is a very complex and expensive undertaking. A simplified launch sequence is described here. A multi-stage launch vehicle injects the spacecraft into an elliptical orbit with an apogee altitude of

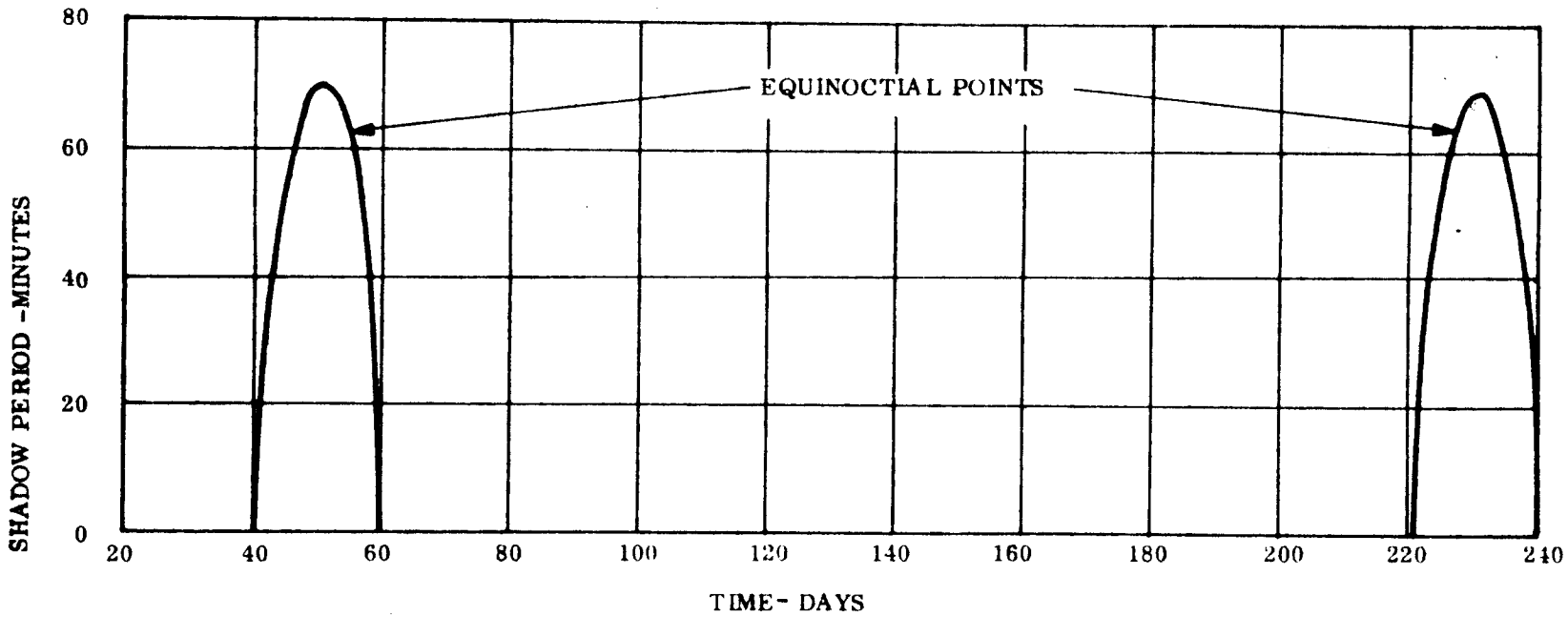


Figure 3-20. Stationary Orbit Shadow History

65-323
001 II

approximately 19,300 nautical miles and a 30 degree inclination. Propulsion on the spacecraft then simultaneously circularizes the orbit and performs the plane change necessary to bring the orbit into the equatorial plane. A slight undercorrection is made in period so that the spacecraft drifts into its correct longitudinal station. A low thrust device on the spacecraft then serves to stop the drift and later perform station keeping as the satellite is perturbed from its position due to the earth's elliptical shape at the equator and solar gravitational effects.

To obtain this orbit, velocities considerably in excess of escape velocity are required. Therefore, except for the solar probe case, this orbit has the largest booster requirement of the orbits under consideration. Based on the results of Section 2, an ATLAS-AGENA D vehicle is needed to achieve a stationary earth synchronous orbit.

### 3.3.7 SOLAR PROBE ORBIT

A detailed study of solar probe orbits has been made by the General Electric Spacecraft Department in connection with the NASA-AMES Solar Probe Studies. A summary of this work is presented in Reference 3-3. The principal feature of this class of orbits, for a solar thermionic experiment, is the capability to achieve continuous daylight for indefinite periods. The solar probe orbit is also of great scientific interest. Its major disadvantage is the large variation encountered in solar intensity throughout the orbit.

As indicated in Section 2, this type of orbit requires at least an ATLAS-AGENA D launch vehicle, preferably with the addition of the X-259 as a third stage. Figure 3-21 indicates the perihelion obtainable with the ATLAS-AGENA D-X-259 and the ATLAS-CENTAUR-X-259 launch vehicles. The ATLAS-AGENA D without the third stage X-259 can only obtain a perihelion of approximately 0.55 AU with a 350 pound payload. To obtain the maximum scientific return, it is essential that the spacecraft pass as close to the sun as possible. For this reason, the addition of a third stage to the ATLAS-AGENA D is considered highly desirable. The ATLAS-CENTAUR-X-259 is not recommended because of the priority and availability problems associated with the CENTAUR stage.

65-323
Vol II

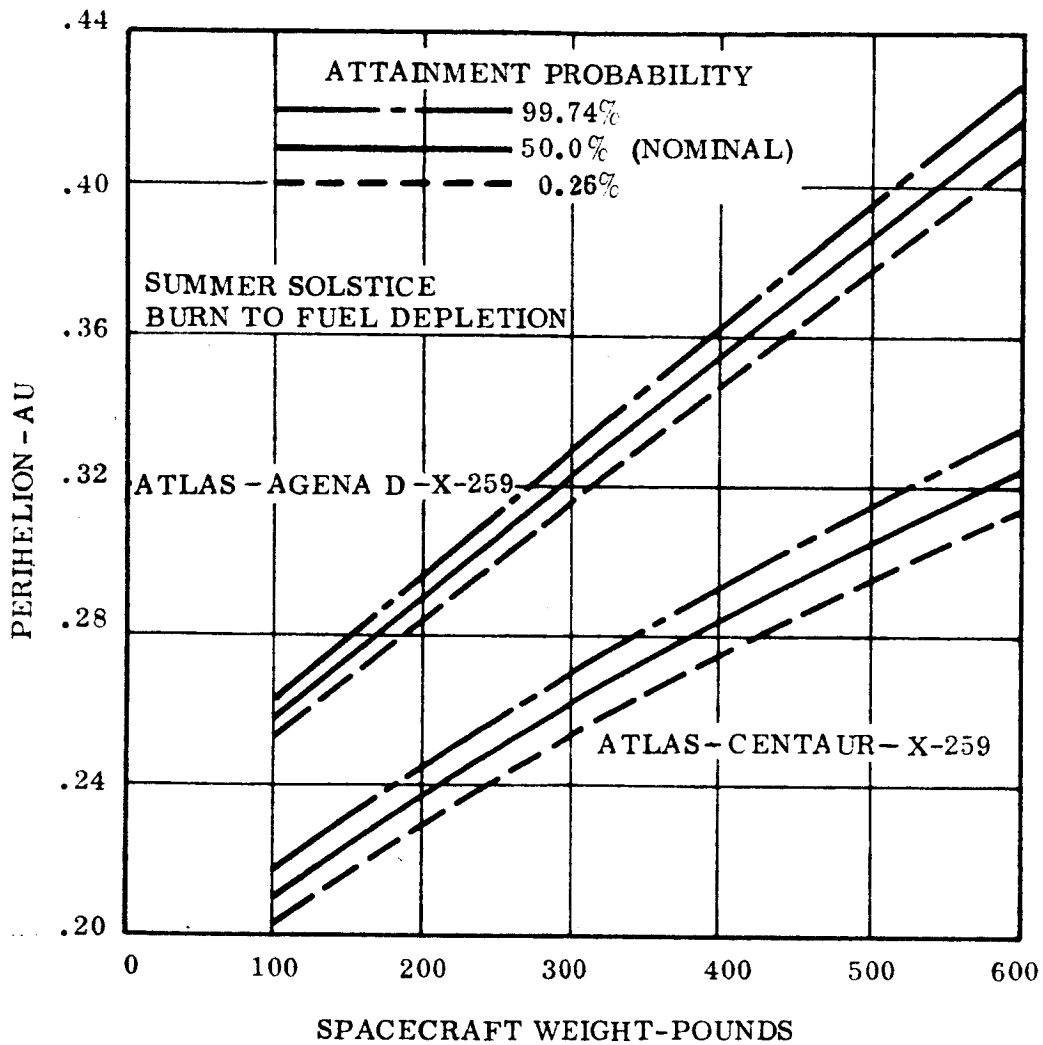


Figure 3-21. Perihelion Performance vs. Spacecraft Weight for Solar Probe Orbit

A typical solar probe orbit is shown in Figure 3-22. A rotating, sun-centered coordinate system is employed such that the earth-sun line remains fixed.

## 3.4 COMMUNICATIONS CONSIDERATIONS

The Deep Space Instrumentation Facility (DSIF) and the Satellite Tracking and Data Acquisition Network (STADAN)* represent the two ground networks available for handling the telemetry, tracking and command functions. These ground station facilities are described in Section 10 (Volume III). Considering the extent of these networks, it is obvious that adequate coverage can be assured for a spacecraft in any of the orbits previously discussed. However, it is desirable to have as few ground stations as possible involved. This will reduce the chances of priority problems, simplify the operation and greatly reduce the cost of data acquisition and reduction. It would be ideal if the telemetry, tracking and command functions could be handled from one station. The spacecraft would not have to be observed by this station on every orbit, since some onboard data storage is possible. Of course, onboard data storage increases the spacecraft weight and power requirements. There is obviously a compromise between the number of ground stations required and the increase in spacecraft weight and power requirements. This trade-off is treated in Section 10 (Volume III).

Of the orbits considered, three types, the stationary earth synchronous, circular polar, and circular sun-synchronous appear to offer the best opportunity for operating with one ground station. Obviously, the stationary earth synchronous, because of its stationary position with respect to the earth, represents the simplest orbit from the communications standpoint. Only one ground station is required and fixed antenna positions can be employed.

*The STADAN network represents a recent combination of the Minitrack Stations and the Wideband Data Acquisition Net. There are fifteen ground stations in this network.

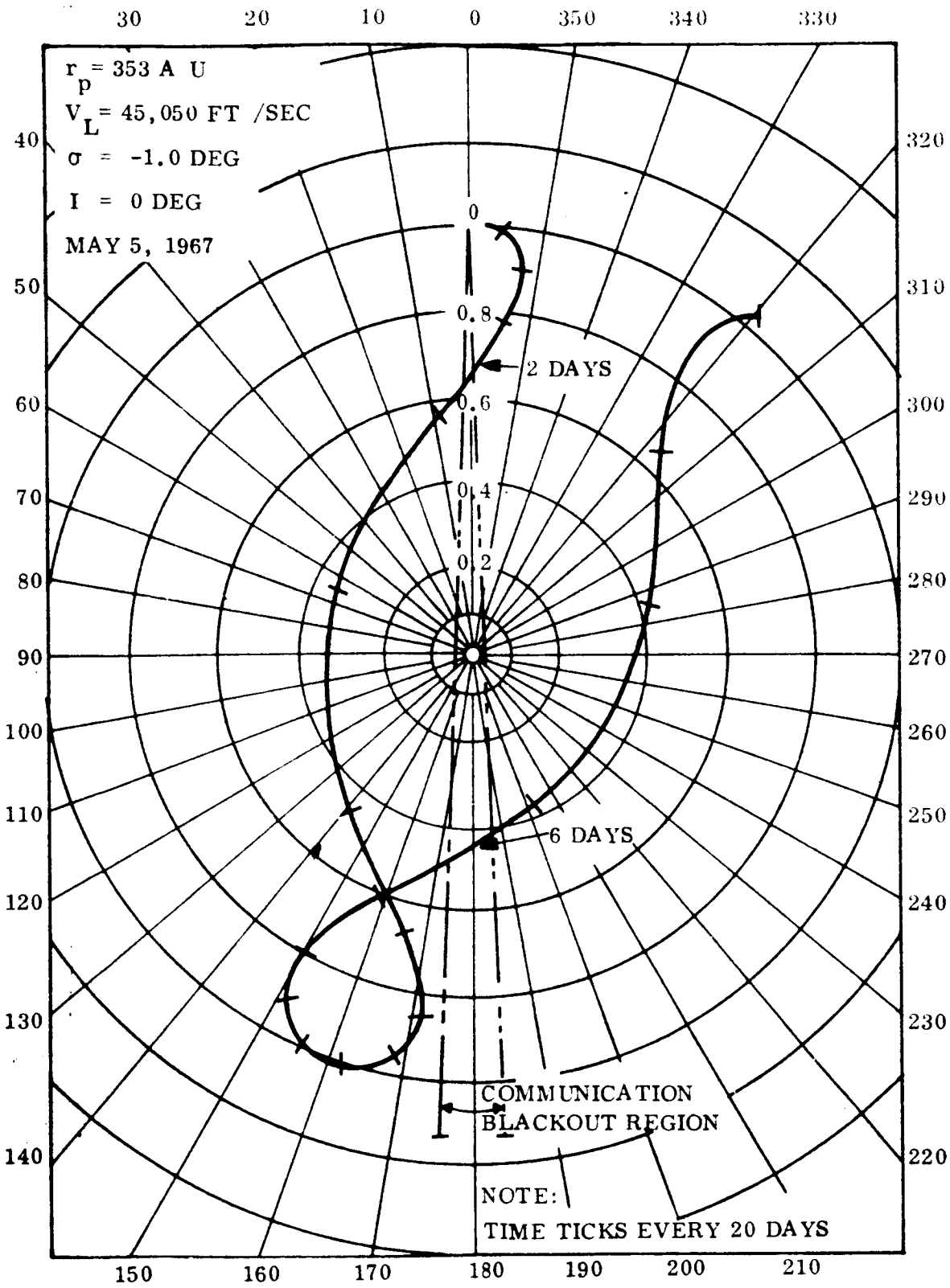


Figure 3-22. Ecliptic Trajectory in Rotating Sun-Centered Coordinate System Using ATLAS-AGENA D-X-259

65-323

The circular polar and circular sun-synchronous orbits do not provide the simplicity of communications of the stationary earth synchronous orbit, but they do offer promise of operating with only two (possibly one) ground station and some data storage onboard the spacecraft. Figure 3-23 illustrates this quantatively. These approximate "gap" (orbits not visible) curves were obtained graphically for zero minutes time in view by drawing tangents to the station visibility ellipse from the North Pole (for polar orbits; actual orbit traces were used for non-polar orbits). The angle from the two tangency points subtended at the pole, divided by 180 is taken to be the fraction of visible orbits. This is somewhat optimistic since the satellite may have just passed the point where its orbit plane becomes tangent to the visibility ellipse and in fact require almost another full revolution to become visible. Subtracting from unity gives the fraction of orbits which are not visible, and multiplying this by the number of orbits per day gives the gap values plotted in Figure 3-23, which are a measure of the number of orbits in a given day when communication is possible.

Since a minimum of ten minutes of time in view is a more realistic limitation, considering acquisition and readout time, a corresponding gap curve was computed using an approach similar to that described above and the results are also presented in Figure 3-23. While the results presented in Figure 3-23 are slightly optimistic, they provide a simple, common basis for comparison purposes. Polar orbits show less gap than the sun-synchronous class. Polar orbits above 1000 nautical miles are visible for at least 10 minutes on every orbit, while sun-synchronous orbits are visible approximately half the time. A data storage requirement of about six hours can be inferred for the latter case, which is not an excessive requirement. Utilization of a second ground station located approximately 90 degrees in longitude from the first would greatly reduce the data storage requirement.

For various reasons, the remaining orbits are not exceedingly attractive from the communications standpoint. Because of its low altitude, the 325-nautical mile circular orbit has very short line of sight times with any given ground station. For this reason, numerous ground stations would be required to perform the telemetry, tracking and command functions.

65-323
Vol. II

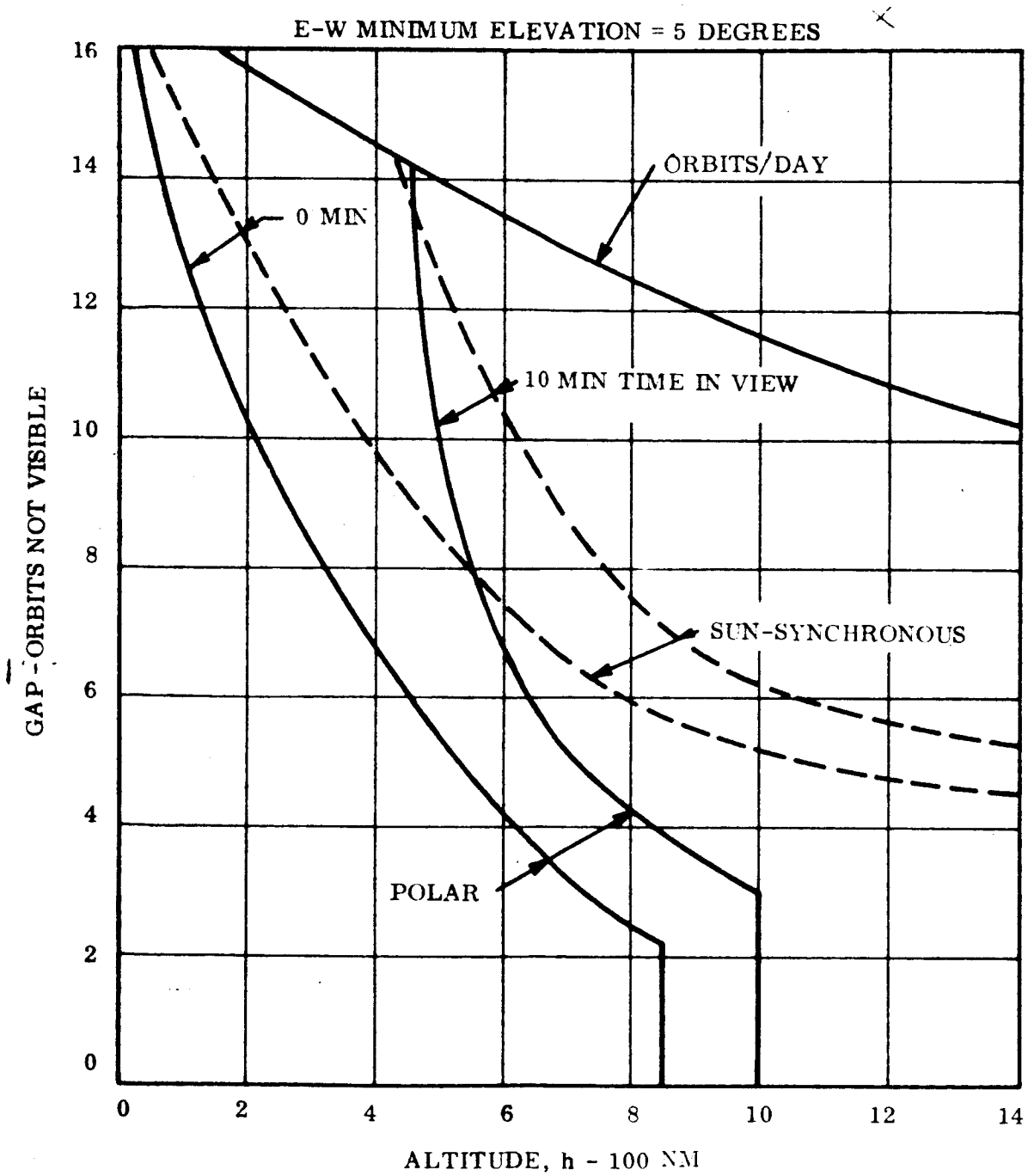


Figure 3-23. Communications Gap as a Function of Altitude for Circular Orbits

65-323

Vol II

Highly elliptical orbits offer a difficult communications problem because of their wide variation in orbit altitude. The spacecraft power required for communications varies as the slant range distance squared. Therefore, for a 200 by 25,000 nautical mile elliptical orbit, the power required to communicate at perigee is 2190 times greater than that needed at apogee (this assumes the same data rate). As a result, communication with the spacecraft is generally confined to orbit altitudes near perigee or low data rates at altitudes near apogee. Of course, at the lower altitudes, the spacecraft velocity is high and the line of sight time for a given station is short. This coupled with the high nodal and aspidal rates associated with elliptical orbits results in a requirement for numerous ground stations.

For all of the orbits considered, except the solar probe class, the communication functions would be handled by the STADAN Network (See Section 10-Volume III). However, a solar probe orbit would require the DSIF Network for communications. This is considered a major disadvantage of a solar probe orbit because of the priority problems associated with use of the DSIF Network. In the 1967 to 1969 time period, the DSIF will be deeply involved with the APOLLO Program and the chances of using these facilities for a program of this type seem remote.

One final orbit selection criterion can be established in connection with communications. This factor may be termed the semi-synchronous criterion. Figure 3-24 indicates the orbital altitudes for this case. The potential advantage of a semi-synchronous orbit is that if a favorable ground pattern is initially established, it will thereafter continue. The disadvantage is that, lacking station keeping, the orbit will drift, so that extended periods of unfavorable position will occur. For the present, it is felt that the disadvantage is predominant and semi-synchronous altitudes should be avoided. Orbits which begin to repeat in two, three, or more whole number of days also exhibit synchronism, but the signficance of these harmonics for the present application remains to be established.

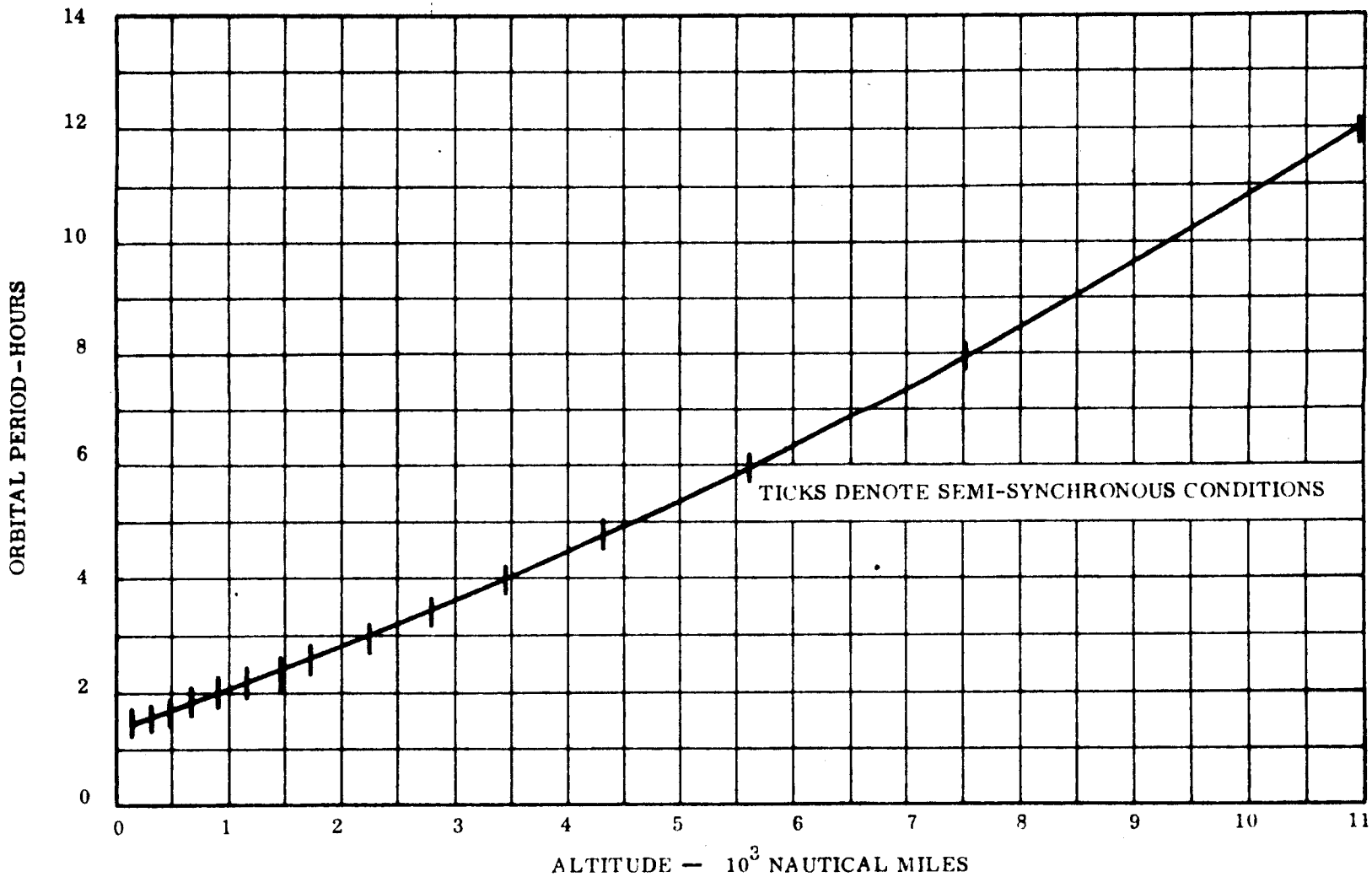


Figure 3-24. Semi-Synchronous Circular Orbit Conditions

65-3[illegible]
Vol II

## 3.5 LAUNCH VEHICLE REQUIREMENTS

The most attractive launch vehicles for achieving the various orbits under consideration were identified in Section 2. The results of the orbit analysis do not alter any of these initial conclusions.

## 3.6 SUMMARY AND CONCLUSIONS

To investigate, in detail, each of the orbits under consideration would constitute a very extensive analysis which is beyond the scope of this study. However, the depth of analysis presented here identifies the predominant advantages and disadvantages of each type of orbit; permitting selection of the most attractive orbits for a solar thermionic flight experiment. This analysis is also performed in sufficient detail to provide the basic orbit information (orbit period, maximum shadow period, etc.) needed for the conceptual spacecraft design phase. Having identified the most desirable orbit or orbits, a more detailed analysis will be required to better define the effects of launch window, orbit inclination, orbit injection errors, etc.

Although a solar thermionic experiment could be conducted from any of the orbits considered, some are definitely better suited than others. The modified sun synchronous orbit (1000 -nautical mile altitude and 101.84-degree inclination) is considered the most attractive orbit for the first solar thermionic flight experiment. Its major advantage is that it permits the first phase (up to approximately six months) of the experiment to be conducted in continuous sunlight with a shadow period being introduced in the latter phase. Having a shadow free period initially, eliminates numerous problems* associated with thermal cycling of the spacecraft and, therefore, maximizes the chances of conducting a successful experiment. In addition, this orbit provides a shadow period in the latter phase of the experiment so that the effect of dark periods can also be evaluated. This feature

*These problems are outlined in Section 6.

of the modified sun-synchronous orbit sets it apart from the other orbits and makes it a highly desirable selection for the first flight of a solar thermionic system. In addition, this type of orbit can be obtained with a low cost, reliable DELTA class launch vehicle. This orbit is also attractive from the communications standpoint since it appears that a maximum of two, and perhaps only one, ground station will be required to handle the telemetry, tracking and command functions. The only major disadvantage of this orbit is that the 1000 - nautical mile altitude places the spacecraft in a very severe portion of the Van Allen belt. This implies weight penalties associated with oversizing the shielding the solar cell array and perhaps shielding some of the more sensitive electronic components.

Since they have equal altitudes (1000 nautical miles) and nearly equal inclinations (90 and 101.84 degrees) the circular polar orbit is very similar to the modified sun-synchronous orbit. The polar orbit can be obtained with the same launch vehicle employed with the modified sun-synchronous orbit. The communication situation is slightly better with the polar orbit since only one ground station is required compared with two (maximum - may need onle one) for the modified sun-synchronous orbit. The major difference between these two orbits is that the polar orbit does not appear to permit a shadow free period of more than one or two months (six months can easily be obtained with a modified sun-synchronous orbit) and a detailed study of the effects of inclination error and launch pad holds may reduce this further. For this reason the modified sun-synchronous orbit is preferable. Since these two orbits are almost identical in all other respects, there is no advantage to considering the polar orbit further.

Next to the modified sun-synchronous orbit, a highly elliptical orbit appears the most suitable for a solar thermionic experiment. However, this type of orbit is considered far less attractive than the modified sun-synchronous orbit. An elliptical orbit with a perigee of 200 nautical miles and an apogee of 25,000 nautical miles is selected because it is within the capability of the IMPROVED DELTA launch vehicle which affords low cost, high reliability and maximum thermionic concentrator diameter. These altitude extremes also allow the spacecraft to make measurements completely through the Van Allen belt.

An orbit inclination of 45 degrees was chosen because this passes the spacecraft through interesting areas of the Van Allen radiation belt and Earth's magnetic field. The major advantage of the elliptical orbit is the long period and high light to shadow ratio. The selected orbit has a period of 14 hours, of which 12 or more are always spent in daylight. Thus, long light periods are provided for operation of the solar thermionic experiment and the long orbit period reduces the number of thermal cycles (approximately 625 light-dark cycles per year). It appears that a initial shadow free period of two months maximum might be obtainable, but inclination errors and launch pad holds would probably reduce or eliminate this entirely. The maximum two-hour shadow period is not desirable since the power requirements during the dark must be supplied by rechargeable batteries which implies significant weight penalties. In addition, the lengthy dark period may cause thermal control problems.

Of the five basic types of orbits considered, the 325 nautical mile circular orbit is ranked third in order of preference. Actually, this orbit is not attractive for this application but as described below, it is more suitable than the stationary earth synchronous or solar probe orbits. The 325 nautical mile circular orbit has no significant advantages other than it can be achieved with any of the launch vehicles considered. Of course, this means a DELTA class vehicle could be used which affords low cost and high reliability. However, this orbit has numerous disadvantages. First, it makes very inefficient use of any of the launch vehicles that might be used because they all have significantly greater boost capability than this type of orbit requires. Since a 325 -nautical mile circular orbit has a short period (1.61 hours) the spacecraft will be subjected to considerable thermal cycling (approximately 5450 light-dark cycles in a one year period). This short period also means that the "line of sight" times from ground stations is very short. This necessitates the use of numerous ground stations to handle the communication functions. Finally, the 325-nautical mile circular orbit is of least scientific interest since, relative to the other orbits, more scientific measurements have been made in this altitude range.

The stationary earth synchronous orbit has two major advantages. First, it provides a significant (five months) shadow free period and secondly, because of its fixed position

with respect to the earth, all communications can be handled from one ground station. In spite of these two highly desirable features, the stationary earth synchronous orbit, primarily because of the complexity and expense associated with establishing and maintaining it, is not considered attractive for the first solar thermionic flight experiment. This orbit also has other disadvantages. It requires an ATLAS-AGENA D launch vehicle which, compared with the other boosters considered, is expensive and has relatively low reliability. Since shadow periods of 1.17 hours duration are encountered, significant weight penalties are expected in connection with the rechargeable batteries necessary to supply the power requirements during shadow. These long dark periods are also likely to create thermal control problems.

Finally, a solar probe orbit is not considered suitable for a solar thermionic experiment. This orbit does offer an opportunity to conduct the thermionic experiment in complete sunlight and to perform important scientific measurements of solar phenomena, but the disadvantages far outweigh these advantages. The major disadvantage of this orbit is the large variation in solar intensity encountered between 1 AU and 0.3 AU. This variation is shown in Figure 3-25 and amount to a factor of 11 to 1 between 1 AU and 0.3 AU. This large difference in available input energy presents a difficult control problem for both the thermionic experiment and the spacecraft solar cell power supply. The varying solar intensity also presents spacecraft thermal control problems. In addition, this orbit has numerous other disadvantages: (1) it does not allow the effect of shadow periods to be evaluated; (2) it requires an unproven, expensive and relatively unreliable launch vehicle; (3) it requires the DSIF Tracking Network which probably means priority problems; and (4) the spacecraft design is complicated by the need for a directional antenna.

In summary then, of the five basic types of orbits considered, the modified sun-synchronous orbit (1000 - nautical mile circular orbit with an inclination of 101.84 degrees) is considered the most attractive for the first solar thermionic flight experiment. The highly elliptical orbit (200 - nautical mile perigee by 25,000 - nautical mile apogee with an inclination of 45 degrees) and the 325 - nautical mile circular orbit (30-degree inclination) represent the second and third orbit selections respectively. The latter two orbits are considered far less attractive compared to the number one selection.

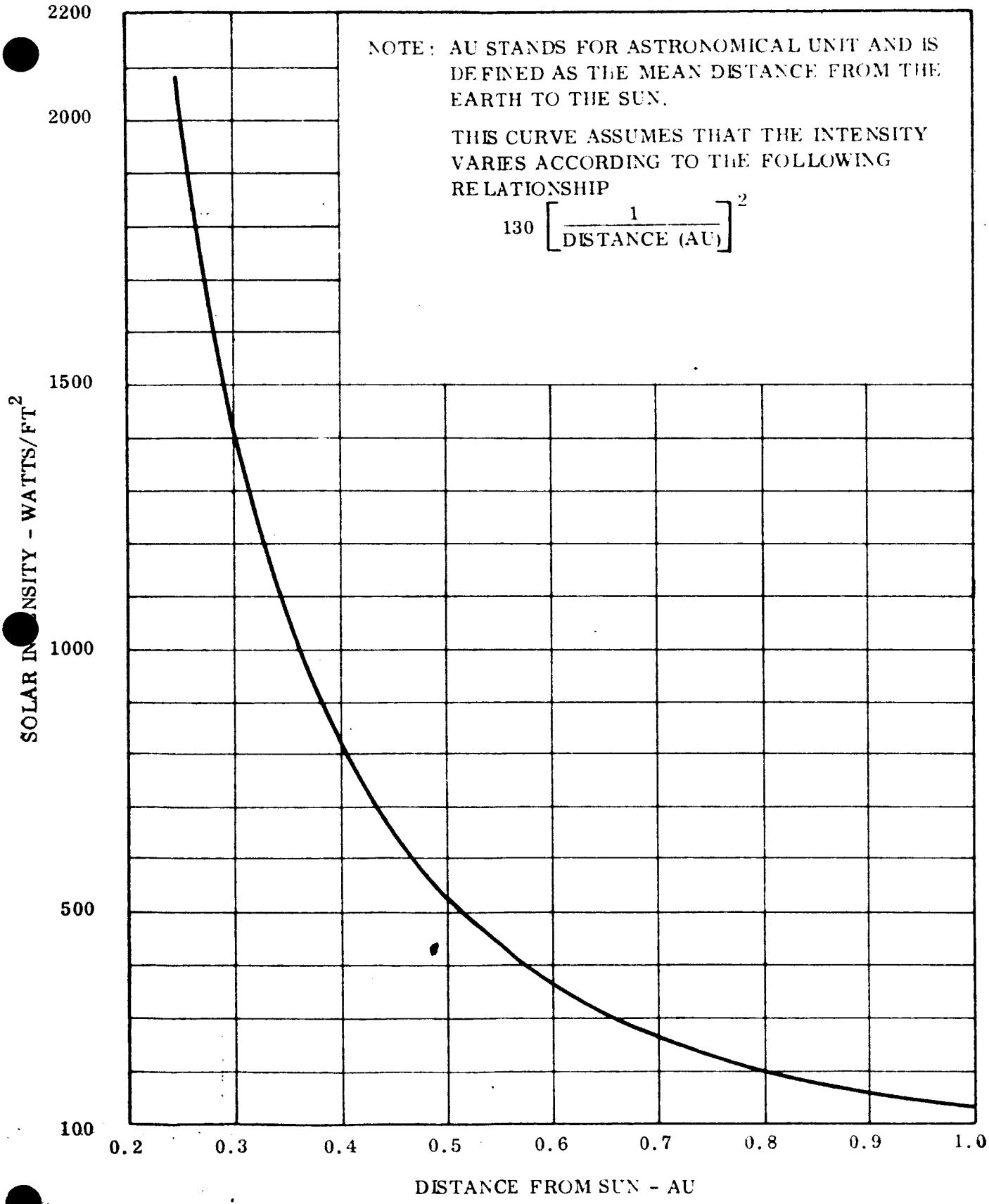


Figure 3-25. Solar Intensity vs. Distance From Sun

## 3.7 REFERENCES

3-1 E. A. Strawbridge, "Digital Computer Program for the Shadow History of a Satellite," General Electric, Missile and Space Division, Report No. TIS 62SD184, July, 1962.

3-2 "Flight Performance Handbook for Orbital Operations", John Wiley and Sons, 1963.

3-3 B. A. Galman, M. M. Levinson, and J. J. Weinstein, "Solar Probe Orbit Design," AIAA Paper No. 64-646, 1964.

65-323

Vol. II

SECTION 4

# SOLAR THERMIONIC SYSTEM PERFORMANCE

PRINCIPAL CONTRIBUTORS:

Dr. P. Brosens
E. W. Williams
L. L. Dutram

140

65-323
Vol II

# SECTION 4

# SOLAR THERMIONIC SYSTEM PERFORMANCE

## 4.1 INTRODUCTION

This section establishes the solar thermionic system performance on which this study was based. The performance estimates presented are considered achievable for a 1967 flight date.

For the mission analysis phase, these performance estimates were used to determine the generator power output as a function of concentrator diameter. Concentrator diameter was then directly related to launch vehicle fairing diameter; thus, defining, for a given launch vehicle, the maximum generator power output. Since a study ground rule required the thermionic generator to produce a minimum of 100 watts, this information was necessary in selecting the launch vehicle.

For the purpose of making performance estimates, the solar thermionic system was treated in three major parts: (1) thermionic converters, (2) generator structure, and (3) solar concentrator. The performance for each of these components is presented in the following sections.

## 4.2 THERMIONIC CONVERTER PERFORMANCE

The performance of the thermionic converters depends heavily on the operating temperature of the emitter. In this study, an emitter temperature of 2000$^{\circ}$K was selected for the following reasons.

a. Most of the existing life data on hardware converters has been obtained at 2000$^{\circ}$K.

b. The performance of thermionic converters increases with emitter temperature, however, prolonged operation at temperatures in excess of 2000$^{\circ}$K are known to cause excessive grain growth in the emitter structure which is considered objectionable. Also, at higher cavity temperatures, the attendant decrease in cavity absorber efficiency tends to nullify the improvement obtained in converter performance.



141

All converter performance in the study is based on a 2000°K emitter temperature unless otherwise specified.

### 4.2.1 SELECTION OF EMITTER MATERIAL

Based on power density, reproducibility, and performance stability; tantalum and rhenium represent the most attractive emitter materials at present. A comparison of these materials follows.

#### 4.2.1.1 Thermionic Performance

The selection of 2000°K as the emitter operating temperature makes it attractive to operate at as close a spacing as possible, the minimum value being determined by reliability considerations. State-of-the-art converters, namely the Solar Energy Thermionic series VIII and TE-100's (Advanced Solar Energy Thermionic Converter), operate at nominal values of spacing of two and one mils respectively. Reasonable life testing, of the order of 3000 hours of continuous operation, has been accomplished only on converters with two mil spacing; although no difficulties have yet been encountered on one mil converters. It is because of the considerably larger amount of experience on two mil converters that the recommendation is made here to operate at a value of interelectrode spacing of two mils.

At this value of spacing, the difference between the best performance obtained in tantalum and rhenium converters is small. Figure 4-1 shows the performance of converters VI-S-15 and VIII-F-3 which are those that have exhibited the best performance to date and which have a tantalum and rhenium emitter respectively. These converters have different collector materials, these being tantalum and molybdenum respectively. However, this difference can be neglected, as demonstrated by specific tests on tantalum and molybdenum collectors.

#### 4.2.1.2 Performance Reproducibility and Stability

While the performance levels obtained in the best rhenium and tantalum converters are not materially different, there is considerable difference in both the reproducibility and the stability of converters made with these emitter materials. Table 4-1 shows the performance levels achieved in different converters as measured by Thermo Electron Engineering



142

NASA 65-323
Vol II

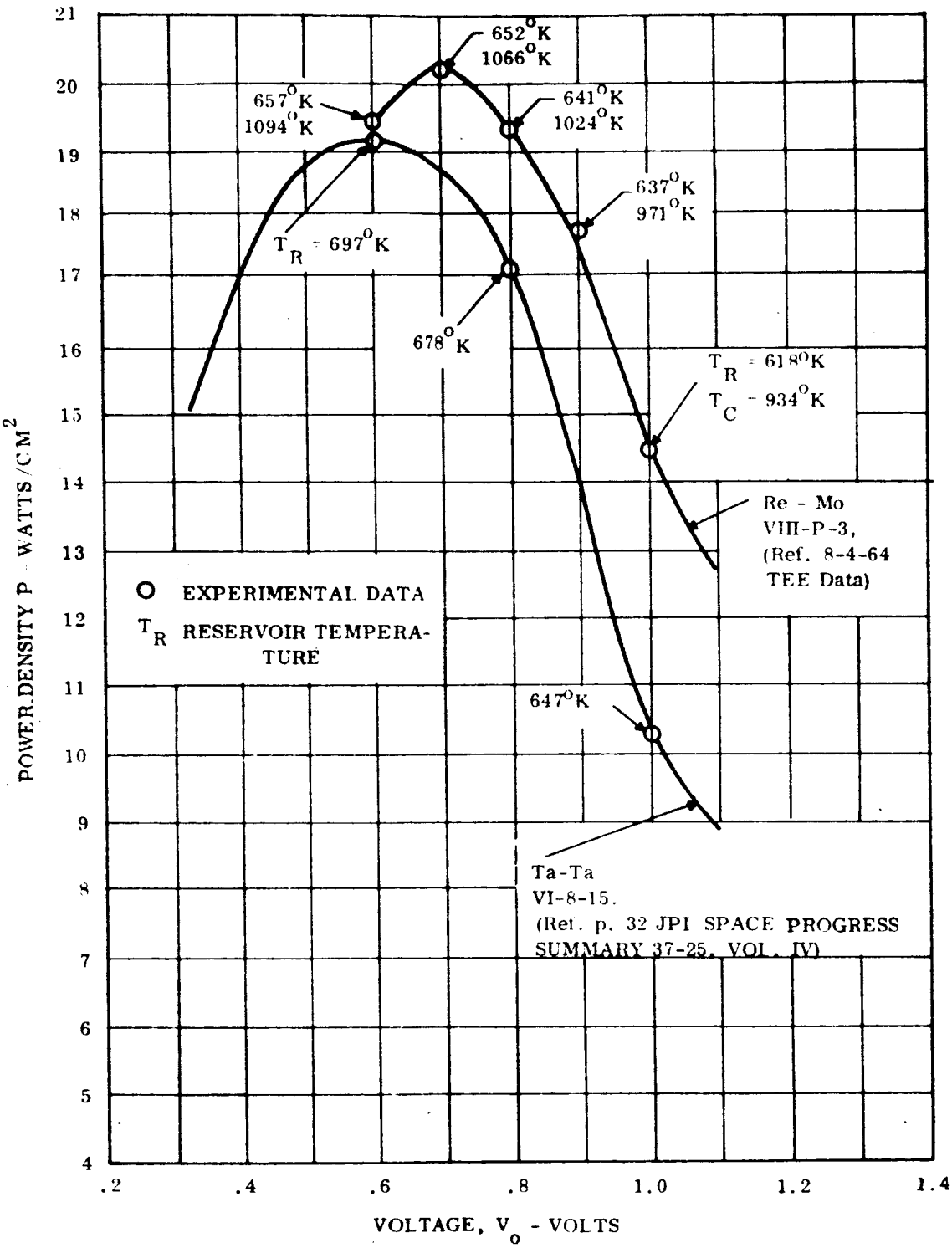


Figure 4-1. Output Power Density of Solar Energy Thermionic Converters With Rhenium and Tantalum Emitters at 2000°K



143

Corporation (TEECO) and JPL. Because of minor differences in emitter temperature measurement techniques, it is not always possible to make a direct comparison between the data measured at the two locations. However, the trend of output variations observed from converter to converter by TEECO and JPL is quite consistent as indicated in Table 4-1. Also, it is apparent in the table that the better the performance, the more difficult it has been to reproduce it. In particular, it may be seen that the performance of VI-S-15, presented in Figure 4-1, is unusually high and has been seldom reproduced. Although only four rhenium converters are listed in the table, it is seen that except for one there is reproducibility within ± 1.5 percent, as compared to a typical value of ± 15 percent for tantalum converters. Converter VIII-P-2b, which does not follow the trend, has been examined and found to have had a contaminated emitter resulting from the use of different fabrication techniques which have since been abandoned.

As far as performance stability is concerned, the lack of standard degradation measurement techniques has made it impossible to gather meaningful records of converter stability. The overall experience may be summarized as follows:

a. Tantalum converters need to be fabricated with exceeding care to avoid performance degradation. Highly refined techniques for cleaning of parts, outgassing and cesium charging have been developed to solve the problem of performance degradation in tantalum converters. The solution has been marginal, because in certain other prototypes degradation has still been observed in spite of the use of such techniques. The rate of degradation is usually of the order of 0.1 to 1 percent per hour of operation, and this rate continues until the output is approximately 1/4 to 1/2 of the initial value at which point the performance levels off.

b. Rhenium converters do not appear to display any degradation. Of approximately 16 converters fabricated to date with rhenium emitters, using standard converter processing techniques and which have been tested for 80 hours or more, none have displayed output variations indicative of a performance degradation problem.

4.2.1.3 Other Comparison Criteria

Table 4-2 lists other desirable properties for an emitter material as well as, indicating which of the two materials considered possesses these properties to a higher degree. The

RE-ORDER No. 65-323
Vol II

Table 4-1. Reproducibility of Solar Energy Thermionic Converter Performance
(Emitter Area = 2 $cm^2$)

| Tantalum Converters Output Current at 1.0 Volt, Emitter Temp = 1700°C | | | Rhenium Converters Output Current at 0.8 Volt, Emitter Temp = 1700°C | | |
|---|---|---|---|---|---|
| Converter | Current Measured at TEECO(AMPS) | Current Measured at JPL(AMPS) | Converter | Current Measured at TEECO(AMPS) | Current Measured at JPL (AMPS) |
| Va | 13.0 | 10.0 | VIII-P-1 | 47.2 | 46.9 |
| Vb | 11.5 | | VIII-P-2a | 47.8 | 50.3 |
| Vc | 12.5 | | VIII-P-2b | 25.6 | - |
| Vd | 13.2 | | VIII-P-3 | 48.5 | - |
| 7007-2 | 12.0 | | | | |
| VI-S-1 | 12.2 | | | | |
| VI-S-2 | 12.4 | | | | |
| VI-R-3 | 12.4 | | | | |
| VI-S-4 | 12.4 | | | | |
| VI-S-5 | 11.7 | | | | |
| VI-R-6 | 12.4 | | | | |
| VI-S-7 | 12.8 | 17.5 | | | |
| VI-S-8 | 12.6 | | | | |
| VI-S-9 | 14.4 | | | | |
| VI-S-10 | 13.8 | | | | |
| VI-S-11 | 15.0 | 17.1 | | | |
| VI-S-12 | 15.0 | | | | |
| VI-S-13 | 15.0 | | | | |
| VI-S-14 | 14.5 | 19.5 | | | |
| VI-S-15 | - | 20.6 | | | |
| VI-S-16 | 14.6 | | | | |
| VI-S-17 | 15.0 | | | | |
| VI-S-18 | 18.7 | 16.6 | | | |
| VI-S-18 | 13.5* | | | | |
| VI-S-19 | 14.0 | 20.5 | | | |
| VI-S-20 | 16.9 | 25.0 | | | |
| VII-S-4 | 19.1** | | | | |
| VII-S-5 | 18.0** | 12.6 | | | |
| VII-S-6 | 14.4 | 11.5 | | | |
| VII-S-7 | 13.0 | 11.1 | | | |
| VII-S-8 | 15.5 | 12.1 | | | |
| VII-S-9 | 12.0 | 8.1 | | | |
| VII-S-10 | 12.0 | 9.7 | | | |
| VII-S-11 | 17.3 | 14.3 | | | |
| VII-S-12 | 17.4 | 12.9 | | | |

Notes

*Measured at 1.0 volt, 1655°C Emitter Temperature
**Measured at 0.8 volt, 1655°C Emitter Temperature



145

Table 4-2. Comparison of Rhenium and Tantalum as Emitter Materials

| Desired Property | Rhenium | Tantalum |
|---|---|---|
| High thermionic performance | B* | - |
| High reproducibility | B | - |
| Low degradation rate | B | - |
| Low required cesium pressure | B | - |
| High thermal conductivity | - | B |
| Low thermal emissivity | - | B |
| Low vapor pressure | - | B |
| Low affinity for trace vacuum impurities | B | - |
| High hot strength | B | - |
| Ease of fabrication | - | B |
| Low rate of grain growth | B | - |

Notes

*Indicates the material which best provides the desired property.

criteria presented in this table do not lead to significant evidence for selection of one or the other of the two materials. The choice must then be made based on performance level, reproducibility, and stability and for the present state of the art, rhenium is definitely superior to tantalum.

4.2.1.4 Conclusions

The preceding discussion leads to the conclusions that, for the purposes of this study, rhenium be chosen as the emitter material and that the nominal value of interelectrode spacing considered be two mils. The arguments to substantiate these choices are not very extensive because of the limited amount of state-of-the-art information; but they are judged nonetheless to be sufficient, and forthcoming tests on the new Solar Energy Thermionic series VIII converters are expected to strengthen them by further establishing the ability of rhenium converters to reproduce high, stable levels of performance consistently.

### 4.2.2 ESTIMATED CONVERTER PERFORMANCE

Having selected rhenium as the emitter material, an emitter operating temperature of 2000°K, and an interelectrode spacing of two mils; the converter performance as a function of emitter area can be calculated. It is necessary to present the converter performance as a function of emitter area because the final emitter area cannot be determined until a launch vehicle is selected and the maximum diameter solar concentrator defined. The data given in Figure 4-1 was used as the basis for these performance calculations. This reference converter (TEECO VIII-P-3) had a rhenium emitter, a two mil interelectrode spacing, a lead resistance of 1.61 millivolts per ampere, an emitter area of two square centimeters, and the measured performance was obtained at an emitter temperature of 2000°K. Therefore, the reference converter exactly matches the operating point selected for use in this study. The effect of varying the emitter area on the performance of the reference converter is calculated in the following sections.

#### 4.2.2.1 Converter Losses

In order to estimate converter efficiency it is necessary to calculate the converter losses. The procedure used to calculate these losses is presented below.

a. Interelectrode Radiation

The interelectrode radiation is calculated assuming an emitter temperature of 2000°K, a collector temperature of 1000°K and emissivities for these surfaces of 0.25 and 0.40 respectively. The somewhat high value chosen for the collector is intended to make allowance for the possible formation of a thin absorptive coating on the collector; which is usually observed. The value of 0.25 chosen for rhenium is lower than the 0.30 value at 2000°K reported in Reference 4-1. The reason for this is that the authors of the referenced article describe their sample as having a matte finish, a description which would not seem to apply to rhenium thermionic emitters which are usually quite shiny. For reference, the emissivity of tantalum at 2000°K is 0.232 and that of tungsten, at the same temperature, is 0.259 (Reference 4-2). Using the formula for radiation heat exchange between parallel plates:

$$q_r = \frac{\sigma\,(T_E^{\,4} - T_C^{\,4})}{\frac{1}{\epsilon_E} + \frac{1}{\epsilon_C} - 1}$$

The calculated value of interelectrode radiation is:

$$q_r = 15.5 \text{ watts/cm}^2.$$

b. Cesium Conduction

The heat transfer by cesium conduction in thermonic converters has been the subject of a special research effort by S. Kitrilakis and M. Meeker (Reference 4-3). These investigators have arrived at the empirical equation:

$$H = \frac{\lambda_m \Delta T \times 1000}{2.5d + 1.15 \times 10^{-2} (T_E + T_C)/p},$$

which is used to evaluate the heat transfer at all possible values of spacing, cesium condensation pressure, and electrode temperature difference. In this expression the high-pressure conductivity of the gas, $\lambda_m$, is expressed in watts/cm-$^{o}$K, the temperature difference, $\Delta T$, is in $^{o}$K, the interelectrode spacing, d, in mils, and the condensation pressure, p, in millimeters of mercury. The value of $\lambda_m$ is relatively constant for usual thermionic converter operating conditions. Arithmetic spot checks indicate that the cesium conduction equation can be simplified with a minimum of error by assuming for $\lambda_m$ the value of $6.11 \times 10^{-5}$ watts/cm-$^{o}$K and for $(T_E + T_C)$ a value of 2930$^{o}$K. The empirical equation then simplifies to

$$H = \frac{0.0244 \Delta T}{d + 13.5/p}.$$

Figure 4-2 shows this simplified equation plotted assuming a value for $\Delta T$ of 900$^{o}$K. In the case of this study, the $\Delta T$ value is expected to be 1000$^{o}$K, and therefore the heat transfer flux given by Figure 4-2 should be increased by 11 percent. Assuming that the converters are operated at a reservoir temperature of 630$^{o}$K (as suggested by Figure 4-1) the cesium conduction predicted by Figure 4-2, with the appropriate $\Delta T$ correction and for an interelectrode spacing of two mils, is:

$$q_{cs} = 6.4 \text{ watts/cm}^2.$$

c. Electron Cooling

The electron cooling loss of converter VIII-P-1 was measured experimentally and is given in Figure 4-3. This is believed to be the best available data on electron

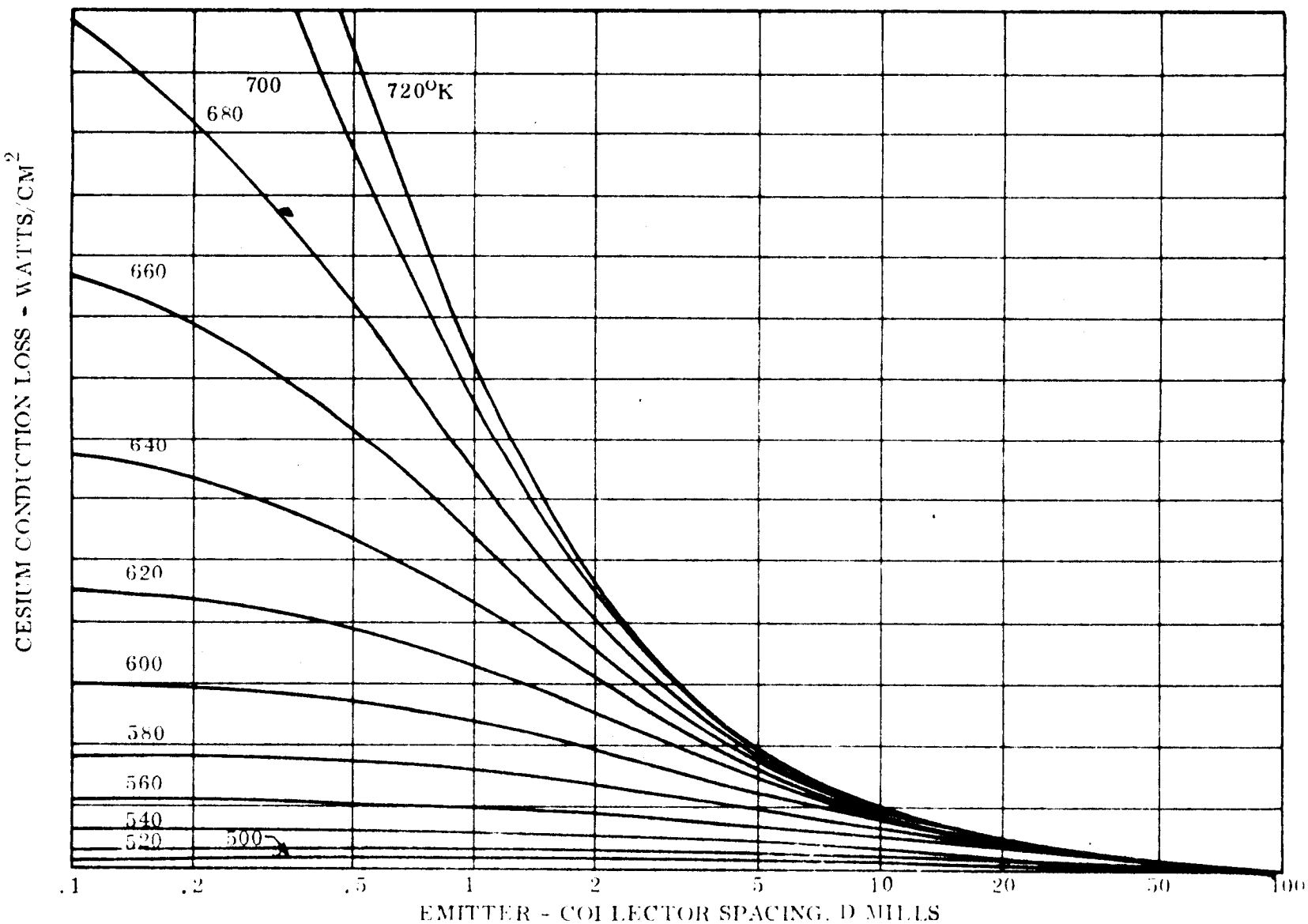


Figure 4-2. Cesium Conduction Loss

cooling for converters operated at 2000°K with a rhenium emitter. In Figure 4-3, it is noted that the value of the electron cooling loss is 2.47 watts per ampere. The cesium reservoir temperature for Figure 4-3 was in the vicinity of 670°K. Operating at a different reservoir temperature would tend to change the electron cooling value because the emitter work function depends on cesium pressure. This dependence is given in Figure 4-4 (taken from Reference 4-4). It can be seen that the value of 2.47 watts per ampere at 670°K falls slightly below the 2.54 ev value of emitter work function at this reservoir temperature. This is contrary to theory in that the electron cooling per ampere would be expected to have a value slightly in excess of the emitter work function. The discrepancy is probably due to edge effects by the emitter support sleeve of VIII-1-1. The temperature of this element is below the emitter temperature, consequently it gets coated with cesium to a greater extent than the emitter and has a lower work function. In this study, the electron cooling per ampere will be assumed equal to the emitter work function as given by Figure 4-4. The corresponding values are listed in Table 4-3 and plotted in Figure 4-5.

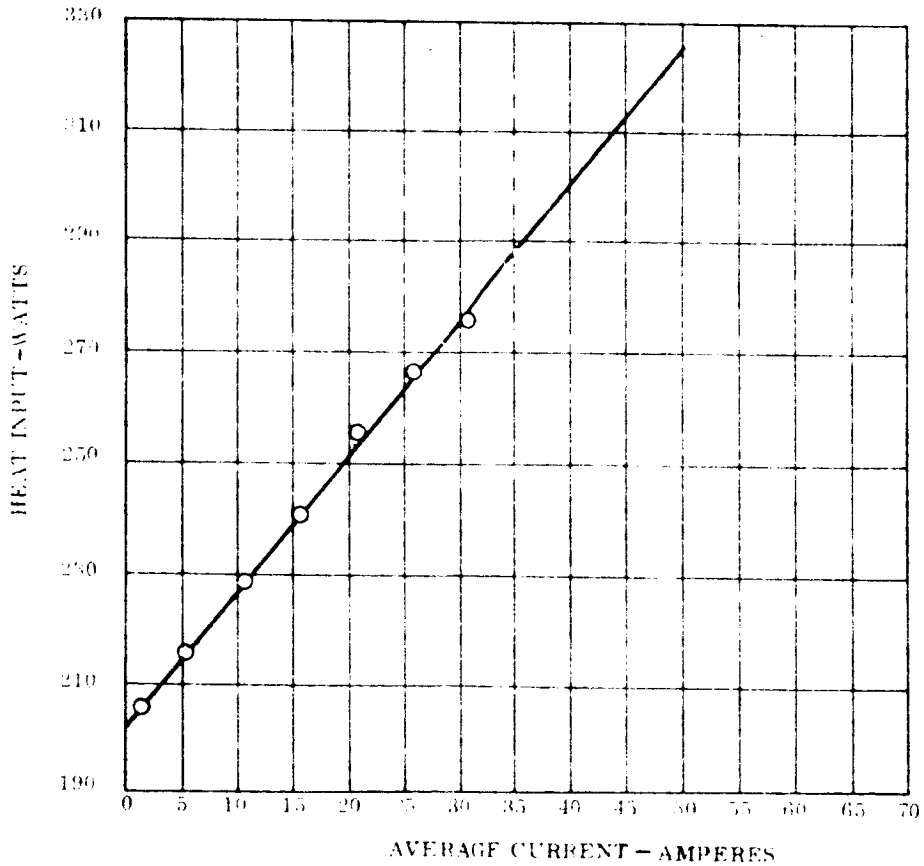


Figure 4-3. Measured Bombardment Power Input vs. Average Current for VIII-P-1 Converter



150

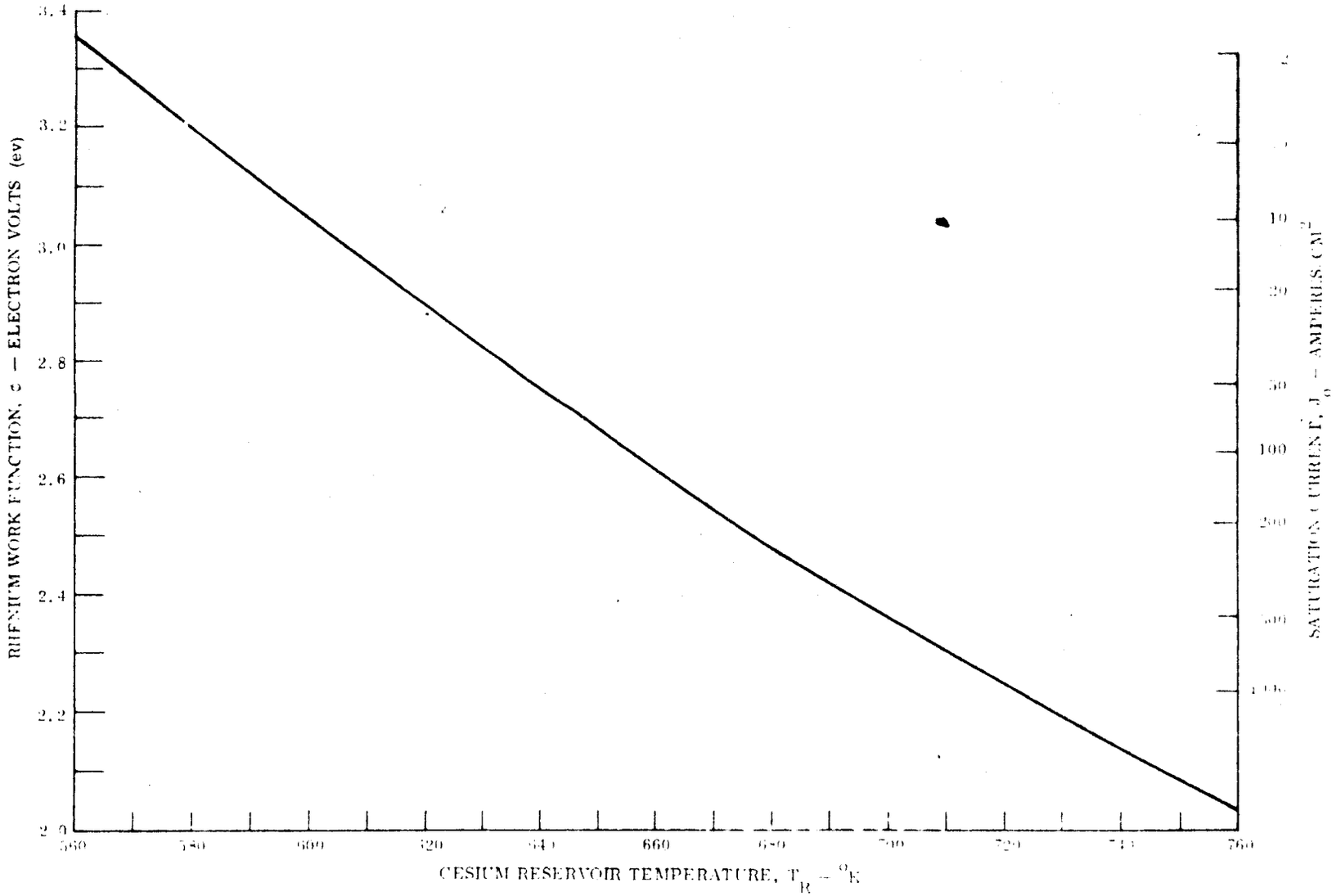


Figure 4-4. Work Function and Saturation Current of Rhenium at 2000°K vs. Reservoir Temperature

d. Conduction and Voltage Drop

The emitter sleeve thermal conduction loss and voltage drop are generally dependent on the size of the converter and on the geometry of the sleeve. For a sufficiently large converter it would be possible to optimize the geometry so that the heat loss per ampere of output current and the voltage drop become independent of size. However, the converter sizes considered in this analysis are two small to meet the size requirement for optimization* and therefore for the purpose of making performance estimates in this study, the basic sleeve geometry considered is that of converter VIII-P-3. This choice is logical since VIII-P-3 represents the most advanced state-of-the-art converter and it has an emitter area of two square centimeters which is close to the size required for this application. However, one change is made; the wall thickness of the thin sleeve considered is 0.0025 inches instead of 0.0030 inches. Although sleeves have been made smaller than 0.0025 inches, this value is considered to be the minimum value consistent with good strength and reliability characteristics. Appendix A shows the details of the assumed geometry and the corresponding calculations. For an emitter diameter of 1.60 centimeters(two square centimeter area), the losses found are:

$$q_L = 49.3 \text{ watts}$$

$$\Delta V_L = 1.93 \text{ millivolts ampere}^{**}$$

The analysis shows that for other emitter diameters, the heat loss will be linearly proportional to diameter and the voltage drop will increase in inverse proportion to the diameter. Table 4-4 shows the resulting values for different emitter areas.

*This statement cannot be substantiated without a calculation based on ideal efficiency which shows that even for the largest converters considered, the emitter sleeve losses are such that increasing the sleeve thickness over the value of 0.0025 inches increases the losses. The reader can use the values of ideal efficiency calculated later in this report to verify that for all practical outputs and converter sizes an increase in sleeve thickness increases the heat conduction to a greater extent than it reduces the heat equivalent of the electrical power loss in the sleeve.

**For a sleeve thickness of 0.003 inches, this value would be 1.61 mv/amp which is the value given at the beginning of Section 4.2.2.1.

Table 4-3. Electron Cooling Loss at 2000°K

| $T_R$, °K | $T_E/T_R$ | $\phi_E$, ev | $J_o$, A/cm$^2$ | $q_e$ Watts/cm$^2$ |
|---|---|---|---|---|
| 618 | 3.24 | 2.88 | 14.5 | 41.8 |
| 637 | 3.14 | 2.74 | 19.5 | 53.5 |
| 641 | 3.12 | 2.71 | 24.5 | 66.5 |
| 652 | 3.06 | 2.63 | 29.0 | 76.3 |
| 657 | 3.04 | 2.60 | 32.5 | 84.5 |

Table 4-4. Emitter Sleeve Heat Loss and Voltage Drop

(Sleeve Thickness - 0.0025 inches)

| $A_E$, cm$^2$ | $D_E$, cm | $Q_L$, Watts | $q_L$, Watts/cm$^2$ | $V_L$, mv/amp |
|---|---|---|---|---|
| 1.0 | 1.13 | 34.8 | 34.8 | 2.73 |
| 1.5 | 1.38 | 42.5 | 28.4 | 2.24 |
| 2.0 | 1.60 | 49.3 | 24.7 | 1.93 |
| 2.5 | 1.78 | 55.0 | 22.0 | 1.73 |
| 3.0 | 1.96 | 60.4 | 20.1 | 1.58 |

### 4.2.2.2 Converter Performance at Peak Power

Figure 4-6 gives the electrode power developed by rhenium converters of the series VIII type. This is the same curve as that of Figure 4-1 except that the voltage is now the voltage at the electrodes. The voltage at the electrodes was obtained by adding to the output voltage of VIII-P-3 the voltage drop in the emitter sleeve at the various currents corresponding to the conditions given in Figure 4-1, assuming a resistance of 1.61 millivolts per ampere. Figure 4-6 also gives the output power curves for converters with the emitter sleeve resistances listed in Table 4-4. The values of voltage drop calculated for the curves of Figure 4-6 are listed in Table 4-5. The following example illustrates the calculation procedure used:

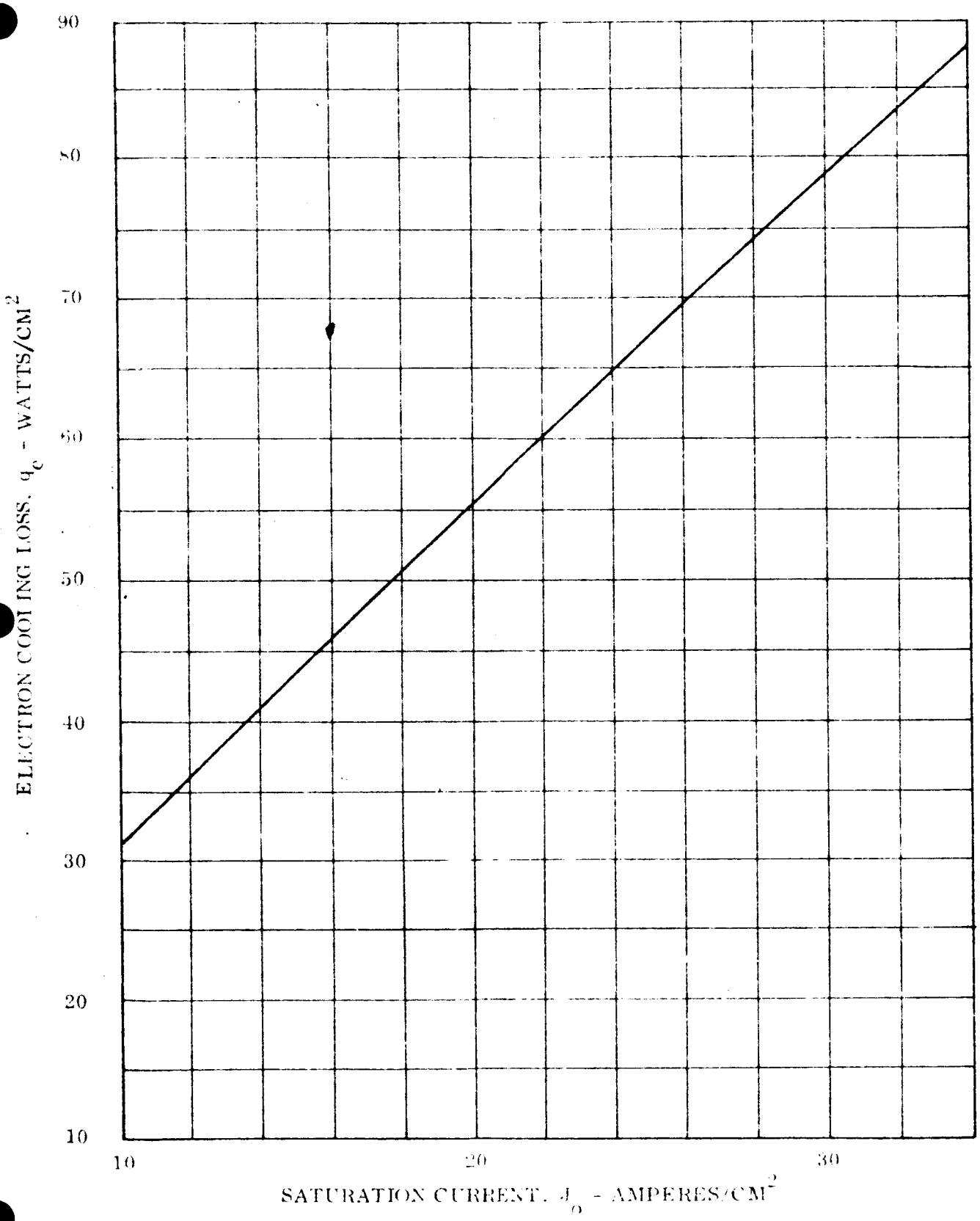


Figure 4-5. Electron Cooling Loss vs. Saturation Current at 2000°K

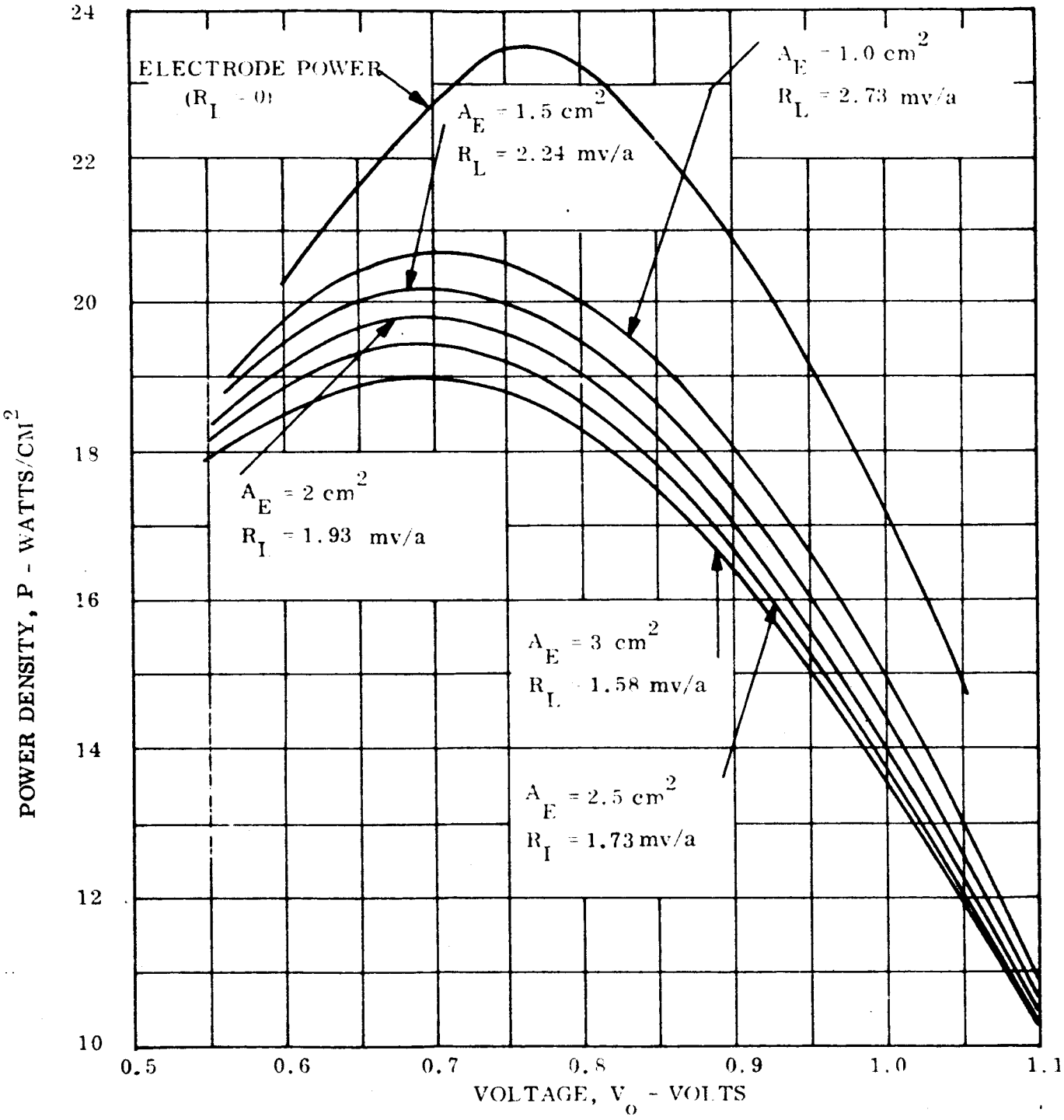


Figure 4-6. Output Power Density of Rhenium Converters

$$A_E = 2.0 \text{ cm}^2$$

$$R_L = 1.93 \text{ mv/A}$$

$$J_o = \text{Select } 24.5 \text{ A/cm}^2,$$

then

$$I_o = 24.5 \times 2.0 = 49.0 \text{ amperes,}$$

and

$$\Delta V_L = 1.93 \times 49.0 = 95 \text{ millivolts.}$$

This current density corresponds to an electrode voltage

$$V_e = 0.879 \text{ Volts, then}$$

$$V_o = 0.879 - 0.095 = 0.784 \text{ volt,}$$

and

$$P = 24.5 \times 0.784 = 19.2 \text{ watts/cm.}^2$$

The curves of Figure 4-6 show that for the range of emitter areas considered, peak power is always achieved at 0.7 volt output. The corresponding power and current densities can be deduced from Figure 4-6 and the electron cooling data of Figure 4-5. Adding the other converter losses calculated previously, the converter efficiency can be calculated as a function of emitter area. These values are given in Table 4-6 and the more significant ones are plotted in Figure 4-7.

#### 4.2.2.3 Converter Performance at Peak Efficiency

Following the same calculation procedure outlined previously, the efficiency may be calculated at other converter voltages and the point at which the efficiency is maximum determined. The results of this calculation are presented in Table 4-7 and plotted in Figure 4-8.

## 4.3 GENERATOR PERFORMANCE

The Generator efficiency is defined by:

$$\eta_g = \frac{\text{Generator Power Output}}{\text{Net Energy Available in the Cavity}}$$

Table 4-5. Lead Voltage Drop and Power Density for Various Voltages and Emitter Areas

| $A_E$, $cm^2$ / $R_L$, mV/A | $V_e$, volts | $J_o$, $A/cm^2$ | $I_o$, amps | $\Delta V_L$, volts | $V_o$, volts | P, watts $cm^2$ |
|---|---|---|---|---|---|---|
| | 1.046 | 14.5 | 14.5 | .039 | 1.007 | 14.6 |
| 1.0 | 0.963 | 19.5 | 19.5 | .053 | 0.910 | 17.8 |
| 2.73 | 0.879 | 24.5 | 24.5 | .067 | 0.812 | 19.9 |
| | 0.793 | 29.0 | 29.0 | .079 | 0.714 | 20.7 |
| | 0.705 | 32.5 | 32.5 | .089 | 0.616 | 20.0 |
| | 1.046 | 14.5 | 21.7 | .048 | 0.998 | 14.5 |
| | 0.963 | 19.5 | 29.2 | .065 | 0.898 | 17.5 |
| 1.5 | 0.879 | 24.5 | 36.7 | .082 | 0.797 | 19.5 |
| 2.24 | 0.793 | 29.0 | 43.5 | .097 | 0.696 | 20.2 |
| | 0.705 | 32.5 | 48.7 | .109 | 0.596 | 19.4 |
| | 1.046 | 14.5 | 29.0 | .056 | 0.990 | 14.3 |
| 2.0 | 0.963 | 19.5 | 39.0 | .075 | 0.888 | 17.3 |
| 1.93 | 0.879 | 24.5 | 49.0 | .095 | 0.784 | 19.2 |
| | 0.793 | 29.0 | 58.0 | .112 | 0.681 | 19.8 |
| | 0.705 | 32.5 | 65.0 | .125 | 0.580 | 18.8 |
| | 1.046 | 14.5 | 36.2 | .062 | 0.984 | 14.2 |
| 2.5 | 0.963 | 19.5 | 48.7 | .084 | 0.879 | 17.2 |
| 1.73 | 0.879 | 24.5 | 61.2 | .106 | 0.773 | 19.0 |
| | 0.793 | 29.0 | 72.5 | .125 | 0.668 | 19.4 |
| | 0.705 | 32.5 | 81.2 | .140 | 0.565 | 18.4 |
| | 1.046 | 14.5 | 43.5 | .069 | 0.977 | 14.2 |
| 3.0 | 0.963 | 19.5 | 58.5 | .092 | 0.871 | 17.0 |
| 1.58 | 0.879 | 24.5 | 73.5 | .116 | 0.763 | 18.7 |
| | 0.793 | 29.0 | 87.0 | .138 | 0.655 | 18.9 |
| | 0.705 | 32.5 | 97.5 | .154 | 0.551 | 17.9 |

Table 4-6. Converter Performance at Peak Power ($V_o$ = 0.700 Volts)

| $A_E$, $cm^2$ | P watts/$cm^2$ | $J_o$, $A/cm^2$ | $q_e$, watts/$cm^2$ | $\Sigma_q$, watts/$cm^2$ | $\eta_{pp}$, % |
|---|---|---|---|---|---|
| 1.0 | 20.7 | 29.6 | 78.0 | 134.7 | 15.4 |
| 1.5 | 20.2 | 28.8 | 76.0 | 126.3 | 16.0 |
| 2.0 | 19.8 | 28.2 | 74.9 | 121.5 | 16.3 |
| 2.5 | 19.44 | 27.7 | 74.0 | 117.9 | 16.5 |
| 3.0 | 19.0 | 27.2 | 72.0 | 114.0 | 16.7 |

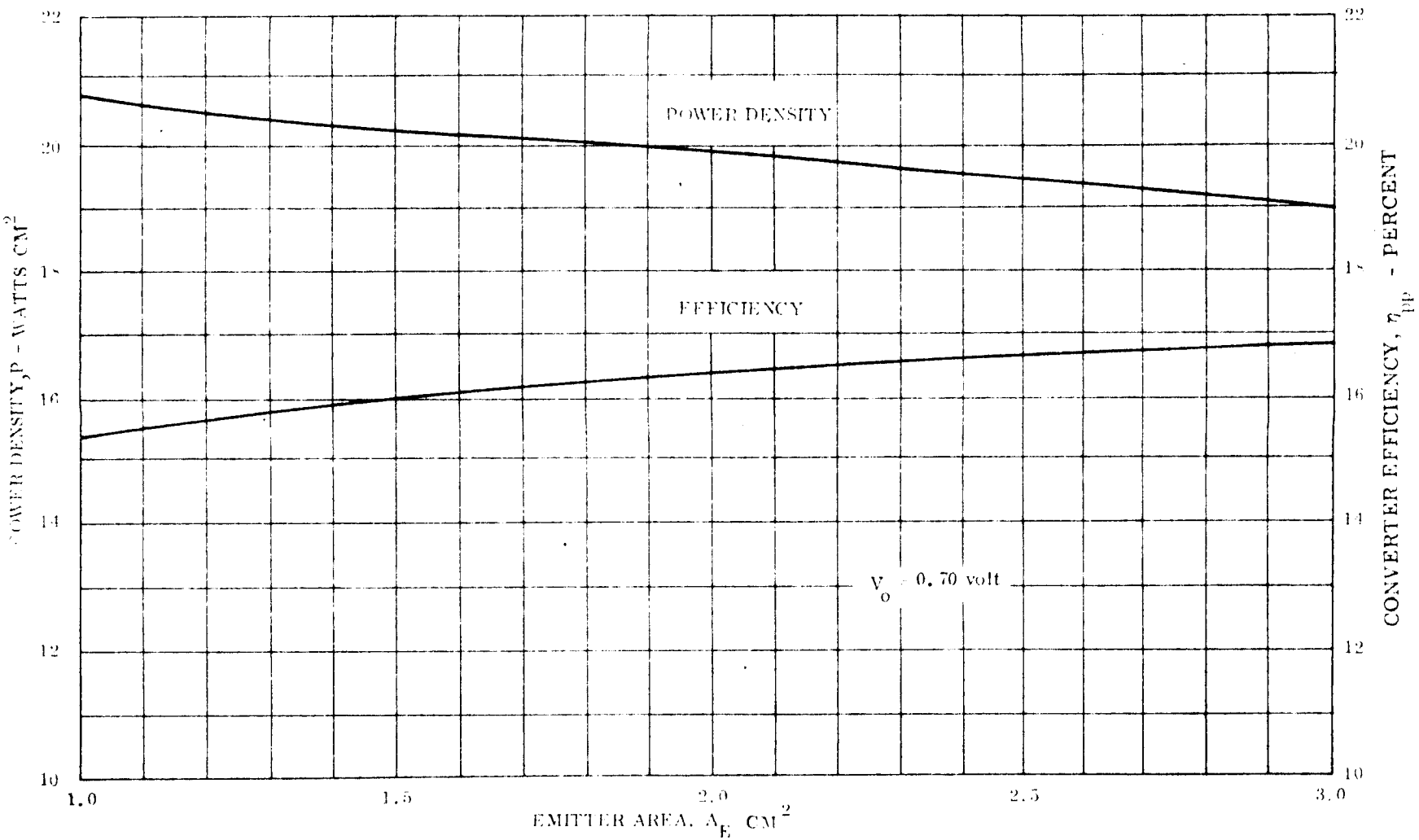


Figure 4-7. Converter Performance at Peak Power $V_o$ = 0.70 Volts

Table 4-7. Converter Performance at Peak Efficiency

| $A_E$, $cm^2$ | $V_o$, volts | P, watts/$cm^2$ | $J_o$, amps/$cm^2$ | $q_e$, watts/$cm^2$ | $\Sigma q$, watts/$cm^2$ | $\eta$, % | $\eta_{pe}$, P * |
|---|---|---|---|---|---|---|---|
| | 0.8 | 20.0 | 25.0 | 66.5 | 123.2 | 16.2 | |
| | 0.9 | 18.1 | 20.1 | 55.0 | 111.7 | 16.2 | 16.3% |
| 1.0 | 1.0 | 14.8 | 14.8 | 42.5 | 99.2 | 14.9 | 19.0 watts/$cm^2$ |
| | 1.1 | 10.7 | 9.7 | 30.2 | 86.9 | 12.3 | at 0.85 volts |
| | 0.8 | 19.5 | 24.4 | 65.2 | 115.5 | 16.9 | |
| | 0.9 | 17.5 | 19.4 | 53.3 | 103.6 | 16.9 | 17.0% |
| 1.5 | 1.0 | 14.4 | 14.4 | 41.5 | 91.8 | 15.7 | 18.5 watts/$cm^2$ |
| | 1.1 | 10.5 | 9.5 | 29.8 | 80.1 | 13.1 | at 0.85 volts |
| | 0.8 | 19.0 | 23.8 | 63.7 | 110.3 | 17.2 | |
| | 0.9 | 17.0 | 18.9 | 52.2 | 98.8 | 17.2 | 17.4% |
| 2.0 | 1.0 | 13.9 | 13.9 | 40.2 | 86.8 | 16.0 | 18.0 watts/$cm^2$ |
| | 1.1 | 10.4 | 9.4 | 29.6 | 72.2 | 13.6 | at 0.85 volts |
| | 0.8 | 18.7 | 23.4 | 62.8 | 106.7 | 17.5 | |
| | 0.9 | 16.6 | 18.4 | 51.0 | 94.9 | 17.5 | 17.6% |
| 2.5 | 1.0 | 13.7 | 13.7 | 39.7 | 83.6 | 16.4 | 17.6 watts/$cm^2$ |
| | 1.1 | 10.3 | 9.3 | 29.3 | 73.2 | 14.1 | at 0.85 volts |
| | 0.8 | 18.3 | 22.8 | 61.5 | 103.5 | 17.7 | |
| | 0.9 | 16.4 | 18.2 | 50.5 | 92.5 | 17.7 | 17.8% |
| 3.0 | 1.0 | 13.5 | 13.5 | 39.2 | 81.2 | 16.6 | 17.3 watts/$cm^2$ |
| | 1.1 | 10.2 | 9.3 | 29.3 | 71.3 | 14.3 | at 0.85 volts |

Notes

*Obtained from a plot of $\eta$ vs. $V_o$.

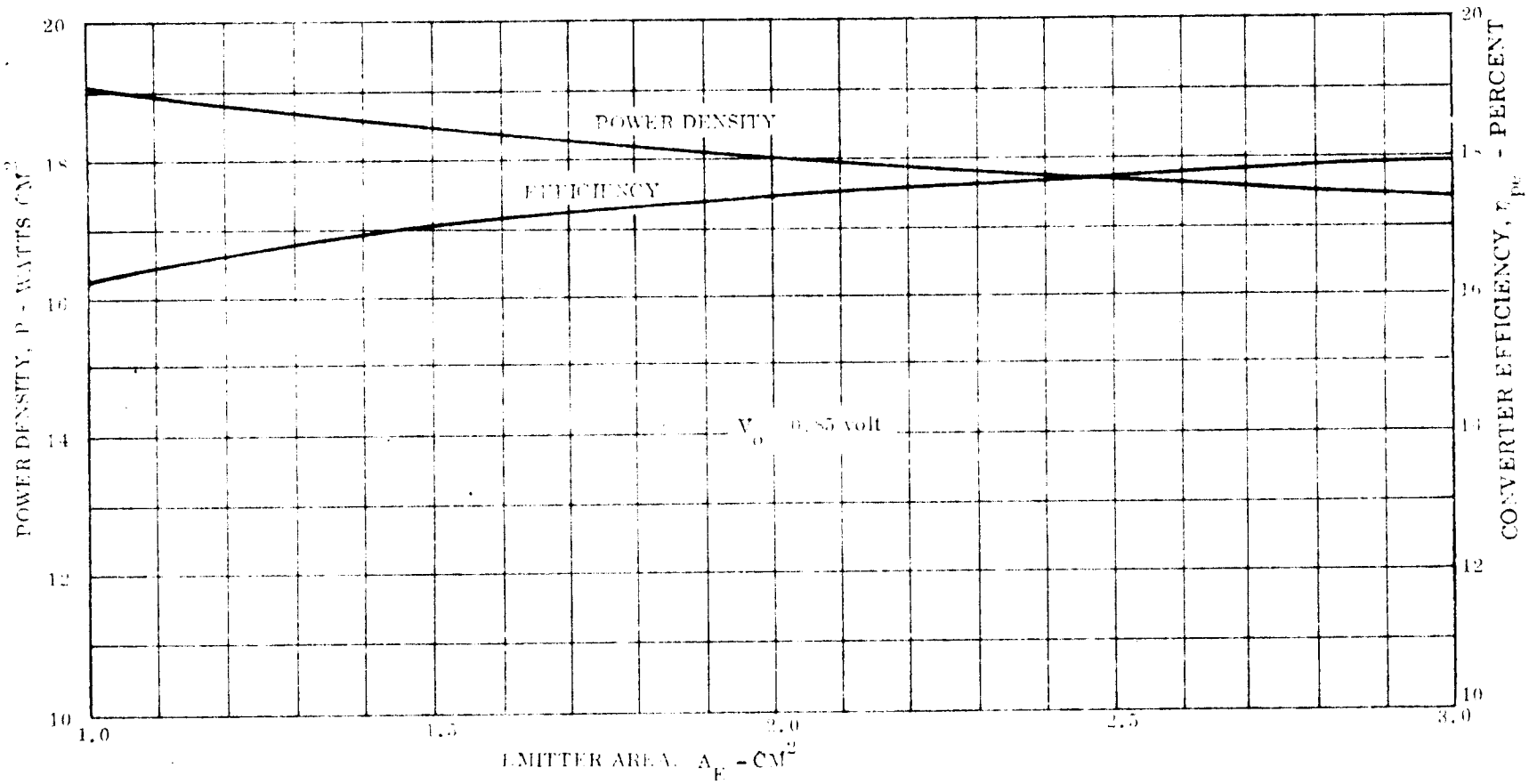


Figure 4-8. Converter Performance at Peak Efficiency $V_o$ = 0.85 Volts

Vol II

The net energy available in the cavity is defined as the energy entering the generator aperture minus that energy lost by reflection and re-radiation back out the cavity opening. If black body radiation is assumed to closely approximate the sum of the reflection and reradiation losses the above equation can be expressed as:

$$\eta_g = \frac{P_g}{Q_{in} - A_o \sigma T^4},$$

where $A_o$ is the aperture area and T is the cavity temperature. Based on the solar test results from the Cavity Vapor Generator Program (Reference 4-5) the black body radiation assumption is a good approximation for the total aperture loss.

The term $Q_{in} - A_o \sigma T^4$ represents the energy available in the cavity for use by the thermionic converters plus that lost as thermal energy through the generator insulation and structure. Therefore, the efficiency of the thermionic converters multiplied by the thermal efficiency of the generator insulation, also, yields the overall generator efficiency. The thermionic converter efficiency is available from Section 4.2, but it is difficult to estimate the thermal efficiency of the generator insulation before the generator design has been layed out. However, experience with recent four converter generator designs such as JG-3 indicate that the generator efficiency can be approximated by

$$\eta_g = 0.7\ \eta_c,$$

where $\eta_c$ is the converter efficiency. This equation is used to express the generator efficiency for the purpose of these system calculations. The thermal losses will be estimated when the generator design is established to check the validity of the above expression (see Section 8.4.1-Volume III).

## 4.4 CONCENTRATOR-ABSORBER PERFORMANCE

The major concentrator performance parameters of interest are net energy available in the generator cavity as a function of concentrator diameter, and the concentrator-abosrber efficiency.

In this study concentrator-absorber efficiency is defined by:

$$\eta_{ca} = \frac{\text{Net Energy Available in Cavity } (Q_n)}{\text{Concentrator Projected Area } (A_c) \times \text{Solar Intensity } (S)}$$

Therefore, the reradiation and reflection losses out of the generator aperture are included in the concentrator-absorber efficiency. Also, in determining the net energy available in the cavity, the misorientation effects are included.

### 4.4.1 ASSUMED CONCENTRATOR PARAMETERS

The assumed parameters from which the concentrator-absorber performance is calculated are listed below.

a. Solar intensity of 130 watts/ft$^2$ (1 AU)

b. Thermal distortion of the concentrator is assumed to be either zero or to be compensated for in the design

c. The concentrator surface reflectivity is 90 percent

d. The concentrator geometric errors are assumed to occur only in the radial plane and not in the circumferential direction. The geometric errors are assumed to have a gaussian distribution centered about zero error with a 3 $\sigma$ value equal to 12 minutes*

e. The area blockage factor is five percent

f. The orientation angle error is assumed to be six minutes and invarient with time

g. The absorber behaves as a blackbody cavity having an emissivity and absorptivity of 1.0 with a temperature of 2000$^{\circ}$K

*1 $\sigma$ is defined as the geometric slope error which is not exceeded over 68.3 percent of the area. 3 $\sigma$ is the geometric slope error which is not exceeded over 99.7 percent of the area.

h. The concentrator-absorber performance was computed for rim angle values of 45 and 60 degrees.

Assumptions c through h are discussed in greater detail in the following sections.

4.4.1.1 Reflectivity

Only two pure metals, aluminum and silver have reflectances high enough for solar concentrators. It is also possible to obtain high reflectance using multilayer interference filters of alternating metallic and dielectric materials, but they are beyond the present state of the art. Vapor deposited aluminum or silver on optically smooth substrates will yield reflectance values in the 88 to 93 percent range over the total solar spectrum.

A concentrator reflectivity value of 90 percent was assumed for this study based on the results of recent (March 5, 1965) reflectivity measurements made by the General Electric Spacecraft Department on Liberty Mirror Coating 747. General Electric supplied the Liberty Mirror Division of the Libby-Owens-Ford Company with six two-inch by two-inch samples of electroformed nickel, 15 mils thick.* These samples were coated by Liberty Mirror with their 747 aluminum coating and returned to General Electric. The samples are shown in Figure 4-9. The reflectivity of each sample was measured using a Bechman 24500 reflectance unit (Model DK-1).

The measured total reflectance, over the solar spectrum, for the six samples is given below.

| Sample | Total Reflectance |
|---|---|
| 1 | 0.896 |
| 2 | 0.904 |
| 3 | 0.904 |
| 4 | 0.901 |
| 5 | 0.907 |
| 6 | 0.907 |

The specular reflectance as a function of wavelength for Sample 5 is given in Figure 4-10. This plot is representative of the measured results on all the six samples.

*This is the same substrate proposed for the parabolic solar concentrator surface (see Section 8.3.1-Volume III).

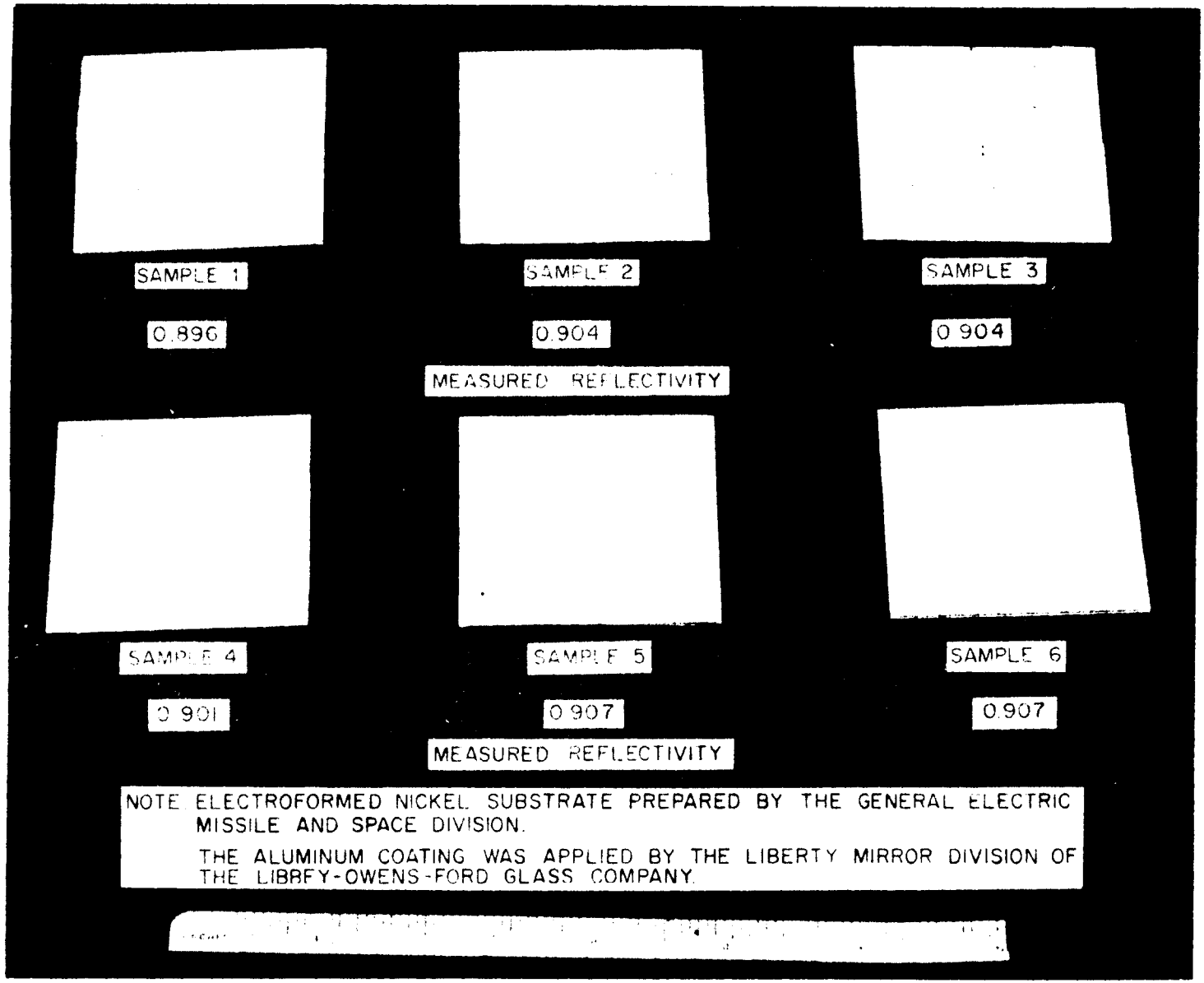


SUBSTRATE-ELECTROFORMED NICKEL (15 MILS THICK)
COATING-LIBERTY MIRROR ALUMINUM COATING 747

Figure 4-9. Reflectivity Samples

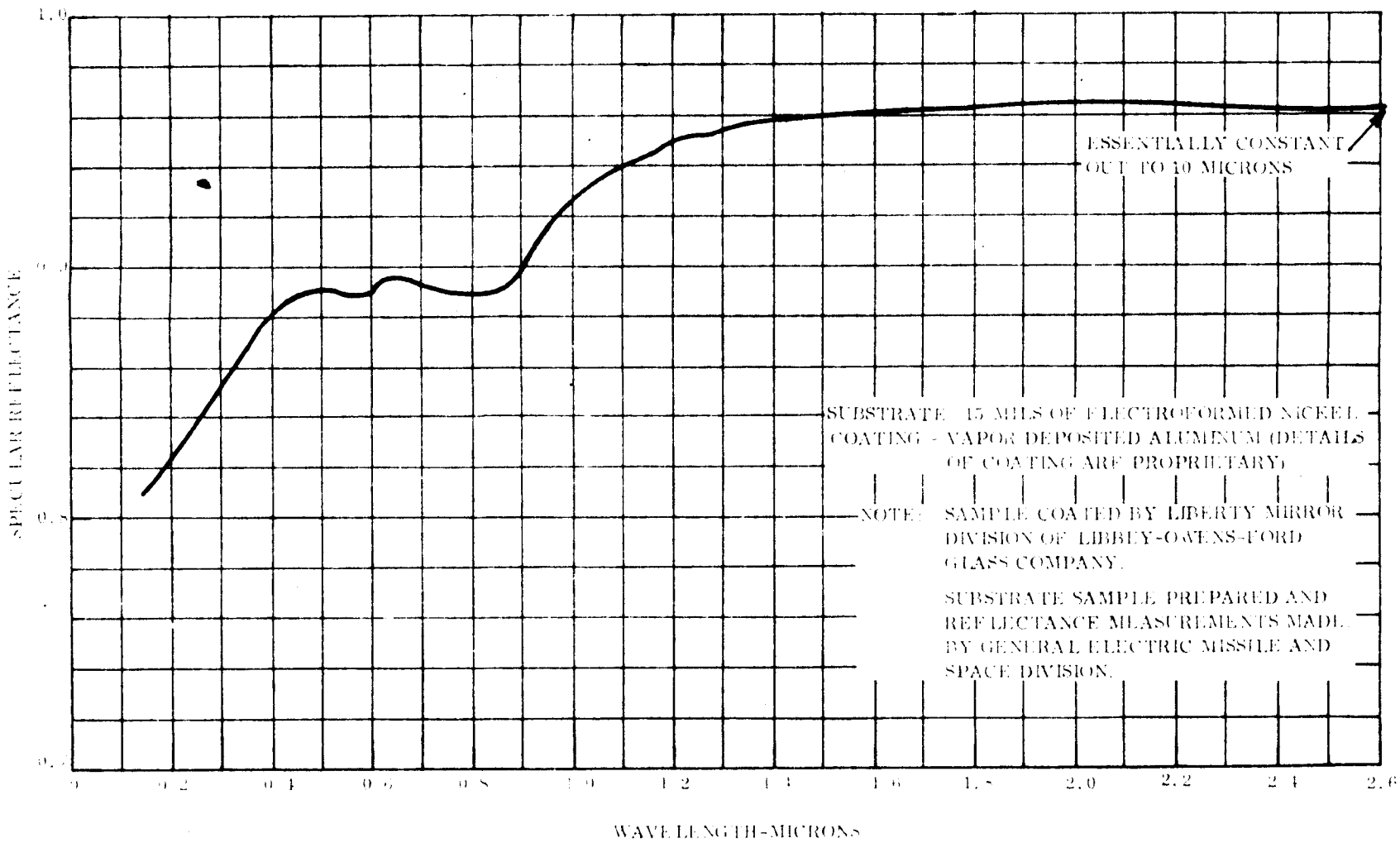


Figure 4-10. Measured Spectral Reflectance for Liberty Mirror Coating 747 (Sample 5)

Integrating the curve over the range from zero to ten microns gave the total reflectance value of 0.907 shown above. For comparison purposes, the sun's energy spectrum in space (at 1 AU) is given in Figure 4-11.

On the basis of these measurements a reflectivity value of 90 percent appears to be a reasonable assumption.

4.4.1.2 Geometric Errors

Optical inspections of fabricated concentrators have demonstrated that the largest geometric errors generally occur in the radial rather than the circumferential direction. The radial and circumferential error nomenclature is defined in Figure 4-12. This is particularly true of concentrators formed by the spin-cast-electroform method. In addition, circumferential errors have a smaller effect on concentrator-absorber efficiency than do radial errors of equal magnitude (Reference 4-8). For these reasons concentrator-absorber performance can be closely approximated neglecting the circumferential errors. This is very fortunate since assuming errors in only one direction greatly reduces the cost of analyzing concentrator-absorber performance with existing computer programs.*

Also, through optical inspection of fabricated concentrators, it has been estalished that in most cases the geometric error distribution is closely approximated by a Gaussian distribution (References 4-6 and 4-7). An example of this is given in Figure 4-13 (taken from Reference 4-7). This data was measured by NASA Langley Research Center on a five-foot diameter, stretch-formed aluminum concentrator (S/N-2) fabricated by the TAPCO Division of Thompson-Ramo-Wooldridge. This parabolic concentrator was made from aluminum with a 16-mil skin thickness. Dr. Schrenk of the University of Pennsylvania has made an extensive statistical study of geometric errors in the TAPCO S/N-2, and S/N-4 concentrators. Only a limited amount of Dr. Schrenk's work in this area has been published but it should be available in the near future. The validity of assuming that the geometric errors can be approximated by a normal distribution was discussed with Dr. Schrenk and based on the results of his work on the TAPCO series of concentrators this appears to be a reasonable assumption.

*Because the concentrator-absorber performance can be closely approximated by considering only radial errors, most of the existing computer programs will not handle circumferential errors.

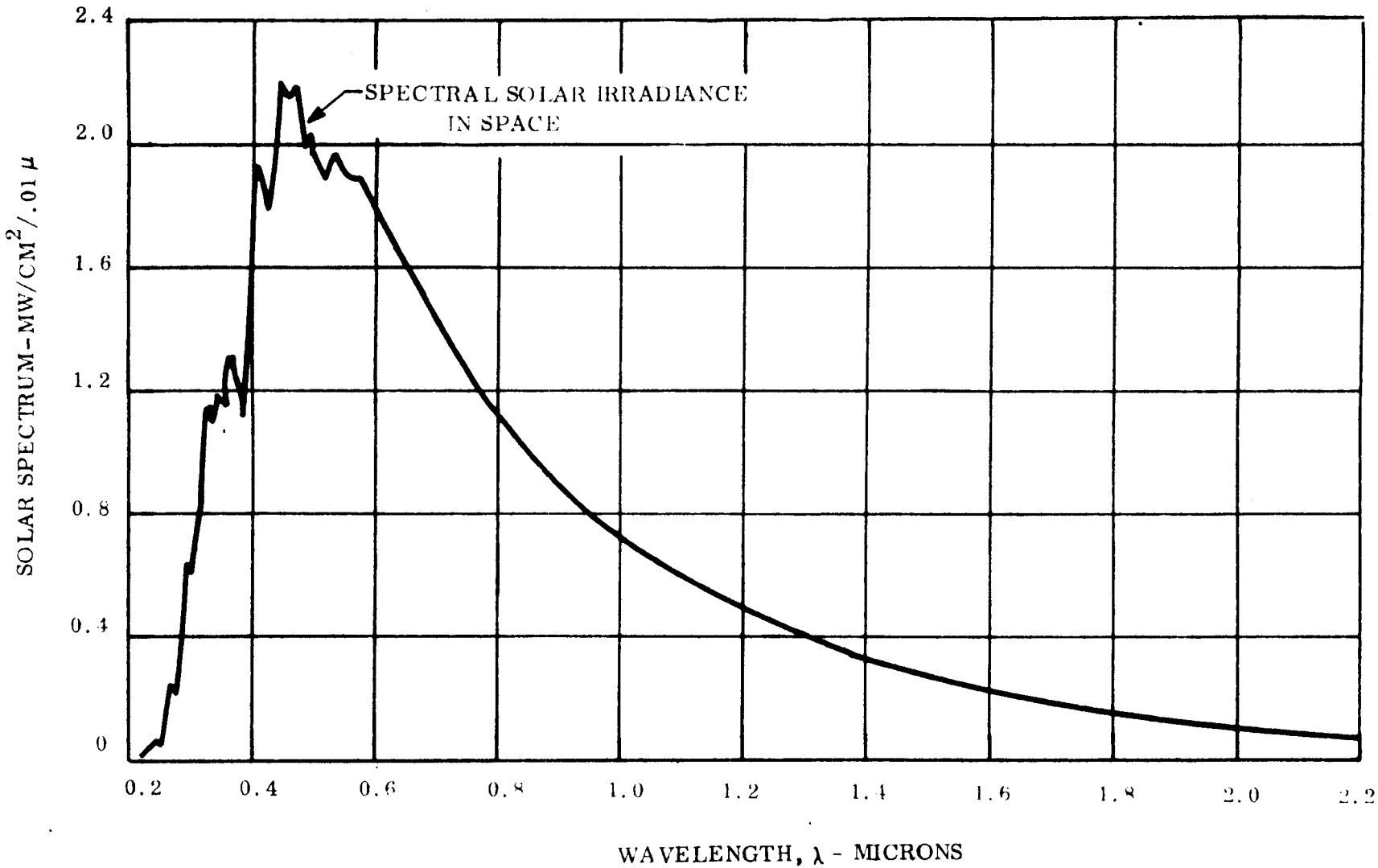


Figure 4-11. Solar Spectrum in Space

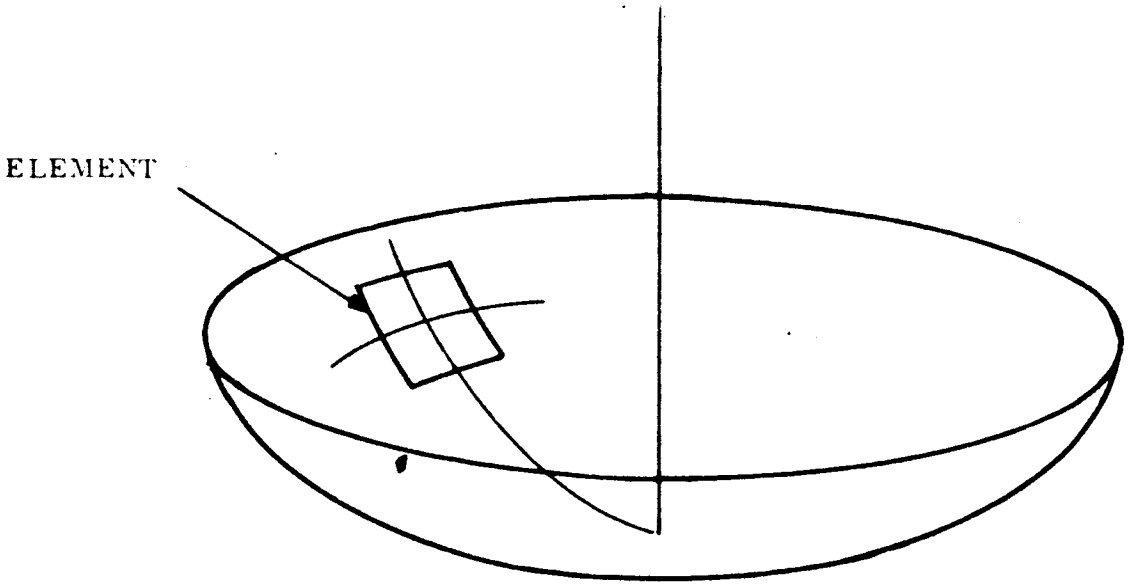


PARABOLIC SOLAR CONCENTRATOR

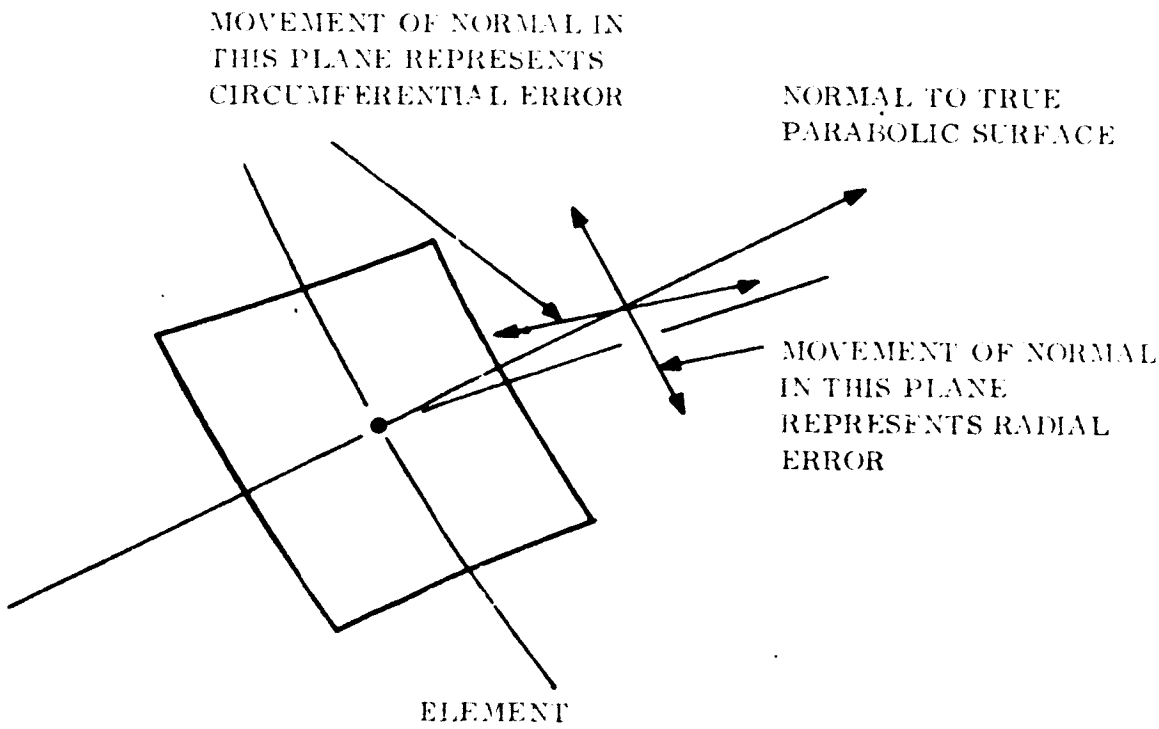


Figure 4-12. Definition of Geometric Error Nomenclature

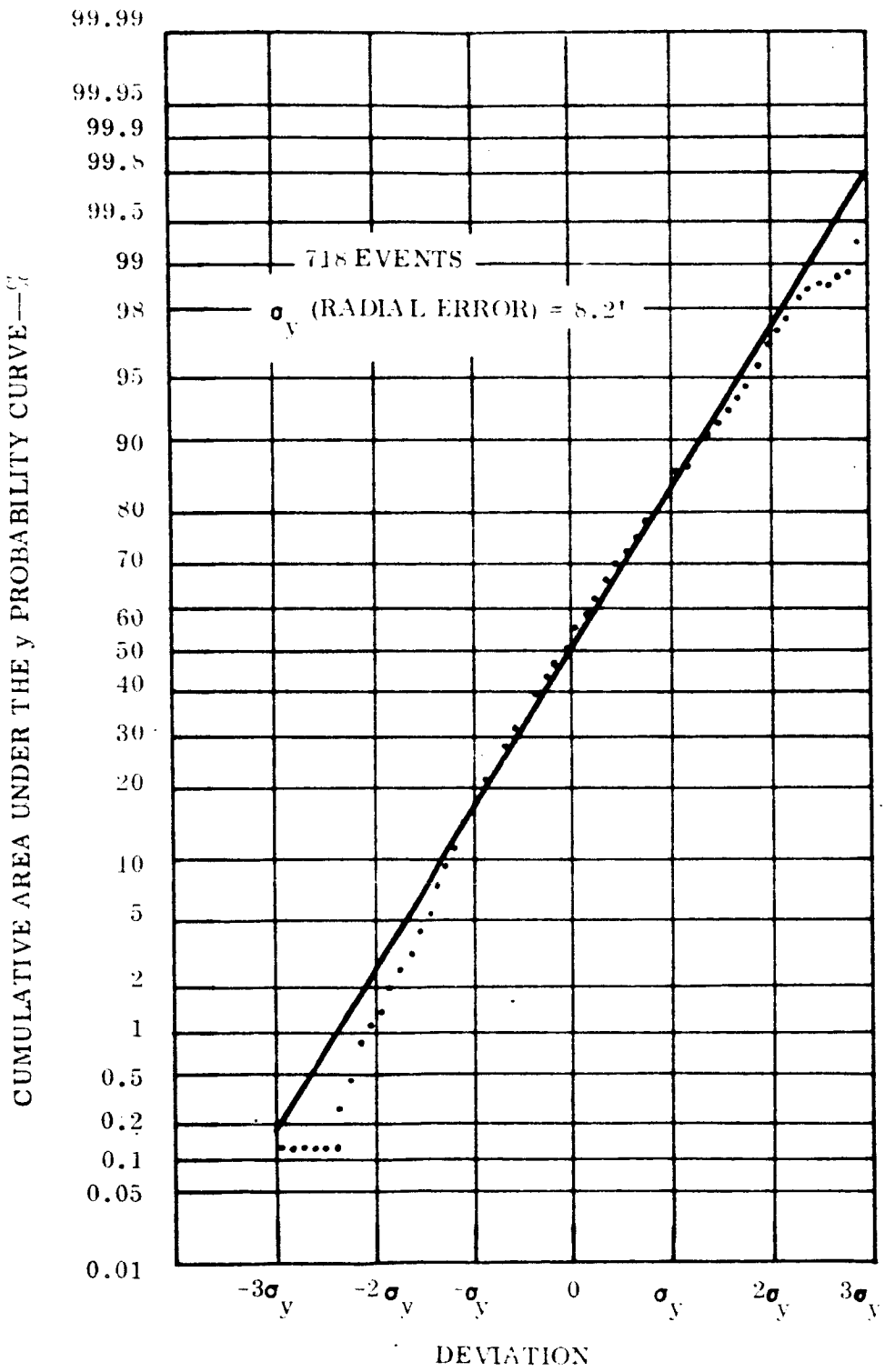


Figure 4-13. Y-Cumulative Distribution Function for the TAPCO S/N-2 Concentrator

This effect of radial geometric errors on concentrator-absorber performance was studied in Reference 4-9* and the results are shown in Figure 4-14. This curve assumes zero orientation error. For the range covered, the concentrator-absorber efficiency drops approximately 2.5 percent with each five minute increase in the three $\sigma$ value of geometric error.

A three $\sigma$ radial geometric error value of 12 minutes was chosen for this study because it was felt to be representative of the accuracy with which concentrators in the five-foot diameter range can presently be fabricated. As an example of this consider the TAICO S/N-2 and S/N-4 concentrators. Dr. Schrenk has reduced the geometric error data on these two concentrators (718 and 5771 points respectively). The results of this complete evaluation have not been published to date but Dr. Schrenk was consulted and he discussed the general nature of the results. Considering the total concentrator surface the one $\sigma$ value of radial geometric error for the S/N-2 and S/N-4 were 8.2 and 2.9 minutes respectively. Since the error distribution was closely approximated by a normal distribution for both of these concentrators then the three $\sigma$ values were approximately 25 and 9 minutes respectively. Obviously there was considerable improvement in the geometric accuracy of the S/N-4 compared to the S/N-2. Since this was a third generation of the same basic design this might be expected. Based on the S/N-4 results the assumed 3$\sigma$ = 12 minutes is slightly pessimistic. However, considering the implications of being unable to match the assumed performance with actual hardware lead to the conclusion that a slightly conservative approach was in order. If hardware could not be fabricated that would approximate the level of performance assumed here then either the concentrator diameter would have to be increased or the size of the thermionic converters reduced. Either of these might be difficult, or impossible, to achieve without significantly altering the experiment concept developed in this study. However, an improvement in concentrator performance over that assumed could be accommodated by reducing the concentrator diameter or increasing the thermionic converter size and either of these could be accomplished without seriously altering the proposed experiment concept. The slightly conservative value for three $\sigma$ was also favored because the circumferential errors were neglected in the performance calculations.

*The study conducted in Reference 4-9 was based on the same assumptions and employed the same computer program for calculating the concentrator - absorber performance that was used in this study.

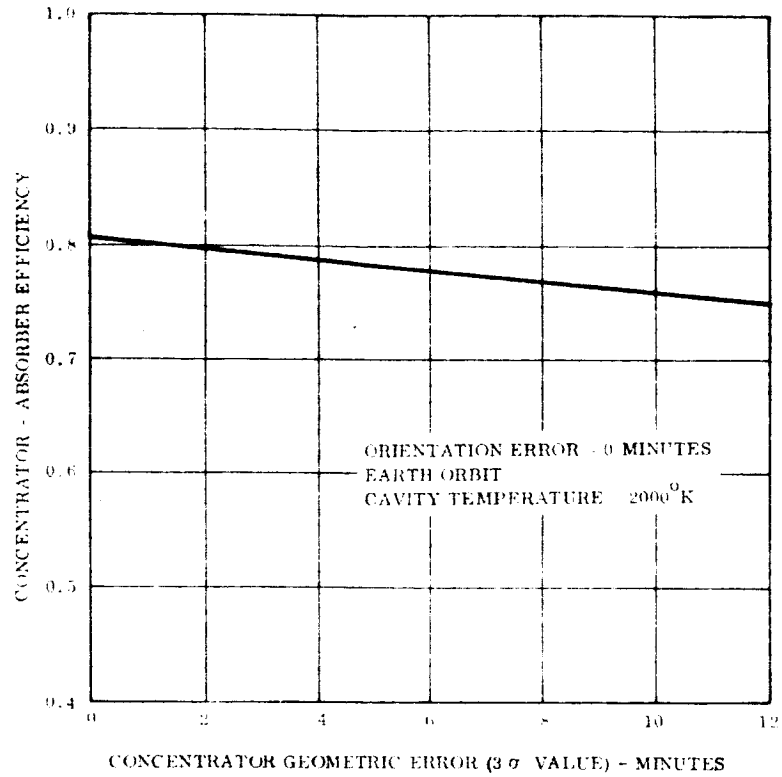


Figure 4-14. Converter-Absorber Efficiency vs. Concentrator Geometric Error for Zero - Orientation Error

#### 4.4.1.3 Blockage Factor

The blockage factor is defined as the percentage of concentrator projected surface area shadowed by the thermionic generator and the generator support arms. Experience with thermionic systems which have been built and tested (Solar Energy Thermionic, STEPS I and STEPS II) indicate that a blockage factor of five percent is typical.

#### 4.4.1.4 Orientation Error

Solar thermionic system performance is very sensitive to orientation error. Since the absorber cavity operates at such high temperatures any increase in the aperture diameter yields a significant increase in the reradiation loss from the cavity and subsequent decrease in the system efficiency. Therefore, the greater orientation error the system is designed for, the larger the resulting optimum aperture diameter will be, and the lower the system efficiency. A study of the effect of misorientation on concentrator-absorber efficiency was conducted in Reference 4-9 and the results are shown in Figure 4-15. This figure indicates a decrease

in concentrator-absorber efficiency of over ten percent in going from 0 to 12 minutes mis-orientation for a geometrically perfect concentrator. The decrease in performance is even more pronounced when geometric errors are included. Obviously, it is important that the orientation error be kept as small as possible.

A maximum orientation error of ± 6 minutes is considered obtainable for an application of this type. A solar thermionic orientation system was developed and ground tested on the STEPS I Program (Reference 4-6). This system had a measured capability of maintaining the orientation error within ± 6 minutes. Although the hardware employed in the application was not "flight type" the basic sensing and logic concepts used in this system would apply equally well in a space system. The importance of obtaining an orientation accuracy of ± 6 minutes and methods of accomplishing this are considered further in Section 11.2.

From Figure 4-15 a six minute orientation error results in a decrease of collector-absorber efficiency of approximately five percent (for a geometrically perfect concentrator). However, the assumption that the error is a constant six minutes is conservative since in actual practice the error will probably vary between plus six minutes and minus six minutes. As a result, the majority of the time the system will be oriented to the sun with an error less than six minutes.

4.4.1.5 Cavity Temperature

A temperature of 2000°K is assumed for the purposes of computing the reradiation loss from the generator cavity. This value was chosen because for state-of-the-art thermionic generator designs, the cavity temperature is essentially equal to the converter emitter temperature and the converter emitter temperature selected in Section 4.2 was 2000°K.

The sum of the reflection and reradiation losses out the generator aperture are assumed to be approximated by computing the reradiation loss through the aperture assuming black-body radiation. Therefore, the total aperture loss (reflection and reradiation) is assumed to be approximated by:

$$Q \text{ (Aperture Loss)} = \sigma A_o T^4.$$

Where $A_o$ is the aperture area and T is the cavity temperature. As indicated in Section 4.3, the ground testing of actual solar thermionic systems has shown this to be a good approximation (Reference 4-5).

### 4.4.1.6 Concentrator Rim Angle

For given concentrator geometric and orientation angular errors, the minimum aperture diameter which will pass all the energy reflected from the concentrator occurs when the concentrator rim angle* is slightly less than 45 degrees; the actual value of this rim angle being given by (Reference 4-6):

$$\phi = 45^{o} = 1/2\ (\beta_s + 2\ \beta_c + \beta_o)$$

where:

$\phi$ = The concentrator rim angle, degrees

$\beta_s$ = Half angle subtended by the sun (approximately 16 minutes at the earth), degrees

$\beta_c$ = Maximum concentrator error angle, assumed to occur at the rim, degrees

$\beta_o$ = Orientation angle error, degrees.

However, the optimum aperture diameter for a given set of concentrator geometric and orientation errors and generator cavity temperature will be something less than that diameter which passes all the reflected energy from the concentrator. This occurs because of the trade-off between energy entering the aperture and that reflected and reradiated back out through the aperture as aperture diameter is varied. Moreover, the higher the cavity temperature, the smaller this optimum diameter will be; assuming the other factors are held constant. Furthermore, in considering the nature of the flux distribution in the plane of the aperture for geometrically perfect concentrators, having zero orientation angle error, the peak flux density, occurring within the sunspot diameter, increases as the rim angle increases. As cavity temperature increases, the optimum rim angle for maximum net energy to the generator will, therefore, increase for concentrators having zero geometric and orientation angle errors. On the other hand, effects of geometric and orientation angle errors increase with rim angle. It is apparent that detailed analysis is required to determine the optimum rim angle for a specific case, but generally, it can be said that it should not be less than approximately 45 degrees and will increase as the cavity temperature increases.

*Concentrator rim angle is defined as the angle between the axis of symmetry of the concentrator and a line drawn from the focal point to a point on the rim.

The effect of rim angle variation on concentrator-absorber efficiency for various values of geometric angular error was also studied in Reference 4-9 and the results are summarized in Figure 4-16. For zero orientation error the concentrator-absorber efficiency decreases slightly with increasing rim angle. With orientation error included, this decrease in efficiency would be more significant.

Concentrator hardware development for solar thermionic applications has dealt primarily with 45 and 60 degree rim angles. Because of the interest in these two values, the concentrator performance calculations will be carried out for both 45 and 60 degree rim angles. A decision on the rim angle value to be used in this study will be made after the performance calculations are completed.

### 4.4.2 CONCENTRATOR-ABSORBER PERFORMANCE CALCULATIONS

The concentrator-absorber performance calculations were carried out on an IBM 7090 Computer using a procedure developed previously. *

For the assumptions outlined in Section 4.4.1, plots of energy entering the cavity for various values of aperture diameter were prepared for concentrator diameters of 2, 3.5 and 5 feet. These plots were made for 45 and 60-degree rim angles and the results are presented in Figures 4-17, 4-18, and 4-19.

Computing the black-body reradiation loss as a function of aperture diameter (Figure 4-20) and subtracting this loss from the "energy entering the aperture" values given in Figure 4-17, 4-18, and 4-19 yields the net energy available in the cavity as a function of aperture diameter. These net energy values peak at distinct values of aperture diameter and these peak points are presented in Figure 4-21. Therefore, Figure 4-21 gives the net energy available in the cavity as a function of concentrator diameter for a cavity temperature of 2000°K and rim angles of 45 and 60 degrees. Figure 4-22 presents optimum aperture diameter as a function of concentrator diameter. These optimum aperture diameter values correspond to the net energy values given in Figure 4-21.

*The computer program employed was developed by the General Electric Company in 1960. Since the concentrator-absorber performance calculations used in this study were performed, Dr. Schrenk of the University of Pennsylvania has developed a new computer program for predicting concentrator performance. Dr. Schrenk's program does not rely on customary approximations and assumptions and will handle both radial and circumferential errors. For future performance calculations, Dr. Schrenk's program is recommended.

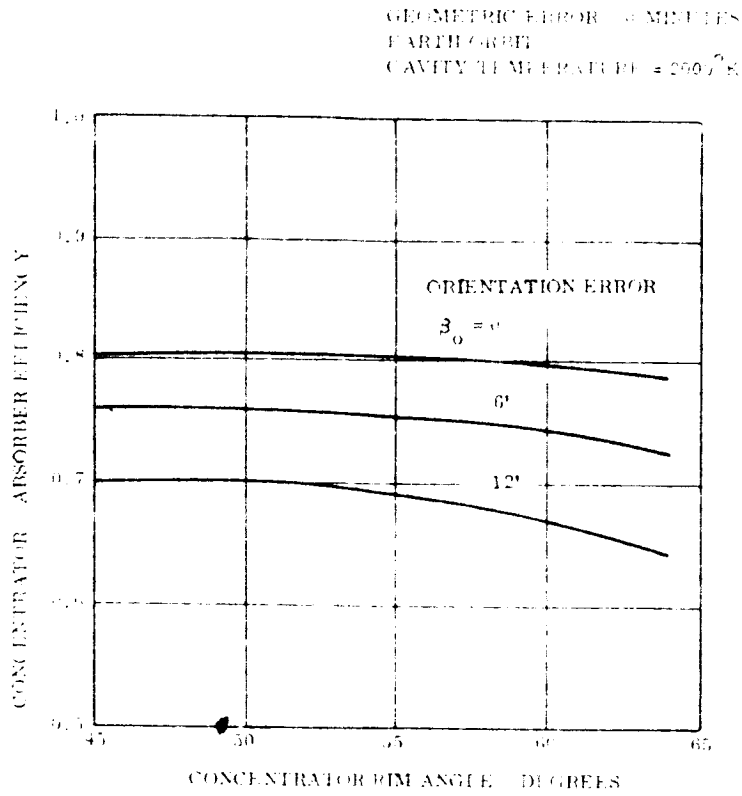


Figure 4-15. Concentrator-Absorber Efficiency vs. Rim Angle for Various Values of Orientation Error

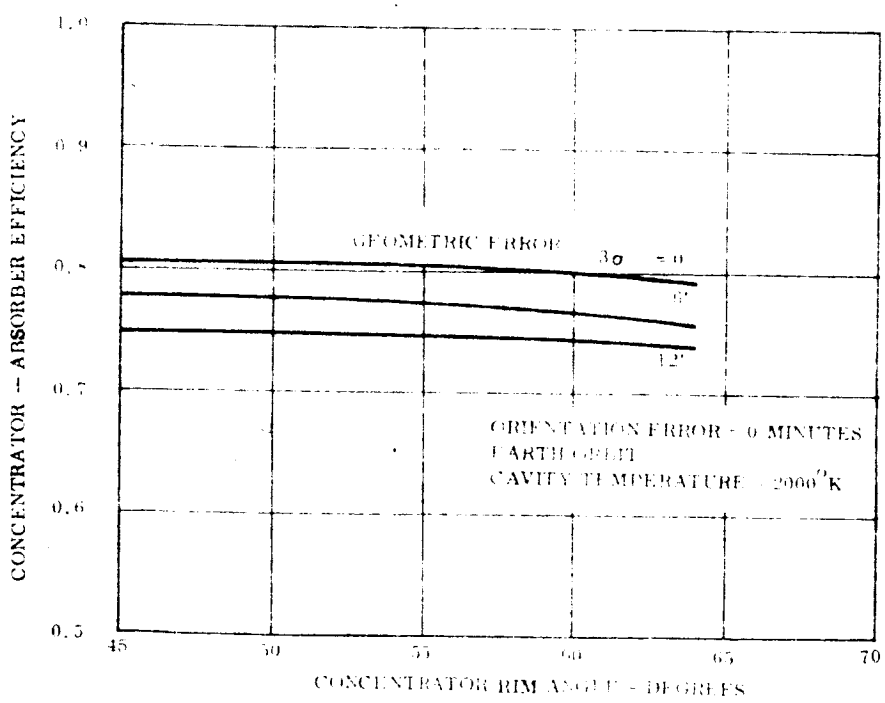


Figure 4-16. Concentrator-Absorber Efficiency vs. Rim Angle for Various Values of Geometric Error

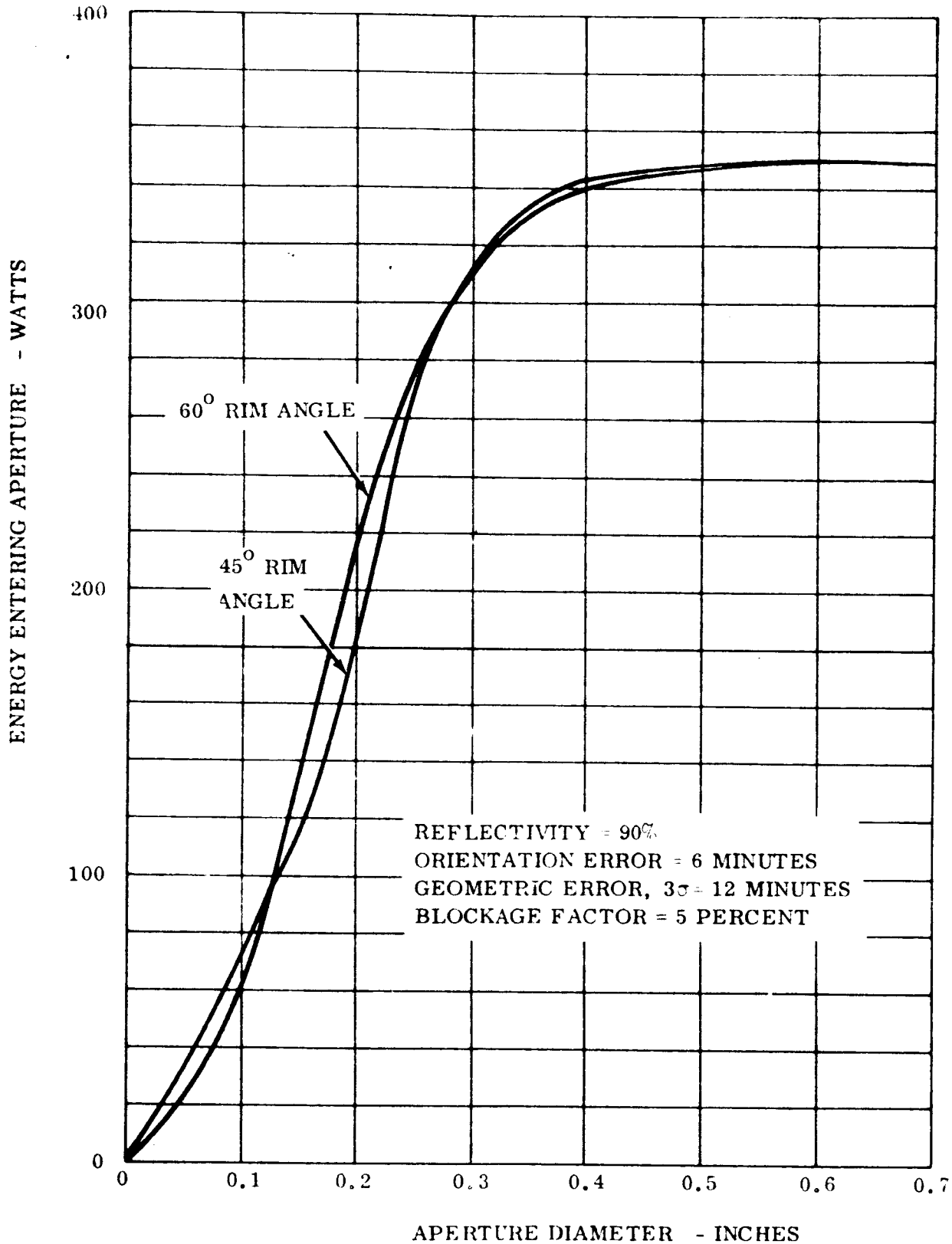


Figure 4-17. Energy Entering Aperture vs. Aperture Diameter (Concentrator Diameter = 2 Feet)

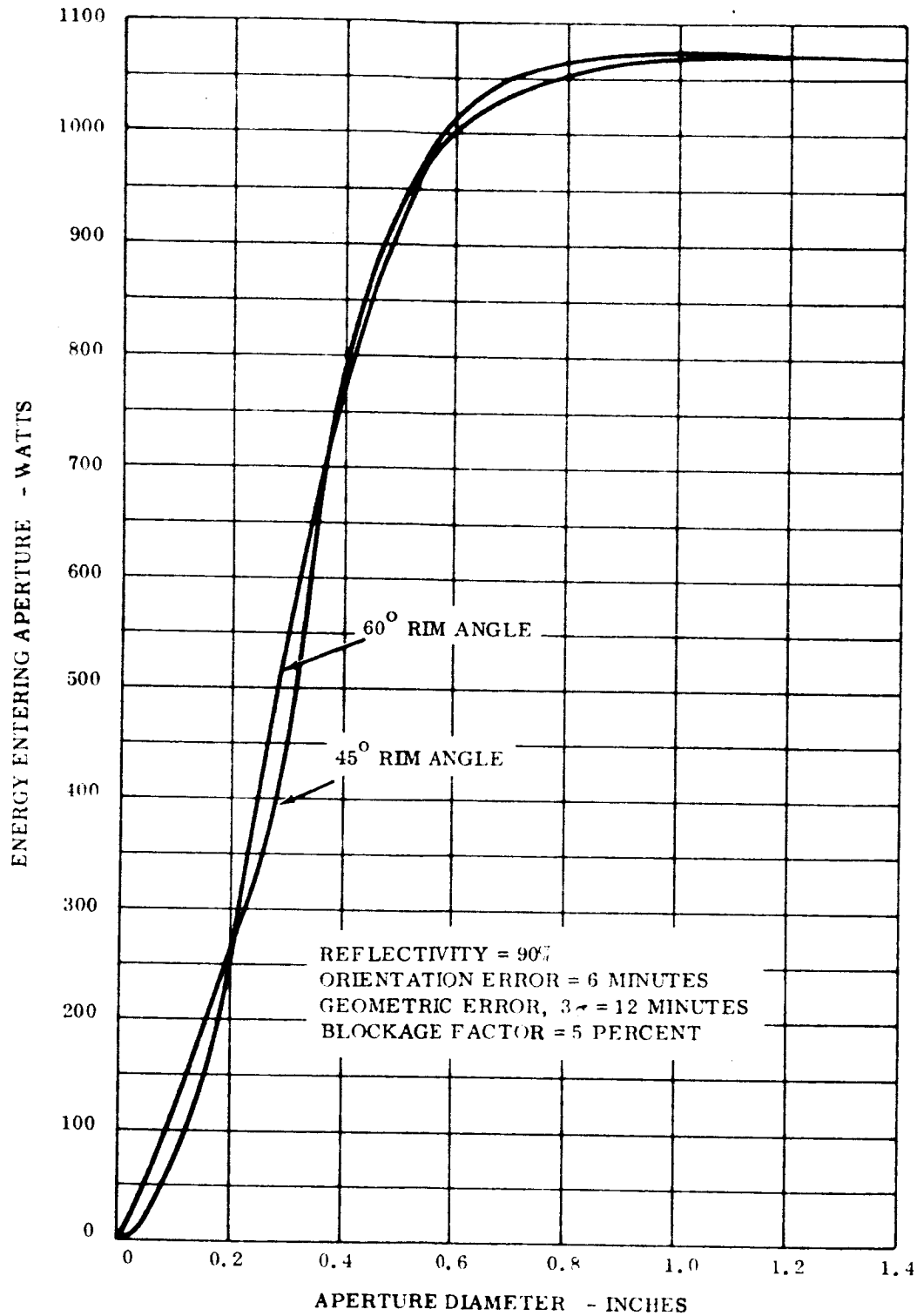


Figure 4-18. Energy Entering Aperture vs. Aperture Diameter (Concentrator Diameter = 3.5 Feet)



177

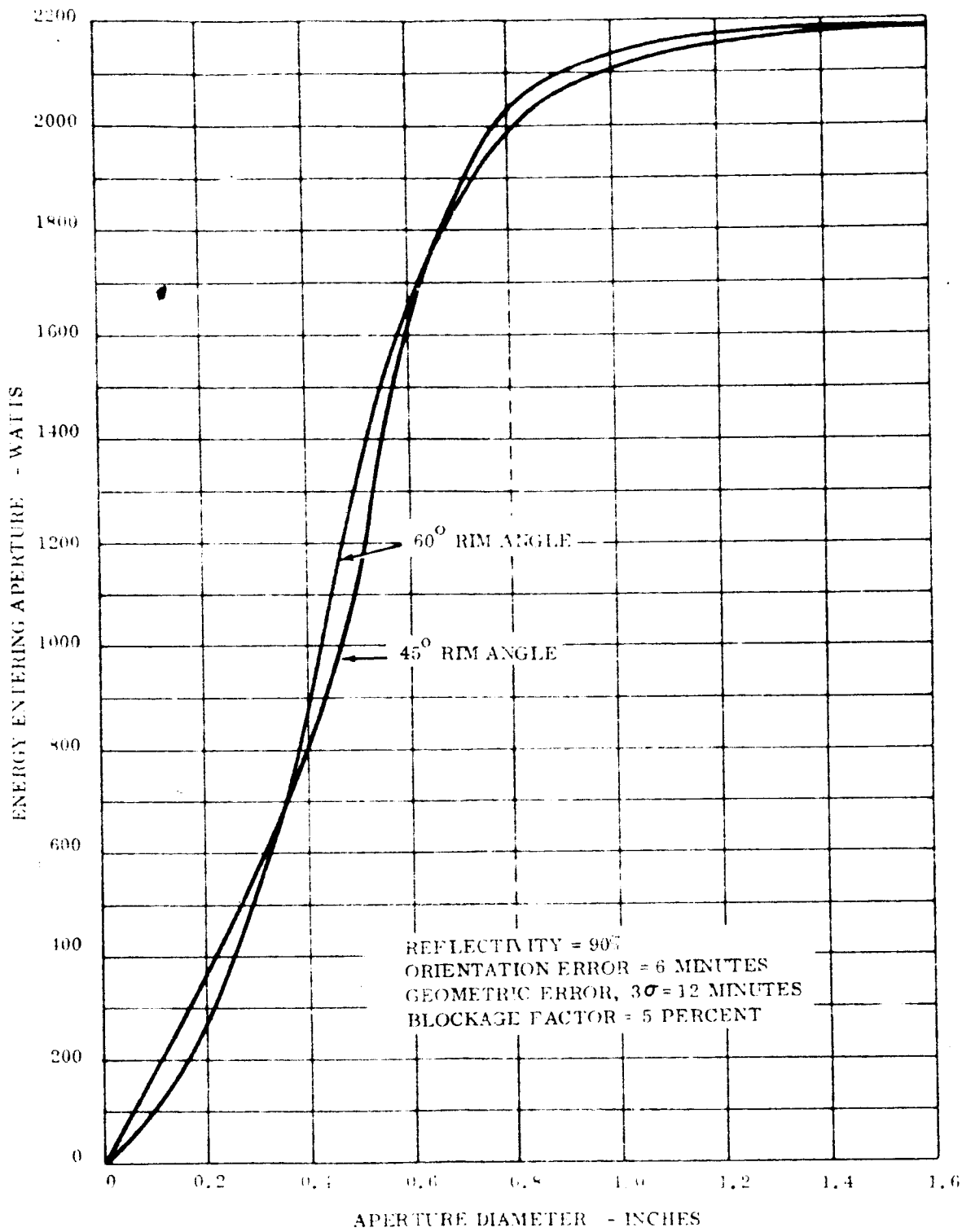


Figure 4-19. Energy Entering Apeture vs. Aperture Diameter (Concentrator Diameter = 5 Feet)

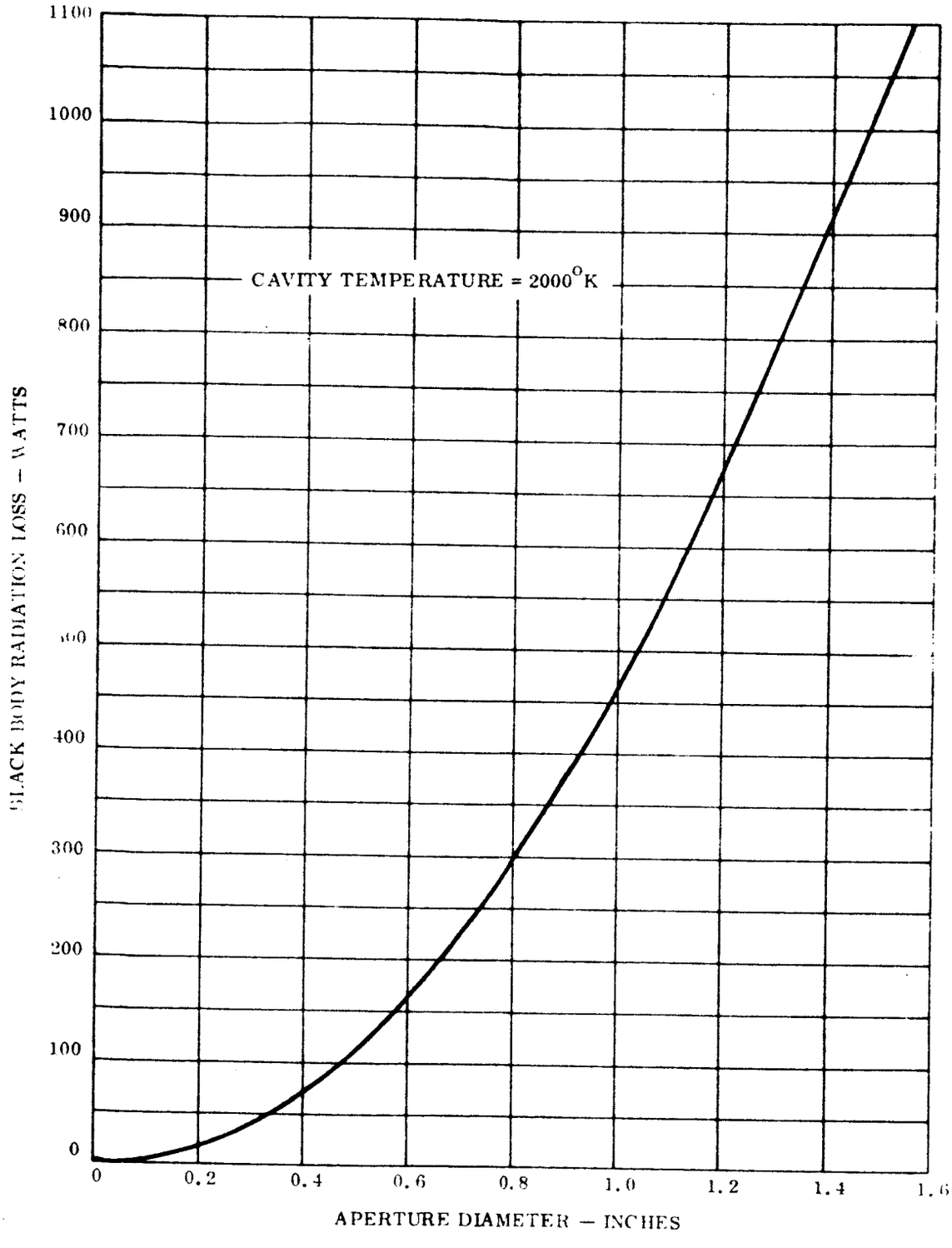


Figure 4-20. Blackbody Radiation Loss vs. Aperture Diameter

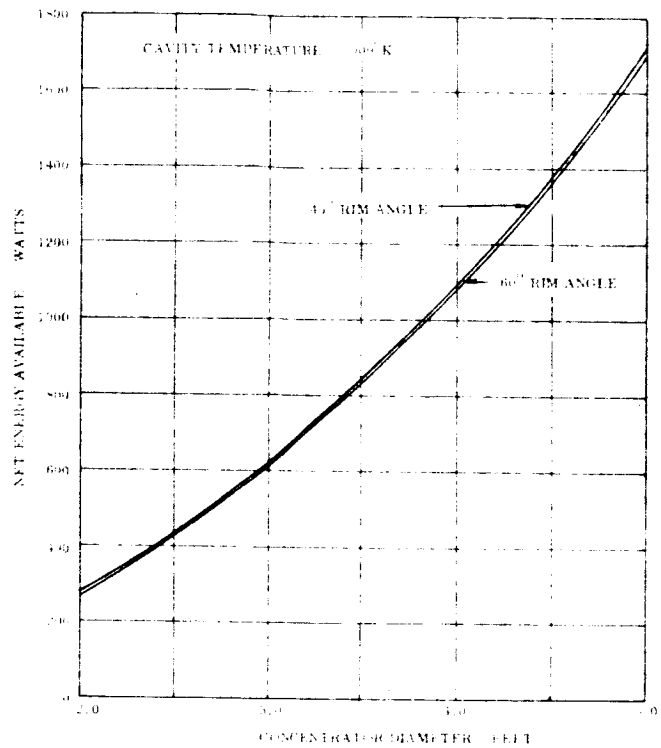


Figure 4-21. Net Energy Available vs. Concentrator Diameter at Optimum Aperture

Having the "net energy available" as a function of aperture diameter from the preceding calculations the concentrator-absorber efficiency can be computed using

$$\eta_{ca} = \frac{Q_n}{A_c \times S} ,$$

where:

$Q_n$ = Net energy available, watts

$A_c$ = Concentrator projected area, $ft^2$

S = Solar intensity, watts/$ft^2$

= 130 watts/$ft^2$ at 1 AU.

Since the same assumptions were used in computing the concentrator-absorber efficiency for the 2, 3.5, and 5-foot diameters, the resulting efficiency values will be the same. However, the two rim angle values considered will yield different concentrator-absorber efficiencies.



180

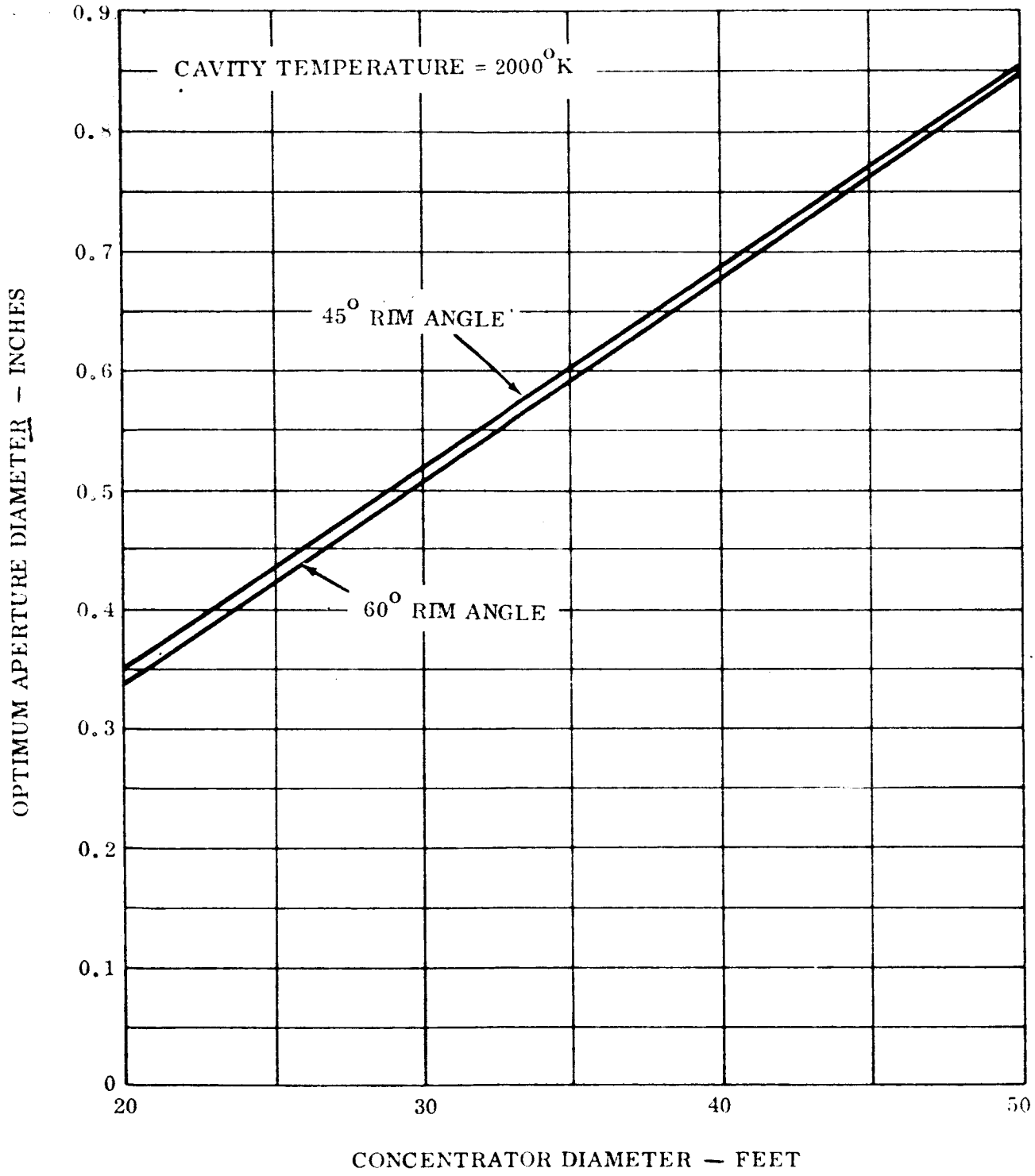


Figure 4-22. Optimum Aperture Diameter vs. Concentrator Diameter

These values are computed below:

$$\eta_{ca}\ (45^{o}\ \text{Rim Angle}) = \frac{276 \times 100}{3.14 \times 130} = 67.7 \text{ percent}$$

$$\eta_{ca}\ (60^{o}\ \text{Rim Angle}) = \frac{273.5 \times 100}{3.14 \times 130} = 67.0 \text{ percent}$$

It is apparent that the high cavity temperature has made the concentrator-absorber efficiency relatively insensitive to concentrator rim angle in the range from 45 to 60 degrees.

### 4.4.3 RIM ANGLE SELECTION

The concentrator-absorber efficiency for the 45 and 60-degree rim angles being essentially equal, a selection of a specific rim angle value on which to base this study cannot be made on performance alone. However, there are practical considerations beyond concentrator-absorber efficiency which resulted in the selection of a 60-degree rim angle for use in this study. The reasons for chosing the 60-degree rim angle rather than 45 degrees are outlined below.

a. The 60-degree rim angle yields a shorter focal length which results in several advantages.

   1. The generator support arms are shorter and, therefore, weigh less.

   2. If the generator is launched in its fixed position with respect to the concentrator (not folded on launch and deployed in space) then a 60 degree rim angle allows the spacecraft to be shorter. This in turn simplifies packaging the spacecraft within the launch vehicle fairing. For example, for a concentrator diameter of 50 inches there is a difference in the focal length of 8.45 inches between a 45 and 60-degree rim angle.

   3. If after the system is in space, for some reasons such as thermal distortion, there is a displacement of the generator with respect to the concentrator optical axis, the performance will be least affected in the system with the shorter focal length. For example, in the case of a 50-inch diameter concentrator, an angular misalignment of 6 minutes represents a lateral displacement in the focal plane of 0.053 and 0.033 inches for rim angles of 45 and 60 degrees respectively.

b. The 60-degree rim angle results in a deeper parabola which has two major advantages.

1. The deeper parabola is structurally more rigid for withstanding the launch vibration and acceleration loads.

2. The deeper parabola provides a recess for the generator in cases where the generator must be folded down during launch and deployed once the vehicle is in space. For example, the parabola depth for a 50-inch diameter concentrator is 5.4 and 7.25 inches for rim angles of 45 and 60 degrees respectively.

c. The 60-degree rim angle yields a better generator cavity design. The energy entrance conditions for 45 and 60-degree rim angles are illustrated in Figure 4-23.

In the 60-degree rim angle case the energy impinges on a point closer to the front of the generator. This allows the converters to be located closer to the front of the

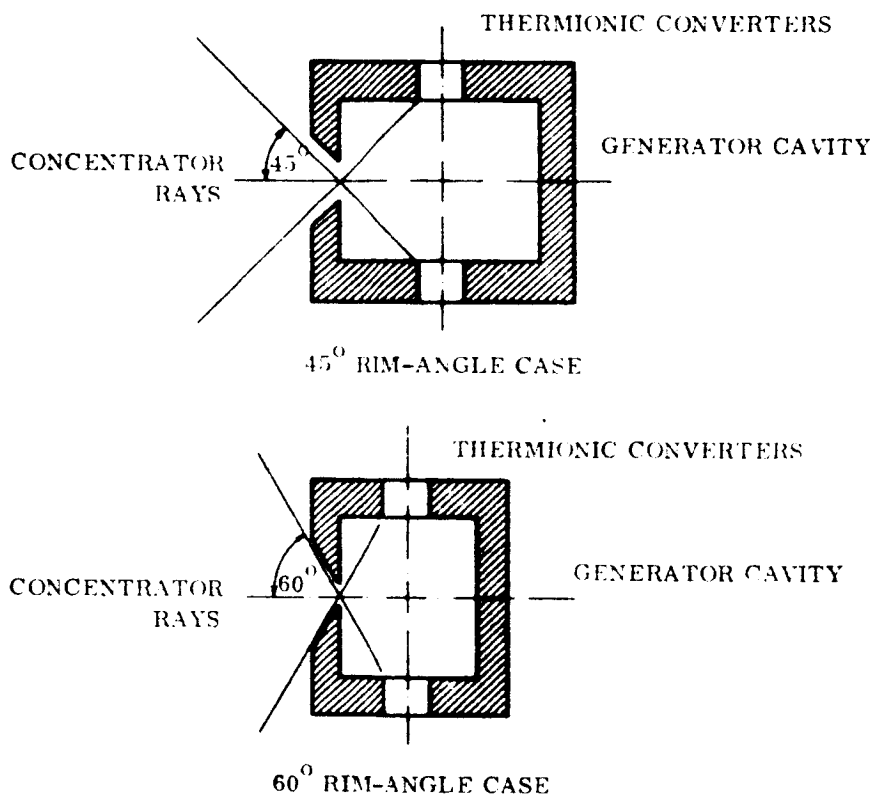


Figure 4-23. Energy Entrance Conditions, 45 and 60-Degree Rim Angles

generator which reduces the size of the generator cavity and subsequently the generator weight and thermal losses.

The remainder of this study is based on a concentrator rim angle of 60 degrees.

## 4.5 THERMIONIC SYSTEM PERFORMANCE

Now that the thermionic converter, generator and concentrator performance have been estimated the solar thermionic system performance can be predicted.

Since the thermionic generator is to contain four converters (study ground rule) the generator power output is given by

$$P_o = 4 \times A_E P.$$

Where $A_E$ is the converter emitter area in square centimeters and P is the converter power density in watts per square centimeter. The generator efficiency is given by:

$$\eta_g = \frac{P_o}{Q_n},$$

or

$$P_o = Q_n \eta_g.$$

Using the generator efficiency expression given in Section 4.3, this becomes

$$P_o = 0.7\, Q_n \eta_c.$$

Substituting this equation in the original generator power output expression and solving for $Q_n$ yields

$$Q_n = \frac{5.71\, A_E P}{\eta_c}$$

Using this expression and the data given in Figures 4-7 and 4-8 the net energy required ($Q_n$) can be computed for various values of converter emitter area ($A_E$).

This was done for both peak power and peak efficiency operation and the results are given in Figure 4-24. Also presented in Figure 4-24 are the corresponding values of generator power output $P_o$.

Figure 4-21 gives concentrator diameter versus net energy available ($Q_n$). Therefore, for a selected value of emitter area, $A_E$, the generator power output, $P_o$, and net energy required, $Q_n$, are defined from Figure 4-24. Entering Figure 4-21 with this value of $Q_n$ yields the required concentrator diameter. This procedure was followed and generator power output versus concentrator diameter plotted in Figure 4-25. Also included in Figure 4-25 are the maximum concentrator diameters that the various launch vehicles will accommodate (see Section 2.).

Several interesting conclusions can be drawn from Figure 4-25. For a minimum acceptable generator power output of 100 watts, the lower limit on concentrator diameter is approximately 42 inches. An upper limit is established by the maximum allowable concentrator diameter compatible with the launch vehicles considered. This is represented by the THOR ABLESTAR vehicle which can accommodate a concentrator diameter of 58 inches. The range of concentrator diameters of interest then is 42 to 58 inches. For this range of concentrator diameters, generator power outputs of from 100 to 185 watts can be obtained.

The thermionic system efficiency is defined as

$$\eta_s = \eta_g \times \eta_{ca}$$

Using the generator efficiency expression from Section 4.3 and substituting the concentrator-absorber efficiency value for the 60-degree, rim angle case (0.67) the above expression becomes

$$\eta_s = 0.7 \times 0.67 \quad \eta_c = 0.469 \quad \eta_c.$$

For a given concentrator diameter Figure 4-19 gives the generator power output ($P_o$) for either peak power or peak efficiency operation. Using this value of generator power output Figure 4-24 defines the thermionic converter emitter area ($A_E$). This value of emitter area ($A_E$) used in conjunction with Figures 4-7 or 4-8 yields the thermionic converter

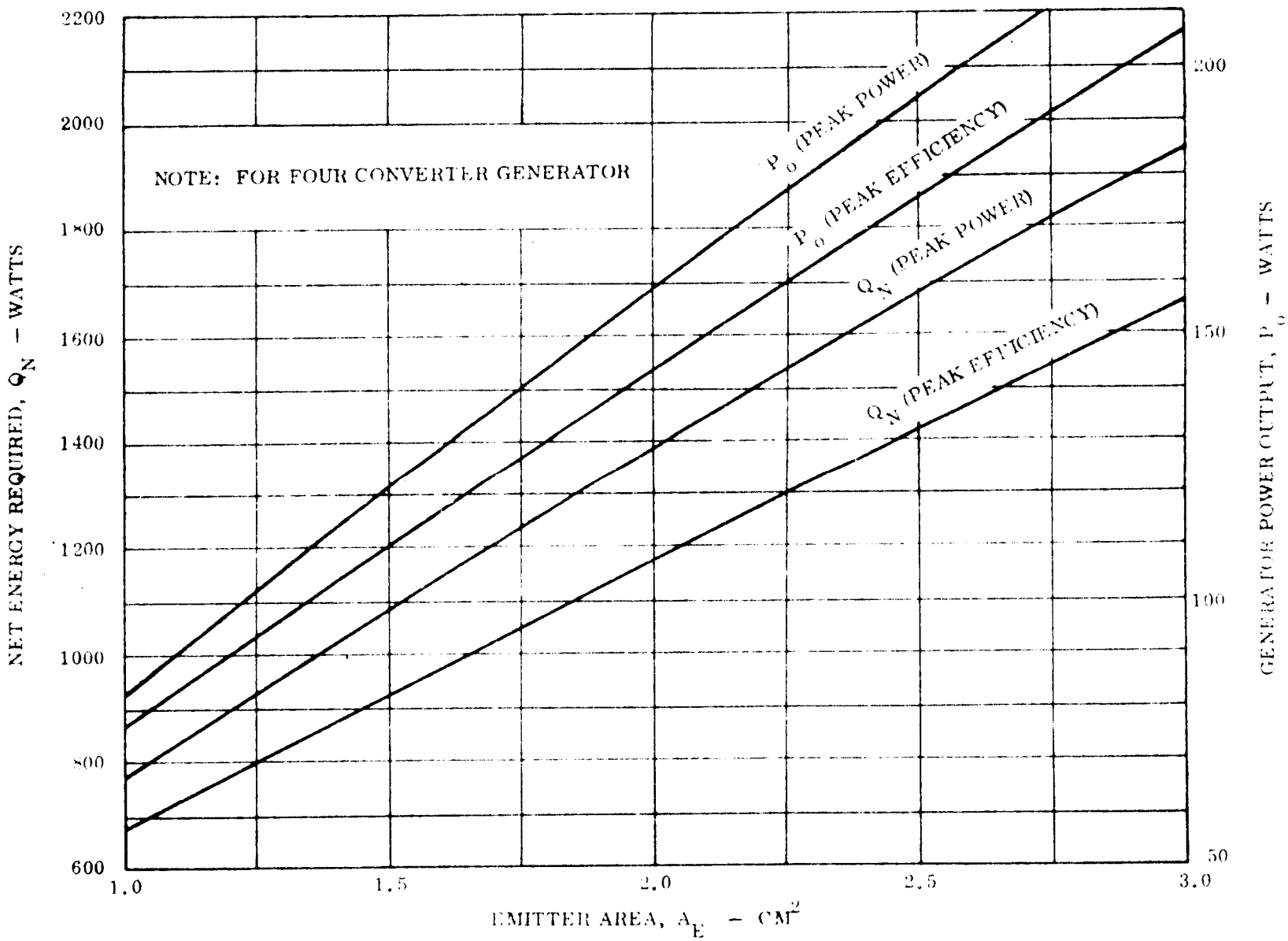


Figure 4-24. Generator Net Energy Required and Power Output vs. Converter Emitter Area

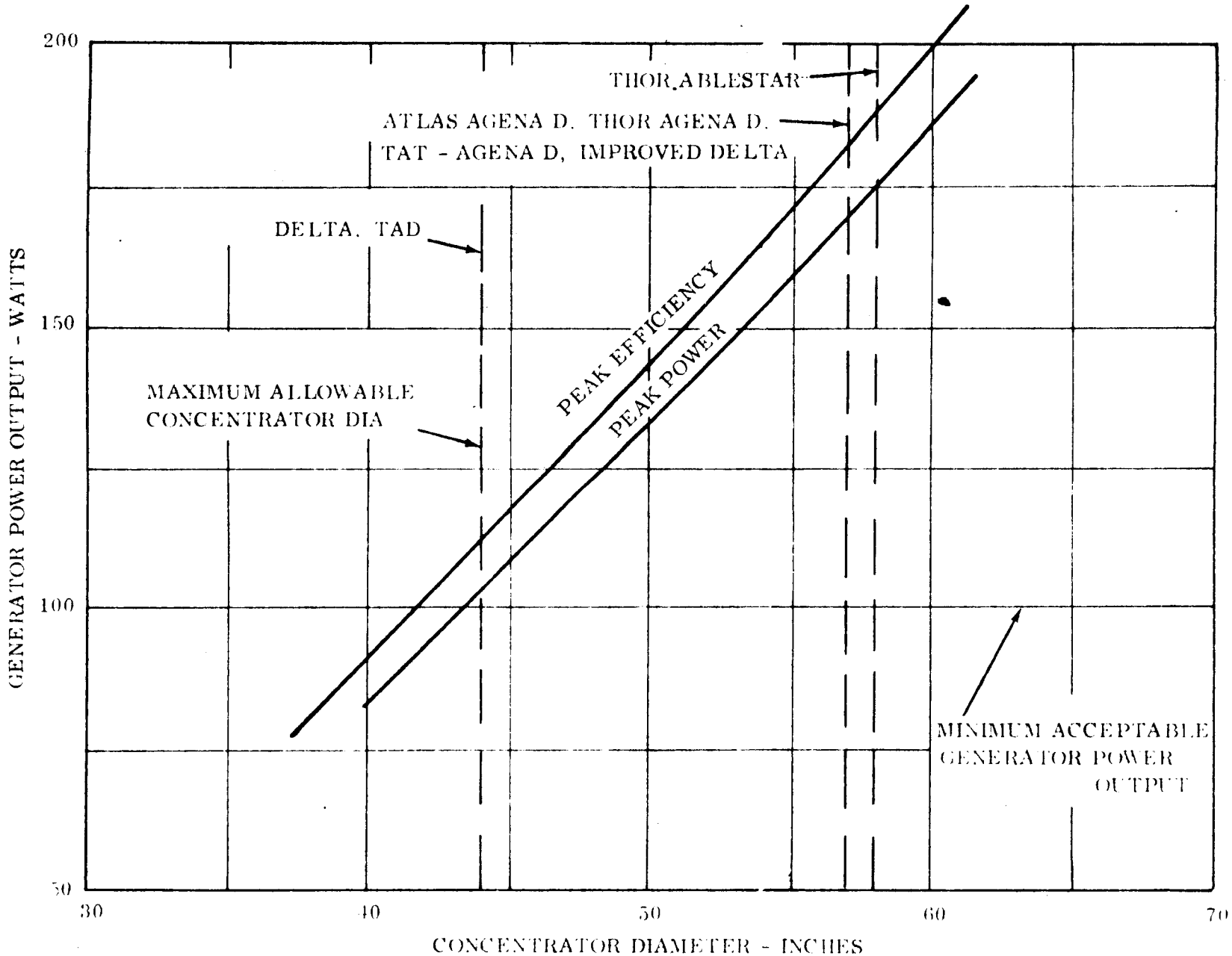


Figure 4-25. Thermionic Generator Power Output vs. Concentrator Diameter

efficiency. Substituting this value of converter efficiency in the above expression yields the system efficiency. Following this procedure, thermionic system efficiency as a function of concentrator diameter was computed and the results are presented in Figure 4-26. The thermionic system efficiency increases with concentrator diameter for both peak power and peak efficiency operation. This occurs because for the larger concentrator diameters the converter emitter area is larger and converter efficiency increases as the emitter area increases (see Figures 4-7 and 4-8).

## 4.6 SELECTION OF CONVERTER OPERATING POINT

Figures 4-25 and 4-26 indicate the following advantages for operating the thermionic converters at their peak efficiency rather than peak power point.

a. As indicated by Figure 4-25 peak efficiency operation yields a 7.5 to 9 percent higher generator power output for a given concentrator diameter.

b. Peak efficiency operation yields a lower weight thermionic system because for a given power level the concentrator will be smaller while the remainder of the system is essentially the same size regardless of operating point.

c. The voltage output per converter is approximately twenty percent higher for peak efficiency operation (0.7 volt compared to 0.85 volts). Therefore, for a four converter generator the series voltage output would be 2.8 compared to 3.4 volts for peak power and peak efficiency operation respectively.

For these reasons the thermionic system will be designed to operate at the converter peak efficiency point.

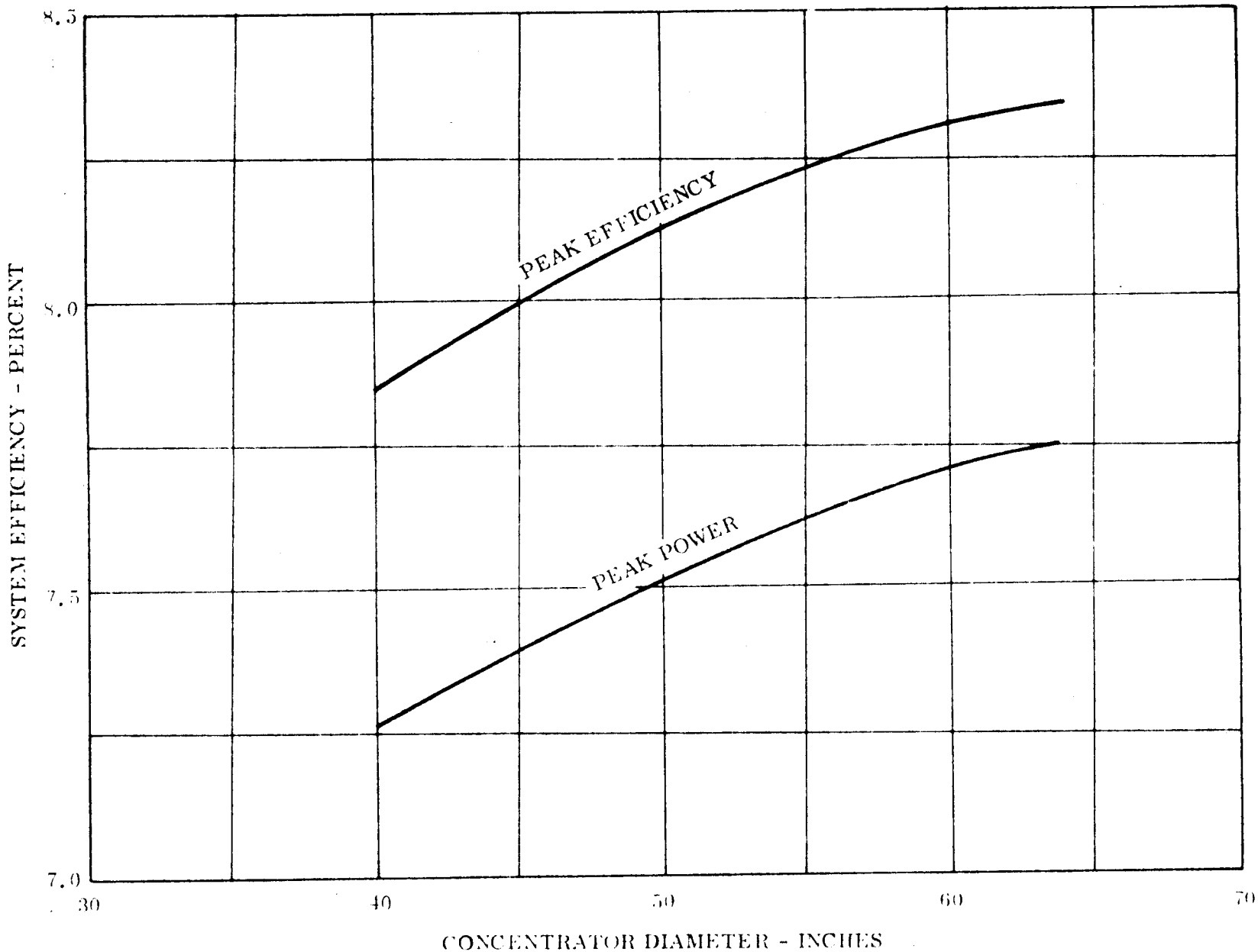


Figure 4-26. Thermionic System Efficiency vs. Concentrator Diameter

## 4.7 SUMMARY AND CONCLUSIONS

The major thermionic system performance parameters established in this section are summarized below.

THERMIONIC CONVERTER

| | | |
|---|---|---|
| Emitter Temperature | - | 2000°K |
| Emitter Material | - | Rhenium |
| Emitter Spacing | - | 2 mils |
| Emitter Sleeve Thickness | - | 0.0025 inches |
| Converter Power Density and Efficiency (Peak Power) | - | Figure 4-7 |
| Converter Power Density and Efficiency (Peak Efficiency) | - | Figure 4-8 |

THERMIONIC GENERATOR

| | | |
|---|---|---|
| Generator Efficiency | - | $\eta_g = 0.7\ \eta_c$ |

CONCENTRATOR-ABSORBER

| | | |
|---|---|---|
| Concentrator Reflectivity | - | 90 percent |
| Concentrator Geometric Error, 3 σ | - | 12 minutes |
| Concentrator Blockage Factor | - | 5 percent |
| Concentrator Orientation Error | - | 6 minutes |
| Concentrator Rim Angle | - | 60 degrees |
| Absorber Cavity Acts as Black Body at | - | 2000°K |
| Concentrator-Absorber Efficiency | - | 67.0 percent |

THERMIONIC SYSTEM

| | | |
|---|---|---|
| Generator Power Output Versus Concentrator Diameter | - | Figure 4-25 |
| Thermionic System Efficiency Versus Concentrator Diameter | - | Figure 4-26 |
| Operate the Thermionic Converters at the Peak Efficiency Point | | |

The range of concentrator diameters of interest is from 42 to 58 inches. Based on the performance figures stated above, a concentrator of 42 inches is needed to achieve the required minimum generator power output of 100 watts. The maximum concentrator diameter (58 inches) will yield a generator power output of 188 watts at the converter peak efficiency operating point.

The maximum thermionic generator power outputs (see Figure 4-25) compatible with the promising launch vehicles identified in Section 2 are summarized below:

| | |
|---|---|
| DELTA (DSV-3C)<br>TAD (DSV-3D) | 112 watts |
| IMPROVED DELTA (DSV-3E)<br>(DSV-3F)<br>(DSV-3G)<br>(DSV-3H)<br>ATLAS-AGENA D<br>ATLAS-AGENA D-X-259<br>THOR-AGENA D<br>TAT-AGENA D | 182 watts |
| THOR-ABLESTAR | 188 watts |

It appears that any of the launch vehicles under consideration can provide the required minimum generator output of 100 watts. However, it should be noted that the figures given in this section are maximum values based on the assumption that the effective concentrator diameter is equal to the maximum allowable payload diameter the fairing can accommodate. When the spacecraft design is formulated, this may be difficult to achieve and the concentrator diameter may have to be reduced, resulting in a lower generator power output.

## 4.8 REFERENCES


4-1 G. Gaines and C. Sims, "Total Emittance or Rhenium," Bulletin of the American Physical Society, p. 2922, 1962.

4-2 W. Kohl, "Materials and Techniques for Electron Tubes," Rheinhold, 1960, p. 340 and 274.

4-3 S. Kitrailakis and M. Meeker, "Experimental Determination of the Heat Conduction of Cesium Gas," Advance Energy Conversion Journal, Volume 3, January-March, 1963.

4-4 A. Shavit, "Characteristics of Cesium Thermionic Energy Converters," Sc.D. Thesie, Mechanical Engineering Department M.I.T., May, 1964, Figure 19.

4-5 F. Blake and R. Herrick, "Cavity Vapor Generator Performance-Endurance Solar Test Program," General Electric Spacecraft Department, ASP-TM-022, July 1963.

4-6 "Solar Thermionic Electrical Power System," General Electric Missile and Space Division, December 1961, ASD Technical Report 61-121.

4-7 "Final Report-Analysis of Solar Reflectors Mathematical Theory and Methodology for Error Model Synthesis from Experimental Ray Trace Data," Allison Division of General Motors, Engineering Department Report No. 3958, September 1, 1964.

4-8 G. Schrenk, "Solar Collection Limitations for Dynamic Converters," University of Pennsylvania, Paper Presented at the AGARD Conference Held in Cannes, France, March 16-20, 1964.

4-9 "9 1/2 Foot Diameter Master and Mirror," General Electric Spacecraft Department, Final Report Prepared for JPL, March 26, 1964, Document No. 64SD540.

Vol II 65-

# SECTION 5

# SECONDARY EXPERIMENTS

PRINCIPAL CONTRIBUTORS:

Dr. K. Coulson
Dr. G. Bouricius
E. W. Williams
H. E. Brown
E. Fried
A. B. Grafinger
J. C. Peden
J. K. Baker

## SECTION 5
## SECONDARY EXPERIMENTS

### 5.1 INTRODUCTION

In addition to the primary solar thermionic experiment, numerous secondary experiments were considered and a recommended list established for each of the selected missions. These secondary experiments were treated in two categories: Engineering Experiments and Scientific Experiments. A description of each of the secondary experiments considered, along with a summary of the selection procedure used to establish the recommended list of experiments, is included in Sections 5.2, 5.3 and 5.4.

Twenty experiments were considered in total: ten engineering and ten scientific. These experiments are listed below.

Engineering Experiments

Radiation Effects on Solar Cells

Solar Thermoelectrics

Thermal Coatings

V-Ridge Concentrating Photovoltaics

Thin-Film Solar Cells

Solar Concentrator Reflective Surfaces

Thermal Contact Resistance

Infrared Detector

Laser Experiment

Low Thrust Electric Engine

## Scientific Experiments

Interplanetary Dust (Micrometeoroids)

Solar Wind

Proton and Electron Spectra and Direction

Magnetic Field

Heavy Nuclei

Solar X-Rays

Solar $\gamma$-Rays

Earth Albedo

Ultraviolet Radiation Measurement

Lyman-Alpha

By necessity, a study of this size is limited in the number of secondary experiments it can consider and the depth in which each experiment can be studied. This program considered those experiments which were felt to be of major importance to the development of solar thermionics and to the total space program. In addition secondary experiments were selected for consideration on the basis of their compatibility with the primary experiment and their ability to take advantage of the unique requirements of the primary experiment such as highly accurate sun orientation.

The results of this portion of the study are illustrative of secondary experiments that could be included on a spacecraft whose primary objective was the evaluation of solar thermionics. As subsequent studies of the solar thermionic flight experiment are undertaken, it will be necessary to continually evaluate potential secondary experiments to insure that those finally selected represent the best possible choice. Before a final selection is made, it will be necessary to evaluate these experiments in greater detail than this study would allow.

## 5.2 ENGINEERING EXPERIMENTS

Each of the secondary Engineering Experiments considered is described in this section.

### 5.2.1 RADIATION EFFECTS ON SOLAR CELLS

The basic design for this experiment was taken from Reference 5-1.

#### 5.2.1.1 Background

Of all the components found on present state-of-the-art spacecraft the solar cell array generally exhibits the highest vulnerability to space radiation damage. As a result considerable attention must be given, when designing a space vehicle, to the shielding required to protect the solar array from the expected space radiation environment. The required shielding and over sizing of the solar array to account for the expected radiation damage can represent a very significant weight penalty. To minimize this weight penalty it is important to: (1) know the radiation environment accurately, (2) thoroughly understand the effect of radiation on solar array performance, and (3) be able to accurately predict the protection afforded by shielding. However, present methods of predicting damage are approximate and, in addition, a large uncertainty in the expected environment exists. Space experiments are needed to better understand this problem and to provide the necessary design information.

The normal solar array configuration consists of solar cells covered with a fused silica cover glass. The cover glass shields the solar cells from the radiation environment. A filter is vapor deposited on the cover glass which is held to the solar cell by an organic bond. Each of these four components: solar cell, cover glass, filter and organic bond to some degree exhibit a damage vulnerability.

In general, solar cell damage results from lattice defect production generated by collisions between higher energy particles and the lattice atoms. This produces a reduction in the minority carrier lifetime which lowers the short circuit current.

Degradation in the organic bond results from a change in its chemical composition induced by ionizing interactions with the incident radiation. Similar ionizing interactions with ultraviolet and particle radiation cause reduction in the transmittance of the filter and fused silica shield. These other effects, then, also degrade the short-circuit current since they reduce the amount of light reaching the cell surface.

5.2.1.2 Experiment Objectives

This experiment is designed to accomplish the following objectives:

a. Separate and determine the relative importance of damage in the solar cell, organic bond, filter and shield

b. Determine the relative degree of protection afforded by shielding of different thickness and provide evidence on the "hardness" of the incident spectrum

c. Monitor the spacecraft solar array degradation

d. Verify, or provide information for correcting, laboratory damage estimates to improve the efficiency of solar array design.

5.2.1.3 Experiment Definition

The selection of appropriate combinations of components for the solar cell assembly will allow damage in either the cell, shield, filter, or bond to prevail in producing degradation in the short circuit current. Therefore, the experiment would contain various combinations of shield, bond, etc., to allow a determination of the relative significance of damage in each. Shields of varying thickness would be used to indicate the effectiveness of this parameter on radiation hardening and the hardness of the incident spectrum. To complete the complement, cell assemblies, identical to those in the spacecraft array,

would be included for the purpose of monitoring the array degradation. Specifically, the experiment would be composed of these solar cell assemblies.

Type A Assembly - This assembly would consist of solar cell and shield with no filter or bond. The shield would be mechanically clamped to the cell and any degradation in the short circuit current would be due mainly to cell damage induced by the residual spectrum. There would be two Type A assemblies present; the shield on one would be 6 mils thick while the other would be 60 mils. Comparison of data for these two shields would indicate relative shield effectiveness and the incident spectrum hardness.

Type B Assembly - This assembly would consist of a pre-irradiated solar cell, shield, and filter with bond. Pre-irradiation of the solar cell would render it relatively immune to additional damage, therefore, any degradation in the output would be due mainly to damage in the shield, filter, and bond.

Type C Assembly - This assembly would consist of a pre-irradiated solar cell, bond, and shield with no filter. Therefore, degradation in the output should be due solely to damage in the bond and shield. A comparison of data from this assembly with data from Type B would indicate the amount of damage incurred by the filter.

Type D Assembly - This assembly would consist of a pre-irradiated cell, with shield, filter, and no bond. Therefore, degradation in the output should result mainly from damage in the shield and filter. A comparison of data from this assembly with Type B would indicate the degree of damage incurred by the bond.

Type E Assembly - This assembly would consist of a pre-irradiated cell and shield with no filter or bond. Any degradation occurring greater than approximately five percent would indicate damage in the shield.

Type F Assembly - This assembly would be representative of the vehicle array. It would contain identical bonding, shield thickness, filter and cells. Therefore, this data would be used to monitor the vehicle array degradation. Also, comparison with data from Type B would indicate the degradation that would be suffered by the cell alone.

5.2.1.4 Experiment Design

In an experiment of this nature, duplication to gain statistical confidence in the data is a necessity since no two samples will exhibit the same damage sensitivity. Therefore, in order to gain sufficient duplication using one vehicle, a scheme has been adopted which utilizes ten, 1/2 by 1/2 centimeter solar cell segments connected as shown in Figure 5-1. Each segment for an assembly would be cut from a different 1 by 2 centimeter cell. The remaining segments cut from the cell would be used in other assemblies. Every assembly would then consist of segments from ten different cells, however, the total output for each of the assemblies would represent the average of the ten cells. This is equivalent to using identical cells on each assembly and duplicating the entire experiment ten times. The segments in an assembly would be mounted in thermal contact with, but electrically insulated from, a common base plate. All would be covered by a single shield and filter piece. If $V_T$ is the voltage across the total string and $V_i$ is the voltage on each cell, then

$$V_T = \sum_{i=1}^{10} V_i$$

To measure the short-circuit current, a one ohm resistor would be connected across each segment. Therefore, the average short-circuit current would be

$$\bar{I}_{sc} = \frac{V_T}{10}$$

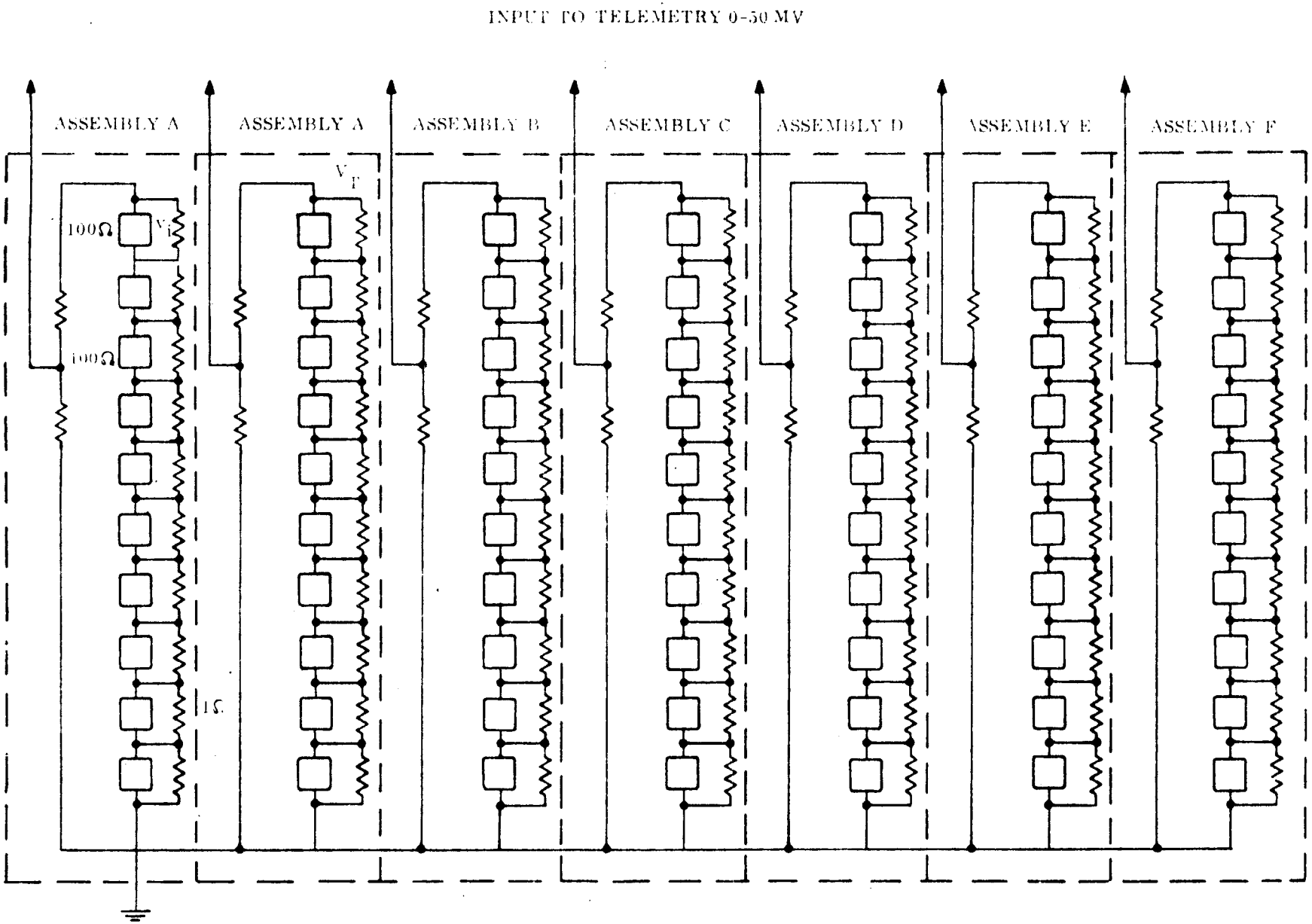


Figure 5-1. Schematic of Solar Cell Radiation Effects Experiment

Then only one quantity, $V_T$, must be measured to obtain the average short circuit current for the ten segments and the same statistical validity is obtained as if ten separate cell assemblies were exposed and measured separately. This scheme enables each assembly to be effectively duplicated ten times with no increase in the number of readings required and an increase in required surface area of only about one square centimeter. Although the size of a segment is 1/8 that of a normal cell, no insurmountable mounting or soldering problems are foreseen since the technology in this area is well advanced.

The short-circuit current is a temperature sensitive quantity, and since variations in temperature are expected, the requirement for temperature information exists. If all the assemblies were mounted on a good common thermal sink, all the cell temperatures should be approximately equal and only the sink temperature would have to be measured.

Solar cell output is also sensitive to sun orientation. The experiment would be sun oriented making use of the orientation system employed by the primary solar thermionic experiment. Since measurement of the orientation accuracy will be required for evaluation of the solar thermionic experiment, this information would be available for the secondary experiments as well.

5.2.1.5 Experiment/Spacecraft Interface Requirements

The interface requirements for the solar cell experiment (assuming a total number of seven solar cell assemblies) are summarized below:

| | |
|---|---|
| Electrical Power Required | 0.04 watts for operation of 2 thermistors |
| Weight | Less than 0.5 pounds |
| Size | 4.5 in.$^2$ by 1 in. deep |
| Instrumentation | 7 voltages (0-50 mv)<br>2 temperatures (thermistors 0-5v) |
| Telemetry Accuracy Required | 1 percent of full scale reading |

The experiment must be sun oriented within approximately $\pm$ 5 degrees.

## 5.2.2 SOLAR THERMOELECTRICS

### 5.2.2.1 Background

One of the potentially attractive means of supplying electrical power in space is by means of solar thermoelectrics. Development efforts in solar thermoelectrics have concentrated on two approaches: (1) a parabolic concentrator system under development by Hamilton Standard (Reference 5-2), and (2) a flat panel system being developed by General Atomic Division of General Dynamics (References 5-3 and 5-4). The development of both of these approaches has been supported by the Space Systems Division of the Air Force. Of the two, the flat panel system is in a more advanced state of development, having proceeded to the point where two earth orbiting flight tests have been carried out. Either of these two concepts could be tested in conjunction with the solar thermionic experiment, but since the recent emphasis has been on the flat panel concept it was selected for consideration in this study.

In the flat panel, solar thermoelectric generator design, heat from the sun is used to provide the temperature difference between the hot and cold junctions. A sandwich type construction is used wherein the thermoelectric elements are bonded between two thin aluminum sheets. One sheet, called the collector, is coated to produce a surface having a high solar absorptivity and a low infrared emissivity. This side of the panel is oriented toward the sun, absorbs energy from it, and produces the hot junction temperature. The heat absorbed is partially converted into electrical energy, and the remainder is transferred through the thermoelectric elements to the cold junctions and radiated from the other side of the panel. Figure 5-2 indicates a typical construction for this type of design. The honeycomb is added to provide structural strength. It should be noted that there is a radiation heat leakage path between the collector foil and the cold honeycomb surface through the area not covered by thermoelectric elements. In this connection, the cross sectional area of the thermoelectric elements is negligible with respect to the panel surface area (less than one percent in a typical design).

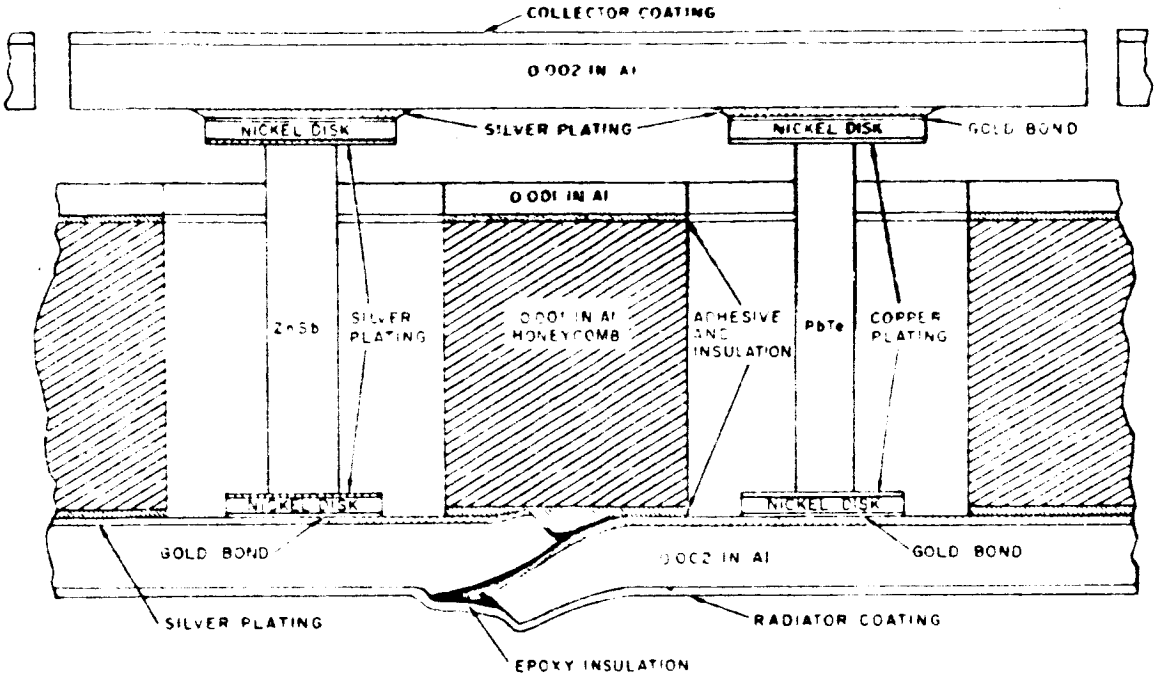


(a) Cross-section view of panel construction

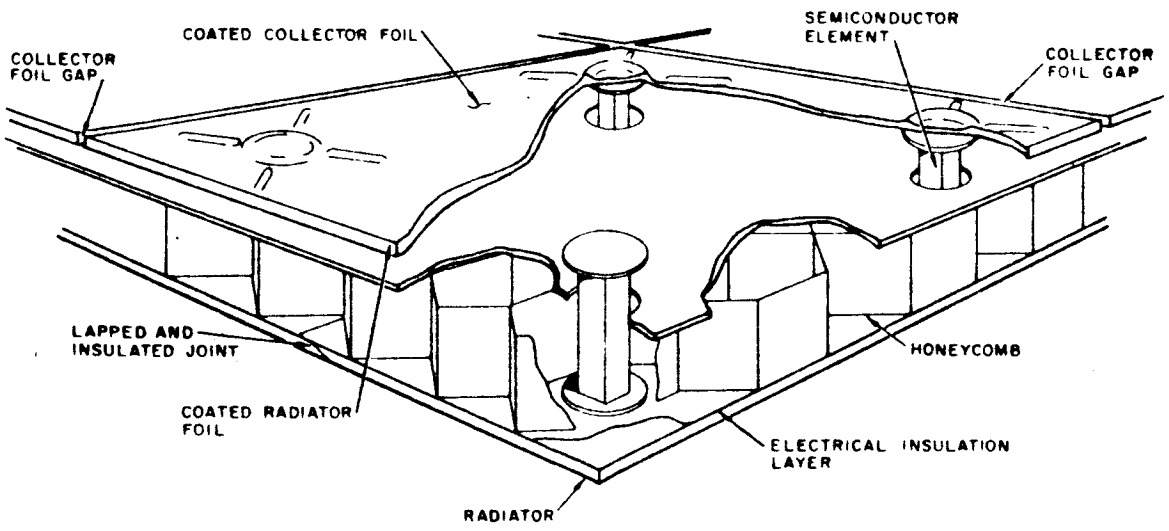


(b) Cutaway view of panel section

Figure 5-2. Construction Details of Solar Thermoelectric Panel

To date, effort at General Atomics has concentrated on the use of zinc antimonide as the p-type thermoelectric material and lead telluride as the n-type material, although other materials are now being actively investigated. The collector coating, which has a most important effect on performance, is a multi-layer optical coating consisting of four alternate layers of elemental aluminum and silicon monoxide, with silicon monoxide forming the outer layer. The total coating is less than one micron thick.

An indication of the state of the art of the flat panel solar thermoelectric design is provided by the following statements.

a. Two flight tests have been made for this type of design. In each test, three panels, each 4 inches square, were mounted in a magnesium frame. This frame was then mounted on a boom which swung out perpendicular to the vehicle after orbit had been achieved. The nature of the mission and orientation was such that the panels were perpendicular to the sun only once during each orbit, and performance measurements made during that time.

   The n-type material used was lead telluride; the p-type material was zinc antimonide. Flight test data covered a period of less than 100 relatively low altitude earth orbits in both flights.

   Based on telemetry data, the power output varied widely from panel to panel. In the first test particularly, there was a significant decrease in power output with time for each panel. In the second test the power output per panel remained essentially constant or increased slightly with time. The range of power outputs for the first set of data in each flight was in the range of 0.8 to 1.8 watts per square foot. These compared with a range of measured values for the same panels made during ground acceptance testing in a solar simulator of about 2.0 to 2.8 watts per square foot. The ratio of flight test power output to acceptance test power output for the individual panels ranged from approximately 40 percent to

85% percent. Also, the power output obtained in the space experiment can be compared to the calculated value of 2.66 watts per square foot for these flight models.

b. Some difficulties were experienced with the telemetry data as to consistency, accuracy, and completeness. These difficulties throw some question on the accuracy and interpretation of the flight test results. Principal areas of question in comparing the flight test results to the ground acceptance tests are the behavior of the collector coating, and of the bond between the thermoelectric elements and the collector and radiator surfaces plus, uncertainty in the actual value of solar intensity experienced by the panels during flight. There is reason to suspect, particularly for the first flight test, that some handling damage may have occurred both to the collector coating and possibly the elements themselves. In addition, there is no data available on the effects of the space environment on the collector coating material, e.g., radiation, ultra-violet, high vacuum, etc. It is considered quite probable that the deterioration in output with time observed in the first flight tests is due in large measure to deterioration of the bonds between the elements and the collector and radiator surfaces.

c. Subsequent to carrying out the flight tests, an improved technique has been developed for bonding the thermoelectric elements to the collector and radiator surfaces. Extensive tests of this process indicate that the bonding problem has been solved. For example, thermal cycling test comprising 900 cycles between 573$^{o}$K and 303$^{o}$K have been carried out with satisfactory performance. Also, measurements of bond strengths have been carried out on a statistical basis; these were found to be much higher than the buckling strength of the radiator and collector sheets.

d. Based on extensive life testing, zinc antimonide-lead telluride couples are expected to be operable at a hot junction temperature of 573$^{o}$K for periods from six months to two years in this type of configuration without experiencing significant deterioration. This is the design hot junction temperature for the flight test models.

e. Measured weights of the 4-inch square flight test panels are 0.14 pounds per square foot. It appears that this figure can be reduced to 0.10 pounds per square foot without any major breakthroughs.

f. In preparation for the flight test, all of the panels flown were subjected to shock, vibration and vacuum-solar simulation acceptance test. Each panel passed these tests satisfactorily.

From this description of the current state of the art of the solar thermoelectrics, it is apparent that further development will require additional space testing, preferable under better experimental conditions than the previous tests were conducted.

5.2.2.2 Experiment Objectives

The objectives of this experiment are:

a. Demonstrate the feasibility of solar thermoelectrics as a means of supplying space power

b. Conduct a long term evaluation of a solar thermoelectric power supply in the space environment.

5.2.2.3 Experiment Definition

A spacecraft designed to conduct a solar thermionic flight experiment offers a very attractive platform for evaluating solar thermoelectrics. Unlike the space experiments conducted to date, the panels would always be oriented to the sun when the spacecraft was not in the earth's shadow. In addition, measurements of the solar intensity, radiation environment, orientation error and micrometeoroid density would be available from the primary solar thermionic experiment. Therefore, the solar thermoelectric experiment

would only require the addition of temperature and voltage instrumentation to provide a more complete evaluation than was possible from the previous space experiments.

5.2.2.4 Experiment Design

The experiment would consist of three, solar thermoelectric panels of the construction shown in Figure 5-2. Each of these samples would be approximately 4 inches by 4 inches by 0.115 inches. In each panel, a row of six n-type elements alternates with a row of six p-type elements. The elements in adjacent pairs of rows are connected in an electrical parallel circuit, and the three pairs of rows are connected in series. A wiring diagram is shown in Figure 5-3.

Three panels would be used to allow evaluation of relative performance between samples and also to improve the chances of obtaining performance data over a long period (months) of time.

The power output for each sample is determined by measuring the voltage drop across a precision resistor located in the electrical circuit. In addition to the required voltage measurement, four temperatures would be measured on each panel (two on each surface). The orientation of the panels to the sun would be accomplished by the same orientation system employed by the solar thermionic system. Also, the orientation accuracy would be obtained from measurements made in connection with the primary solar thermionic experiment.

A summary of the expected panel performance is presented in Table 5-1.

5.2.2.5 Experiment/Spacecraft Interface Requirements

The interface requirements for the solar thermoelectric experiment (assuming three test panels mounted together in one magnesium support frame) are summarized on the following page.

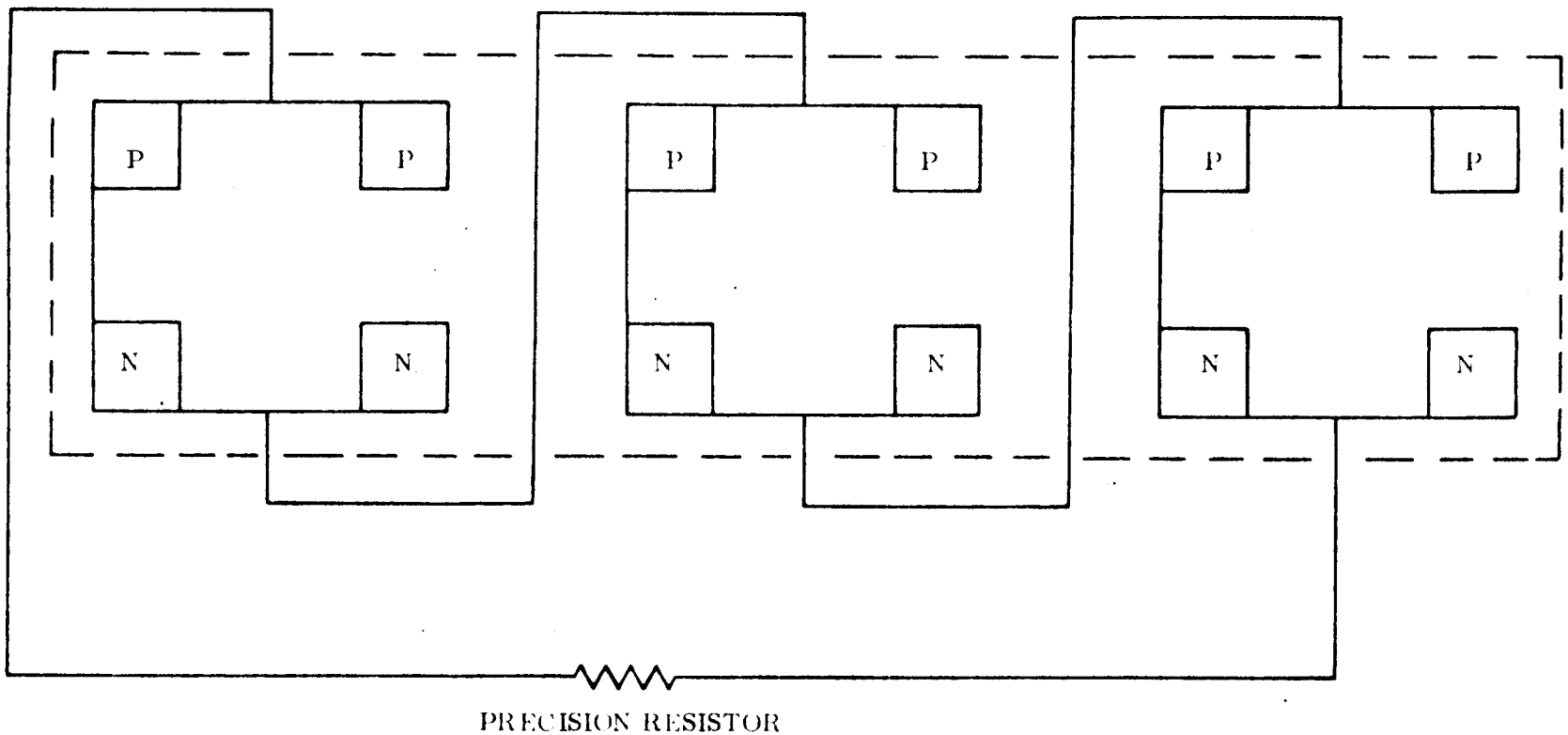


Figure 5-3. Schematic Diagram, Solar Thermoelectric Test Panel

| | |
|---|---|
| Electrical Power Required | 0.12 watts for 6 thermistors |
| Weight | 1 pound |
| Surface Area Required | 14 in. x 5 in. |
| Volume | 8 in.$^3$ |
| Instrumentation | 3 volts (0-1.2v) |
| | 6 temperature (thermistors (0-5v) |

This experiment requires sun orientation and, if possible, a measure of the orientation error. This could be obtained for the primary experiment. Although not absolutely necessary, it would be desirable to also have a measure of the radiation environment and micrometeoroid density. These two items might be obtained from other secondary experiments included on the spacecraft.

Table 5-1. Calculated Performance of Solar Panel Illuminated with 130 Watts/Square Foot Solar Intensity at Normal Incidence*

| | |
|---|---|
| Collector Temperature, $^oK$ | 573 |
| Radiator Temperature, $^oK$ | 358 |
| Collector Efficiency, % | 57.7 |
| Thermoelectric Efficiency, % | 3.74 |
| Over All Converter Efficiency, % | 2.05 |
| Area Ratio, n-Leg to p-Leg | 0.544 |
| Cross Section Area, p-Leg, cm$^2$ | 0.0196 |
| Cross Section Area, n-Leg, cm$^2$ | 0.01068 |
| Length of Legs, cm | 0.268 |
| Dimensions of p-Leg, cm | 0.140x0.140x0.268 |
| Dimensions of n-Leg, cm | 0.103x0.103x0.268 |
| Area of Collector or Radiator, cm$^2$/couple | 6.10 |
| Output Voltage at Design Load, mv/couple | 39.5 |
| Output Current at Design Load, mw/couple | 18.3 |
| Power Density, w/ft$^2$ | 2.66 |
| Output Power per Panel, 6 couples, mw | 110 |

Note:

*These performance estimates were taken from Reference 5-4.

### 5.2.3 THERMAL COATINGS

Reference 5-5 and 5-6 provided the basic information on which this experiment is based.

#### 5.2.3.1 Background

The optical characteristics of the surfaces of a spacecraft are fundamental parameters in controlling the spacecraft temperature. Thus, a major effort has been made in recent years to determine the optical properties of various surfaces and even to develop surfaces which have special desired optical characteristics and environmental stability.

The need for adequate temperature control of spacecraft was never more apparent than during the anxious hours in December of 1962 as Mariner II approached the Planet Venus, and the temperature inside the vehicle rose well above that considered safe for the electronic components and batteries. The difficulty apparently stemmed from incomplete knowledge of the required pattern of temperature-control coatings on the spacecraft (Reference 5-7). In addition, the coatings undoubtedly deteriorated somewhat during the three-month voyage. This event in the Mariner flight points up the importance of the role of thermal control in space vehicles.

The NASA-Marshall Space Flight Center (NASA-MSFC) has been a leader in space evaluation of thermal coatings. MSFC has developed a sensor for determining effects of ascent and/or space environments on the optical properties of thermal control surfaces. Several attempts have been made by MSFC to place such a sensor into orbit on board satellites which were shielded from the ascent environment. The first such attempt (S-46 payload which flew on Juno II AM-19C) on March 23, 1960 failed when orbit was not achieved. A second try also failed with the S-45 payload on AM-19F, February 25, 1961. Success was achieved with Explorer XI (S-15 payload, AM-19E vehicle) which was launched on April 27, 1961. The "surface of interest" on this sensor was multilayered and prepared by Dr. G. Hass of the Corps of Engineers, Fort Belvoir, Virginia. The first layer on the aluminum disk was a 9000 angstrom layer of SiO followed by 200 angstrom layer of

Germanium and topped with 1500 angstrom layer of SiO giving initial $\epsilon_S$ and $\epsilon_T$ values of 0.71 and 0.12, respectively. A comparison of theoretical and measured temperatures is given in Figure 5-4. From this figure (showing two temperature curves as a function of position in orbit where the satellite egresses from the earth's shadow), it can be seen that there is good correlation between the theoretical curve and the measured data. From a comparison of measured data (on June 19 and October 8, 1961) having about the same orbital and altitude parameters, as shown in Figure 5-5, it is apparent that the radiative characteristics of the coating changes very little (no more than 10 percent) during 3 1/2 months between these two dates.

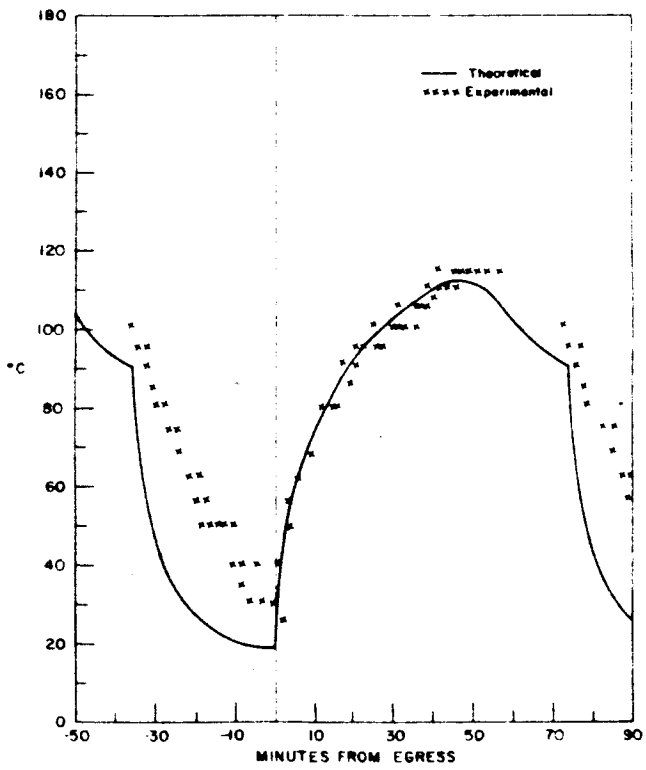


Figure 5-4. Temperature of Sensor for 19 June 1961

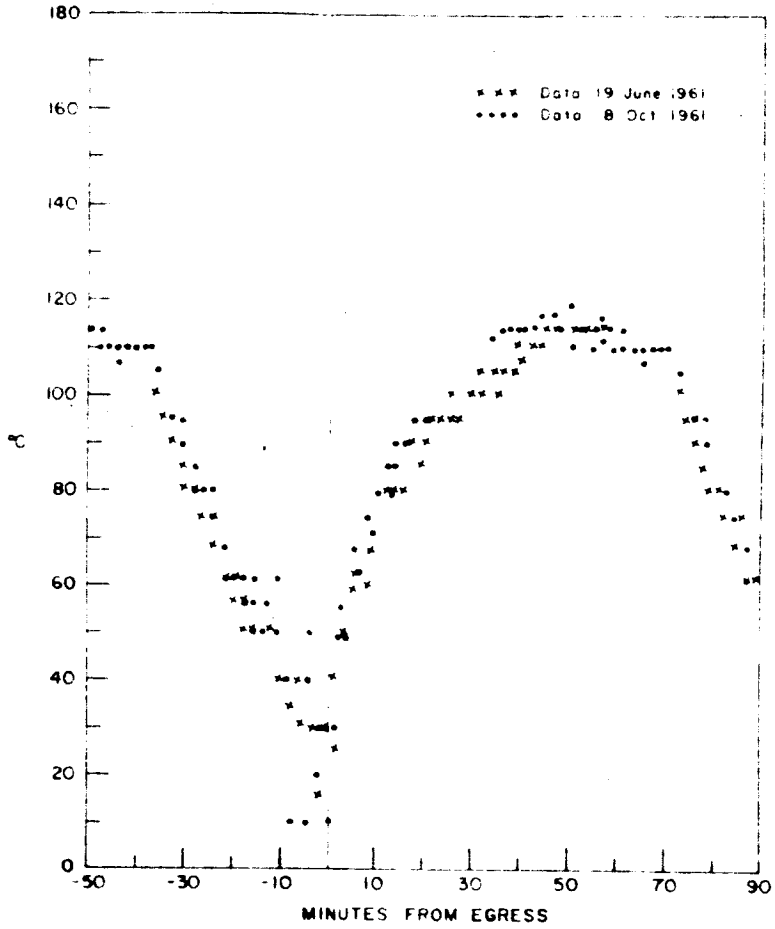


Figure 5-5. Comparison of Experimental Temperature of Explorer XI Sensor for 6/19/61 and 10/8/61 (Approximately Same Thermodynamic Orbit)

In addition to MSFC's efforts in this field, the Ames Research Center and the Jet Propulsion Laboratory have also been very active in research on the stability of thermal-control coatings for spacecraft. A series of flight experiments is being performed by the Ames Research Center on the stability of thermal-control surfaces in space. In the first of these, six test surfaces and one reference were installed on the first Orbiting Solar Observatory. The satellite was launched on March 7, 1962, and data have been obtained for a period of 16 months, thus providing information on the long-term stability of temperature control coatings.

From the preceding, it is apparent that the space evaluation of thermal coatings is well underway. However, the need for a wide variety of thermal coatings which possess, in addition to their thermal characteristics, such properties as: (1) stability to ultraviolet, (2) electrically conductive, (3) prelaunch stability, (4) launch ascent stability, etc., has created the requirement for conducting many space tests of the type described above.

5.2.3.2 Experiment Objectives

The objectives of this experiment are:

a. To measure, in the space environment, the solar absorptance and total hemispherical emittance of selected thermal coatings.

b. To determine the chances with time of the optical and adhesive characteristics of the selected thermal coatings in the space environment.

5.2.3.3 Experiment Definition

The two most important optical properties in thermal design are the absorptance of the surface with respect to solar radiation, $\alpha_S$, and the total hemispherical emittance of the surface in the far infrared, $\epsilon_T$, (T denotes surface temperature). Of somewhat lesser importance, generally, are the absorptance of the surface to earth radiation, $\alpha_E$, the spectral absorptance and emittance, $\alpha_\lambda$, and $\epsilon T_\lambda$, the directional absorptance and emittance, $\alpha_\theta$ and $\epsilon_{T\theta}$, and polarization effects. This experiment will be designed to measure the absorptance and total hemispherical emittance of selected thermal coatings.

The exact thermal coatings to be tested will not be proposed here. These coatings would be selected at a time closer to the flight date. The interest in development of (1) directional surfaces, (2) interference coatings, (3) non-spectral coatings, (4) controlled degradation coatings, (5) self-regulating surfaces, etc., insures that there will be numerous coatings to be tested.

5.2.3.4 Experiment Design

A thermal surface environment effect sensor has been designed and fabricated at the NASA-Marshall Space Flight Center. It is used for determining effects of the ascent and/or space environment on the optical properties of thermal control surfaces. The

sensor, shown in Figure 5-6, consists of 3.175 centimeter diameter disks flush with the skin of the spacecraft using Kel-F posts for thermal isolation. The optical properties of the disk surfaces are determined in flight by monitoring the temperature of the disks as a function of time and by solving the thermal design equations backwards to obtain $\alpha_S$ and $\epsilon_T$.

The Ames Research Center has developed a similar sensor and mounted six of them on a common structure. In this sensor, each test coating is applied to a metal-disk substrate one-inch in diameter which is placed in a mounting cup, as illustrated in Figure 5-7. The disks are mounted on three small plastic supports to minimize the conduction path. Radiant heat exchanges with the mounting cup are minimized by the use of four radiation shields. Surface temperature is measured by means of a thermistor soldered to the underside of the test disk. The radiation sensors are arranged in a circular cluster with a reference surface in the center (Figures 5-8 and 5-9). Figure 5-8 illustrates the design of the reference surface. The surface is composed of razor blades stacked together to form a large number of notches, which cause multiple reflections and eventual absorption of most of the incident radiation. As a result, the reference surface is essentially a black body. Because of the large number of reflections, any change in the emittance or reflectance of the individual surfaces in the notches would have only a very small effect on the overall emittance or absorptance of the reference surface. To permit correction of heat exchanges between the test surfaces and the sensor mounting cups, the temperature of the base plate is measured with a thermistor. Since the cups are in intimate thermal contact with the base plate, it is assumed the cups are at all times at base-plate temperature.

Either the Marshall or Ames sensors could be used but since the latter incorporates six samples in one unit, it is recommended and used as the example in this study.

### 5.2.3.5 Experiment/Spacecraft Interface Requirements

The interface requirements for the thermal coatings experiment (assuming an experiment composed of six sensors) are summarized on the following page:

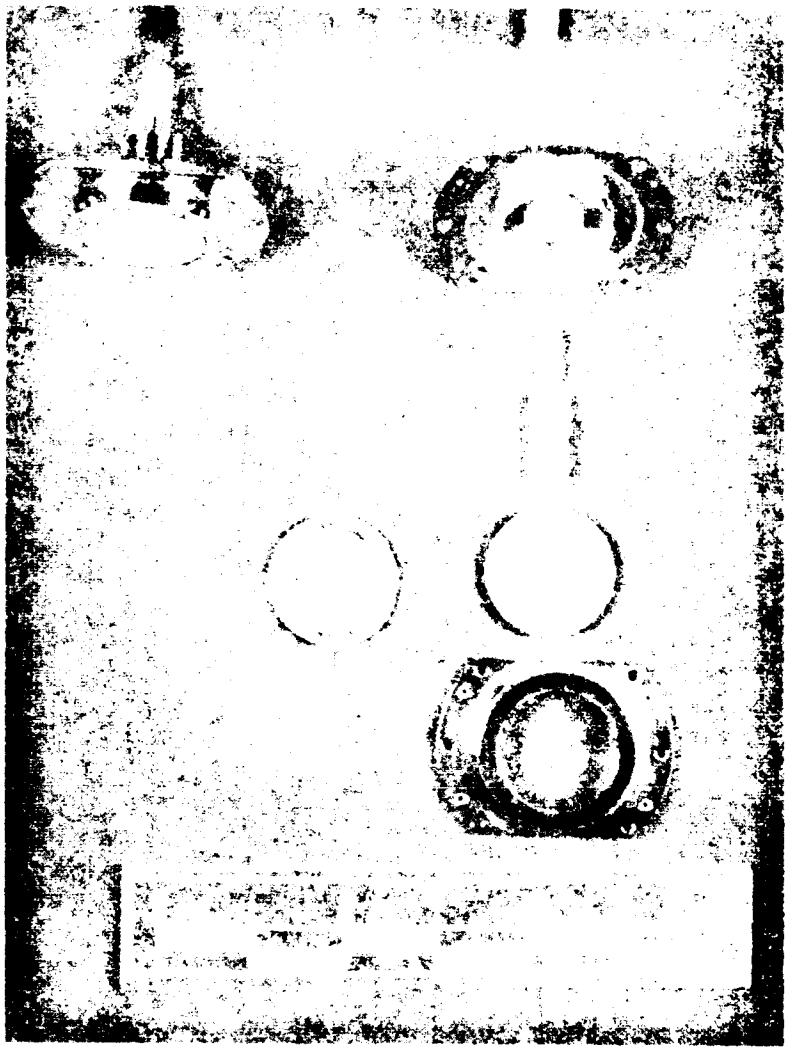

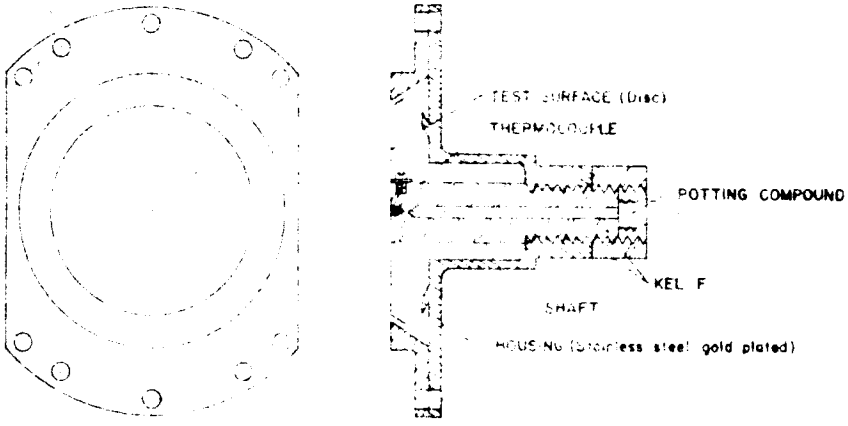


Figure 5-6. Thermal Surface Environment Effects Sensor

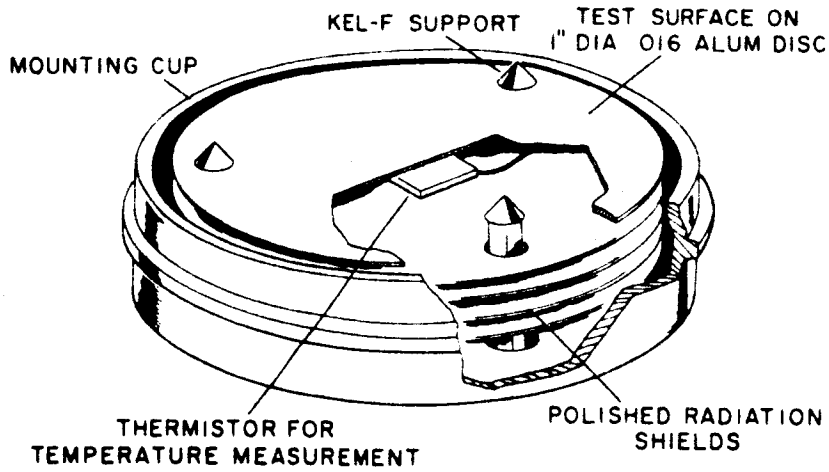


Figure 5-7. Construction Details of Radiation Sensor

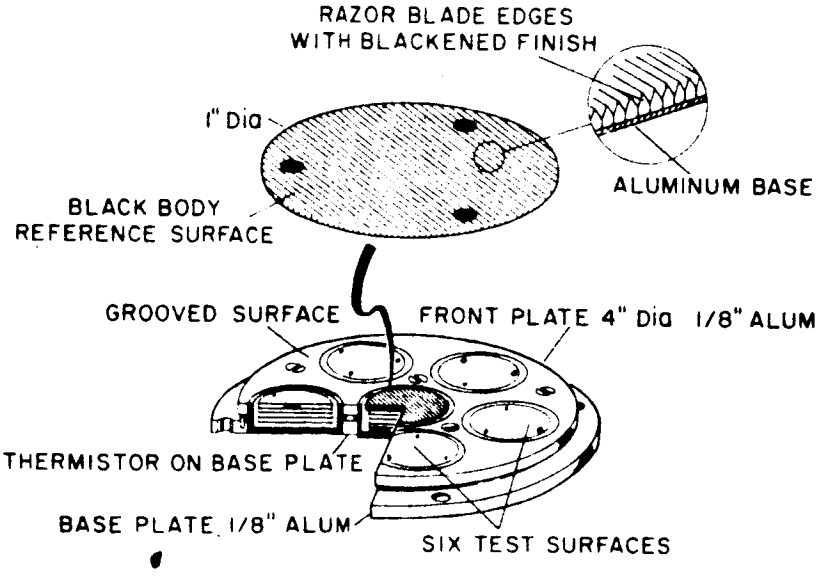


Figure 5-8. Mounting of Radiation Sensor

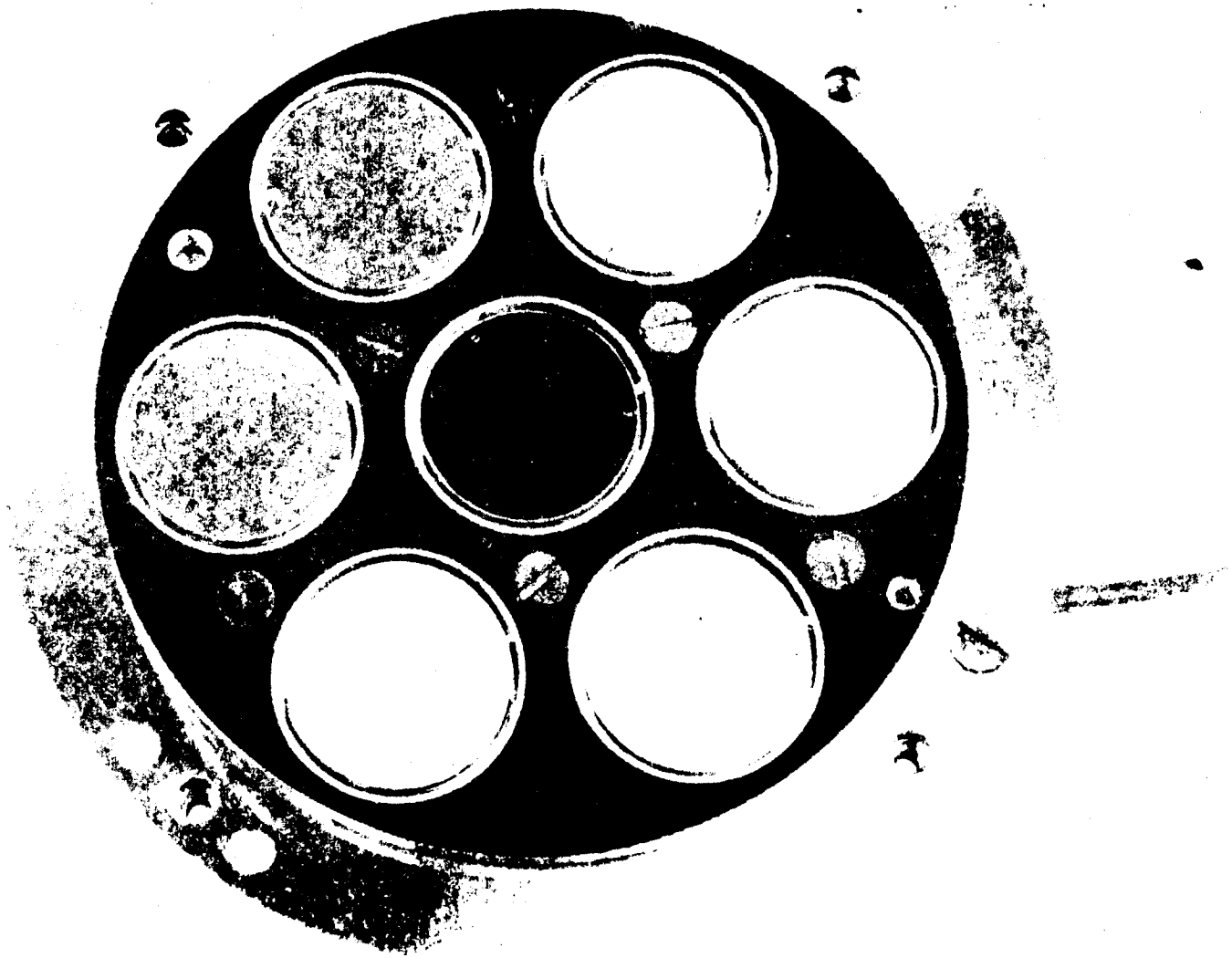

Figure 5-9. S-16 Orbiting Solar Observatory Radiation Sensor Plate

Vol II

| | |
|---|---|
| Electrical Power Required | 0.16 watts for 8 thermistors |
| Weight | 2 pounds |
| Size | 8 inch diameter by 3 inches deep |
| Instrumentation | 8 temperatures (thermistors 0-5v) |
| Telemetry Accuracy Required | 1 percent of full scale reading |

The experiment must be sun oriented and have an unobstructed view. The required exposed surface area is 50.3 square inches (8 inch diameter circle).

### 5.2.4 V-RIDGE CONCENTRATING PHOTOVOLTAICS

#### 5.2.4.1 Background

Solar photovoltaic arrays are currently the major means of supplying electrical power in space and are expected to be the best source of power for many missions in the future. The state of the art has evolved to the solar-oriented flat paddle of the Ranger, Mariner, Nimbus, and OGO systems. The present paddle designs will continue to be improved with the use of more efficient and more radiation resistant solar cells and other innovations. However, an advance in the state of the art of photovoltaic arrays to the use of V-ridge concentrators offers two potentially significant advantages: (1) a weight saving of 15 to 30 percent, and (2) a decrease in cost of up to 45 percent. A typical V-ridge concentrating photovoltaic panel is shown in Figure 5-10. The V-ridge reflective surfaces result in more solar energy being concentrated on the solar cells. This allows more power to be obtained from the same number of cells. This means a given power output can be achieved with a smaller number of solar cells which accounts for the reduction in cost. Since the concentrating surfaces are lighter in weight than the solar cells they replace, this also yields an overall decrease in weight.

In the past three years, several companies, including General Electric and Boeing, have successfully developed and ground tested experimental V-ridge concentrating modules similar to the one shown in Figure 5-10. The major uncertainty remaining is what effect,

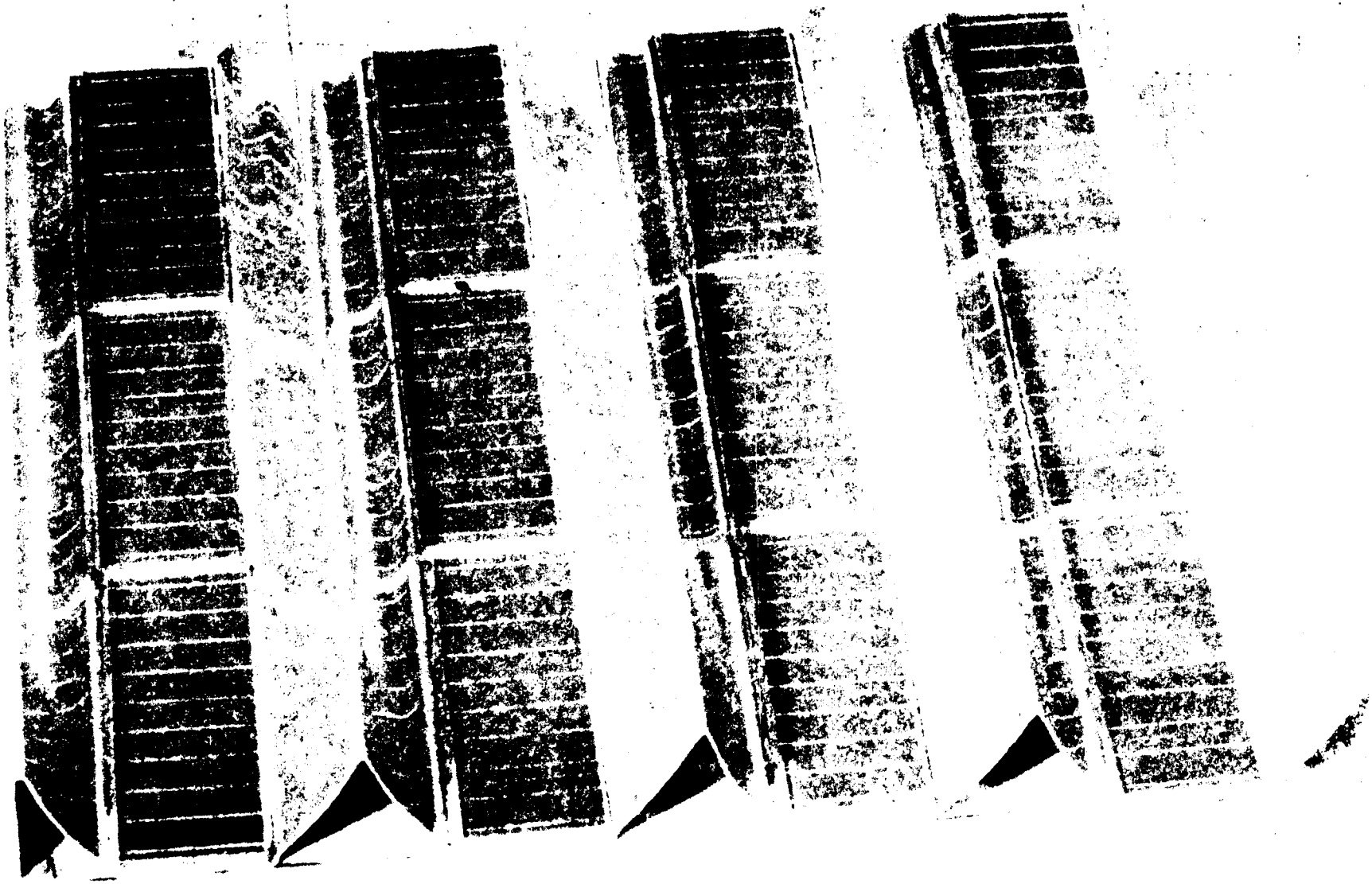

Figure 5-10. Photovoltaic V-Ridge Concentrator Panel

if any, will the space environment have on the performance of the concentrator surfaces. A space experiment is required to find the answer.

5.2.4.2 Experiment Objectives

This experiment is designed to verify the space performance of a typical photovoltaic array employing V-ridge concentrators. Of particular interest are the effects of ultraviolet radiation, ionizing radiation, micrometeorites, and thermal cycling on the performance of the reflecting surfaces.

5.2.4.3 Experiment Definition

The selection of appropriate combinations of solar cells and concentrator surfaces will enable separate determination of solar cell performance for both concentrated and non-concentrated cases; and separate determination of any solar cell or concentrator performance degradation. The experiment would be composed of three assemblies.

Type A Assembly - This assembly would consist of a a typical V-ridge concentrator panel from which temperature and power output measurements would be made.

Type B Assembly - This assembly would be a non-concentrating section. Power output and solar cell temperature would be measured. A comparison of the performance between Assemblies A and B would provide a measure of the concentration ratio. Also, the data from these two assemblies would allow the solar cell performance to be factored out and the concentrator performance isolated.

Type C Assembly - This assembly would be identical to the Type A section but smaller. Solar cell temperature and short-circuit current would be measured. Since short-circuit current is primarily dependent on energy impinging on the solar cells and not cell temperature, it is another measure of concentrator degradation.

5.2.4.3 Experiment Design

Assembly A would consist of an 8-inch x 12.8-inch panel constructed similar to the sample shown in Figure 5-10. This panel would contain 32 groups of five, one by two centimeter, solar cells wired as indicated in Figure 5-11. The 32 groups would be divided into two modules of 16 each. The five cells in each group would be connected in parallel and then loaded with a series resistor. The resistor would be sized to operate the solar cells near the peak power point (approximately 1.33 ohms). The voltage drop across the 16 resistors would be added yielding the average current. In this manner only two voltage readings, one for each 16-group module, would be required to monitor the panel power output. The solar cell temperature would be measured at four points with thermistors.

Assembly B would contain twenty, one by two centimeter solar cells without a concentrator. The twenty cells would be wired in two strings of ten cells as indicated in Figure 5-11. To measure the short-circuit current, a one-ohm resistor would be connected across each cell. The voltage across each ten cell string would be measured which would allow the average short-circuit current to be computed from

$$I_{SC} = \frac{V_T}{10} .$$

The temperature of the solar cells would be measured with two thermistors.

Assembly C would be a V-ridge concentrator sample of the same construction as Assembly A, but smaller (approximately four inches by four inches). This panel would consist of four groups of five, one by two centimeter solar cells wired as shown in Figure 5-11. This is the same wiring arrangement used for Assembly B to measure the average short-circuit current. The solar cell temperature would be measured by two thermistors.

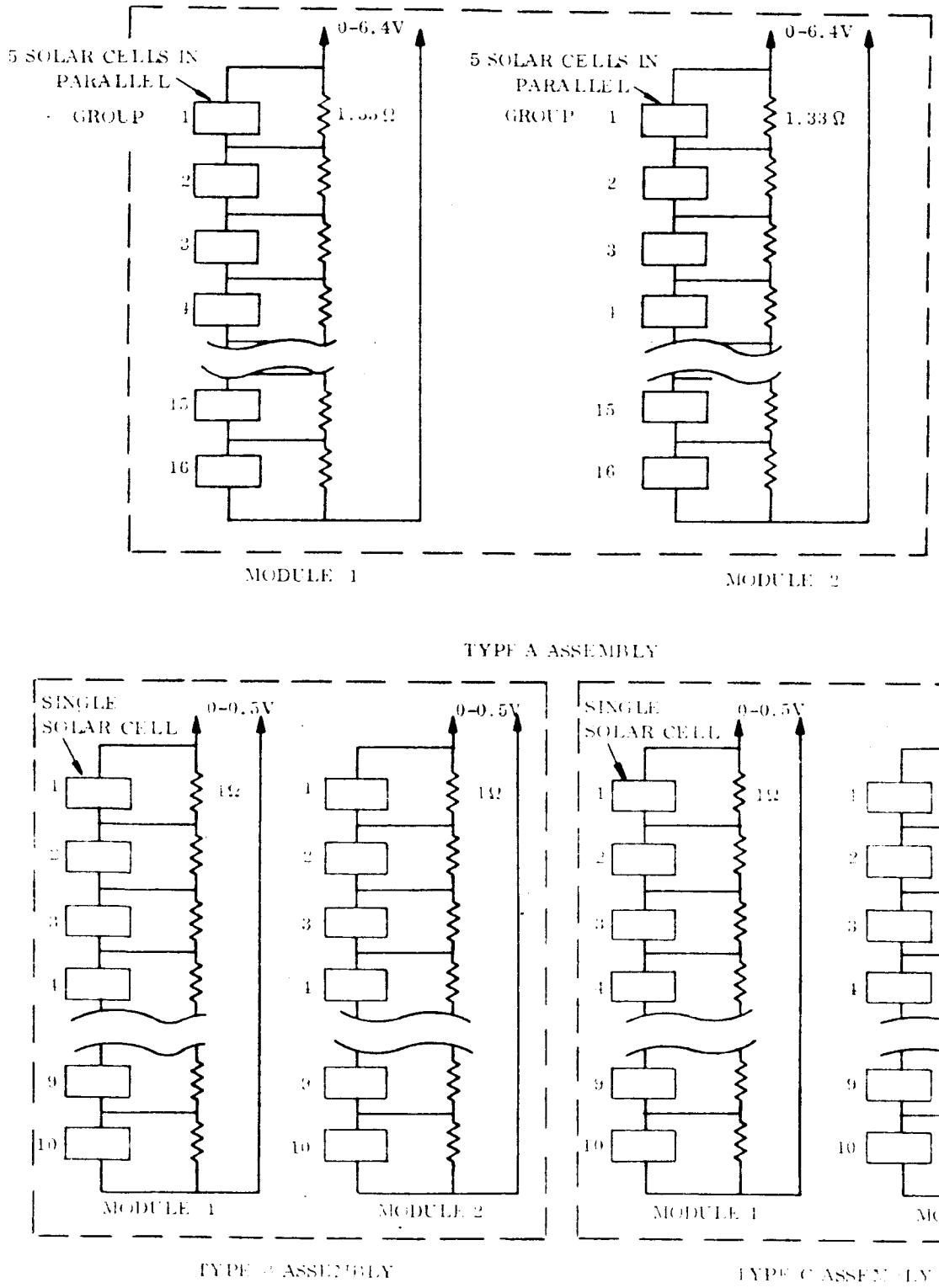


Figure 5-11. V-Ridge Concentrator Experiment Schematic

5.2.4.4 Experiment/Spacecraft Requirements

The interface requirements for the V-ridge concentrator experiment are summarized below:

| | |
|---|---|
| Electrical Power Required | 0.16 watts (8 thermistors at 20 mw per thermistor) |
| Weight | 2 pounds |
| Surface Area Required | 130 $in^2$ |
| Volume | 260 $in^3$ |
| Instrumentation | 6 voltages (0-6.4 volts) 8 temperatures (thermistors 0-5v) |
| Telemetry Accuracy Required | 1 percent of full scale reading |

The experiment must be sun oriented with an accuracy on the order of $\pm 3$ degrees. It is also desirable to have a measure of the orientation accuracy. This could be obtained from the primary experiment.

5.2.5 THIN-FILM SOLAR CELLS

5.2.5.1 Background

The development of high efficiency, thin-film solar cells could result in extremely light-weight space power systems. Consequently, research and development of thin-film cells is presently receiving considerable attention. However, this work is still in a very early state of development. This is true both from the standpoint of the theoretical understanding of thin-film cell operation and also from the standpoint of materials and fabrication techniques for making usable cells for space experimentation and application. A brief synopsis of the present state of the art* of thin-film solar cells is given below, and will serve as a background upon which a space experiment will be defined.

*The present state of the art of thin-film solar cells is presented in Reference 5-8.

The materials being most agressively investigated at present are cadmium sulfide (CdS), cadmium telluride (CdTe), and to a lesser degree, gallium arsenide (GaAs) and silicon (Si). Several techniques are being pursued in fabricating the CdS cells. These include the following:

a. CdS, Type A Cell - The Harshaw Chemical Company is fabricating CdS cells by the evaporation of a CdS film onto a metallic substrate such as molybdenum or titanium. The barrier layer is formed by immersing the CdS film into a CuCl water solution. This type of cell appears to be very susceptible to degradation due to moisture and must be encapsulated in a plastic case such as Dupont H-Film or Mylar for earth storage. Recovery of the cell after moisture degradation, however, can be made by drying; depending, apparently, on the extent of the degradation. Reliable space efficiencies appear to be two to three percent with open circuit voltages of approximately 0.5 volts.

b. CdS, Type B Cell - The National Cash Register Company is fabricating CdS cells by first evaporating a CdS film onto a CdCu alloy substrate and forming the barrier layer by chemically spraying the CdS film with CuS. These cells do not appear to be moisture sensitive and apparently do not require encapsulation. The efficiencies are generally about two percent with open circuit voltages of approximately 0.9 volts. This high open circuit voltage is not presently understood, however, NCR states these cells can be made with a high degree of reproducibility with the spraying technique.

c. CdS, Type C Cell - Still another type of CdS cell is under development by the Clevite Corporation. This is called the "Back-wall" CdS cell. These cells are made by evaporating a CdS film onto a transparent substrate such as Dupont H-film. The barrier layer is formed with a cuprious oxide slurry. The cell is operated with the light energy incident on the transparent substrate. These cells are apparently not effected by moisture. The efficiencies are one to two percent with an open circuit voltage of 0.5 volt.

The General Electric Company is presently developing fabrication techniques for the CdTe cell. These cells are made by evaporating the CdTe onto a molybdenum substrate that is coated with CdS. The barrier layer is formed by controlling the dopant during the evaporation process. The major fabrication problem with these cells has been the application of proper gridding material that does not deteriorate the cell characteristics with age. The only material that appears to be acceptable as gridding material at this time is gold. There does not appear to be a moisture problem, although this has not been thoroughly investigated as yet. The efficiencies are in the range of two to four percent with open circuit voltages of approximately 0.5 volt.

The development of fabrication techniques for thin-film GaAs and silicon cells are such that they cannot be considered for a space experiment at this time.

The laboratory work that has been done on the radiation effects on CdS and CdTe cells indicates that these cells are very radiation resistant. Some test results on CdS cells, fabricated by the techniques described previously, are given below.

Tests with electrons ranging in energy from 0.6 to 2.5 Mev show degradations of only five to ten percent for doses of $10^{17}$ electrons per square centimeter. Similar results are seen for protons ranging in energy from 2 to 10 Mev for doses of $10^{15}$ protons per square centimeter. These are extremely high radiation doses for space application. However, an interesting aspect of the electron irradiations, was that for doses above approximately $10^{16}$ electrons per square centimeter, the effects of the radiation appears to be very dose rate dependent. Degradations of 50 to 90 percent have been seen immediately after an irradiation of $10^{17}$ electrons per square centimeter at a high dose rate. Complete recovery of the cells occurred; however, within a few days after the irradiation with the cells exposed to room ambient light and under no load. This recovery shows a strong dependence on cell loading during the annealing.

5.2.5.2 Experiment Objectives

A space experiment with CdS and CdTe cells could shed light on a number of questionable areas. For example, will the moisture degradation for at least one type of CdS cell be a problem, or will the cells quickly recover once they are in space, regardless of the previous moisture degradation history? Will the CdS be stable in the combined space environment of deep vacuum, ultraviolet radiation, particle radiation, and temperature; or will a protective coating have to be applied to stabilize the surface? Are the cells stable against the low dose-rate space particle radiation while under full solar illumination and power loading conditions? Do the cells have to have some minimum shielding against the intense very low energy particle radiation? Will micrometeorites create an erosion problem on unshielded film surfaces?

A space experiment can be designed that would attempt to answer some of these questions for the CdS and CdTe cells. Specifically, the objectives of the experiment would be to investigate:

a. The recovery of moisture degraded cells in space

b. The effect of intense low energy particle radiation and micrometeorites on thin film surfaces

c. The need for surface stabilization against evaporation in the space environment

d. The effect of low dose-rate energetic particle radiation on cell output

e. An accurate determination of thin-film cell efficiencies in space.

5.2.5.3 Experiment Definition

The experiment would be composed of various combinations of cell assemblies, surface

coatings, and shielding in order to investigate the above listed objectives. Specifically, these cell assemblies would be:

Type A Assembly - This assembly would utilize the Type A CdS cell described previously. The cells would be encapsulated in Dupont H-film and would not have suffered moisture degradation prior to launch. No additional shielding would be used. This assembly would indicate the stability of this cell type and construction in the space environment. It would also measure the space conversion efficiency of this cell type.

Type B Assembly - This assembly would utilize the Type A CdS cell, however, it would not be encapsulated and would have had considerable moisture degradation prior to launch. The assembly would be shielded; however, to prevent low energy particle radiation and micrometeorites from impinging on the film. The shield would be mechanically clamped over the cell assembly. The degree of recovery of this assembly in space would give a measure of the need for ground protection against degradation.

Type C Assembly - This assembly would also utilize Type A CdS cells. The cells would be encapsulated with an evaporative material to prevent moisture degradation prior to launch. The films would also have a surface coating such as $SiO_2$ to stabilize the surface against evaporation in space. A mechanical shield similar to that in Type B assembly would also be used. This assembly would test the stability of the films in space.

Type D Assembly - This assembly would also utilize Type A CdS cells. The cells would be encapsulated in an evaporative material to prevent moisture degradation prior to launch. No shield would be used. This assembly would expose the film surface to the space environment of low energy particle radiation and micrometeorites and would give a measure of the effects of this environment on cell output.

Type E Assembly - This assembly would utilize the Type B CdS cells. No shielding or surface coatings would be used. This assembly would give an indication of the effect of the space environment on this cell type and would also measure its space conversion efficiency.

Type F Assembly - This assembly would utilize the Type B CdS cells with a shield similar to that used in the Type B assembly to prevent low energy particle radiation and micrometeorites from impinging on the film surface. This assembly would indicate the degree of evaporation of the film in space.

Type G Assembly - This assembly would be the same as Type F except a surface coating would be used to stabilize the films from evaporation. This assembly would serve as a reference for assemblies Type E and Type F so that the radiation, micrometeorite and evaporation degradation could be related.

Type H Assembly - This assembly would utilize Type C CdS cells. No shielding would be used. This assembly would indicate how well this cell type could withstand the space environment and would also give a measure of its space conversion efficiency.

Type I Assembly - This assembly would utilize the Type C CdS cells with a shield similar to that used in the Type B assembly. This assembly along with the Type H assembly would give a measure of the effects of the radiation and micrometeorite environment on cell output.

Type J Assembly - This assembly would utilize the CdTe cell. No shielding would be used. This assembly would indicate how well this cell type can withstand the space environment and would also give a measure of its space conversion efficiency.

Type K Assembly - This assembly would utilize the CdTe cell with a shield similar to that used in the Type B assembly. This assembly along with the Type J assembly would give a measure of the effects of the radiation and micrometeorite environment on cell output.

5.2.5.4 Experiment Design

A detailed design of the cell assemblies will not be attempted at this time. This will require some development work on techniques of mounting and encapsulating the cells. However, the general layout would be similar to that described for the Radiation Effects on Solar Cells experiment described in Section 5.2.1. It is anticipated that each of the cell assemblies would contain at least five, one by two centimeter cells connected in series. Each cell would have an individual loading resistor to load it to its short-circuit condition. The overall voltage of each assembly would be measured. This voltage would be approximately 50 mv for these cells with a one ohm load on each cell in the five cell assembly.

5.2.5.5 Experiment/Spacecraft Interface Requirements

The interface requirements for the thin-film solar cell experiment (assuming a total of eleven assemblies) are estimated below:

| | |
|---|---|
| Electrical Power Required | 0.04 watts (2 thermistors at 20 mw per thermistor) |
| Weight | Less than 0.5 pounds |
| Surface Area Required | 30 $in^2$ (10 in. x 3 in.) |
| Instrumentation | 11 voltages (0-50 mv) |
| | 2 temperatures (thermistors 0-5 v) |
| Telemetry Accuracy Required | 1 percent of full scale reading |

In addition the experiment would have to be solar oriented and the solar orientation error measured.

## 5.2.6 SOLAR CONCENTRATOR REFLECTIVE SURFACES

Reference 5-9 provided the basic information on which this experiment is based.

### 5.2.6.1 Background

The energy sources which various space power systems employ can be grouped into three categories: (1) solar, (2) nuclear, and (3) chemical. This experiment deals with those power systems deriving their input energy from the sun.

The majority of the solar power systems, such as:

a. Solar Thermionics
b. Solar Thermoelectrics (Concentrating Design)
c. Concentrating Photovoltaics
d. Solar Dynamic (Rankine, Stirling, Brayton).

depend on a solar concentrator to collect and concentrate the solar energy. A great deal of effort has already been expended on development of the potential space power supplies listed above. Considerable progress has been made in the development of accurate, light weight, highly reflective concentrators. However, the question of how well highly reflective surfaces will perform, and resist degradation in the space environment must be answered before any of these systems can seriously be considered for space applications. Actually, very little has been done on this problem for two reasons: (1) the uncertainty in the space environment, and (2) the difficulty in simulating effectively those characteristics known to be present. The problems of simulation become particularly difficult when the necessity for long duration tests and combinations of physical effects are considered.

The solution to this critical problem is a long term space evaluation of concentrator reflective surfaces. In November, 1963, Electro-Optical Systems, Inc. (EOS) completed, for NASA-Langley, a feasibility study of a flight experiment for accurate determination of

the performance of the reflective properties of solar concentrators. The results of the Electro-Optical Systems study, although altered somewhat to be compatible with this application, served as the basis for the experiment proposed here. The primary difference between the experiment as proposed by EOS and the version described here is that the EOS results were for a primary experiment with its own launch vehicle, attitude control system, telemetry systems, etc., and in the application being studied here the experiment would be secondary to the solar thermionic flight experiment. In this capacity the experiment would make use of many of the spacecraft functions associated with the primary experiment and therefore most of the supporting subsystems required for the EOS experiment would not be needed. However, the basic experiment is the one designed by EOS in Reference 5-9.

At present, it appears likely that an experiment similar to the one described here will be flown before a solar thermionic flight experiment could be orbited. This is highly desirable since it would provide information for selecting a surface for use on the concentrator employed in the solar thermionic flight experiment. Even if several experiments of this type were flown before the solar thermionic experiment, it is very likely that additional space experiments would be needed to completely evaluate concentrator surfaces in the space environment.

5.2.6.2 Experiment Objectives

The objective of this experiment is to perform a long term performance evaluation, in the space environment, of the reflective properties of solar concentrators.

5.2.6.3 Experiment Definition

Environments to which materials in space will be exposed can be classified into the following:

a. Temperature
b. Pressure

c. Meteoroids

d. Electromagnetic Radiation

e. Geomagnetic Fields

f. Charged Particles.

The effect of these various factors was investigated in Reference 5-9 and the conclusion was reached that the most predominant causes of reflectivity degradation would be:

a. Sputtering due to low energy protons

b. Ultraviolet radiation which produces photo-chemical changes in dielectric and anodic coatings

c. Micrometeoroids.

To be truly effective then, a flight experiment must measure the relative effect of these three primary sources of degradation on concentrator performance.

The basic measure of performance for a concentrator surface is reflectivity. The experiment then would measure reflectivity versus time for various concentrator surface samples. The samples would consist of combinations of the following surface components:

a. Substrate (plus backup structure)

b. Undercoating

c. Reflective Layer

d. Overcoating.

The samples would be selected to represent the material combinations from which concentrator surfaces are currently constructed.

Since reflectivity degradation may be a function of temperature, the experiment would be designed such that the surface samples will operate in the temperature range comparable to what they will see in a typical space application. The temperature of each sample would be measured.

The samples would be oriented to the sun and for complete evaluation, measurements would also be made of the low energy proton spectra, ultraviolet radiation and the micrometeoroid population.

5.2.6.4 Experiment Design

The basic experiment configuration is shown in Figure 5-12. It consists of a 24 inch diameter cylinder, approximately 8 inches long. The reflective samples (1.5 inches in diameter) are mounted on the flat end of the cylinder which would be oriented to the sun. A total of 25 to 28 samples would be tested. Separating the effects of the various degradation factors would be accomplished by occluding the sun from some samples so that essentially only particle radiation strikes them, covering other samples with fused quartz so that essentially only electromagnetic radiation strikes them, and exposing the other samples to the total space environment.

The samples are arranged in a circle at the center of which is a rotating arm which is a part of the reflectometer. This arm would measure all samples; plus, 0 and 100 percent calibration points. The zero percent calibration point is a cavity and the 100 percent point a fused quartz roof prism. The arm only rotates when measurements are performed and covers the calibration positions in the standby mode thus leaving the samples exposed.

A temperature measurement would be made on each sample to evaluate its performance and allow the calculation of absorptivity/emissivity ratios and emissivity. These temperature measurements would be made with thermistors. The range of temperature variation of the samples would be controlled by careful design of their surrounding thermal environment.

In addition to measuring reflectivity and temperature of the samples, measurements would also be made of the low energy proton spectra, ultraviolet radiation, and micrometeoroids. The means of making these measurements are covered under secondary scientific experiments (Section 5.3).

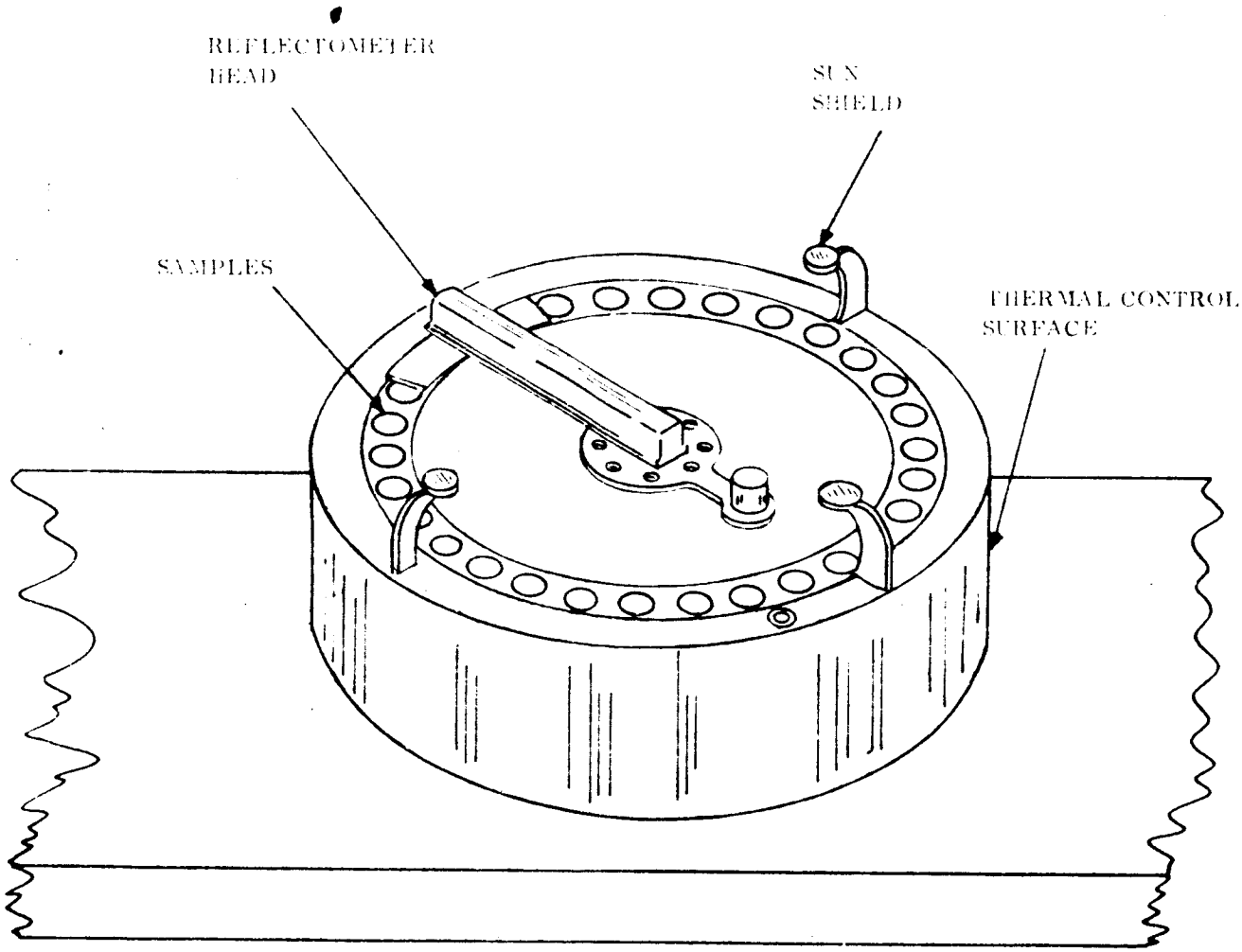


Figure 5-12. Reflective Surfaces Experiment Configuration

A list of preferred experiment samples are given in Table 5-2. These samples represent those surfaces presently being used on concentrators. Various arrangements of shielding are used to evaluate the relative effects of the major degradation factors.

An ideal orbit altitude for this experiment would be 10,000 nautical miles, since this altitude exposes the samples to the maximum low-energy proton fluxes. However, the actual orbit selected must represent a trade-off between launch vehicle capability, cost, reliability, etc. The EOS study recommended a compromise elliptical orbit with a apogee of 4000 to 5000 nautical miles and a perigee of 300 nautical miles. This recommended orbit had an inclination of 37 degrees.

5.2.6.5 Experiment/Spacecraft Interface Requirements

The interface requirements for the solar concentrator reflective surfaces experiment are summarized below:

| | |
|---|---|
| Electrical Power Required | 2.6 watts (2 watts for reflectometer and 0.6 watt for 30 thermistors) |
| Weight | 27.0 pounds |
| Surface Area Required | 452 in.$^2$ (a 24 in. diameter circle) |
| Volume | 3616 in.$^3$ (cylinder 24 in. diameter by 8 in. long) |
| Instrumentation | 1 voltage (0-20 mv)<br>30 temperatures (thermistors 0-5 v) |
| Telemetry Accuracy Required | 1 percent of full scale reading |

Table 5-2. Experiment Sample Selection and Separation of Effects

| NO. | SUBSTRATE | UNDERCOAT | REFLECTIVE COATING | OVERCOAT | SEPARATION OF EFFECTS |
|---|---|---|---|---|---|
| 1 | Ni | SiO | Al | | Surface mounted, no shield |
| 2 | Ni | SiO | Al | | Partially recessed |
| 3 | Ni | SiO | Al | | Fully recessed |
| 4 | Ni | SiO | Al | $Si_2O_3$ | No shield |
| 5 | Ni | SiO | Al | $Si_2O_3$ | Sun shield |
| 6 | Ni | SiO | Al | $Si_2O_3$ | Particle shield |
| 7 | Ni | | Ag | | No shield |
| 8 | Ni | | Ag | | Sun shield |
| 9 | Ni | | Ag | | Particle shield |
| 10 | Ni | | Ag | | Total shield (control) |
| 11 | Foam/Mylar | | Al | | No shield |
| 12 | Foam/Mylar | | Al | | Sun shield |
| 13 | Foam/Mylar | | Al | | Particle shield |
| 14 | Foam/Mylar | | Al | High $\epsilon$ | No shield |
| 15 | Foam/Mylar | | Al | High $\epsilon$ | Sun shield |
| 16 | Foam/Mylar | | Al | High $\epsilon$ | Particle shield |
| 17 | Al/Epoxy | SiO | Al | SiO | No shield |
| 18 | Al/Epoxy | SiO | Al | SiO | Sun shield |
| 19 | Al/Epoxy | SiO | Al | SiO | Particle shield |

Table 5-2. Experiment Sample Selection and Separation of Effects (Cont)

| NO. | SUBSTRATE | UNDERCOAT | REFLECTIVE COATING | OVERCOAT | SEPARATION OF EFFECTS |
|---|---|---|---|---|---|
| 20 | Epoxy | SiO | Al | Barrier layer | No shield |
| 21 | Epoxy | SiO | Al | Barrier layer | Sun shield |
| 22 | Epoxy | SiO | Al | Barrier layer | Particle shield |
| 23 | Epoxy | | Al | | No shield |
| 24 | Epoxy | | Al | | Sun shield |
| 25 | Epoxy | | Al | | Particle shield |

In addition to the indicated instrumentation, measurements of the low energy proton spectra, ultraviolet radiation, and micrometeoroids would be required for complete evaluation of the experiment. Measurement of these quantities is covered in Section 5.3.

This experiment also requires sun orientation and a measure of the orientation error. This information would be available from the primary solar thermionic experiment.

The basic experiment designed in Reference 5-9 and described here was designed to be compatible with a considerably different spacecraft configuration. A redesign of this experiment should be considered to make it easier to integrate with this spacecraft and to reduce the weight if possible.

## 5.2.7 THERMAL CONTACT RESISTANCE

### 5.2.7.1 Background

The designer of moderate to long-life spacecraft containing heat sources and heat sinks is frequently faced with the problem of providing adequate heat flow paths between heat generating devices such as electronics, power sources or energy converters and structural heat

sinks. This problem is complicated even further, when such components and subsystems are attached by means of bolted or riveted connections to allow for their removal at any time prior to launch. Such methods of fastening often introduce an undesirable additional temperature drop at the plane of attachment, which is due to the thermal contact resistance.

Several applied research, as well as engineering studies, are currently underway on the subject of thermal contact resistance in vacuum to: (1) improve our undertstanding of this phenomenon, and (2) to find practical ways to control it by means of filler and shim materials. A research study on this topic is currently being conducted by the General Electric Spacecraft Department under NASA Contract NAS 8-11247. A report on an earlier study (NAS 8-5207) is available (Reference 5-10). These efforts have been directed primarily toward item (1) above; to improve understanding of the basic phenomena and methods of predicting performance. The areas of practical applications, and engineering type studies have received little systematic attention (Reference 5-11), although they are urgently needed for many spacecraft applications. For example, heat transfer promoting fillers such as high-vacuum silicone grease have been shown to be excellent contact resistance reducers and are currently used on electronics parts (Reference 5-12). However, little or no knowledge exists on their behavior under extended space flight conditions. Evaporation effects, if any, and subsequent deterioration or condensation effects can only be studied effectively in space flight experiments.

5.2.7.2 Experiment Objectives

The objectives of this experiment are:

a. To study the thermal performance of metallic joints under load during long term exposure in vacuum

b. To observe by thermal contact means the possible "cold welding" effects of a metallic joint under load, since this may have significant effects on contact heat transfer

c. To study the thermal performance of metallic joints with a non-metallic heat transfer promoting filler during long term high-vacuum exposure (in particular de-gassing effects will be considered).

d. To study the degree of thermal performance deterioration of the above joints during launch and other severe environments associated with flight preparation.

5.2.7.3 Experiment Definition

Most previous studies (References 5-10 and 5-13) provide new insight into the short range thermal problem, but do not consider the long term effects which could manifest themselves in the form of elastic recovery, plastic flow, and most importantly vacuum effects on evaporation of surface material or filler material. The elastic-plastic effects have been studied in a vacuum to a limited degree by Cordier (Reference 5-14) in France. However, only qualitative data is available at present. There is no doubt that such effects will have a bearing on the thermal performance of joints in long-life space vehicles. Such effects deserve study in the space environment under controlled conditions, since poor performance of such a joint could jeopardize thermal reliability of a mission. The proposed experiment would require a concurrent ground based experiment to permit laboratory checks and verification of unusual flight experiment results. There is very little reliable data on the time-relaxation effects of thermal contacts or joints and the thermal performance effects on such joints in a gravitational field. There is no such data available for reduced or non-gravitational systems. Yet such effects can have an important bearing on a spacecraft's thermal performance. The proposed experiments should provide such data.

A further problem of interest is the frequently mentioned "cold welding" effects of metallic surfaces under load in high vacuum. The effects of such cold welding should be observable by a change in the thermal contact heat transfer; this would be monitored.

The effects of outgassing of the contact interface containing a low volatility, non-metallic shim or a very thin layer of high-vacuum silicone grease is another area of interest.

Current practice in spacecraft mounting of high heat dissipation components makes use of an electrically insulating, thin glass-epoxy laminate shim to improve heat transfer. There exists a high degree of uncertainty on the long term thermal performance and reliability of such materials in vacuum. The proposed experiment using such a shim is of vital interest for long-life planetary exploration vehicles.

A related area of need for more information is the use of high-vacuum silicone grease, which is currently used on spacecraft for improving (by a factor of 2 or more) the heat transfer of metallic joints. Data in References 5-12 and 5-13 supports this remarkable improvement. Data from a flight experiment should prove highly useful for future programs to indicate the degree of heat transfer deterioration, if any, due to a gradual loss of grease volatiles. This portion of the experiment would have to be enclosed and vented to the outside of the vehicle in order to avoid any possible interference with adjacent experiments.

5.2.7.3 Experiment Design

The flight experiment would utilize three samples (approximately 1.3 centimeters in diameter by 3 centimeters long) of the configuration shown in Figure 5-13. The temperatures would be measured by thermistors. One of the problems still to be solved is how to handle the power dissipation of the thermistor and its effect on the measurement accuracy. It may be possible to solve this problem by ground calibration in a vacuum chamber.

The heat flux measurement would be accomplished by use of the measured temperature gradient and the previously measured thermal conductivity k of the sample cylinders. Thus:

$$\frac{q}{A} = k \frac{dT}{dx} ,$$

where all quantities, except q, are known or measured. The multiple use of the thermal gradient for both heat flux as well as interface thermal resistance temperature drop measurement is one example of maximum utilization of telemetry information. It should be

noted that the flight experiment would not use guard heaters, but would accomplish the same effect by careful thermal design.

The heat flux would be provided by an embedded resistance heater on one end of the sample cylinder. A heater made from a material that exhibits a small resistance variation with temperature would be used and the voltage would be monitored to avoid fluctuations. Therefore, a regulated power supply would be required.

The means for heat rejection on the heat sink side of the contact cylinder assembly would be one of the major items to be considered during the experiment design phase.

The initial design would attempt to operate with sufficiently large thermal mass and limited radiation coupling with the spacecraft skin to avoid cyclical temperature variations. It is expected that such a system can be made to work. Should analysis indicate differently, then a simple, passive type thermal control utilizing a thermal switch or a bi-metallic radiation shutter would be installed between the heat sink and the vehicle skin or stringer.

The experiment modules would be stacked as shown in Figure 5-14. For continuous operation each module would require two watts of heater power. If the power available is limited, the experiment could be operated on a periodic basis with the modules being energized by program or command. However, in the silicone grease sample continuous operation would be required to obtain meaningful results.

The mechanical load on the sample would be provided by a structural frame made of a hollow box section as shown in Figure 5-14. The load adjustment would be made by means of screw-type loadcell assemblies.

The temperature of the test specimens would be measured at eight points as shown in Figure 5-13. Each measurement would be performed through the use of glass bead thermistors imbedded in, and in good thermal contact with, the specimen metal. In order

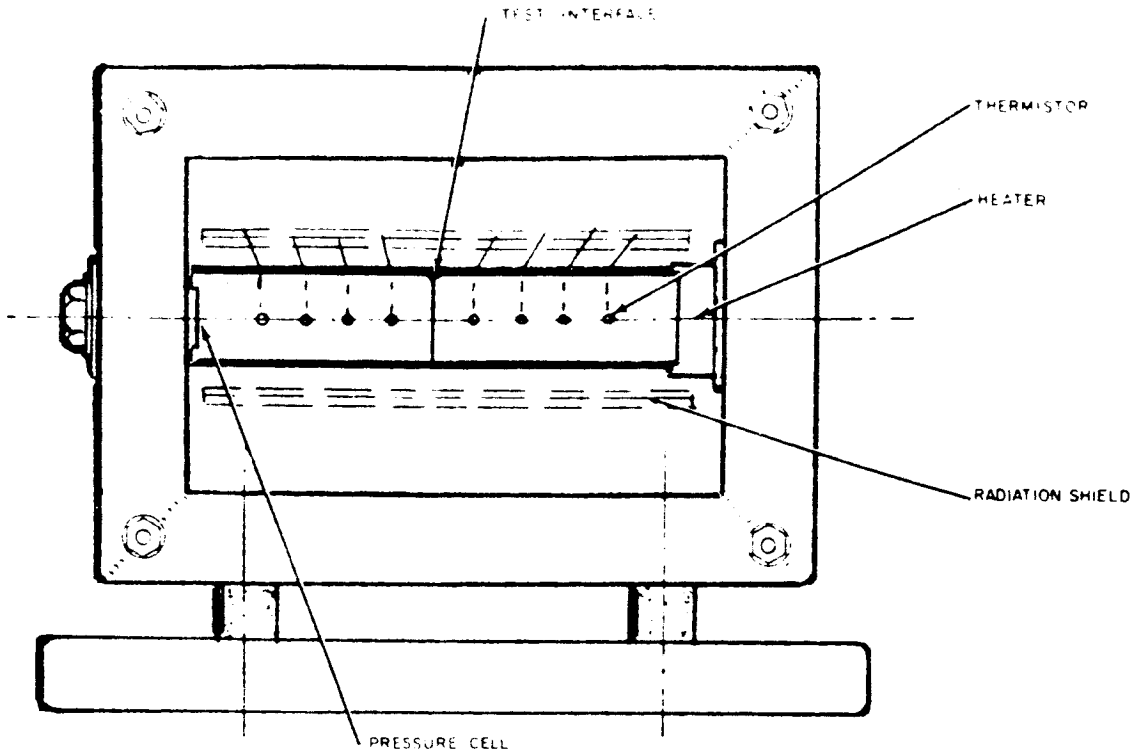


Figure 5-13. Thermal Contact Resistance Experiment Module

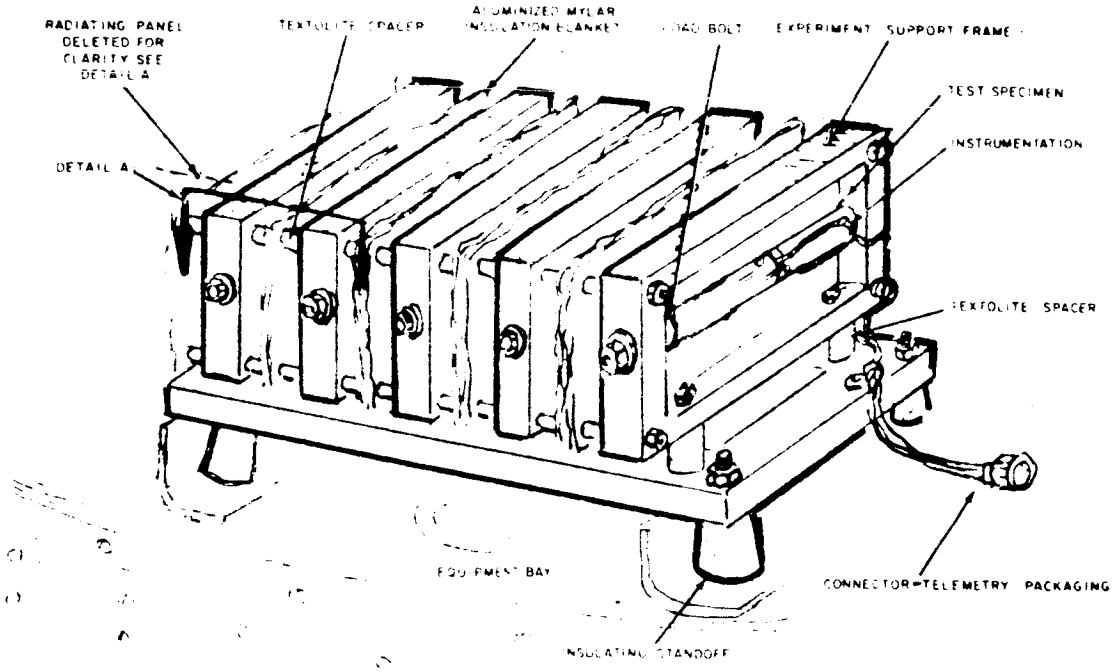


Figure 5-14. Assembly Technique for Several Modules

to minimize error in the data, a certain number of measurements involving temperature differences would be made with thermistors connected in bridge circuits such that only signals representing temperature differences would be generated and presented to the telemetry subsystem. For small temperature differences, the signal voltage V is very nearly directly proportional to the temperature difference between thermistors $\theta_1$ and $\theta_2$.

Each temperature measurement would require approximately 20 milliwatts and would generate a 5.0-volt full scale output signal when operated on 20 to 30 volts.

5.2.7.4 Experiment/Spacecraft Interface Requirements

The interface requirements for the thermal conductance experiment (assuming three modules) are:

| | |
|---|---|
| Electrical Power Required | 6 watts for heaters<br>0.6 watt for 30 thermistors |
| Weight | 7.2 pounds |
| Overall Dimensions | 6 in. x 6 in. x 10 in. |
| Instrumentation | 30 temperatures (thermistors 0-5 v) |
| Telemetry Accuracy Required | 1 percent of full scale reading |

A regulated power supply is required.



243

Vol II

## 5.2.8 INFRARED DETECTOR

### 5.2.8.1 Background

The Materials and Processes Laboratory of the General Electric Spacecraft Department has developed a new concept in infrared detectors. It utilizes a semiconductor material (silver-doped tellurium) in a vacuum-deposited thin film as a thermoelectric detector with an exceptionally high thermoelectric power. The result is a thermal detector with high sensitivity and a flat spectral response.

A good thermal detector has several advantages over the commonly used thermistor bolometer. It requires no bias supply, eliminating this source of noise; signal voltage is the only potential in the detector circuit, minimizing microphonic noise from stray lead capacitance; and the detector is self-referencing, eliminating the need to chop the input radiation to avoid reference tracking error. Eliminating the chopping requirement suggests the possibility of a completely passive (no moving parts) sensor with good accuracy and greatly increased reliability.

A versatile, conceptual design of an earth sensor employing the new detector has been devised. It includes simple, reflective-cone optics in a radiometer balance configuration. At least three separate detection heads, and possibly four, would view segments of the earth and space at equal intervals around the horizon. Use of relatively large viewing angles would provide maximum signal as well as minimize the effect of local variations in earth radiance.

Based on early Tyros data, the use of a narrow infrared passband centered on 15 microns has been proposed as ideal for earth sensing (Reference 5-15). This is the carbon dioxide absorption band in which, if a sufficiently narrow band is chosen, the earth's atmosphere is opaque. The atmosphere thus tends to average out variations in surface radiance and present a more uniform surface. Calculations have shown that interference filters passing

only a two-micron band can be used in the sensor configuration proposed and the sensitive detectors will still produce a usable signal with one degree or less change in vehicle attitude.

A highly reliable earth sensor of the type proposed here will find many applications on long-life earth referenced vehicles, including meteorological and communication satellites.

Since the solar thermionic flight experiment will not maintain an attitude with respect to earth, it will not be practical to check out a complete earth sensing system. However, the important sensor feasibility questions can be answered equally well with a sun-referenced vehicle. Sensing heads can be located such that the earth will pass through their fields-of-view during each satellite orbit, thus cycling the sensors to alternately view earth and space. Valuable information concerning detector stability in the space environment would be gained. In addition, calculations of expected signal level and 14 to 16 micron radiance variations can be checked experimentally. Specific information on the variations in radiance in the narrow, 14 to 16 micron band is especially important since this determines the limiting accuracy of the radiometer balance sensor.

5.2.8.2 Experiment Objectives

The objectives of the infrared sensor experiment are:

a. Obtain stability data on a new infrared detector in the space environment

b. Check calculations of expected signal levels from a detector head accepting energy only in the 14 to 16 micron band

c. Measure variations in earth radiance, in the 14 to 16 micron band.

5.2.8.3 Experiment Definition

A satellite oriented to the sun offers some positive advantages in evaluating this new earth sensing concept. Since the solar direction will be nominally fixed with respect to the vehicle,

the infrared sensing heads can readily be located such that the sun is never in their fields-of-view. Thus, no special design precautions, either optical or electronic need be taken to avoid problems caused by the sun. The extent that the sun would be a problem in a sensor system can be determined in a laboratory and need not be evaluated in space. However, a flight experiment will provide the missing information required to properly determine the feasibility of the sensor design concept. This information, in sufficient detail, can be obtained in no other way.

5.2.8.4 Experiment Design

A very simple experiment is proposed, consisting of cone-detector sensing heads and associated electronics for amplifying and conditioning of the signals for telemetering. In addition to the telemetered signals, several diagnostic readouts including temperature and power monitors would be desirable. A command on/off capability would be required, since data need be taken only periodically to meet all experiment objectives.

Figure 5-15 shows schematically the sensor head configuration proposed, and Figure 5-16 is a block diagram of the electronics. The electronic circuitry consists basically of a chopper stabilized amplifier. The input signal will be electronically chopped using the basic concepts of a low level, solid state multiplexing circuit developed by General Electric. This is followed by a low-pass, ac-coupled amplifier. The signal then passes through a delayed gate synchronized with the chopper/modulator such that short term switching transients are eliminated. Finally, a synchronous demodulator provides a d-c output signal for processing to provide the correct level and output impedance for the telemetry circuit.

5.2.8.5 Experiment/Spacecraft Interface Requirements

The interface requirements for the infrared detector experiment are summarized below:

| | |
|---|---|
| Electrical Power Required | 1 watt for electronics |
| | 0.1 watt for 5 thermistors |

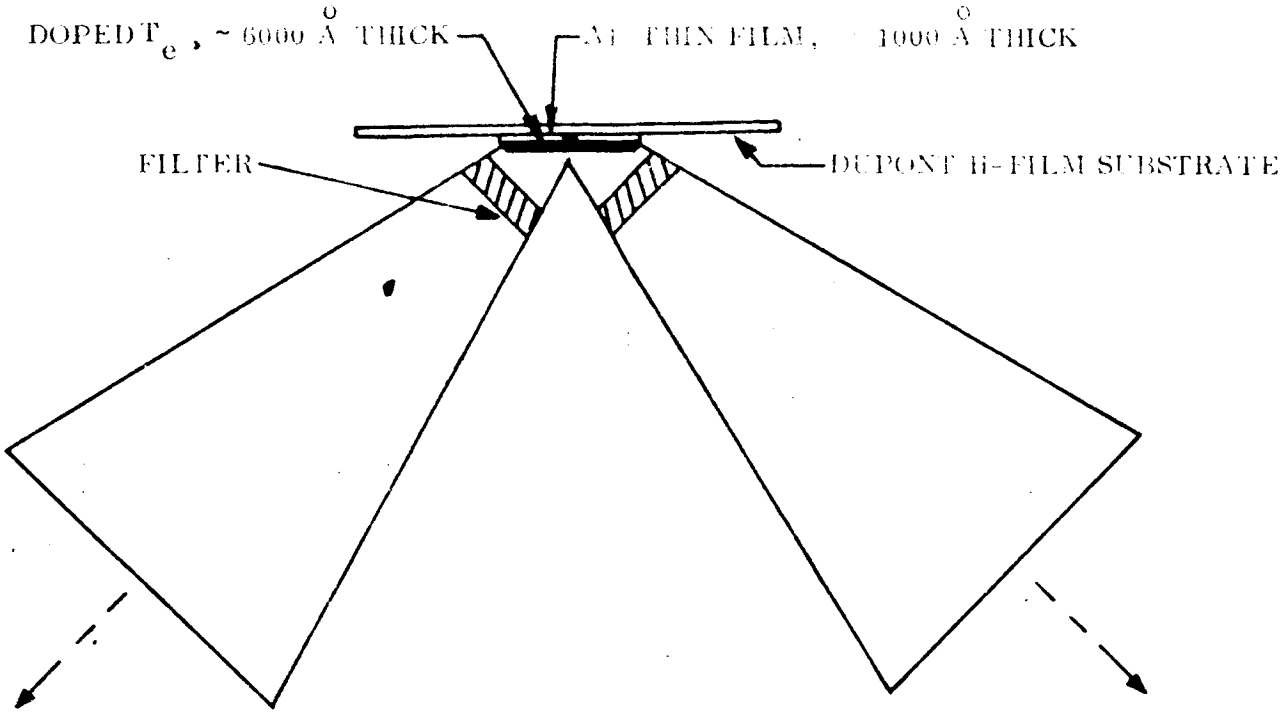


Figure 5-15. Sensor Head Configuration - Schematic

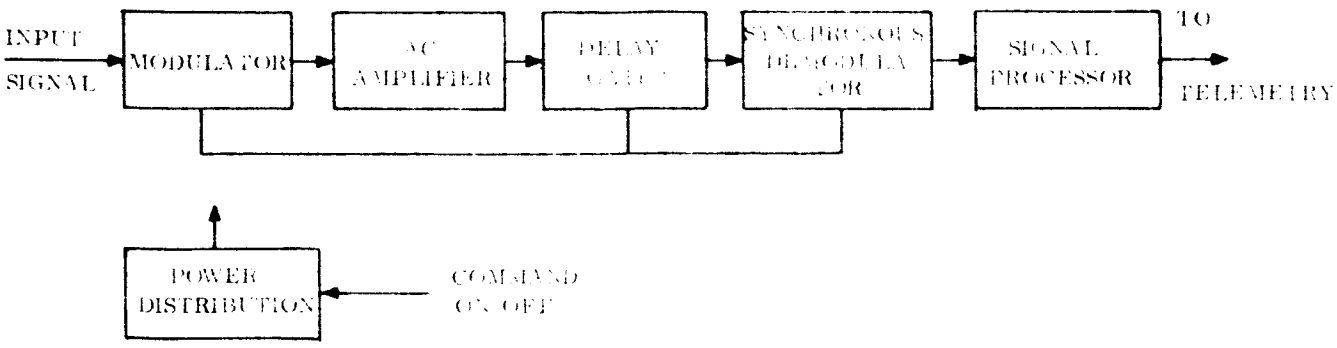


Figure 5-16. Infrared Detector Electronics, Block Diagram

| | |
|---|---|
| Weight | 3 pounds |
| Overall Dimensions | 4 in. x 6 in. x 8 in. |
| Instrumentation | 1 voltage (0-5v)<br>5 temperatures (thermistors 0-5v) |
| Telemetry Accuracy Required | 1 percent of full scale reading |

The sensing heads must be located on the spacecraft in such a position that the earth will pass through their field-of-view during the orbit.

### 5.2.9 LASER EXPERIMENT

#### 5.2.9.1 Background

The use of lasers and applied optical technology for space communication and tracking has been the subject of several recent investigations and considerable interest has been generated in this field. This area of laser application is in the very early stage of development. The first laser satellite experiment was launched on the NASA-GSFC S-66 satellite on October 9, 1964 (see Reference 5-16). The objective of this experiment was satellite tracking by means of a ground based laser and corner retroreflectors located on the spacecraft. NASA announced successful laser tracking of the S-66 satellite on November 9, 1964.

In connection with the work performed to date, several areas have been identified which presently constitute limitations on the confident prediction of optical space system performance. Presently available data is mostly derived from astronomical observations, laboratory experiments, and deductions based on theory. This data, based on terrestrial observations and usually taken for an unrelated purpose, is often inadequate for the design of space optical systems. Before lasers can be established as an operational means of

space communication and tracking, many experiments of the type performed on the S-66 satellite must be conducted. The types of information needed can be classified in four categories:

a. Measurement of the optical properties of the earth's atmosphere

b. Measurement of the optical properties of the space background

c. Determination of the effects of the space environment on optical and related components and systems

d. Demonstration and evaluation of prototype communication and tracking systems under space conditions.

Obviously, numerous space experiments will be required to obtain this information so that a variety of experiments could be proposed for inclusion on the solar thermionic flight experiment spacecraft. In this study, a modulatable corner reflector experiment is proposed. This experiment falls under (d) above and would demonstrate the feasibility of using a laser system for telemetering data from space vehicles to earth. This experiment was selected because it is considered typical of the type of laser experiments that will be of interest in the 1967 to 1969 time period.

5.2.9.2 Experiment Objectives

The objective of this experiment is to obtain an early demonstration of retroreflector communication, including a test of the space environment effects on modulatable corner reflectors. Also, such an experiment will provide valuable data on the attenuation, scattering, and refracting properties of the atmosphere.

5.2.9.3 Experiment Definition

Modulatable optical corner reflectors have been proposed as a means for transmitting data from a satellite to a ground station by means of semi-passive satellite equipment. The

corner reflectors have the property of returning incident light in a reciprocal direction in a narrow beam. Thus, if the satellite carrying the corner reflectors is illuminated by an earth based laser, the return beam will be detected by an adjacent receiver. This has been demonstrated in the NASA-GSFC S-66 satellite experiment. The corner reflectors consist of three orthogonal plane reflecting surfaces. If the planeness or orthogonality of the reflecting surfaces is even slightly disturbed, the collimation of the return beam will be decreased and the ground receiver will detect a change in signal amplitude. A method of distorting the corner reflectors according to a function of the data to be transmitted thus produces amplitude modulation in the received signal which can be processed to recover the data. The advantage of this communication technique is that the signal power is generated in the ground station, the power required to distort the corner reflectors being very small. Further, the corner reflectors do not need to be pointed accurately; the acceptance angle can be hemispheric or more.

Figure 5-17 shows a developmental model of a piezo-electric modulatable retro-reflector. Figure 5-18 shows the S-66 satellite retro-reflector panel, giving near hemispheric coverage.

5.2.9.4 Experiment Design

The major components of the experiment are:

a. Ground based laser
b. Ground based receiver
c. Satellite reflector panel
d. Modulating electronics (located on satellite).

The ground based laser and receiver can be readily adapted from equipment now available at NASA-GSFC, GE-MSD, or elsewhere. This equipment would provide a data rate of about one bit per second. Further development of ground equipment may increase the data rate to tens of bits per second, depending on the available pulse rate of the laser.

Figure 5-17. Piezo-Electric Modulatable Retroreflector

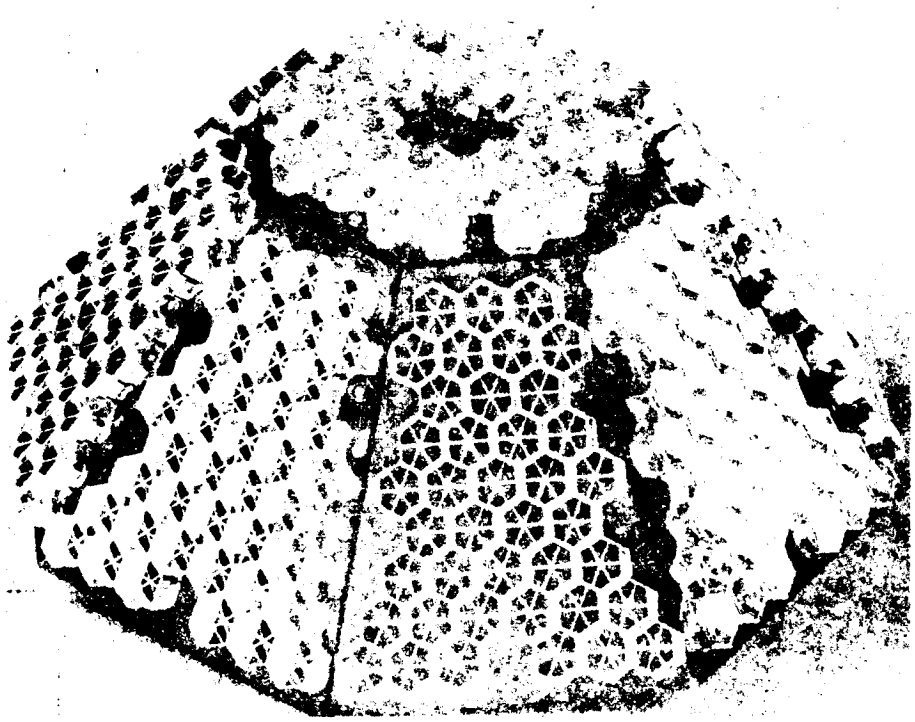

Figure 5-18. S-66 Satellite Retroreflector Panel

Several types of modulatable corner reflectors have been investigated, including piezo-electric quartz or ferro-electric ceramics, magneto-strictive deflection, and electrostatic or electromagnetic deflection (Reference 5-17). Further work is needed to select and optimize the most suitable type for this experiment. Depending on the type chosen, the driving electronics will consist of a low power source of voltage or current excitation which in the simplest case will be triggered by ground radio command.

The retroreflectors will be mounted in a panel on the shade side of the satellite. The total area of the panel should be at least 16 square inches, and preferably larger.

The proposed method of modulation by ground radio command provides a demonstration of retroreflector communication, without however, the capability of actually transmitting satellite generated data. If desired, this capability could be provided by including a satellite laser receiver as described in Reference 5-18.

5.2.9.5 Experiment/Spacecraft Interface Requirements

The interface requirements for the laser experiment are:

| | |
|---|---|
| Electrical Power Required | 1 watt for electronics<br>0.06 watt for 3 thermistors |
| Weight | 10 to 15 pounds |
| Exposed Surface Area | 16 in.$^2$ (minimum) |
| Overall Dimensions | 2 in. x 2 in. x 1 in. (electronics only) |
| Instrumentation | 2 voltages (0-5v)<br>3 temperatures (thermistors 0-5v) |
| Telemetry Accuracy Required | 1 percent of full scale reading |

The retroreflectors must be mounted on the shade side of the spacecraft in a location that will allow them to be "seen" from a ground station for some portion of the satellite orbit.

## 5.2.10 LOW THRUST ELECTRIC ENGINE

### 5.2.10.1 Background

The low thrust electric engine consists of a propellant, a propellant feed arrangement and a means for generating an electrical discharge across a surface of the propellant. The electric arc is used to ablate a solid or semisolid fuel and then to eject the resulting material from a nozzle formed by the arc electrodes. The device can be considered a form of pulse plasma accelerator with a novel method of propellant feed. By changing the energy, the number, and frequency of the discharges; the amount and physical characteristics of the gas resulting from the propellant ablation can be varied and thus thrust and specific impulse can be varied.

Low thrust electric engines appear very attractive for space propulsion applications such as spacecraft attitude control, orbit station keeping, and orbit eccentricity changes. Some of the advantages of this low thrust device compared with the more conventional cold gas means of propulsion are listed below:

a. No pneumatic tubing, fittings, or valving are needed. The only connection to the engine is electrical. The fuel is stored at each engine or cluster of engines.

b. Lower fuel weight, and since high pressure gas is not used, very low tank weight. Furthermore, no catastrophic gas leakage is ever possible.

c. Large range in thrust level is possible by simply varying the power input.

d. Redundancy is easily provided and reliability is inherently higher since failure of one engine (or pair of engines if common fuel storage is used) does not affect the remaining engines.

e. More precise attitude control performance can be attained due to the very small impulse bit generated by the engine.

f. Problems associated with valves capable of metering and/or sealing small flows are avoided.

g. This means of propulsion permits the design of high performance electrical propulsion devices in the very low ranges of thrust previously unobtainable.

h. The system has no mechanical moving parts, is rugged and compact, and offers long-life operation at very high reliability.

Although their approaches differ somewhat, numerous companies (GE, EOS, Ford, Philco, American Standard, Rocket Research, etc.) are actively developing low thrust devices. The development of low thrust electric engines for a wide range of applications was initiated by the General Electric Spacecraft Department in 1962. This work has been carried to a point where successful performance has been demonstrated for many thousands of operations. A family of experimental electric engines is shown in Figure 5-19. Work is presently underway on measuring the very low values of thrust associated with this type of propulsion system. Figure 5-20 shows a thrust measurement being made on an electric engine. The next logical step is demonstration of the low thrust electric engine in the space environment.

5.2.10.2 Experiment Objectives

The objectives of this experiment are:

a. To demonstrate the performance, reliability, and long life of a low thrust electric engine in the space environment

b. To demonstrate the use of low thrust electric engines to perform spacecraft attitude control functions

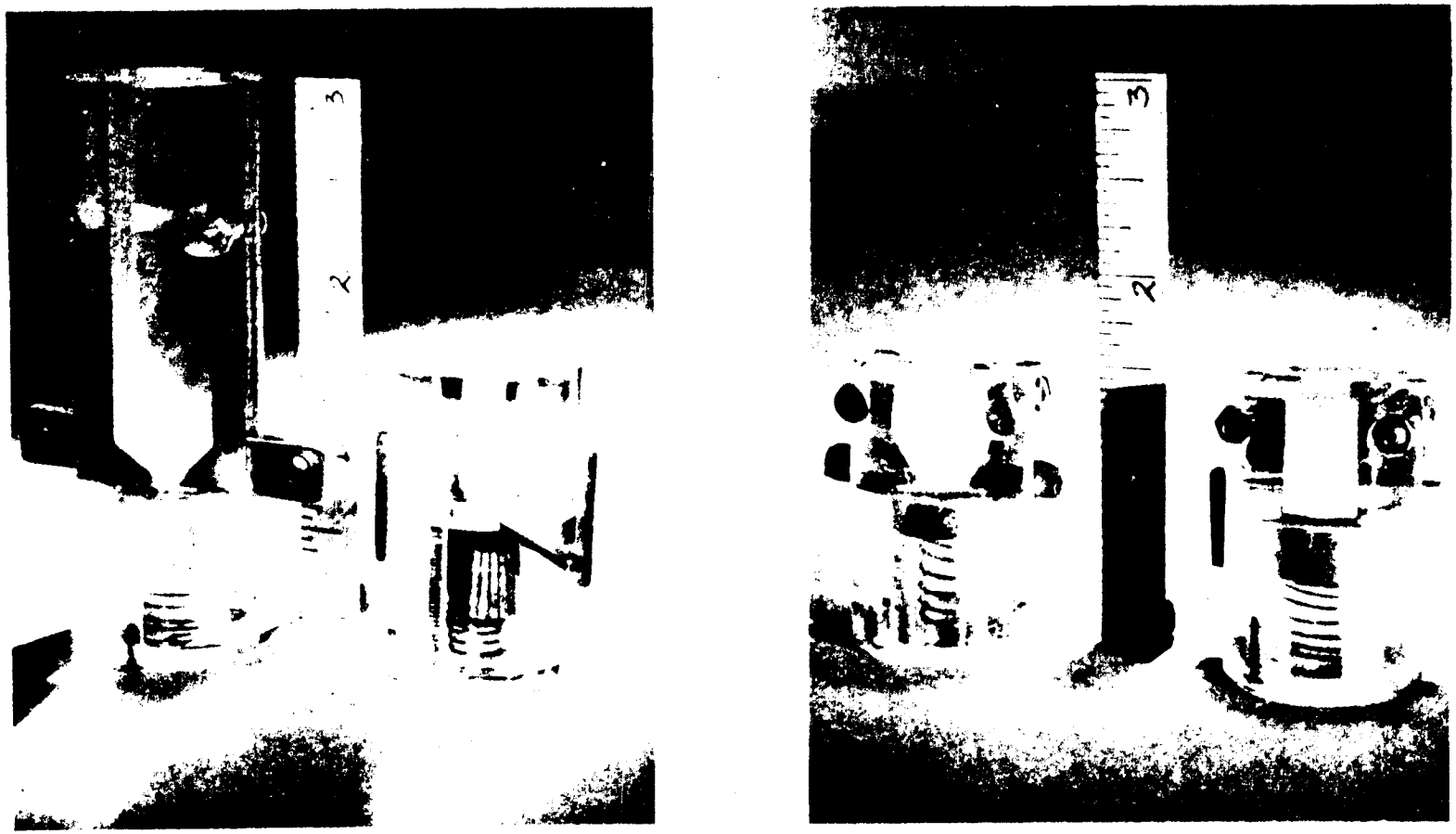

Figure 5-19. Family of Experimental Electric Engines

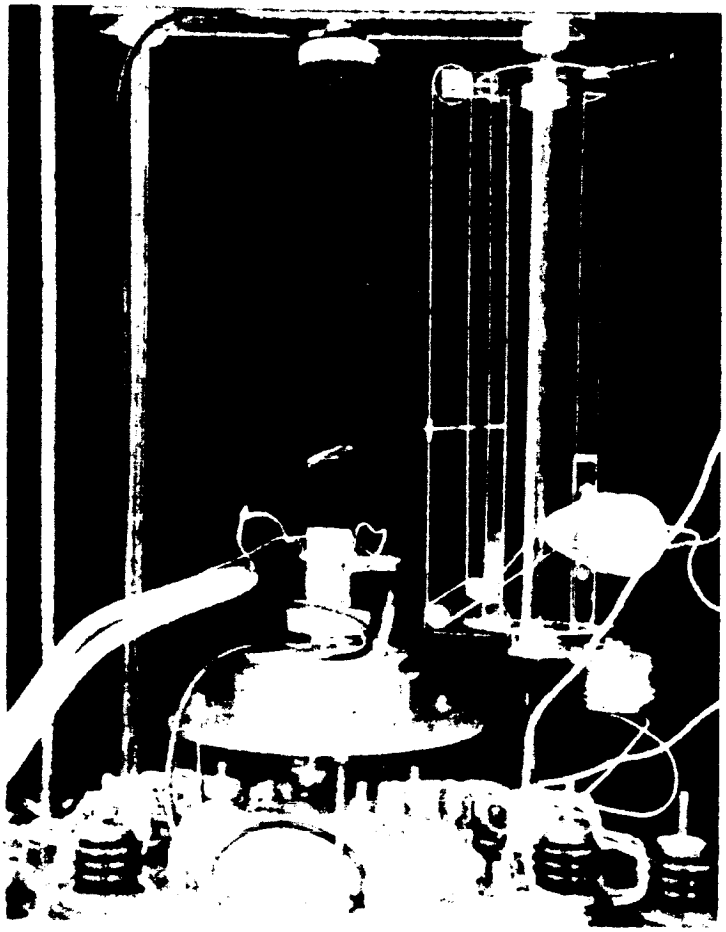

Figure 5-20. Electric Engine on Thrust Stand (In Instrumented Vacuum Chamber)

c. To measure the engine thrust in the space environment and correlate it with the calculated values and measurements made on earth.

5.2.10.3 Experiment Definition

The state of development of the low thrust electrical engine has reached the point where a space experiment is in order. The primary reason for such an experiment is to prove this type of propulsion in the space environment. Also, space offers an ideal environment for measuring the electric engines extreme low thrust ($10^{-6}$ to $10^{-5}$ pounds), which because of the need for a zero g environment, isolation from vibration and a deep vacuum is difficult to do on earth.

In addition to evaluating the engines performance and reliability under actual space conditions, it is desirable to have the engine perform some useful function on the spacecraft. In connection with this particular application, it appears feasible to use low thrust electric engines as an alternate or experimental means of controlling the spacecraft roll rate.

5.2.10.4 Experiment Design

The solar thermionic experiment only requires that the spacecraft be oriented about two axes (pitch and yaw). There is no requirement for roll axis orientation. However, in order to avoid gyroscopic cross-coupling problems or torques from inertia products, it is necessary to keep the spacecraft roll rates low. The spacecraft attitude control system would accomplish this by the use of cold gas jets. When a preset roll rate was reached, the cold gas jets would fire with sufficient impulse to reduce the roll rate to essentially zero. The disturbance torques would then slowly increase the roll rate again until the threshold value was reached and the propulsion cycle repeated.

This experiment proposes to use electric engines for control of the spacecraft roll rate. The experiment would be designed so that upon ground command, control of the spacecraft roll rate would be switched from the cold gas system to the low thrust electric engine experiment. The capability would also be provided to switch back to the primary cold gas system by means of ground command.

Based on the anticipated disturbance torques, a total impulse of approximately $10^{-3}$ lb-sec per cycle would be required once every 1.2 days. This would be accomplished by two sets of engines firing in the roll plane. Each set of engines would have thrust capability in two opposite directions. Thus, if thrust were desired to counter a clockwise roll of the spacecraft, the counter clockwise engine in each engine set would be fired. Assuming an engine thrust of $10^{-7}$ pounds per pulse this means that to obtain a total impulse of $10^{-3}$ lb-sec, the two engine couple would have to fire for approximately 1.4 hours. Electric engines of this size would require approximately two watts per set and operate on a voltage input of 24 to 28 volts.

A circuit voltage measurement would be made on each of the four engines to monitor their performance. Information from the roll rate gyro would be used to calculate the engine thrust.

### 5.2.10.5 Experiment/Spacecraft Interface Requirements

The interface requirements for the low thrust electric engine experiment are:

| | |
|---|---|
| Electrical Power Required | 2 watts for each pair (couple) of engines |
| Weight, Electronics | 2 pounds (total) |
| Engines | 0.25 pounds (4 engines) |
| Overall Dimensions, Electronics | 4 in. x 3 in. x 3 in. each pair of engines |
| Engine | 1 in. diameter x 2 in. long (per engine) |
| Instrumentation | 5 voltages (0-5v) |

Since the mode of operation only requires that two of the engines operate at a time, the power requirements would never exceed two watts. The engines operate on an input voltage of 24 to 28 volts. It is desirable to keep the electronics as close to the engines possible.

The engines would be mounted so as to form couples acting in a plane perpendicular to the spacecraft roll axis.

## 5.3 SCIENTIFIC EXPERIMENTS

Each of the scientific experiments considered is described in this section.

## 5.3.1 INTERPLANETARY DUST (MICROMETEOROIDS)

The micrometeoroid experiment, as presented here, is designed to measure interplanetary dust. As such, it would require an escape orbit of the solar probe type. However, it is typical of a micrometeoroid experiment and would require only minor modifications for an earth orbiting case in which measurement of the micrometeoroid population would be confined to the region around earth.

### 5.3.1.1 Background

The zodiacal light, a phenomenon observed for the past three centuries, has at various times been attributed to the scattering of sunlight by dust particles whose radius lies in the range 0.2 to 100 microns, free electrons with a number density in the order of 600 $cm^{-3}$ at 1 AU from the sun, and a combination of both. Before 1953, it was generally accepted that interplanetary dust was the principal scattering agent. Behr and Siedentopf (Reference 5-21) performed a series of polarization measurements from which they concluded (assuming that the degree of polarization produced by light scattered from dust particles is near zero) that half of the observed surface brightness of the zodiacal light near elongation 35 degrees was due to the scattering of sunlight by free electrons in interplanetary space. Their assumption that the coefficient of scattering is unity for micron size particles has been disputed by a number of investigations (Reference 5-22). Evidence that interplanetary dust may also scatter highly polarized light has been introduced by van de Huls (Reference 5-23). Recently, Blackwell and Ingham, (Reference 5-24) using the facilities at Chacaltaya (Bolivia), have carried out an extensive optical measurements program in an effort to more accurately define the constitutive make up of the zodiacal light. While far from being conclusive, it is apparent that both dust and free electron components exist. Furthermore, it is generally now believed that the zodiacal light can be regarded as the outer part of the solar corona in which there exists a K (free electron) and F (dust particle) component. Additional observations made at Chacaltaya also report a fluctuation in the surface brightness of the zodiacal light at times of increased solar activity.

Recent in-space measurements from satellite probes, conducted primarily by McCracken, Alexander and Dubin (Reference 5-25), in the vicinity of the earth yield higher spatial densities than those obtainable from the zodiacal measurements. This led Whipple (Reference 5-26) to postulate a geocentric "dust belt" around the earth.

The results from Mariner II, on the other hand, lead to a much lower value than expected; recording only one or two impacts during the flight with no impacts recorded in the vicinity of Venus. This is four orders of magnitude less than that recorded in the vicinity of the earth by the Explorer VIII satellite.

5.3.1.2 Experiment Objectives

Therefore, to resolve some of these problems, it is proposed that the environment in interplanetary space lying in the region $0.3 < r < 1.0$ AU from the sun be monitored for the dust component; and that in the event of a strong solar flare be correlated, if possible, with any brightness fluctuations in the zodiacal light. (The latter would be recorded via earth based observations.) An understanding of the nature, origin, and dynamics of this dust component may be an important clue to our understanding of the origin and evolution of the solar system.

5.3.1.3 Experiment Definition

The proposed experiment is designed to measure the flux and momentum of cosmic dust particles (momentum range $2.5 \times 10^{-4}$ to $2.5 \times 10^{-1}$ dyne-seconds) in interplanetary space. These measurements are to be obtained as a function of the distance from the sun. The mass range covered, assuming that the particles have a velocity relative to the vehicle of 25 km $sec^{-1}$, lies in the range of $10^{-10}$ to $10^{-17}$ grams. This is compatible with the findings obtained over the last several years of measurement. The experiment is directed toward providing direct observational data to aid in a separation of the zodiacal light source into a dust and an electron component. The escape orbit probe would provide the only vehicle to date that allows direct sampling of one of these, the dust component near the sun. The

parameters of the cosmic dust environment requiring investigation are size, mass, structure, chemical composition, speed and direction of motion, number density, and distribution in space. Present non-recovery techniques measure only size and the combination of mass and velocity (i.e., momentum and/or energy).

Obviously, a solar probe orbit would be ideal for this type of experiment since it would allow measurements over the total range of interest (1.0 to 0.3 AU). However, measurements in near earth orbits are also valuable since they provide a more complete picture of the micrometeoroid environment near earth. This is of great importance in designing spacecraft and evaluating the effect of micrometeoroid erosion on spacecraft components such as concentrator reflective surfaces, thermal coatings, etc. Near earth measurements also provide partial information from which a better understanding of the zodiacal light may be derived.

### 5.3.1.4 Experiment Design

The instruments developed to date together with the quantity that they measure are given below:

| Type | Measurement |
|---|---|
| Crystal Microphone | number density - momentum* |
| Wire Grid | number density - size |
| Flash Detector | number density - energy |
| Thin Film (Photosensitive or Pressure) | number density - size |

*Note - The response characteristics of the microphone detector have been the subject of numerous debates with regard to just what quantity is being measured. The arguments run from mv to $mv^{4/3}$ to $mv^2$. It is considered here to be an mv detector, the commonly accepted view held by the majority of investigators active in this field.

The crystal microphone detector will probably be most suitable because of its reliable past performance, its simplicity, and its inherent long life. The latter characteristic is not found in the wire grid and thin film types of instruments.

Two units are employed in an effort to record the momentum spectra of those particles overtaking the probe and those being overtaken by the probe. This arrangement would help define the number, densities and momenta for particles having direct and retro-grade orbital motions. This latter point is of interest in cosmological studies. A conventional crystal microphone of small size and appropriate sensitivity would be directly mounted against a sounding plate which is acoustically isolated from the remainder of the vehicle by rubber, polyethylene, or other suitable grommets. Additional acoustical isolation could be provided by tuning the crystal to provide a maximum signal at ultrasonic frequencies thus reducing any effects due to vehicle vibrational frequencies in the order of 100 kc.

A conventional 120 db gain voltage sensitive amplifier with a passband of $\pm$ 10 kilocycles centered at 100 kilocycles would receive the signal from the microphone. The pulse rate from this amplifier would be recorded by four counters of two binaries each fed from amplifier taps separated by 30 db in gain. Thus, a crude momentum spectrum would be obtained.

Each instrument would have 4 channels of output:

$2.5 \times 10^{-4}$ to $2.5 \times 10^{-3}$ dyne-cm

$2.5 \times 10^{-3}$ to $2.5 \times 10^{-2}$ dyne-cm

$2.5 \times 10^{-2}$ to $2.5 \times 10^{-1}$ dyne-cm

$> \quad 2.5 \times 10^{-1}$ dyne-cm

Each impact ($\approx 2.5 \times 10^{-4}$ dyne-cm) will appear as a signal in one of the four channels. The maximum impact acceptance rate is determined by the physical vibration characteristics of the impact plate and the instrument will begin to saturate at an impact rate greater than one impact per minute.

A problem area exists in the calibration and interpretation of impact as a function of location on the plate where the impact occurred.

5.3.1.5 Experiment Spacecraft Interface Requirements

The interface requirements for the interplanetary dust experiment are:

| | |
|---|---|
| Special Instruments | 2 crystal microphones |
| Size - Microphone | 1/2 in. diameter x 1 in. long |
| Plate | 5 in. wide x 10 in. long x 1/8 in. thick |
| Amplifier | 2 in. x 2 in. x 1 in. |
| Weight | 4 pounds (2 pounds per unit) |
| Power | 1 watt (0.5 watt per unit) |
| Output Signal | 8 volts 0-5v range |
| Telemetry Accuracy Required | 1 percent of full scale reading |

The impact receiving plate (5 in. x 10 in. x 1/8 in.) must be mounted so as to have an unobstructed forward view and be oriented perpendicular to the vehicle line of motion. Also, an identical plate must be mounted perpendicular to the vehicle line of motion with an unobstructed backward view.

The primary experiment does not require that the vehicle be oriented about the roll axis. Therefore, it may be difficult to have the same side of the vehicle always facing in the direction of motion. If this is the case, microphones should be placed on four opposite sides of the spacecraft and the number of instruments, size, weight, power and output signal figures given above would be doubled.

## 5.3.2 SOLAR WIND (INTERPLANETARY PLASMA)

This experiment requires a solar probe orbit and is not suitable for inclusion on earth orbiting spacecraft.

### 5.3.2.1 Background

The presence of an interplanetary plasma streaming outward from the sun has been detected recently by instruments aboard Luniks II and III (Reference 5-27), Explorer 10 (Reference 5-28) and most recently by Mariner II (1962). The presence of this solar wind has been inferred earlier from a variety of indirect evidence, including the airglow and aurorae, geomagnetic fluctuations, Forbush events and the appearance of certain types of comet tails.

Based on the data which are available and the most widely accepted theory of the solar wind, it is believed that the solar wind is an extension of the sun's corona which is expanding hydrodynamically into interplanetary space. The plasma consists mainly of fully ionized hydrogen with a measurable fraction of helium nuclei. It is considered likely that traces of other elements (fully or perhaps partially ionized) are present in the plasma, but their detection awaits more sensitive experiments than have been flown to date.

Because of the high electrical conductivity of the plasma, magnetic lines of flux present in the corona tend to be effectively frozen into the plasma. Since the kinetic energy density of the plasma is greater than the magnetic energy at distances greater than a few hundredths of an AU, the magnetic field is carried along by the plasma as it expands into interplanetary space. Thus the structure of the interplanetary magnetic field is intimately connected with the presence of the solar wind.

The recurrence of magnetic disturbances with successive passages of active regions across the face of the solar disc suggests that more intense beams of plasma flow in certain directions and that these rotate with the sun. The Mariner II plasma instrument gave the

first direct measurement of these beams, and showed that during the time of observation, the plasma current in the beams was an order of magnitude higher than the average plasma current. A strong correlation was found between the time of occurrence of peak plasma current and the time of peak disturbance in the geomagnetic field, with allowance for the difference in heliocentric longitude of the probe and earth.

The occurrence of a Forbush decrease in galactic cosmic ray intensity in conjunction with intense magnetic storms is interpreted as due to the deflection of the cosmic ray particles by large scale magnetic field systems associated with unusually dense plasma clouds which reach the vicinity of the earth. The Pioneer V experiments showed that the Forbush decrease is indeed associated with large scale increases in the interplanetary field, but the spatial extent needs investigating. Since the magnetic fields carried by these plasma clouds act to guide solar cosmic rays, the shapes of the clouds and the manner of their connection to the sun requires further study in regions as close as possible to the sun.

The present experimental situation relating to the solar wind leaves open a large number of questions; nevertheless, the Mariner II experiment has provided several fundamental facts about the solar wind. The plasma instrument was a narrow angle device which was always pointed directly towards the sun; at all times during the flight measurable, although at times rapidly fluctuating, plasma current was detected. The current is believed to move out approximately radially from the sun, although it is not certain that the Mariner instrument was viewing the direction of the stream. Indeed, Biermann's comet tail work indicates that the plasma moves out in slighly curved paths which make angles with the radial direction of between 6 and 16 degrees. Thus a possibility exists that the plasma flux and density, as determined by the Mariner experiment, might have occasionally been on the low side. It would therefore be desirable to examine the interplanetary plasma with a wide angle instrument to obtain a better measure of the total plasma density. To study plasma direction, complementary narrow angle instruments are indicated. The density measured by the Mariner II instrument was of the order of four ions per cubic centimeter at approximately one AU.

The Mariner II instrument measured a spectrum of each telemetry frame from which a measure of the mass motion velocity and temperature of the ionic component of the plasma was determined. The mass transport velocity varied considerably (314 to 1250 km/sec) but had an average value of about 500 kilometers per second. The ion temperature can be estimated to be approximately $10^5$ to $10^6$ °K, the specific value depending on the particular spectrum analyzed. At times during the flight, rapid changes in the plasma spectrum were detected; at least one of these can be ascribed to the passage of a plasma shock front. However, the sampling rate of the spectrum was too slow (3.7 minutes) to study the energy turbulence in the shock front.

An escape orbit probe should carry plasma instruments capable of looking in several directions about the sun-probe line to determine plasma stream directions. A wide angle instrument should also be provided to obtain a better measurement of the total plasma density. The coarseness of the Mariner energy spectra makes temperature determinations and observations of helium ions subject to considerable uncertainty. Therefore, more energy resolution should be provided than was available for Mariner II.

Thus far no mention has been made of the electron component of the plasma. The kinetic energy of electrons due to the plasma mass transport velocity is expected to be much lower than that of the ions due to their small mass. On the other hand, approximate equipartition of random thermal energy would be expected between ions and electrons. Based on plasma temperatures deduced from the Mariner II experiments, the random thermal electron velocity is expected to be much greater than the plasma mass transport velocity so that the electrons should have a nearly isotropic distribution. Since the average electron energy is expected to be only of the order of tens of volts, based on the ion temperatures measured by Mariner II, the vehicle electrostatic potential may act as a serious perturbation on any measurements of plasma electron spectra, since plasma currents and photoelectric effect could easily result in a vehicle potential on the order of ten volts which cannot easily be measured. Since there are other difficult technical problems associated with measuring the electron portion of the solar wind, no specific consideration has been given to any instruments designed to measure their spectrum.

5.3.2.2 Experiment Objectives

The objective of this experiment would be to measure the solar wind magnitude and direction as a function of the heliocentric distance, going as close to the sun as is feasible.

5.3.2.3 Experiment Definition

The requirements for the interplanetary plasma experiments in order to furnish a quantitative understanding of the flow outward from the sun, the dimensions and propagation of intense beams originating in active solar regions, and interplay with the interplanetary magnetic field, are the following.

a. Instruments capable of determining the direction of the main plasma stream with an angular resolution of the order of 5 to 10 degrees are necessary.

b. Based on the Mariner II spectrum measurements, the plasma analyzer should cover the range of plasma ion mass velocities from about 200 kilometers per second to perhaps as high as 2500 kilometers per second in about 30 energy steps.

c. Although the electron component of the plasma is of considerable interest, the problems of making clear cut measurements of the electrons do not appear to be solved at present. Therefore, a separate electron plasma probe need not be provided.

d. One of the unique sets of data to be gathered by an escape orbit probe is the plasma density as a function of heliocentric distance. A wide angle instrument should be employed to insure a good measurement of the density.

e. The most valuable spectrum data would be a series of snapshot-like spectra. A spectrum gathered in a time of the order of a few seconds would be desirable.

f. The aberration effect of an escape orbit probe orbital velocity should be taken into account when the pointing directions for the plasma probes are selected.

The above requirements can be satisfied by combining narrow angle and wide angle instruments. Narrow angle instruments have been developed (Reference 5-29) which can examine plasma current in a number of directions lying near a given plane by utilizing hemispherical electrostatic deflection plates and multiple collectors. Two such instruments can be used to examine the angular direction of plasma flow near the plane of the ecliptic and near another plane perpendicular to the ecliptic and pointing toward the sun. Since vehicle aberration effects will be different for ions of widely different velocities, the maximum current directions are not expected to be the same for widely different energy channels.

A large aperture, wide-angle, Faraday Cup type of plasma probe would give a sensitive measurement of weak plasma currents (Reference 5-30). The importance of the plasma measurements justifies a certain amount of redundancy in the plasma instrumentation.

5.3.2.4 Experiment Design

The solar plasma wind will be measured with a Faraday Cup and two electrostatic analyzers. The range of measurement would be from 200 to 20 keV. Each of the two electrostatic analyzers measures four angles and 32 energy levels (20 protons plus 12 electron) for each angle, the single Faraday cup instrument would measure 12 energy levels (8 proton plus 4 electron) for each of three plates.

5.3.2.5 Experiment/Spacecraft Interface Requirements

The interface requirements for the solar wind experiment are:

| | |
|---|---|
| Special Instruments | 2 Narrow Angle Electrostatic Analyzers (4 angles each instrument)<br>1 Wide-Angle Faraday Cup |

65-325

Vol II

| | | |
|---|---|---|
| Volume | 2 Electrostatic Analyzers | - 216 $in^3$ |
| | 1 Faraday Cup | - 216 $in^3$ |
| Weight | 2 Electrostatic Analyzers | - 8 pounds |
| | 1 Faraday Cup | - 5 pounds |
| Power | 2 Electrostatic Analyzers | - 3 watts |
| | 1 Faraday Cup | - 1.5 watts |
| | with 10 watt peaks of 30 ms duration | |
| Output Signal | 2 Electrostatic Analyzers | - 256 voltages (0-5v) |
| | 1 Faraday Cup | - 36 voltages (0-5v) |
| Telemetry Accuracy Required | 1 percent of full scale reading | |

The Electrostatic Analyzers and the Faraday Cup require exposed surface areas of approximately 20 square inches (per instrument) and six square inches respectively. These instruments must be mounted on the spacecraft so they have an unobstructed view of space.

### 5.3.3 PROTON AND ELECTRON SPECTRA AND DIRECTION

#### 5.3.3.1 Background

Despite the large number of experiments which have been carried out to determine the space radiation environment, there still exists a need for additional information in order to assess the effects of this environment for specific satellite missions. There are several reasons for the uncertainties which remain despite the measurements carried out to date, one being the lack of adequate particle discrimination in the early experiments which were performed.

Another is the large perturbation in the environment which was introduced into the natural radiation environment by the detonation of high altitude nuclear devices during the latter half of 1962. Besides the complex time decay pattern followed by the artifically injected electrons, recent experiments indicate that the intensity of the proton belt at the low altitudes is increasing with time, but data are sparce. Many satellites have been flown at altitudes too high to permit adequate mapping of the lower altitude regions of the trapped radiation belts which are important to manned space station applications. For example, the radiation data on which present MOL environment studies are being carried out is mostly the result of an intensive series of experiments carried out in late 1962.

Proton spectra were obtained by Naugle and Kniffen (Reference 5-31) using emulsions aboard the recoverable NERV vehicle. From their data, it can be seen that the dose can be reduced by as much as an order of magnitude as the shield thickness is increased from one to eight grams per square centimeter, corresponding to the successive removal of protons in the energy range 30 to 100 Mev. It would appear that from the standpoint of computing shielded radiation dose, it would be desirable to measure the intensity of proton energy groups, within this energy interval, over extensive regions, at low altitudes (approximately 300 nautical miles).

Freden and Paulikas (Reference 5-32) have made measurements of protons using lithium ion drift detectors behind hemipsherical shielding of thicknesses appropriate to stop protons below 5 and 60 Mev. When such a detector is used as an omnidirectional instrument, the upper energy limit of a given channel depends upon the direction of the incident particle due to variations in lengths of oblique paths through the detector.

Proton measurements in the energy group 40 to 110 Mev have been made on Explorer XV by McIlwain (Reference 5-33) using a spherical scintillator covered by a hemispherical shield. These data do not cover the altitude range covered by many low altitude satellites and it is desirable to divide this energy range into two or three subintervals.

The electrons most likely to be of interest for prediction of radiation dose inside the thin walls of a manned orbiting laboratory are those in the energy range just above that required for wall penetration. It is unlikely that the walls of most vehicles will be thick enough to stop electrons above, say 1.5 Mev, and hence the dose from penetrating electrons will far exceed that due to bremsstrahlung. Because of the uncertain picture of time decay of the electron fluxes in the low altitude regions, it is desirable to make a number of measurements of integral electron fluxes from above thresholds up to about 3 Mev.

McIlwain has made measurements of the integral electron fluxes above 0.5 Mev in a collimated instrument, and omnidirectional measurements with a threshold of 5 Mev. These Explorer XV results are insufficient for use in environment specification in the altitude range below 200 to 300 nautical miles. Other measurements were obtained in late 1962 by Katz, White, Smith and West (Reference 5-34, 5-35, and 5-36). The latter used a magnetic spectrometer and obtained a large amount of differential spectrum data. Because of the complex time decay of the aritificial electron belt, it is desirable to make repetitive measurements of electron fluxes in order to keep information on present status of the electron environment more up to date than has been possible in the past, particularly at low altitudes.

5.3.3.2 Experiment Objectives

The objectives are to obtain measurements of proton and electron spectra in well-defined energy intervals as a function of direction. The energy intervals chosen will depend upon the particular orbit of the satellite upon which the experiment is conducted.

5.3.3.3 Experiment Definition

The proposed experiment is designed to measure proton and electron spectra in the following ranges:

| Protons | Electrons |
|---|---|
| 30 - 50 Mev | 0.5 - 1.5 Mev |
| 50 - 100 Mev | 1.5 - 2.8 Mev |
| 100 - 200 Mev | > 2.8 Mev |

Three directions would be measured. These ranges are most suitable for a circular orbit at approximately 325 nautical miles. The ranges may be tailored to fit other orbits as required.

5.3.3.4 Experiment Design

Solid state detectors are used in a telescope configuration backed by electronic amplifiers, coincidence circuits, discriminator gates, and a data conditioning section. The data conditioning section converts raw pulses from the coincidence circuits to a form ready for telemetering. At present, the conditioning circuit accepts pulses from five pulses $sec^{-1}$ to $1.5 \times 10^5$ pulses $sec^{-1}$ and produce logarithmically a d-c voltage varying from 0 to 5 volts, where each volt corresponds approximately to a decade.

5.3.3.5 Experiment/Spacecraft Interface Requirements

The interface requirements for the proton and electron spectra and direction experiment are:

| | |
|---|---|
| Special Instrument | 3 Charged Particle Telescopes |
| Volume | 300 $in^3$ (total package including electronics) |
| Weight | 24 pounds (total package including electronics) |
| Power | 9 watts |
| Output Signal | 20 voltages (0-5v) |
| Telemetry Accuracy Required | 1 percent of full scale reading |

The three telescopes are to be mounted on mutually perpendicular axes with one of the axis pointed to the sun. The telescopes are to be mounted so that they have an unobstructed

view of space. In order to evaluate the measured data, it is also necessary to know the spacecrafts position and orientation in space.

The primary experiment does not require that the spacecraft be oriented about the roll axis. As a result it may be difficult to determine the spacecraft orientation in space. If this is the case, only one telescope (instead of three) pointing to the sun would be used. This would alter the interface requirements summarized above to the following:

| | |
|---|---|
| Special Instrument | 1 Charged Particle Telescope |
| Volume | 100 $in^3$ (total package including electronics) |
| Weight | 8 pounds (total package including electrics) |
| Power | 3 watts |
| Output Signal | 6 voltages (0-5v) |

As before the telescope requires an unobstructed view.

### 5.3.4 INTERPLANETARY MAGNETIC FIELD

The magnetic field experiment as presented here is designed to measure interplanetary magnetic fields. This is typical of a magnetic field experiment and would require only minor modification for a earth orbiting case in which measurements of the earth's magnetic field would be of interest.

#### 5.3.4.1 Background

A considerable body of evidence regarding the nature of the interplanetary magnetic field is available from observations of the following phenomena:

a. Appearance of filaments in the solar corona

b. Modulation of galactic cosmic radiation, including Forbush events

c. Terrestrial magnetic disturbances and ionospheric absorption events resulting from arrival of low energy solar cosmic rays

d. Observation of energetic solar particles originating in flares.

Recently, preliminary space measurements, notably on the Pioneer V spacecraft, have become available. The Pioneer V data indicated the presence of a rather steady field of approximately four $\gamma$, with occasional increases by an order of magnitude. This probe measured the component of the field perpendicular to its spin axis, which lay generally along the line towards the sun. A report on the experiment (Reference 5-37) indicates that the results are difficult to reconcile with many theories of the interplanetary magnetic field. More recent measurements aboard the Mariner II spacecraft showed variations in the interplanetary magnetic field over heliocentric distances from 1.0 to 0.7 AU with a period of the same order as the solar rotational period, but a lack of zero calibration and suspected vehicle induced fields prevented the attainment of a picture of the interplanetary field at these distances. Considerable fluctuations were observed and the data were consistent with an interplanetary field whose radial direction near the ecliptic does not change, except possibly over regions extending on the order of half way around the sun.

Coronal filaments which appear to outline magnetic field lines show evidence for a rather ordered field in the immediate neighborhood of the sun's poles. An overall dipole field is excluded by the fact that the Pioneer V and Mariner II data would, if extrapolated in this manner to the surface of the sun, give field strengths far in excess of those obtained by measurements of Zeeman splitting of optical lines (Reference 5-38). A comparison of plasma particle energy densities and magnetic field energy densities deduced at a heliocentric distance near unity shows that any systematic intergalactic field penetrating through the solar system should be swept out by the plasma wind.

At latitudes corresponding to those containing most solar surface activity, the coronal streamers show evidence of closing at distances not exceeding a solar radius or so, while lines emanating from the less active polar regions appear to extend to great distances from

the sun. It has been pointed out (Reference 5-39) that this general structure is consistent with the expectation that clouds of plasma ejected from active regions would sweep away the magnetic fields at small and intermediate latitudes, and that ultimate detachment of the corresponding field lines from the solar surface must occur through dissipative processes. The magnetic pressures available in the coronal regions should be completely inadequate to prevent the expansion of such relatively dense and energetic clouds of highly conducting plasma.

That systems of magnetic field lines carried out to the earth's orbit must, in many cases, retain a high degree of attachment to the solar surface is indicated by the high degree of correlation between observations of the Forbush decrease and the frequency and intensity of solar proton events observed at the earth from chromospheric flares. Pioneer V served to prove that the Forbush decrease was not a geocentric phenomenon but is connected with large scale magnetic field increases in the interplanetary space. The magnetic field strengths observed during disturbed times were of the order of 40 $\gamma$, which are known to be adequate to cause a Forbush type decrease if the regions involved extend over distances of the order of an astronomical unit. The high degree of probability of occurrence of geomagnetic disturbances from large disturbed regions of the solar surface indicates that, at least in many cases, the plasma clouds presumably giving rise to increases in the interplanetary magnetic field must extend over extremely large regions.

The fact that geomagnetic disturbances can occur periodically with successive solar disc passage of M regions and the recent direct observations aboard Mariner II of plasma current peaks with the periodicity of the solar rotation suggests that magnetic lines swept out by the plasma may retain a high degree of attachment to the sun. A high degree of overall order to the interplanetary field may therefore exist despite the dominance of magnetic field pressure by plasma particle pressure, but this field structure must be considerably more complicated than, for example, the geomagnetic field. Evidence from solar energetic particle events (Reference 5-40) indicates that, following the expulsion of large plasma clouds from active solar regions, the interplanetary magnetic field between the earth and sun tends to lie near the plane of the solar equator. Analysis of two solar

RE-ORDER NO. 65-323
Vol II

cosmic ray events indicated that the direction of the field near the earth's orbit must have made an angle of approximately 60 degrees from the earth-sun line. Analysis of the relative frequency of occurrence of solar flares resulting in energetic particle arrival at earth shows that particle arrival is most probable for events occurring near the western solar limb. The fact that, for the events analyzed, rise times for energetic particle fluxes are much more rapid for flare events occurring near the western limb, while flares near the central solar meridian give slow rise times. This strongly indicates that during these disturbed times, magnetic lines of force connect the earth with the western portions of the sun. The difference in rise times of the energetic particle fluxes is understandable, from this hypothesis, since particles from flares near the western limb can reach the earth quickly by spiralling along field lines, while those originating from flares near the center of the solar disc must diffuse across magnetic field lines in order to reach earth. This interpretation is further confirmed by the fact that for the latter type of events, the delay times are longer for the particles with lower energies.

The hydrodynamical expansion theory of the solar plasma (Reference 5-41) and evidence from the orientation of comet tails (Reference 5-42) indicates that the plasma motion in the vicinity of the inner planets should be principally in the radial direction. The plasma currents measured by the narrow angle Mariner II instrument, which was pointed at the sun, appear to give some confirmation of this expectation. On the other hand, if there is the expected correlation between the direction of the plasma flow and the direction of field lines swept out by it, the large deviations of the apparent field direction from the radial direction, deduced as mentioned above from solar energetic particle events on two occasions, need to be explained. It is of course possible that the pitch angle of the outward spiral described by the plasma flow and the field lines changes radically during solar disturbances. The mean plasma velocity (500 km/sec) measured by Mariner II corresponds to arrival at the earth at a time when the responsible active region would be near the western limb but the shorter transit times sometimes observed from geophysical evidence indicates that the tightness of the spiral paths may be highly variable.

The importance of the overall structure of the interplanetary field and its time variations indicates the desirability of performing in space magnetometer measurements at various distances from the sun. These can complement and perhaps reconcile the evidence based on other types of studies. In particular it is desirable to make measurements as close as possible to the sun in order to observe the transition to a more ordered field and to search for possible field detachment processes.

A recent theory (Reference 5-43) for the sunspot cycle which seeks to explain the periodic reversal of polarity of the leading spot in groups in northern and southern hemispheres could be tested by measurements of the ordered solar field. Magnetometer measurements aboard a solar probe might thus have far-reaching implications for solar physics as well as for the field and particle physics of the interplanetary space.

In addition to the interest in making magnetic field measurements in a solar probe orbit, it is also desirable to make further measurements in near earth orbits to improve our understanding of the earth's magnetic fields.

5.3.4.2 Experiment Objective

The objective of this experiment is to measure the interplanetary magnetic field strength as a function of time and position. The region for investigation is to be $0.3 < r < 1.0$ AU from the sun.

5.3.4.3 Experiment Defination

The proposed experiment is designed to measure the interplanetary magnetic field (field strength $0.12\gamma$ to approximately $500\gamma$). These measurements are to be obtained as a function of time and position for $0.3 < r < 1.0$ AU from the sun. The magnitude of the field fluctuations already observed in interplanetary space indicates that the greater sensitivity of the gas-type magnetometer such as the rubidium device (sensitivity $0.01\gamma$)

would not be warranted. Neither do the temperature limitations of the sensing element ($40^{o}$ to $55^{o}$C) appear suitable for boom mounting in an environment in which the solar heating flux would be highly variable over the orbit.

5.3.4.4 Experiment Design

For the measurement of the interplanetary magnetic field, the most suitable instrument appears to be the saturable core flux gate magnetometer. This instrument has adequate sensitivity (to 0.12 $\gamma$), adequate range, and has been proven in other space experiments. It is assumed that the instrument would be similar to one recently developed by the Schoenstedt Instrument Company for measurement of small fields. This would be a three-axis instrument which would cover the range between instrument noise level (0.12$\gamma$) and 500$\gamma$. For periodic zero calibration, it is necessary to mechanically reverse the direction of each separate sensor axis. Two axes can be reversed simultaneously by a rotation about the third axis, but the third sensor must be mounted separately with its own reversing mechanism. Operation of the reversing mechanism could be provided by an on-board clock several times per day. Override capability could be provided by radio command so that possible development of periodic instrument zero drifts could be distinguished from fluctuations in field direction or strength.

The accuracy of the magnetometer depends upon the range setting. For the low range (high responsivity) the limit is set by the noise level, and is $\pm$ 0.125$\gamma$. For the high range it may be $\pm$ 1$\gamma$. The sensitivity stability of the electronics (from $-25^{o}$ to $+50^{o}$C) is better than two percent, and the sensitivity stability of the sensor from ($-55^{o}$ to $+65^{o}$C) is better than two percent. The stability of the signal output (zero field) is $\pm$ 0.6 percent each for both the electronics ($-25^{o}$ to $+50^{o}$C) and the sensor ($-55^{o}$ to $+65^{o}$C).

5.3.4.5 Experiment/Spacecraft Interface Requirements

The interface requirements for the interplanetary magnetic field experiment are:

| | |
|---|---|
| Special Instruments | Triaxial Fluxgate Magnetometer |
| Volume of Instrument | 3 in. x 4 in. x 5 in. (does not include boom) |
| Weight | 4.5 pounds (does not include boom) |
| Power | 0.5 watt |
| Output Signal | 3 voltages (0-5v) |
| Telemetry Accuracy Required | 1 percent of full scale reading |

The magnetometer must be mounted on an extended boom of sufficient length to avoid any stray magnetic fields developed on the spacecraft. This is vital in obtaining valid readings and has proved to be a problem in the past (Mariner II experience). Also, for zero calibration purposes it is necessary to periodically rotate the magnetometer boom.

5.3.5 HEAVY NUCLEI

Since very few heavy particles are found within the region of space influenced by the earth's magnetic field, this experiment requires an orbit altitude greater than approximately 55,000 nautical miles. For this reason, of the orbits considered, only the solar probe is compatible with this experiment.

5.3.5.1 Background

In the study of solar physics and galactic cosmic rays, it is necessary to know the relative abundance of the various energetic nuclear particles arriving at the earth during and after major flare activity. There are (Reference 5-44) theoretical reasons to suppose that the composition of the multiple charged components with the same charge to mass ratio, compared in the same velocity interval, should be essentially the same as that deduced for the sun's surface on the basis of spectroscopic measurements. Experiments have

been carried out (Reference 5-45, 5-46, and 5-47) which seem to indicate that the energetic solar nuclei coming from the sun and having charges ranging from 2 to about 18 do reflect the composition of the solar surface. Additional experiments need to be conducted to obtain heavy particle flux values and rates of change as a function of the solar cycle and solar activity.

5.3.5.2 Experiment Objectives

Therefore, as an aid in determining the sun's composition, it is proposed that the spectrum of the flux of heavy particles originating in the sun be measured as a function of solar activity and solar cycle.

5.3.5.3 Experiment Definition

The proposed experiment is designed to measure the differential flux of heavy particles, $z = 2$ to about $z = 20$, emanating from the sun.

5.3.5.4 Experiment Design

Solid state detectors are used in a telescope configuration backed by electronic amplifiers, coincidence circuits, discriminator gates, and a data conditioning section. The data conditioning section converts raw signal pulses from the coincidence circuits to a form ready for telemetering. No instrument has been built for this specific purpose using a telescope configuration of solid state detectors, but a similar one has been built for protons and electrons (refer to Section 5.3.3). The choice of ranges of z and of energy for a given channel of output will be determined at the time of final orbit selection.

65-323

Vol II

5.3.5.5 Experiment/Spacecraft Interface Requirements

The interface requirements for the heavy nuclei experiment are:

| | |
|---|---|
| Special Instrument | 3 Charged Particle Telescopes |
| Volume | 300 in.$^3$ |
| Weight | 25 pounds |
| Power | 9 watts |
| Output Signal | 20 voltages (0-5v) |
| Telemetry Accuracy Required | 1 percent of full scale reading |

The three telescopes are to be mounted on mutually perpendicular axes with one of the axis pointed to the sun. The telescopes are to be mounted so that they have an unobstructed view of space. In order to evaluate the measured data, it is also necessary to know the spacecrafts position and orientation in space.

As outlined in Section 5.3.3.5, the primary experiment does not require orientation about the roll axis and, therefore, it may not be convenient to provide this third axis orientation for one or two secondary experiments. If this is the case, only one telescope (instead of three) pointing to the sun would be used. This would alter the interface requirements summarized above to the following:

| | |
|---|---|
| Special Instrument | 1 Charged Particle Telescope |
| Volume | 100 in.$^3$ |
| Weight | 8 pounds |
| Power | 3 watts |
| Output Signal | 6 voltages (0-5v) |

5.3.6 SOLAR X-RAYS



281

VOL II

5.3.6.1 Background

Among the many avenues leading to a more complete understanding of the sun's operation is the study of solar X-rays. This requires that the intensity of X-radiation as a function of time, wavelength, and source location be observed. First, consider a certain wavelength region and source position. Experiments (Reference 5-48) have shown that solar X-ray emission in the 44 to 60Å band, responsible for most of the E-region ionization, originates sufficiently high in the corona that a total eclipse does not entirely obscure it. Furthermore, the X-rays are closely associated with active regions identified by sunspots and plage formations. Secondly, consider the time dependence of the X-radiation for various wavelength regions. The X-ray intensity varies with time and has a large variation from sunspot minimum to sunspot maximum. The solar cycle increase is about a factor of 200 in the 2 to 8Å band and about a factor of 50 in the 8 to 20Å band (Reference 5-49). The increases in the intensities in the 2 to 8Å and 8 to 20Å bands are even greater at times of solar flares and the characteristic flare-produced X-ray spectrum is considerably harder than that from the quiet sun. Thirdly, consider why the sun emits X-radiation. The radiation of the sun in the wavelength range of X-rays is a consequence of the high temperature of the emitting layers, namely the corona and the region of transition to the chromosphere (Reference 5- 50). The flux from a region depends upon the electron density, relative abundance of the elements, and the temperature. The electron density decreases with latitude and also there is about a factor of two change during the solar cycle. The relative abundance of the elements can be obtained, within about a factor of two from Fraunhofer lines (Reference 5-51). The temperature of the electrons, based upon ionization equilibrium in the corona, inferred from green and red lines of Fe XIV and Fe X, are about $10^6$ °K in the corona. Considerably more data is needed to complete our understanding of solar X rays.

5.3.6.2 Experiment Objective

In order to provide answers to some of the solar problems; e.g., flare mechanisms, temperature gradient in corona, and coronal structure continuous monitoring of solar

X-rays would be helpful. It is proposed that the solar X-ray flux be monitored continuously or at least sampled as often as is practical.

5.3.6.3 Experiment Definition

The proposed experiment is designed to measure the solar X-ray flux in the 2 to 8Å and 8 to 20Å bands. Measurements are to be made once a minute in order to detect any correlation between increased X-ray activity and solar flares.

5.3.6.4 Experiment Design

The solar X-ray fluxes would be measured with Geiger counters. The spectral sensitivity of the counters would be defined by the transmission of the window and by the absorption and photoionization properties of the filling gas (Reference 5-48). The Geiger counter covering the 2 to 5Å band would have an aluminum window having a thickness of 1.534 mg $cm^{-2}$, and the counter covering the 8 to 20Å band would have a beryllium window having a thickness of 24.4 mg $cm^{-2}$. Both counters would be filled with 8.6 millimeters of ethyl formate and 702.6 millimeters of neon. The signal pulses would be amplified, conditioned, and fed into a counting rate circuit. The output would then be a d-c voltage in the range 0 to 5 volts suitable for the telemetry system. The size of each counter would be determined by the expected counting rate range and would be adjusted for the specific orbit finally chosen.

5.3.6.5 Experiment/Spacecraft Interface Requirements

The interface requirements for the solar X-ray experiment are summarized below:

| | |
|---|---|
| Special Instruments | Geiger Counters |
| Size | 100 $in^3$ |
| Weight | 3 pounds |

65-323

| | |
|---|---|
| Power | 1 watt |
| Output Signal | 2 voltages (0-5v) |
| Telemetry Accuracy Required | 1 percent of full scale reading |

The Geiger counters must be oriented to the sun and be mounted on the spacecraft so that they have an unobstructed view of space.

### 5.3.7 SOLAR $\gamma$-RAYS

#### 5.3.7.1 Background

Gamma radiation comes from space to earth. The logical sources would most likely be individual astronomical objects. Gamma radiation in the energy region of 100 Mev is expected to originate in the same regionsin which cosmic rays are produced. These would be regions where hydromagnetic turbulence accelerates charged particles to very high energies in the presence of gas or dust. Such conditions probably exist in flares; old supernovae like the Crab Nebula; our Galaxy as a whole, but most particularly the nucleus identified by some as Sagittarius A (Reference 5-52); other galaxies, e.g., M31; and galaxies in collisiton, e.g., Cygnus A. On this basis, our sun should be considered as a possible source of gamma-rays.

Low energy gamma-rays, say from 0.1 to 5 Mev, result from radioactive decay of excited nuclei, fusion of light elements, and perhaps electron-position annihilations. High energy gamma-rays, say from 50 to 200 Mev, should result from the decay of neutral $\pi$-mesons produced in nuclear interactions with high-energy particles and from the annihilation of matter and antimatter. The high energy range is of greater interest because the expectation of finding something is more definite.

One such experimental investigation was carried out by Danielson (Reference 5-53). A gamma-ray telescope was used on a manned balloon flight. The results showed that the solar produced gamma-radiation, having energy greater than about 200 Mev, had an upper

limit of about 0.008 photon $cm^{-2}$ $sec^{-1}$. This is approximately one percent of the cosmic-ray flux. Danielson set no lower limit on the gamma-ray flux. However, the experiment, as performed, could not detect any increase in gamma-radiation when the telescope was pointed at the sun, compared to pointing it in the general direction of the sun but not at it.

As far as the low end of the energy spectrum of gamma radiation is concerned, there has been an observation (Reference 5-54) of a flash of 0.5 Mev gamma-rays 0.5 minutes before a solar flare. Thus continuous monitoring of solar gamma rays is most important.

5.3.7.2 Experiment Objective

In order to provide answers to some of the solar problems, e.g., flare mechanisms and particle acceleration, continuous monitoring of the solar gamma radiation would be helpful. It is proposed that the solar gamma radiation flux be monitored continuously.

5.3.7.3 Experiment Definition

The proposed experiment is designed to measure the solar gamma-ray flux in the energy range of 0.1 to 200 Mev.

5.3.7.4 Experiment Design

The solar gamma-rays will be measured with scintillation detectors. The signal pulses will go into a pulse height analyzer and will be sorted into six energy ranges. The pulses from each channel will be fed into a counting rate circuit whose output will be a d-c voltage in the range of 0 to 5 volts suitable for the telemetry system.

5.3.7.5 Experiment/Spacecraft Interface Requirements

The interface requirements for the solar gamma-ray experiment are:

| | |
|---|---|
| Special Instruments | Scintillation Detectors |
| Size | 150 $in^3$ |
| Weight | 8 pounds |
| Power | 4 watts |
| Output Signal | 6 voltages (0-5v) |
| Telemetry Accuracy Required | 1 percent of full scale reading |

Each of the six channels would be sampled approximately once per minute in order to detect any correlation between increased gamma-ray activity and solar flares. The scintillation detectors must be oriented to the sun and be mounted on the spacecraft so that they have an unobstructed view of space.

5.3.8 MEASUREMENTS OF PLANETARY ALBEDO

5.3.8.1 Background

It is well known that the albedo of the earth is a very important quantity for investigations of the atmospheric energy budget. Solar radiation which is reflected back to space obviously does not participate in an important way in the development of atmospheric circulations, in the change of water from the liquid to the gaseous phase, or in the other major energy-dependent processes in the atmosphere. Since the solar energy emission is approximately constant throughout much of the spectral range of interest, a knowledge of the planetary albedo permits a determination of the amount of energy which is retained by the Earth and is thus a positive term in the energy budget.

Measurements of the earth's albedo which have been made so far are of the most primitive kind. The first such determination, aside from theoretical estimates, was that of Danjon

(1936) (Reference 5-55) in which the earth-reflected sunlight which was reflected from the dark portion of the Moon was measured. Since the measurements were all made at one location on the Earth, they represented albedo determinations of only a part of the Earth. Furthermore, the measurements covered only a very small part of the total solar spectrum.

A great number of data on the earth-reflected sunlight have been obtained by the TIROS meteorological satellite, but these data are still unsatisfactory from a number of standpoints. Their most serious shortcoming lies in the fact that there is no on-board calibration of the instrument and a serious but quantitatively unknown amount of degradation of the instruments has occurred subsequent to the ground calibration. Consequently, the values of planetary albedo obtained are subject to large errors. The second difficulty with the TIROS data is that the radiometer furnishes data on radiant intensity in a restricted solid angle oriented in only one direction at any given time. Our knowledge of the angular distribution of intensity over the downward hemisphere is still too meager to allow a good determination of total reflectance from a measurement in only one direction. Thirdly, TIROS has so far been restricted to orbits of inclination of less than 60 degrees, with respect to the equatorial plane, so there are large areas of the Earth for which no TIROS measurements are available.

The Ames Research Center of NASA (Reference 5-56) is in the process of building up an experiment for satellite application in which multi-channel measurements of the earth-reflected sunlight will be made. These measurements will, however, be restricted to the range of wavelengths 3200 to 7800Å, while 41.5 percent of the energy of solar radiation is at wavelengths greater than 8000Å. The orbit of the Ames vehicle will be inclined 33 degrees to the equatorial plane, thereby providing data only at relatively low latitudes. Finally, the Ames experiment has yet to be flown.

5.3.8.2 Experiment Objective

The objective of the present experiment is to obtain data for a reliable determination of the earth's albedo and its variation throughout the lifetime of the satellite.

5.3.8.3 Experiment Definition

The experiment should provide data on the intensity of the earth-reflected solar radiation, as a function of location and angle at which the earth is viewed, in six different spectral intervals in the 3000Å to 2.5 μ range. The field of view of each of the six channels should be a 5 degree half-angle cone, the optical axes for all channels should be parallel, and the field of view should be made to sweep across the disc of the earth from horizon to horizon, through the nadir direction (this would be accomplished by mechanical means). Each channel should be made to obtain a burst of approximately twenty measurements at equal angular intervals during the horizon-to-horizon sweep, thereby making a total of approximately 120 individual measurements during a sweep. The sequence should be repeated at intervals of approximately 2 1/2 minutes during the time the satellite was over the sunlit hemisphere.

The spectral intervals for the six channels would be defined by six optical filters, the band passes of which are centered at the following wavelengths:

| Channel | Wavelength |
|---|---|
| 1 | 3500Å |
| 2 | 5500Å |
| 3 | 8000Å |
| 4 | 1.025 μ |
| 5 | 1.35 μ |
| 6 | 2.15 μ |

5.3.8.4 Experiment Design

The optics of each channel would be of the most primitive type, consisting simply of a lens, filter and detector with appropriate optical diaphragms for defining the field of view. The measurements are all in a portion of the spectrum which has been well explored and the necessary instrument components are all available from commercial sources. The

radiation in the spectral range of interest is essentially all continuum radiation, a fact which permits relatively wide passbands for the optical filters. Interference filters of passbands of 150Å would be satisfactory for the first four channels, and absorption filters with bandpasses of 200Å would give sufficient resolution for channels 5 and 6. Commercially available photomultiplier tubes would be the detectors for channels 1, 2, and 3, while lead sulfide or similar detectors would have the required sensitivity for channels 4, 5, and 6.

Lenses made of fused quartz would be recommended for channels 1 and 6, while glass lens would be satisfactory for the other four channels.

The components would be mounted in the most convenient configuration for incorporation into the particular spacecraft, the only special requirements being that all of the optical axes coincide and all channels have an unobstructed view.

5.3.8.5 Experiment/Spacecraft Interface Requirements

The interface requirements for the planetary albedo experiment are:

| | |
|---|---|
| Special Instrument | Multi-Channel Photometer |
| Size | 4 in. x 4 in. x 3 in. |
| Weight | 5 pounds |
| Power | 5 watts during normal operation |
| | 25 watts for 5 seconds during calibration |
| Output Signal | 6 voltages (0-5v) |
| Telemetry Accuracy Required | 1 percent of full scale reading |

The optical field of view of the instrument must be unobstructed. The instrument should be mounted so that its field of view can be swept from horizon to horizon across the disc of the earth at least once for every 10 degree change in orbit position (during the daylight portion of the orbit only).

## 5.3.9 MEASUREMENTS OF ULTRAVIOLET RADIATION FLUX

### 5.3.9.1 Background

The major part of the ultraviolet radiation which would be incident on the satellite will be primarily that directly from the sun, and this direct solar radiation would be mainly responsible for any damage to the satellite components which occurs. Ultraviolet radiation which is reflected or emitted from the earth will not be sufficiently intense to cause appreciable damage, although this ultraviolet radiation is a very information-packed portion of the spectrum and is scientifically interesting. The ultraviolet radiation which comes from outside the solar system is also of great scientific interest, but it is much too weak to be detrimental to exposed surfaces of a satellite.

Because of the nature of the present satellite, it is considered most desirable to concentrate the measurements for this particular experiment in the ultraviolet region between 2000 and 3000Å. There are four reasons for this choice. First, the total energy at wavelengths from 0 to 2000Å is less than 0.0002 of the total solar energy, while that between 2000 and 3000Å is some sixty times greater than this. One would expect degradation effects to be a maximum for the large energy fluxes. Second, most of the radiation at wavelengths below 2000Å is confined to numerous emission lines, so the spectrum is a line spectrum and requires reasonably high resolution spectrometers for proper measurements. Such sophisticated instrumentation, and the attendant high communication requirement, is outside the scope of that anticipated for this satellite. The spectrum in the 2000 to 3000Å region, on the other hand, is largely continuous, thereby being amiable to meaningful measurements with simple instrumentation. The third reason for investigating the 2000 to 3000Å region is a purely scientific one. Radiation at 3000Å $> \lambda$ 2000Å penetrates down in the atmosphere to the ozone layer at altitudes of 30 to 60 kilometers, whereas radiation at the shorter wavelengths is effectively absorbed at the 100 to 150 kilometer altitude. Thus the characteristics of the ozonosphere are observable in the first, but not the second, spectral region.

An added factor in the selection of the 2000 to 3000Å region for this experiment is that other experiments are under definition for the region from 1050 to 1240Å, which encompasses the very strong and scientifically interesting Lyman-Alpha radiation at 1216Å, and for the X-ray region (sections 5.3.10 and 5.3.6 respectively). Fourth and finally, the greatest uncertainty in the determinations of the solar constant is caused by the inability to observe the ultraviolet flux at wavelengths less than 3000Å from the surface of the Earth. It is known, however, that there are large variations in that region, the variations being due to solar activity. From an overall energy standpoint, the 2000 to 3000Å is by far more important than is the region below 2000Å, so a long term continuous monitoring of the solar ultraviolet flux in the 2000 to 3000Å, should decrease the uncertainty in the value of the solar constant by at least an order of magnitude.

5.3.9.2 Experiment Objectives

The objectives of the experiment are threefold. First, the total ultraviolet radiation flux is to be measured in order to assess the effect of such radiation in degrading materials such as the concentrator reflective surface, solar cells, or other satellite components. Secondly, the intensity of the ultraviolet radiation at selected wavelengths in the 2800 to 3000Å region is to be measured in order to determine the large scale distribution of atmospheric ozone. The third objective is to constantly monitor the solar ultraviolet radiation to obtain better values for the solar constant.

5.3.9.3 Experiment Definition

The experiment would make three different types of ultraviolet radiation measurements. For purposes of damage assessment, the total flux is of most interest. The major part of the flux is represented by radiation direct from the sun, so this measurement is of prime importance. A lesser but still considerable amount of radiation is that portion of the solar radiation which is reflected and backscattered by the earth. A second broad-band instrument would measure this component. The third type of measurement,

REPORT NO. 3 5- 3 2 3
Vol II

namely, measurements of the intensity of radiation in the 2800 to 3000Å region, is for a scientific investigation of atmospheric ozone. This type of study has been performed only from a theoretical standpoint, so a successful completion of these measurements would be of basic significance. The three-channel instrument, the design of which is outlined below, should provide the necessary data.

5.3.9.4 Experiment Design

The ultraviolet experiment would consist of three basic parts, as follows.

a. First, a broadband instrument for measuring the direct flux from the sun. The spectral extent would be through the entire 2000 to 3000Å range as defined by a broadband optical filter. The optical system for the direct flux would consist of a simple objective lens made of quartz, a filter, a Fabre lens, and a photomultiplier tube. The filter could be made of nickel sulfate hexahydride crystal as reported by Childs (Reference 5-57). The extra transmission window at $\lambda >$ 3500Å would be of no consequence if an appropriate detector were selected. The detector could be any one of several photomultipler tubes, such as the ITT FW 157-1 with a fused silica window (Reference 5-58). Neutral density filters could be inserted to attenuate the direct solar radiation appropriately for the instrument. Approximately one flux measurement per minute continuously during the time the satellite is in sunlight would be required.

b. Second, a broadband instrument for measuring the Earth-reflected ultraviolet flux. This is essentially a duplicate of the previous instrument, the main difference being that this instrument would view the Earth instead of the sun. The optics would be the same as described above except that no neutral density filters would be required here. A field of view of a 2 1/2 degree, half-angle cone would be reasonable. In order to compute the total flux on the spacecraft components one would have to make a series of measurements as the field of view

of the instrument was swept across the earth disc (accomplished mechanically). A burst of twenty measurements during one 180 degree sweep would furnish the required data, the burst to be repeated once per minute while the satellite is over the sunlit hemisphere of the earth.

c. Third, a narrowband ultraviolet photometer for measuring the intensity of the earth-reflected radiation for the purpose of determining the ozone distribution in the atmosphere. This would be a three-channel instrument for measurements of Earth-reflected sunlight in the 2800 to 3000Å region. The spectral bandwidth should be of the order of 10Å for each channel (Reference 5-59), but a definition of the best wavelengths still requires some computations. This instrument also would take a burst of twenty measurements on each channel as the field of view was swept across the disc of the earth (also accomplished mechanically). A one-minute repetition rate would be adequate. Any of the commercially available photomultiplier tubes of high sensitivity in the 3000Å region would be suitable for this type of measurement and many different materials are available for the optical components. Commercial interference filters of 10Å bandwidth in this range are readily available.

On-board calibration of the photometers would be necessary in order to assure interpretable results throughout the long lifetime of the experiment. A convenient standard for the broadband channels is a mercury source which emits a strong mercury line at 2537Å. For the three narrowband channels a low-intensity continuum source would be indicated.

5.3.9.5 Experiment/Spacecraft Interface Requirements

The interface requirements for the ultraviolet experiment are:

| | |
|---|---|
| Special Instruments | 1 Broadband Radiometer, sun-oriented |
| | 1 Broadband Radiometer, earth-oriented |
| | 1 Narrowband Multi-channel Photometer |



213

| | |
|---|---|
| Size | 4 in. x 4 in. x 3 in. per instrument |
| Weight | Broadband Radiometer (sun-oriented) 1 pound |
| | Broadband Radiometer (earth-oriented) 1.5 pounds |
| | Narrowband Multi-channel Photometer 2.5 pounds |
| Power | 3 watts |
| Output Signal | 5 voltages (0-5v) |
| Telemetry accuracy required | 1 percent of full scale reading |

The sun-oriented radiometer must view the sun whenever the vehicle is in the sunlight. Orientation to within $\pm 1$ degree is sufficient. The other instruments should view the Earth, the fields of view being swept across the disc of the Earth from horizon to horizon by mechanical means. For purposes of data correlation, the fields of view of both earth-oriented instruments should coincide.

The earth sensing portion of this experiment would be eliminated in the case of a highly elliptical orbit because the large variations in altitude would make it difficult to design an experiment that would yield meaningful data.

## 5.3.10 LYMAN-ALPHA EXPERIMENT

### 5.3.10.1 Background

The solar Lyman-Alpha ($\lambda \sim 1216$Å) line has been shown (Reference 5-60) to exhibit an absorption future when viewed with a high dispersion spectograph flown above the earth's atmosphere. This feature is composed of two components; a broad weak reversal, and a deep narrow central absorption core at 1215.67Å. The broad reversal is believed to originate in the solar atmosphere whereas the absorption core is attributed to neutral hydrogen lying between the ionized E-layer of the earth's atmosphere and the sun, but outside the sun's atmosphere. The emission line itself arises in the chromosphere of the sun. The kinetic temperature required to form the line is of the order of Te $\approx$

65-323

60,000 to 100,000°K. However, the temperature characterizing the emergent radiation, averaged over the disk of the sun, is about 7200°K.

To determine the temporal variation of the density of the neutral hydrogen cloud is of great interest and is determined by recording the depth of the absorption core continually from an Earth orbiting satellite. By observing the change in the equivalent width of the core, it will be possible to calculate the number, and time rate of change of number, of atoms $cm^{-2}$ in a column lying between the satellite and the sun. The total as seen from the earth's vicinity has been computed to be of the order of $2 \times 10^{12}$ atoms $cm^{-2}$. How this may vary during intense solar activity is unknown.

Measurements (Reference 5-61) made to determine how much the net solar Lyman-Alpha flux increases during flares indicate that the Lyman-Alpha flux remains essentially unchanged during the occurrence of a flare. This does not imply that the intensity of the Lyman-Alpha may not increase greatly from a flare at the time of a flare, but only that this enhancement does not appreciably alter the total amount of Lyman-Alpha radiation emanating from the solar disk. The Lyman-Alpha line is about five times more intense.

Although no spectra of Lyman-Alpha have been obtained for flares, it is probable that the central reversal will be absent, as it so often is in the Ca II lines. The weak reversal is caused by the partial absorption of the line by hydrogen in the chromosphere at lower temperature than the source of the line. During a flare, it is possible that the upward and outward surge of hot gases would blow the cooler gas away, thus tending to preserve the original line shape. It may be that a flare or a series of flares, whether detected optically or not, will distribute sufficient hydrogen into the region between the sun and earth to measurably affect the depth of the absorption core. While it is known that the rise time of flares is most generally less than 10 minutes (Reference 5-62), it is not known how long flares may take to cause a change in the absorption core; if they do so at all.



385

65-323
Vol. II

5.3.10.2 Experiment Objective

The objective of the experiment is to obtain a knowledge of how the density of neutral hydrogen clouds, between the earth and the sun, changes with time, and to determine any correlation with solar activity.

5.3.10.3 Experiment Definition

The proposed experiment is designed to measure, by means of a spectrometer, the solar Lyman-Alpha line shape continually from an earth orbiting satellite. The detector would measure the spectral range from 1214.37 to 1216.97Å. The output would be sampled at the following wavelengths:

Every 0.1Å from 1214.37 to 1215.37Å
Every 0.1Å from 1215.37 to 1215.97Å
Every 0.1Å from 1215.97 to 1216.97Å

5.3.10.4 Experiment Design

Since the Lyman-Alpha line is quite intense, of the order of 6 erg $cm^{-2}$ $sec^{-1}$, from which the narrow core removes approximately 0.1 erg $cm^{-2}$ $sec^{-1}$, detection problems are minimal. The detector is a photo detector using a tungsten cathode and an LiF window (Reference 5-63). This combination has a spectral passband of $1050Å < \lambda < 1800Å$. The rejection of the scattered near ultraviolet and visible radiation within the spectrometer is an important aspect of this combination of filter and photocathode. The detector is operated at a pressure of $10^{-5}$mm Hg.

The spectrometer, similar to the NRL instrument, would use a 50 centimeter, 1200 line $mm^{-1}$ diffraction grating in the 13th order operated in a Rowland mount with the pre-dispersive grating ahead of the entrance slit mechanically deformed so that the spectra appearing at the exit slit will be stigmatic over the entire slit length. The dispersion

Vol II 65-523

from such a system will be of the order of 2.6Å $mm^{-1}$ with the exit slit scanning across the line having an effective width of 0.01Å. Thus, the entire line, which is one Å wide, and the core, which is 0.04 to 0.05Å wide at the half maximum point, will be resolved in sufficient detail to trace the changes of the core with time. The exit slit will scan thru an arc of one millimeter in length along the Rowland circle, thus covering 2.6Å in wavelength centered at 1215.67Å. This will insure complete coverage of the line plus a portion of the continuum on either side of the line required for a reference comparison. Slit widths are of the order of 10 to 15 microns. The gratings are coated with fresh aluminum overlaid with magnesium fluoride in order to ensure sufficient light efficiency (Reference 5-64).

5.3.10.5 Experiment/Spacecraft Interface Requirements

The interface requirements for the Lyman-Alpha experiment are:

| | |
|---|---|
| Special Instrument | Spectrometer |
| Size | 8 in. x 10 in. x 2 in. |
| Weight | 6 pounds |
| Power | 2 watts |
| Output Signal | 1 voltages (0-5v) |
| Telemetry Accuracy Required | 1 percent of full scale reading |

The total readings per sweep would be 81 and one sweep would be made each minute. No measurements would be made when the sun is not in view. The sweeping rate of the spectrometer must not exceed 1.3 Å $sec^{-1}$ to insure that the response time of the instrument is not exceeded.

The spectrometer must be oriented to the sun and have an unobstructed view. The pointing of the satellite should not change by more than one second of arc during the sweeping operation.



297

## 5.4 SELECTION OF SECONDARY EXPERIMENTS

A total of twenty secondary experiments, ten engineering and ten scientific, have been outlined in Sections 5.2 and 5.3 respectively. The major characteristics and requirements of these twenty experiments are summarized in Table 5-3. Obviously such factors as weight, complexity, data storage and telemetry requirements, etc., may prohibit all of these experiments being included on one spacecraft. Also, some of these experiments are of greater importance than others and some are better suited to certain orbits. Therefore, it is necessary to identify the orbits for which each of these experiments is suitable and to categorize the experiments in order of priority.

### 5.4.1 ORBIT COMPATIBILITY

Table 5-4 indicates the orbits from which each of the twenty experiments considered could be conducted.

The earth orbits are suitable for conducting all of the engineering experiments with one exception. The Radiation Effects on Solar Cells Experiment is not well suited to the low altitude circular or highly elliptical orbits because the radiation environment encountered is of low intensity. The Laser Experiment is not considered suitable for a solar probe orbit because of photon detection problems encountered with present state-of-the-art equipment for greater than lunar distances. The Infrared Detector experiment is not compatible with a solar probe orbit because the earth's horizon is not available for sensing. Engineering Experiments 1, 2, 4, 5, and 6 in Table 5-4 are not recommended for a solar probe orbit because the large variation in solar intensity throughout the orbit complicates their evaluation.

The scientific experiments considered are somewhat more sensitive to orbit than are the engineering experiments. The Interplanetary Dust, Interplanetary Magnetic Field and Solar Wind experiments are only compatible with the solar probe orbit since their objectives require that the space vehicle go out to approximately 0.3 AU. However, there are

REPORT No. 65-303
Vol II

Table 5-3. Summary Of Secondary Experiment Characteristics And Requirements

| NO | EXPERIMENT | SPECIAL INSTRUMENTS REQUIRED | RANGE OF MEASUREMENT | INSTRUMENTATION | | FREQUENCY OF SAMPLING | SENSOR VIEW ANGLE | REQUIRED SUN ORIENTATION ACCURACY | SIZE | EXPOSED SURFACE AREA REQUIRED (in.$^2$) | WEIGHT (lbs) | ELECTRICAL POWER REQUIRED (Watts) | COMMENTS |
|---|---|---|---|---|---|---|---|---|---|---|---|---|---|
| | | | | QUANTITY | OUTPUT SIGNAL RANGE | | | | | | | | |
| 1 | Radiation Effects on Solar Cells | - | - | 7 Voltages<br>2 Temp | 0 - 50 mv<br>0 - 5 v | Once per orbit after steady state has been reached during daylight portion of the orbit. | - | $\pm 5^\circ$ or better | 4.5 in.$^2$ surface area by 1 in. deep | 4.5 | 0.5 | 0.04 watts for 5 minutes during daylight portion of each orbit. | Must be sun-oriented and have an unobstructed view. |
| 2 | Solar Thermoelectrics | - | - | 3 Voltages<br>6 Temp | 0 - 1.2 v<br>0 - 5 v | Once per orbit after steady state has been reached during daylight portion of the orbit. | - | $\pm 5^\circ$ or better | 14 in. x 5 in. x 0.115 in. | 70.0 | 1.0 | 0.12 watts for 5 minutes during daylight portion of each orbit. | Must be sun-oriented and have an unobstructed view. |
| 3 | Thermal Coatings | - | - | 8 Temp | 0 - 5 v | Once per orbit after steady state has been reached during daylight portion of the orbit. | - | $\pm 5^\circ$ or better | 8 in. diameter by 3 in. deep | 50.3 | 2.0 | 0.16 watts for 5 minutes during daylight portion of each orbit. | Must be sun-oriented and have an unobstructed view. |
| 4 | V-Ridge Concentrating Photovoltaics | - | - | 6 Voltages<br>8 Temp | 0 - 6.4 v<br>0 - 5 v | Once per orbit after steady state has been reached during daylight portion of the orbit. | - | $\pm 5^\circ$ or better | 12 in. x 12.8 in. x 1.5 in. deep | 130 | 2.0 | 0.16 watts for 5 minutes during daylight portion of each orbit. | Must be sun-oriented and have an unobstructed view. |
| 5 | Thin-Film Solar Cells | - | - | 11 Voltages<br>2 Temp | 0 - 50 mv<br>0 - 5 v | Once per orbit after steady state has been reached during daylight portion of the orbit. | - | $\pm 5^\circ$ or better | 10 in. x 3 in. x 0.5 in. deep | 30 | 0.5 | 0.04 watts for 5 minutes during daylight portion of each orbit. | Must be sun-oriented and have an unobstructed view. |
| 6 | Solar Concentrator Reflective Surfaces | - | - | 1 Voltage<br>30 Temp | 0 - 20 mv<br>0 - 5 v | Once per orbit after steady state has been reached during daylight portion of the orbit. | - | $\pm 5^\circ$ or better | 24 in. dia. cylinder 8 in. long | 452 | 27 | 2.6 watts for 15 minutes during daylight portion of each orbit. | Must be sun-oriented and have an unobstructed view. |
| 7 | Thermal Contact Resistance | - | - | 30 Temp | 0 - 5 v | Once per orbit at any point in the orbit. | - | - | 6 in. x 6 in. x 10 in. | - | 7.2 | 6.8 watts continuously. | Requires no sun orientation and does not have to see space directly. |
| 8 | Infrared Detector | - | - | 1 Voltage<br>5 Temp | 0 - 5 v<br>0 - 5 v | Once per orbit at any point in the orbit. | Two sensors 30° each | - | 4 in. x 6 in. x 8 in. | 4 in.$^2$ (2 in. x 2 in.) per sensor. Two sensors involved. | 3.0 | 1.1 watts continuously during daylight portion of each orbit. | Sensing heads must be located so the earth disc passes through their field of view during the daylight portion of the orbit. |
| 9 | Laser Experiment | - | - | 2 Voltages<br>3 Temp | 0 - 5 v<br>0 - 5 v | Once per orbit at any point in the orbit. | — | — | 2 in. x 2 in. x 1 in. Electronics only | 16 in.$^2$ Min. for Retroreflectors which are 0.75 in. deep. | 10.0 | 1.06 watts for 20 minutes each orbit. | Retroreflectors must be mounted on the shaded side of the vehicle in a location that can be seen from a ground station during some position of the orbit. |
| 10 | Low Thrust Electric Engine | - | - | 5 Voltages | 0 - 5 v | Once per minute for 1.4 hours every 1.2 days | — | - | 2 Electronic Packages Each 4 in. x 3 in. x 3 in. Each Engine - 1 in. dia. x 2 in. long | — | 2.25 | 2 watts while operating. Estimated operating time 1.4 hours once every 1.2 days. | Engines must be mounted to form couples acting in a plane perpendicular to the spacecraft roll axis. Engines must have a clear path in the thrust direction |



291

REPORT NO. 65-323
VOL II

Table 5-3 (Cont'd). Summary of Secondary Experiment Characteristics And Requirements

| NO | EXPERIMENT | SPECIAL INSTRUMENTS REQUIRED | RANGE OF MEASUREMENT | INSTRUMENTATION | | FREQUENCY OF SAMPLING | SENSOR VIEW ANGLE | REQUIRED SUN ORIENTATION ACCURACY | SIZE | EXPOSED SURFACE AREA REQUIRED (in.$^2$) | WEIGHT (lbs) | ELECTRICAL POWER REQUIRED (Watts) | COMMENTS |
|---|---|---|---|---|---|---|---|---|---|---|---|---|---|
| | | | | QUANTITY | OUTPUT SIGNAL RANGE | | | | | | | | |
| 11 | Interplanetary[b] Dust (Micro-meteoroids) | 4 Crystal Microphones | $2.5 \times 10^{-4}$ to $2.5 \times 10^{-1}$ dyne cm + > $2.5 \times 10^{-1}$ dyne cm | 16 Voltages | 0 - 5 v | Impacts counted continuously and read out once per orbit for earth orbiting case | - | - | 4 plates 5 in. x 10 in. x 1/8 in. thick. Electronics - 2 in. x 2 in. x 4 in. | 4 plates, 50 in.$^2$ each | 8.0 | 2.0 watts continuously | Each plate must have an unobstructed view of space |
| 12 | Solar Wind | 2 Electrostatic Analyzers 1 Faraday Cup | 200 ev to 20 Kev | 256 Voltages 36 Voltages | 0 - 5 v 0 - 5 v | Every 30 seconds | 5° Electro-static Analyzers 90° Faraday Cup | - | 2 Electrostatic Analyzers - 216 in.$^3$ 1 Faraday Cup - 216 in.$^3$ | 20 in.$^2$ each Electrostatic Analyzers. 6 in.$^2$ Faraday Cup | 13.0 | 4.5 watts continuously | Requires solar probe orbit or an elliptical orbit with a very high apogee (55,000 NM) |
| 13 | Proton and[c] Electron Spectra and Direction | 1 Charged Particle Telescope | Proton - 30 Mev to 200 Mev Electrons - 0.5 Mev to 2.8 Mev | 6 Voltages | 0 - 5 v | Once per minute | 5° | ±3° or better | Sensor - 2 in. dia. x 4 in. Electronics 90 in.$^3$ | 3.0 | 8.0 | 3.0 watts continuously | Sensor must have an unobstructed view and a known position in space. The position in space is determined by orienting sensor to the sun |
| 14 | Magnet Field | Triaxial Fluxgate Magneto-meter | 0.12 γ to 500 γ | 3 Voltages | 0 - 5 v | Once per minute | - | - | 3 in. x 4 in. x 5 in. does not include boom. | Mounted on extended boom. | 4.5 Does not include boom | 0.5 watts continuously | Must be able to rotate boom and isolate the magnetometer from stray magnetic fields |
| 15 | Heavy Nuclei[c] | 1 Charged Particle Telescopes | Atomic Number Range from 2 to 20 | 6 Voltages | 0 - 5 v | Once per minute during daylight portion of the orbit. | 5° | ±3° or better | Sensor - 2 in. dia. x 4 in. Electronics - 4.5 in. x 4.5 in. x 4.5 in. | 3.0 | 8.0 | 3.0 watts continuously during daylight portion of the orbit. | Sensor must have an unobstructed view and a known position in space. Requires solar probe orbit or an elliptical orbit with a very high apogee (55,000 NM) |
| 16 | Solar X-Rays | 2 Geiger Counters | 2 to 8 and 8 to 20 Angstrom Bands | 2 Voltages | 0 - 5 v | Once per minute during daylight portion of the orbit. | 2.5° | ±1° | 5 in. x 5 in. x 4 in. total experiment | 1.765 in.$^2$ per instrument (1.5 in. dia circle) | 3.0 | 1.0 watt continuously during daylight portion of the orbit. | Must be oriented to the sun and be shielded from stray x-rays. Sensor must have an unobstructed view |
| 17 | Solar γ -Rays | Scintillation Detectors | 0.1 Mev to 200 Mev | 6 Voltages | 0 - 5 v | Once per minute during daylight portion of the orbit. | 2.5° | ±1° | 5 in. x 5 in. x 6 in. total experiment | 1.765 in.$^2$ (1.5 in. dia circle) | 8.0 | 4.0 watts continuously during daylight portion of the orbit. | Must be oriented to the sun and have an unobstructed view |
| 18 | Earth Albedo | Multi-Channel Photometer | 3000 Å to 2.5μ | 6 Voltages | 0 - 5 v | Once every 2.5 minutes during the daylight portion of the orbit. | 10° | - | 4 in. x 4 in. x 3 in. | 19.6 (5 in. dia circle) | 5.0 | 5.0 watts continuously during daylight portion of the orbit. | Must be mounted on the rear of the spacecraft and be able to sweep through 180°. Must have an unobstructed view |
| 19 | Ultraviolet Radiation | 2 Radiometers 1 Multi-Channel Photometer | 2000 to 3000 Å | 5 Voltages | 0 - 5 v | Once per minute during daylight portion of the orbit. | 5° | ±1° | 4 in. x 4 in. x 3 in. per instrument | 0.785 in.$^2$ per instrument (1 in. dia circle) | 5.0 | 5.0 watts continuously during daylight portion of the orbit. | One sensor must be oriented to the sun and have an unobstructed view. Two other sensors must be mounted on the rear of the spacecraft and be able to sweep through 180° |
| 20 | Lyman-Alpha | Spectrometer | 1214.37 to 1216.97 Å | 1 Voltage | 0 - 5 v | Once per minute during daylight portion of the orbit. | 2.5° | ±1° | 8 in. x 10 in. x 2 in. | 0.785 in.$^2$ (1 in. dia circle) | 6.0 | 2.0 watts continuously during daylight portion of the orbit. | Must be oriented to the sun and have an unobstructed view |

(a) A telemetry accuracy of 1 percent is satisfactory for all the measurements listed in this table. "Telemetry accuracy" is defined as the accuracy with which the measured data is telemetered from the spacecraft to earth.

(b) The version of this experiment that does not require roll axis orientation is presented in this table.

(c) The versions of these experiments that do not require knowledge of the spacecraft position about the roll axis are presented in this table.

TABLE 5-4. ORBIT COMPATIBILITY OF SECONDARY EXPERIMENTS

| | | SECONDARY EXPERIMENTS \ ORBITS | Low Altitude Circular Orbit (325 nm - 30 deg. inclination) | Modified Sun-Synchronous Orbit (1000 nm - 101.84 deg. inclination) | Highly Elliptical Orbit (200 NM x 25,000 nm - 45 deg. inclination) | Stationary Earth-Synchronous Orbit (19,300 nm - 0 deg. inclination) | Solar Probe Orbit (perihelion 0.34 AU) |
|---|---|---|---|---|---|---|---|
| ENGINEERING EXPERIMENTS | 1 | Radiation Effects on Solar Cells | | X | | X | |
| | 2 | Solar Thermoelectrics | X | X | X | X | |
| | 3 | Thermal Coatings | X | X | X | X | X |
| | 4 | V-Ridge Concentrating Photovoltaics | X | X | X | X | |
| | 5 | Thin-Film Solar Cells | X | X | X | X | |
| | 6 | Solar Concentrator Reflective Surfaces | X | X | X | X | |
| | 7 | Thermal Contact Resistance | X | X | X | X | X |
| | 8 | Infrared Detector | X | X | X | X | |
| | 9 | Laser Experiment | X | X | X | X | |
| | 10 | Low-Thrust Electric Engine | X | X | X | X | X |

Vol I.

TABLE 5-4 . ORBIT COMPATIBILITY OF SECONDARY EXPERIMENTS (Cont)

| | SECONDARY EXPERIMENTS \ ORBITS | Low Altitude Circular Orbit (325 nm - 30 deg. inclination) | Modified Sun-Synchronous Orbit (1000 nm - 101.84 deg. inclination) | Highly Elliptical Orbit (200 NM x 25,000 nm - 45 deg. inclination) | Stationary Earth-Synchronous Orbit (19,300 nm - 0 deg. inclination) | Solar Probe Orbit (perihelion 0.34 AU) |
|---|---|---|---|---|---|---|
| SCIENTIFIC EXPERIMENTS | 11 (a) Interplanetary Dust (b) Micrometeoroid Measurements Around Earth | X | X | X | X | X |
| | 12 Solar Wind | | | | | X |
| | 13 Proton and Electron Spectra and Direction | X | X | X | X | X |
| | 14 (a) Interplanetary Magnetic Field (b) Earth Magnetic Field | X | X | X | X | X |
| | 15 Heavy Nuclei | | | | | X |
| | 16 Solar X-Rays | X | X | X | X | X |
| | 17 Solar $\gamma$ - Rays | X | X | X | X | X |
| | 18 Earth Albedo | X | | | X | |
| | 19 Ultraviolet Radiation | X | X | X | X | X |
| | 20 Lyman-Alpha | X | X | X | X | X |



362

similar versions of the Interplanetary Dust and Interplanetary Magnetic Field experiments for earth orbiting applications. These alternate experiments are basically the same as those described in Sections 5.3.1 and 5.3.4 with the measurement ranges changed to be compatible with the environment expected near earth. Of course the information obtained is not interplanetary in scope but is confined to the region of space near earth. These alternate experiments are referred to in Table 5-4 as "Micrometeoriod Measurements Around Earth" and "Earth Magnetic Field Measurements".

As indicated, either of these alternate experiments could be conducted from anyone of the four earth orbits. Since very few heavy particles are found within the region of space influenced by the earth's magnetic field, the Heavy Nuclei experiment is only compatible with the solar probe orbit. The Earth Albedo experiment is not well suited to the modified sun-synchronous or highly elliptical orbits. In the former case, the difficulties arise because the spacecraft is always operating almost directly above the boundary between the illuminated and dark portions of the earth. This presents a confusing field of view to the earth oriented albedo sensor and makes meaningful results difficult to obtain. The highly elliptical orbit, because of its wide variation in altitude, represents a difficult orbit for conducting an albedo experiment.

### 5.4.2 PRIORITY GROUPING OF EXPERIMENTS

It is possible to divide the twenty secondary experiments into groups according to preference. The major factors considered in establishing these groups are:

a. Compatibility with the solar thermionic experiment
b. Importance to the development of solar thermionics
c. Importance to the space program and interest to the scientific community
d. Ease of integration with the spacecraft
e. Size and weight
f. Demands on the telemetry, command, and power subsystems.

The results of such an evaluation are shown in Table 5-5. The major reasons for placing each experiment in a given group are indicated and the experiments compatibility with each orbit specified.

The experiments are divided into four groups: Priority "A", Priority "B", Priority "C", and "Not Recommended". The significance of each of these groups is described below:

Priority "A"

Experiments which should be given first consideration for inclusion on the spacecraft. These experiments are individually of great engineering or scientific interest and also yield information which is needed to completely evaluate the primary experiment.

Priority "B"

Experiments which are to be considered for inclusion on the spacecraft after the priority "A" experiments. The experiments in this second group are also of great engineering or scientific interest, but are not necessary to evaluation of the primary experiment.

Priority "C"

The experiments included in this group have either already been performed or will probably be performed in the near future and, therefore, are of second order interest compared with those included in the first two groups.

"Not Recommended"

As indicated by the title, the experiments included in this group, for various reasons, are not considered suitable.

## 5.5 SUMMARY AND CONCLUSIONS

Those secondary experiments considered most appropriate for inclusion on a spacecraft whose primary objective is the evaluation of solar thermionics are represented by the

| | EXPERIMENT | MAJOR REASONS FOR PRIORITY GROUPING | ORBIT COMPATIBLE* | | | | |
|---|---|---|---|---|---|---|---|
| | | | I | II | III | IV | V |
| PRIORITY "A" | 1 Solar Reflective Surfaces | Results of major importance to the development of solar thermionics and other solar power systems employing concentrators. Also helpful in evaluating the primary experiment and makes use of the sun-pointing feature of the spacecraft. | X | X | X | X | - |
| | 2 Micrometeoroid Measurements | Important scientifically and to evaluation of the primary experiment. Also needed for complete evaluation of Experiment No. 1. | X | X | X | X | X |
| | 3 Proton and Electron Spectra and Direction | Important scientifically and to evaluation of the primary experiment. Also needed for complete evaluation of Experiments No. 1 and 8. | X | X | X | X | X |
| | 4 Measurements of Ultraviolet Radiation Flux | Important scientifically and to evaluation of the primary experiment. Also needed for complete evaluation of Experiments No. 1, 5, and 8, and supplements Experiments No. 10, 11 and 12. | X | X | X | X | X |
| PRIORITY "B" | 5 Thermal Coatings | Relatively simple experiment which yields needed information on thermal coatings to be used on space vehicles. Experiment package already developed. Experiment makes use of sun-pointing feature of the spacecraft. | X | X | X | X | X |
| | 6 Laser Experiment | Important to the development of lasers as a means of space communications. | X | X | X | X | - |
| | 7 Low-Thrust Electric Engine | Important to the development of low-thrust electric engines for use in attitude control systems and space propulsion in general. | X | X | X | X | X |
| | 8 Radiation Effects on Solar Cells | Important to a more complete understanding of solar array degradation from radiation. Results needed to improve solar cell power supply design. Also makes use of the sun-pointing feature of the spacecraft. | X | - | - | X | - |
| | 9 Infrared Detector | Important to the development of better IR detectors for use in attitude control systems. | X | X | X | X | - |
| | 10 Solar X-Rays | Important scientifically and makes use of the sun-pointing feature of the spacecraft. Also supplements Experiments No. 4, 11 and 12. | X | X | X | X | X |
| | 11 Solar $\gamma$-Rays | Important scientifically and makes use of the sun-pointing feature of the spacecraft. Also supplements Experiments No. 4, 10 and 12. | X | X | X | X | X |
| | 12 Lyman-Alpha | Important scientifically and makes use of the sun-pointing feature of the spacecraft. Also supplements Experiments No. 4, 10 and 11. | X | X | X | X | X |
| | 13 Earth Albedo | Required to obtain a better measure of the earth's albedo. This information is of value scientifically and to the thermal design of space vehicles. | - | - | X | X | - |
| | 14 Solar Wind | Of scientific importance to a better understanding of the make up of interplanetary space, and solar phenomenon in general. | - | - | - | - | X |
| | 15 Heavy Nuclei | Of scientific importance to a better understanding of the sun's composition and solar phenomenon in general. Also supplements experiments 4, 10, 11 and 12 and makes use of the sun-pointing feature of the spacecraft. | - | - | - | - | X |
| PRIORITY "C" | 16 V-Ridge Concentrating Photovoltaics | This experiment is considered of secondary priority because the major question of how well the concentrating surface will hold up can be answered by Experiment No. 1. | X | X | X | X | - |
| | 17 Thermal Contact Resistance | It appears likely that this experiment will have already been performed by the time a space vehicle could be developed for this program. Also this experiment does not take advantage of any of the special features of this spacecraft. | X | X | X | X | X |
| NOT RECOMMENDED | 18 Solar Thermoelectrics | This experiment has already been done and, if further space experiments are warranted, they will probably be performed by the time a space vehicle could be developed for this program. | X | X | X | X | - |
| | 19 Thin-Film Solar Cells | The state of the art is not sufficiently advanced at this time to warrant a space experiment. | X | X | X | X | - |
| | 20 Earth Magnetic Field | This experiment is not recommended because of the complexity associated with the spacecraft integration. | X | X | X | X | X |

Table 5-5. Priority Grouping Of Secondary Experiments

Notes

*Orbit I - Modified Sun-Synchronous (1000 NM - 101.84 degree inclination)
Orbit II - Highly Elliptical (200 NM x 25,000 NM - 45 degree inclination)
Orbit III - Low Altitude Circular (325 NM - 30 degree inclination)
Orbit IV - Stationary Earth Synchronous (19,300 NM - 0 degree inclination)
Orbit V - Solar Probe Orbit (Perihelion 0.34 AU)

priority "A" and priority "B" groupings given in Table 5-5. It is unlikely that all thirteen of these experiments can be included on any one of the spacecraft designs. However, it appears that all of the priority "A" experiments and most of the priority "B" experiments can be included in each case. The decision on the priority "B" experiments to be included will be made in the spacecraft design phase of this study. This decision will be based on a more complete consideration of power, weight, telemetry requirements, and compatibility with the spacecraft design.

## 5.6 REFERENCES


5-1 J. Freedman, "Rancom Solar Cell Radiation Effects Experiment," Missile and Space Division, General Electric Company, PIR No. 8123-514, February 22, 1963.

5-2 J. Ferrara, "A Solar Thermoelectric Generator System Study," Hamilton Standard Division, United Aircraft Corporation, ASD Technical Report 61-315, November 1961.

5-3 A. Himle, D. Brush, J. Roes and E. Brady, "Flat-Plate Solar Thermoelectric Conversion Panels," General Atomic Division of General Dynamics Corporation, Technical Documentary Report No. ASD-TDR-62-214, May 1962.

5-4 E. Brady and A. Himle, "Fabrication and Flight Test of Flat-Plate Thermoelectric Solar Energy Converter," General Atomic Division of General Dynamics, Report No. GA-4154, April 15, 1963.

5-5 W. Snoddy and E. Miller, "Areas of Research on Surfaces for Thermal Control," NASA-Marshall Space Flight Center. A paper presented at the Symposium on Thermal Radiation of Solids, March 4, 5, 6, 1964.

5-6 C. Neel, "Research on the Stability of Thermal-Control Coatings for Spacecraft," Ames Research Center, NASA TM X-51, 1963.

5-7 J. James, "The Voyage of Mariner II," Scientific American, Vol. 209, No. 1, July 1963, PP 70-84.

5-8 "Proceedings of the Fourth Photovoltaic Specialists Conference," Vol. II, PIC-SOL 209/5.1, August 1964.

5-9 "Study of a Flight Experiment of Solar-Concentrator Reflective Surfaces," EOS Report 4100-Final, Contract NAS 1-2880, November 1, 1963.

5-10 E. Fried, "Thermal Contact Conductance of Metallic Joints in Vacuum," General Electric Spacecraft Department, Final Report of Contract NAS 8-5207, February 1964.

5-11 E. Fried and F. Costello, "Interface Thermal Contact Resistance Problem in Space Vehicles," ARS Journal, Volume 32, No. 2, 1962.

5-12 E. Fried. "Thermal Joint Conductance in a Vacuum," ASME Paper 63-AHGT-18, March 1963.

5-13 A. Clausing and B. Chao. "Thermal Contact Resistance in a Vacuum Environment," University of Illinois, 1963.

5-14 C. Bory and H. Cordier. "Thermal Contact Resistances," Institute Francais des Combustibles et de L'Energie, Journee de La Transmission de La Chaleur, February. 1961.

5-15 R. Hanel. "Journal of Atmospheric Science," Pages 73-86, 1963.

5-16 "A Proposal for a Laser Satellite Tracking System," by General Electric Missile and Space Division, Submitted to NASA-GSFC on March 19, 1962.

5-17 "A Proposal for Modulation-Inducing Retrodirective Optical System (MIROS) Prototype Development," by General Electric Missile and Space Division, submitted to NASA-GSFC, May 28, 1964.

5-18 "A Proposal for Determination of Optical Technology Experiments for a Satellite," by General Electric Missile and Space Division, submitted to NASA-MSFC, May 28, 1964.

5-19 A. V. LaRocca, "Parametric Performance Studies of Electrical Thrust Generators for Space Applications," Proceedings of Fifth Symposium of Ballistic Missile and Space Technology, Volume II, Los Angeles, August 1960.

5-20 A. V. LaRocca, "An Introduction to the Study of the Application of Advanced Schemes for Space Propulsion," General Electric Spacecraft Department, Advanced Development and Analysis Memo No. 10, October 10, 1961.

5-21 A. Behr and H. Siedentopf, "Zeits. f. Astrophys.," Vol. 32, 1953.

5-22 E. J. Opik, "Zeits. f. Astrophys.," Vol. 35, 1954.

5-23 H. C. Van de Hulst, "Les Particles Solides dans les Astres," Leige, 1955.

5-24 D. Blackwell and M. Ingham, "Monthly Notice of Royal Astronomical Society," Volume 122, PP 114, 1962.

5-25 C. McCracken, W. Alexander and M. Dubin, NASA TN D-1174, Dec. 1961.

5-26 F. L. Whipple, "The Dust Cloud About the Earth," Nature, Vol. 189 (4259), Jan. 1961.

5-27 K. I. Gringauz, "Procedure of Third International Space Science Symposium," Washington, D. C., 1962.

5-28 A. Bonetti, "Explorer 10 Plasma Measurements," Journal of Geophysical Research, Vol. 68, 1962.

5-29 C. Josias and J. Lawrence, "An Instrument for the Measurement of Interplanetary Solar Plasma," JPL Technical Report No. 32-492.

5-30 H. Bridge, C. Dilworth, B. Rossi, and F. Scherb, "An Instrument for the Investigation of Interplanetary Plasma," Journal of Geophysical Research, Vol. 65, 1960.

5-31 J. Naugle and D. Kiffen, "Variations of the Proton Energy Spectrum with Position in the Inner Van Allen Belt," NASA Publication X-611-63-35.

5-32 S. Freden and G. Paulikas, "Trapped Protons at Low Altitudes in the South Atlantic Magnetic Anomaly," Journal of Geophysical Research, Vol. 69, 1964.

5-33 C. McIlwain, "The Radiation Belts, Natural and Aritificial," Science, Vol. 142, 1963.

5-34 J. Mihalov, T. Mozer, R. White, "Artificially Injected Electrons at Low Altitudes," Journal of Geophysical Research, Vol. 69, 1964.

5-35 R. Smith, P. Fisher, W. Imhof and J. Reagan, "Mides IV Proton Measurement in the Inner Van Allen Belt," Lockheed Missile and Space Co. Report 3-77-62-6.

5-36 H. West, L. Mann, and S. Bloom, "Spectra and Fluxes of Electrons Trapped in the Earth's Magnetic Field Following Bursts," Laurence Radiation Laboratory Internal Report.

5-37 Coleman, Davis and Sonett, "Physics Review," Letter 5, 1960.

5-38 H. W. Babcock, "Astrophysics," Vol. 118, 1953.

5-39 T. Gold, "Procedure of the Second International Space Science Symposium," Florence, 1961.

5-40 K. G. McCracken, "Procedure of the Second International Space Science Symposium, Florence, 1961.

5-41 E. N. Parker, "Astrophysics Journal", Vol. 128, PP 664, 1958.

5-42 L. Bierman, Symposium on Plasma Space Science, Catholic University, June 1963.

5-43 H. W. Babcock, Symposium on Plasma Space Science, Catholic University, June 1963.

5-44 S. Biswas, C. Fichtel, and D. Guss, "Study of the Hydrogen, Helium and Heavy Nuclei in the November 12, 1960 Solar Cosmic Ray Event," Physics Review, Vol. 128, 1962.

5-45 S. Biswas, C. Fichtel, D. Guss, and C. Waddington, "Hydrogen, Helium, and Heavy Nuclei from the Solar Event on November 15, 1960," Journal of Geophysical Research, Vol. 68, 1963.

5-46 M. Pomerantz, and L. Witten, "Solar-Produced Heavy Nuclei During November 1960," paper presented at the Third International Space Science Symposium of COSPAR, Washington, D.C., May 1-9, 1962.

5-47 E. Ney, and W. Stein, "Solar Protons, Alpha Particles, and Heavy Nuclei in November, 1960," Journal of Geophysical Research, Vol. 67, 1962.

5-48 R. W. Kreplin, "Solar X-Rays," Annales de Geophysique, Vol. 17, 1961.

5-49 T. Chub, H. Friedman, and R. Kreplin, "Measurements made of High Energy X-Rays Accompanying Three Class 2+ Solar Flares", Journal of Geophysical Research, Vol. 65, 1960.

5-50 G. Elwert, "Theory of X-Ray Emission of the Sun," Journal of Geophysical Research, Vol. 66, 1961.

5-51 A. Unsold, Physik der Sternatmospharen, Springer-Verlag, Berlin, Gottingen, Heidelberg, 1955.

5-52 G. Westerhout, "The Radio Galaxy," Scientific American, Vol. 201, Aug. 1959.

5-53 R. E. Danielson, "An Attempt to Detect Energetic Gamma Radiation from the Sun," Journal of Geophysical Research, Vol. 65, July 1960.

5-54 L. Peterson, and J. Winckler, "Gamma-Ray Bursts from a Solar Flare," Journal of Geophysical Research, Vol. 64, 1959.

5-55 A. DaJon, "Nouvelles Resesches Sur la Photometrie de la Cendree Lalbedo de la terre," Ann. L'obs., Strasburg, Vol. 3, 1936.

5-56 L. M. Ball, NASA Ames Research Center, Private Communication, 1964.

5-57 C. B. Childs, "Broad-Band Ultraviolet Filters," Journal of Optical Society of America, Vol. 51, 1961.

5-58 L. Dunkelman, "Ultra-Violet Photodetectors," NASA Goddard, TN D-1718, August 1963.

5-59 J. Dave and Z. Sekera, "Diffuse Reflection of Solar Ultra-Violet Radiation in the Presence of Ozone," Scientific Report No. 4, Contract AF 19(604)-2429, Department of Meteorology, University of California, Los Angeles.

5-60 J. Purcell and R. Tousey, "The Profile of Solar Hydrogen-Lyman-Alpha," Journal of Geophysical Research, Vol. 65, 1960.

5-61 T. A. Chubb, "Some Results of the NRL Rocket Program for 1960-X-Ray and Ultraviolet Radiation from Flares, Ultraviolet Stars, and Solar Ultraviolet Spectra," Journal of Geophysical Research, Vol. 66, 1961.

5-62 H. J. Smith, "A Study of Sacramento Peak Flares: Distribution, Area, and Growth Curves," Geophysics Research Directorate, Solar Research Note No. 59, AFCRL-600.

5-63 H. Hinteregger, and K. Watanabe, "Photoelectric Cells for the Vacuum Ultraviolet," Journal of Optical Society of America, Vol. 43, 1953.

5-64 G. Hass, and R. Tousey, "Reflecting Coatings for the Extreme Ultraviolet," Journal of Optical Society of America, Vol. 49, 1959.

NO. 65-323
VOL 2

# SECTION 6

# MISSION SELECTION

# SECTION 6
# MISSION SELECTION

## 6.1 INTRODUCTION

This section presents the conclusions reached from the Mission Analysis Phase (Phase I) of this study. To arrive at these conclusions, the results of the Launch Vehicle, Orbit Analysis, Thermionic System Performance and Secondary Experiments Sections were integrated and the most promising combinations of these factors selected. These selected combinations constitute the most attractive missions for a solar thermionic flight experiment.

## 6.2 ORBIT COMPARISON

The advantages and disadvantages of the various orbits considered are summarized in Table 6-1. Based on these advantages and disadvantages, the recommended orbits for the first solar thermionic flight experiment, in order of preference, are summarized in Table 6-2.

Primarily because it can provide an initial shadow free period followed by the introduction of a shadow period in the latter phases of the experiment, the modified sun-synchronous orbit is far more attractive than any of the orbits considered. The advantages provided during the initial shadow free period are:

a. An uninterrupted evaluation of the thermionic experiment can be made.

b. An uninterrupted evaluation can be made of all secondary experiments that require sun orientation.

c. With no shadow periods, the severe thermal cycling problems are eliminated and the solar thermionic system life and reliability increased.

Vol. II

## Table 6-1. Advantages and Disadvantages of Various Orbits

| ORBIT | ADVANTAGES | DISADVANTAGES |
|---|---|---|
| Low Altitude Circular (325 nm) | 1-Can be obtained with a low cost, highly reliable launch vehicle. | 1-Has a short period and low light-to-shadow ratio. This results in frequent thermal cycling and does not provide a long uninterrupted light period for evaluation of the solar thermionic experiment.<br>2-Of least interest for making scientific measurements because a relatively large number of experiments have already been conducted in this altitude range.<br>3-Because the boost capability required is relatively small, this orbit makes very inefficient use of any of the launch vehicles available.<br>4-Requires numerous ground stations for handling the TT&C functions. |
| Modified Sun-Synchronous Daylight (1000 nm) | 1-Provides shadow free period for the early phase of the mission with shadow periods being introduced in the latter phase.<br>2-TT&C functions require a maximum of two ground stations. One station may be sufficient.<br>3-Can be obtained with a low cost highly reliable launch vehicle.<br>4-Altitude is of interest for making scientific measurements and ideal for conducting many of the secondary engineering experiments considered. | 1-Falls in a severe region of the Van Allen radiation belt. |
| Highly Elliptical Orbit (200 by 25,000 nm) | 1-High light-to-shadow ratio.<br>2-Scientific measurements of interest.<br>3-Can be obtained with a medium cost highly reliable launch vehicle.<br>4-Long orbit period reduces thermal cycling. | 1-Requires numerous ground stations for handling TT&C functions.<br>2-Has lengthy shadow periods (2 hours).<br>3-Shadow history is erratic.<br>4-Has a long period which results in large quantities of data being collected per orbit. |
| Stationary Earth Synchronous (19,300 nm circular) | 1-Can handle TT&C functions from one ground station.<br>2-Provides shadow free periods for the early phase of the mission with shadow periods being introduced in the latter phase. | 1-Establishing and maintaining orbit requires a complex station keeping system.<br>2-Expensive launch vehicle (ATLAS-AGENA D) of relatively low reliability required.<br>3-Not very interesting for scientific measurements.<br>4-Has lengthy shadow periods (1.17 hours). |
| Solar Probe | 1-Spacecraft always in the sun.<br>2-Secondary scientific experiments of great interest. | 1-Large variation in solar intensity.<br>2-Effects of shadow cannot be evaluated.<br>3-Desirable orbit requires an unproven launch vehicle (ATLAS-AGENA D-X-259).<br>4-Launch vehicle relatively expensive and of low reliability.<br>5-High priority ground stations required (DSIF).<br>6-Requires directional antenna onboard the spacecraft. |



313

RE-ORDER No. 65-325
Vol II

d. Thermionic generator warm-up problems such as getting the cesium reservoir up to temperature after each dark period are eliminated.

e. The attitude control function is simplified because the sun reference is never shadowed.

f. The spacecraft thermal control problems are reduced.

g. The need for secondary battery power is reduced or eliminated.

Table 6-2. Recommended Orbits

| Recommended Orbits (In Order of Preference) | Altitude (nm) | Inclination (degrees) | Period (hours) | Maximum Dark Period (hours) | Launch Site |
|---|---|---|---|---|---|
| 1. Modified Sun-Synchronous | 1000 | 101.84 | 2.07 | 0.4 | WTR |
| 2. Highly Elliptical | 25,000 (Apogee)<br>200 (Perigee) | 45 | 14.0 | 2.09 | ETR |
| 3. Low Altitude Circular | 325 | 30 | 1.61 | 0.61 | WTR |

The introduction of a shadow period in the latter phase of the mission gives the added advantage of allowing the effect of dark periods to be evaluated. Since the majority of space applications for solar thermionics would involve shadow periods, this information is needed. The other advantages listed in Table 6-1 also contribute substantially to making this orbit the number one selection. Since spacecraft weight does not appear to be a problem, the solar cell shielding weight associated with the severe radiation environment does not appear to be a serious disadvantage.

A highly elliptical orbit is the second choice, however, compared with the modified sun-synchronous orbit, it is considered far less attractive. Its only advantage, compared with the modified sun-synchronous orbit, is that the wide variation in orbit altitude provides a platform for performing interesting scientific measurements of such quantities as the proton and electron spectra. This type of orbit does not offer a completely shadow free period, but it does offer a high light to shadow ratio and a long orbital period. This assures long periods (12 hours or more) of daylight for operating the thermionics experiment and minimizes the thermal cycling. Communication for the highly elliptical orbit is more difficult than it is with the modified sun-synchronous orbit and requires the involvement of more ground stations.

Also, the relatively long shadow period compared with the modified sun-synchronous orbit (2 hours compared with 0.4 hour) may create thermal control problems for the highly elliptical orbit.

Of the five basic types of orbits considered, the low altitude circular orbit is ranked third. Although a solar thermionic experiment could be conducted from this type of orbit, it is not extremely attractive. Compared with the two orbits ranked above it, the low altitude circular orbit has no advantages and, as indicated in Table 6-1, it has numerous disadvantages.

The stationary earth synchronous orbit or the solar probe are not considered suitable for the first solar thermionic flight experiment. The stationary earth synchronous orbit is rejected primarily because of the cost and complexity associated with establishing and maintaining this type of orbit. The major objections to the solar probe are the serious design problems resulting from the change in solar intensity encountered throughout the orbit.

## 6.3 LAUNCH VEHICLE SELECTION

One of the IMPROVED DELTA launch vehicle configurations is recommended for each of the three orbits selected. The specific launch vehicle selected is indicated in Table 6-3.

Table 6-3. Recommended Launch Vehicle

| Orbit | Recommended Launch Vehicle |
|---|---|
| Modified Sun-Synchronous<br>Altitude: 1000 nm<br>Inclination: 101.84 degrees | IMPROVED DELTA<br>DSV-3E |
| Highly Elliptical<br>Altitude: APOGEE - 25,000-nm<br>PERIGEE- 200-nm<br>Inclination: 45 degrees | IMPROVED DELTA<br>DSV-3E |
| Low Altitude Circular<br>Altitude: 325-nm<br>Inclination: 30 degrees | IMPROVED DELTA<br>DSV-3H |

The reasons for selecting a DELTA class launch vehicle are summarized below:

a. Based on actual flight records, the DELTA class of launch vehicles have demonstrated a significantly higher reliability than any of the other vehicles considered .

b. For equivalent payload-orbit capability, the DELTA series has the lowest cost of the vehicles considered.

c. The DELTA series of launch vehicles provide a wide range of payload-orbit capability. As a result, one of the DELTA configurations will generally closely approximate the required payload-orbit capability. This minimizes the chances of paying for booster capability that is not needed.

d. The DELTA series are the only launch vehicles considered that are not engaged in orbiting classified military payloads. In addition, the DELTA series are NASA vehicles. These two conditions should minimize priority problems in obtaining a vehicle and scheduling launches.

The specific reasons for choosing the IMPROVED DELTA from the various DELTA configurations available are:

a. The payload fairings associated with the IMPROVED DELTA allow solar concentrator diameters essentially as large as those obtainable with any of the vehicles considered and substantially larger than allowable with other vehicles in the DELTA series. These allowable concentrator diameters are large enough (57 inches maximum) to obtain the minimum acceptable thermionic generator output of 100 watts, with a sizable margin of safety (a concentrator diameter of 42 inches is required to obtain 100 watts). Having this safety margin can simplify the spacecraft design and offer some space for expansion should the component performance not come up to present estimates, thus, necessitating a larger concentrator diameter. This safety margin will also permit the use of concentrator diameters on the order of 50 inches, which are required if thermionic emitter areas of two square centimeters or greater are to be used. Areas of two square centimeters (or more) are highly desirable since all of the existing experience has been with emitter areas of this size.

b. Since the IMPROVED DELTA can be used in four different configurations, (DSV-3E, 3F, 3G and 3H) which cover a wide range of payload-orbit capability, it represents a very versatile launch vehicle. For example, assume a mission were designed around the DSV-3G vehicle. If for some reason, such as a change in the planned orbit, an overweight spacecraft, etc., greater booster capability were required, a switch to the DSV-3E launch vehicle could be made. Since all of the IMPROVED DELTA configurations are modifications of the same basic vehicle, and they all employ the same payload fairings, this change could be made with the

minimum of difficulty. This might prove particularly attractive for second or third generation missions where a significant change in the spacecraft orbit could be made without a major redesign of the spacecraft.

There are three potential disadvantages with using the IMPROVED DELTA launch vehicle. First, since it is not scheduled to become operational until the third quarter of 1965, it is not now available. Also, since it is not operational, its performance has not been demonstrated. However, if the present schedule is held, the vehicle availability should not present a problem for a solar thermionic flight experiment. Also, this is not an entirely new vehicle since, in general, the IMPROVED DELTA will employ the same basic components as the current DELTA (DSV-3C), and is therefore expected to have the same high reliability.

Secondly, the DELTA class of vehicles do not at present have WTR launch capability which is advantageous for achieving polar or near polar orbits. This capability is scheduled to be available in the first quarter of 1966 and, therefore, should present no problems for this program.

Finally, the DELTA series of vehicles have, in general, a more severe launch acceleration and vibration environment because of the solid stages employed. A detailed design analysis will have to be performed before the effects of the launch environment can be established, but based on past spacecraft design experience, no extremely difficult problems are anticipated.

These three potential disadvantages are not considered serious at this point.

## 6.4 SOLAR THERMIONIC SYSTEM PERFORMANCE

Since one of the IMPROVED DELTA configurations was selected as the launch vehicle for use with each of the missions, the maximum payload diameter is 57 inches for all three cases. A concentrator diameter of 50 inches was selected for the following reasons:

Vol 2

a. A 50 inch diameter concentrator will yield a thermionic generator output of 144 watts which is considerably above the minimum ground rule requirement of 100 watts. Therefore, a substantial decrease in estimated performance could be tolerated without the generator output falling below 100 watts.

b. A 50-inch diameter concentrator allows a converter emitter area of two square centimeters which is highly desirable since the majority of thermionic converter experience has been with this emitter size.

c. Choosing a concentrator diameter smaller than the maximum value the payload fairing will allow has two major advantages.

1. It allows flexibility should the thermionic system performance fall below present estimates and the concentrator diameter have to be increased.

2. It leaves ample space for the concentrator torus and other spacecraft structure that may be required. If it were necessary to design the spacecraft such that the concentrator diameter equaled the maximum allowable payload diameter this could present some difficult spacecraft design problems.

Having selected the concentrator diameter, the thermionic system size is defined. The major performance parameters, consistant with a 50-inch concentrator diameter, are summarized in Table 6-4. The thermionic system design will be the same for all three of the missions.

## 6.5 SECONDARY EXPERIMENT SELECTION

A total of twenty secondary experiments (ten engineering and ten scientific) were considered. These experiments were selected on the basis of their importance to the development of solar thermionics and to the total space program. Also considered in choosing secondary experiments for evaluation was their compatibility with the primary experiment and their



311

Table 6-4. Thermionic System Performance Parameters

| Performance Parameters | |
|---|---|
| Converter Emitter Temperature | 2000°K |
| Converter Electrode Spacing | 2 mils |
| Converter Emitter Material | Rhenium |
| Converter Sleeve Thickness | 0.0025 in. |
| Converter Emitter Area | 2 $cm^2$ |
| Converter Operating Point | Peak Efficiency |
| Converter Power Density | 18 watts/$cm^2$ |
| Converter Voltage Output | 0.85 volts |
| Converter Efficiency | 17.4 percent |
| Concentrator Diameter | 50 in. |
| Concentrator Rim Angle | 60 degrees |
| Concentrator Geometric Error, $3\sigma$ | 12 min |
| Concentrator Reflectivity | 90 percent |
| Concentrator Blockage Factor | 5 percent |
| Concentrator-Absorber Efficiency | 67 percent |
| Thermionic Generator Aperture Diameter | 0.71 in. |
| Thermionic Generator Efficiency | 12.2 percent |
| Thermionic Generator Power Output | 144 watts |
| Thermionic Generator Voltage (Four Converters in Series) | 3.4 volts |
| Thermionic System Efficiency | 8.2 percent |

ability to take advantage of the unique requirements of the primary experiment, such as highly accurate sun orientation.

Table 6-5 presents the most attractive secondary experiments of the twenty evaluated. These experiments are divided into two groups: priority "A" and priority "B." The priority "A" group represents those experiments which should be included on the spacecraft

Table 6-5. Recommended Secondary Experiments (Sheet 1 of 2)

| | | Experiment | Major Reasons for Selection | Orbit Compatibility* I | II | III |
|---|---|---|---|---|---|---|
| PRIORITY A | 1 | Solar Reflective Surfaces | Results of major importance to the development of solar thermionics and other solar power systems employing concentrators. Also helpful in evaluating the primary experiment. | X | X | X |
| | 2 | Micrometeroid Measurements | Important scientifically and to evaluation of the primary experiment. Also needed for complete evaluation of Experiment No. 1. | X | X | X |
| | 3 | Proton and Electron Spectra and Direction | Important scientifically and to evaluation of the primary experiment. Also needed for complete evaluation of Experiments No. 1 and 8. | X | X | X |
| | 4 | Ultraviolet Radiation | Important scientifically and to evaluation of the primary experiment. Also needed for complete evaluation of Experiments No. 1, 5, and 8, and supplements Experiments No. 10 and 11. | X | X | X |
| PRIORITY B | 5 | Thermal Coating | Relatively simple experiment which yields needed information on thermal coatings to be used on space vehicles. Experiment package already developed. Experiment makes use of sun pointing feature of the spacecraft. | X | X | X |
| | 6 | Laser Experiment | Important to the development of lasers as a means of space communication. | X | X | X |
| | 7 | Low Thrust Electric Engine | Important to the development of low thrust electric engines for use in attitude control systems and space propulsion in general. | X | X | X |

Table 6-5. Recommended Secondary Experiments (Sheet 2 of 2)

| | | Experiment | Major Reasons for Selection | Orbit Compatibility* | | |
|---|---|---|---|---|---|---|
| | | | | I | II | III |
| PRIORITY B | 8 | Radiation Effects on Solar Cells | Important to a more complete understanding of solar array degradation from radiation. Results needed to improve solar cell power supply design. Also makes use of the sun pointing feature of the spacecraft. | X | – | – |
| | 9 | Infrared Detector | Important to the development of better IR detectors for use in attitude control systems. | X | X | X |
| | 10 | Solar X-Rays | Important scientifically and makes use of the sun pointing feature of the spacecraft. Also supplements Experiments No. 4 and 11. | X | X | X |
| | 11 | Solar $\gamma$-Rays | Important scientifically and makes use of the sun pointing feature of the spacecraft. Also supplements Experiments No. 4 and 10. | X | X | X |
| | 12 | Lyman-Alpha | Important scientifically and makes use of the sun pointing feature of the spacecraft. Also supplements Experiments Nos. 4, 10, and 11. | X | X | X |
| | 13 | Earth Albedo | Important to a better measure of the earth's albedo. This information is of value scientifically and to the thermal design of space vehicles. | – | – | X |

*ORBIT I - MODIFIED SUN-SYNCHRONOUS (1000-nautical miles - 101.84-Degree Inclination)

ORBIT II - HIGHLY ELLIPTICAL (200 by 25,000 nautical miles - 45 -Degree Inclination)

ORBIT III - LOW ALTITUDE CIRCULAR (325-nautical miles - 30-Degree Inclination)

if at all possible. These experiments are individually of great engineering or scientific interest and also yield information which is needed to completely evaluate the primary experiment.

The priority "B" experiments are to be considered for inclusion on the spacecraft after the priority "A" experiments. The experiments in this second group are also of great engineering or scientific interest, but are not necessary to evaluation of the primary experiment.

Table 6-5 also indicates the orbits which are suitable for conducting each of these experiments. With a few exceptions all of the experiments listed can be conducted from any of the three orbits selected. Experiment No. 3 is not suitable for the low altitude circular orbit because the 325-nautical mile altitude is below the Van Allen Belt and there is no appreciable radiation to measure. The Earth Albedo Experiment (No. 13) is not well suited to the modified sun-synchronous or highly elliptical orbits. In the former case, the difficulties arise because the spacecraft is always operating almost directly above the boundary between the illuminated and dark portions of the earth. This presents a confusing field of view to the earth oriented albedo sensor and makes meaningful results difficult to obtain. The highly elliptical orbit, because of its wide variation in altitude, represents a difficult orbit for conducting an earth albedo experiment.

The final selection of the secondary experiments to be included on each of the three missions will be made in the spacecraft design phase of the study. It may be difficult to include all thirteen of the experiments listed in Table 6-5 on any one of the spacecraft designs; however, it appears that all of the priority "A"-experiments and most of the priority "B" experiments can be included in each case. The decision on which of the priority "B" experiments is to be included with each of the missions will be based on a consideration of power, weight, telemetry requirements, and compatibility with the spacecraft design.

The secondary experiments considered in this study are illustrative of those that could be included on a spacecraft whose primary objective is the evaluation of solar thermionics. As subsequent studies of the solar thermionic flight experiment are undertaken, it will be necessary to continually evaluate potential secondary experiments to insure that those finally selected represent the best possible choice. It will also be necessary to evaluate these experiments in greater detail than this study would allow before a final selection is made.

## 6.6 SUMMARY AND CONCLUSIONS

The missions selected for detailed study are summarized in Table 6-6 and in the subsequent sections will be referred to as Missions A, B and C. In Phase II of the study, conceptual spacecraft designs will be developed for each of these missions.

Table 6-6. Summary of Selected Missions

| MISSION | ORBIT | ORBIT ALTITUDE NM | ORBIT INCLINATION DEGREES | ORBIT PERIOD HOURS | ORBIT MAXIMUM DARK PERIOD HOURS | LAUNCH VEHICLE | LAUNCH SITE | THERMIONIC SYSTEM CONCENTRATOR DIAMETER, INCHES | THERMIONIC GENERATOR POWER OUTPUT WATTS | SECONDARY EXPERIMENTS |
|---|---|---|---|---|---|---|---|---|---|---|
| A | Modified Sun-Synchronous | 1,000 | 101.84 | 2.07 | 0.4 | IMPROVED DELTA DSV-3E | WTR | 50 | 144 | See Table 6-5 |
| B | Highly Elliptical | 25,000 Apogee 200 Perigee | 45 | 14.0 | 2.09 | IMPROVED DELTA DSV-3E | ETR | 50 | 144 | See Table 6-5 |
| C | Low Altitude Circular | 325 | 30 | 1.61 | 0.617 | IMPROVED DELTA DSV-3H | ETR | 50 | 144 | See Table 6-5 |